REFERENCE ONLY

UNIVERSITY OF LONDON THESIS

Degree PhD Year 2006 Name of Author KANAGOTTIY N.T

Neurotransmitter signalling to oligodendrocytes

Ragnhildur Þóra Káradóttir

A thesis submitted to the University of London

for the degree of

Doctor of Philosophy

Department of Physiology, University College London

January 2006

ProQuest LLC
789 East Eisenhower Parkway
P.O. Box 1346
Ann Arbor, MI 48106-1346

For my daughter Melkorka Elea

Abstract

Neurotransmitter signalling to neurons and glial cells plays a key role in brain development, information processing and pathological processes. This thesis focuses on neurotransmitter signalling to oligodendrocytes, the glial cells which provide myelin to speed the propagation of action potentials along neuronal axons. In cerebellar and corpus callosal slices, I used patch-clamping and immunocytochemistry to examine the properties of precursor, immature and mature oligodendrocytes, characterizing their morphology and basic electrical properties, their response to glutamate, GABA and other neurotransmitters, and the neurotransmitter receptor subunits that they express. In contrast to the currently held view, I found that oligodendrocytes express NMDA receptors. These receptors show extremely weak magnesium-block, allowing them to be activated at the resting potential, and they may be composed of NR1, NR2C and NR3 subunits. To investigate the role of these NMDA receptors in pathology, experiments on hippocampal neurons were first used to establish how best to block glycolytic and mitochondrial production of ATP to mimic the energy deprivation which occurs in ischaemia. Ischaemia-evoked glutamate release was found to activate oligodendrocyte NMDA and non-NMDA receptors. Although the normal role of the oligodendrocyte NMDA receptors may be to regulate myelination, they probably contribute to the glutamate-mediated damage which occurs to oligodendrocytes in periventricular leukomalacia (leading to cerebral palsy), stroke, spinal cord injury and multiple sclerosis. Block of these receptors may therefore offer a potential therapeutic approach to treating these disorders.

Statement of the candidate's contribution to this thesis

With the minor exceptions listed below (which contribute about 5% of the work in the thesis), all of the work in this thesis was carried out by Ragnhildur Karadottir. She was responsible, with normal supervisorial input, for planning the work, developing the techniques needed for electrophysiological recording from oligodendrocytes, carrying out the subsequent patch-clamping experiments, adapting immunocytochemistry techniques to work reliably in brain slices after electrophysiological recording, performing the extensive immunocytochemical experiments described in the thesis, and analysing and interpreting the data.

The exceptions are as follows.

(i) In chapter 8 (defining conditions to mimic ischaemia) 40% of the experiments were done by Nicola Allen.

(ii) Some experiments were carried out in collaboration with Pauline Cavelier: these contribute to one figure of the thesis (Figure 4.2 C-E).

(iii) Electron microscopy work on oligodendrocytes by Linda Bergersen is reproduced in one figure of the thesis (Figure 4.8).

(iv) Some experiments were carried out in collaboration with Louise Whiteley: these contribute to one figure in the thesis (Figure 5.2).

Ragnhildur Karadottir wrote all of the thesis.

Signed: David Attwell, Jodrell Professor of Physiology, PhD Supervisor

Acknowledgements

I would like to thank my supervisor Prof. David Attwell, for his support, guidance and encouragement throughout my PhD. Furthermore, I would like to thank all the lab members, both past and present, for a lovely and friendly atmosphere and all their help and support during the course of my PhD: Nicola Allen, Marina Catsicas, Pauline Cavelier, Anna De Simoni, Ines Hans, Clare Howarth, Josef Kittler, Manuela Lahne, Nanna Luneborg, Paikan Marcaggi, Rachael Pearson and Claire Peppiatt.

I specially thank and appreciate the help from: Linda Bergersen, who did all the post-embedding electron microscopic immunocytochemistry and Pauline Cavelier, who contributed some experiments to Chapter 4. In addition, I would like to thank Louise Whiteley who did some recording of GABAergic responses in oligodendrocytes, presented in Chapter 5. Furthermore, a very special thanks to Nicola Allen, for the enjoyable collaboration during the experiments that are presented in Chapter 8.

In addition, I thank Kristján Jessen, for scientific support in the field of myelinating glial cells

Finally, I would like to thank my partner Massimiliano Polli for his patience, support and understanding when I worked long hours in the lab and during these last few months while I have been writing up, and I thank my daughter Melkorka Elea for sharing her mum with oligodendrocytes! In addition, I thank my parents for supporting me to follow my dreams, as well as my previous supervisor Prof. Jóhann Axelson who made me believe I could do it!

The work presented in this thesis was supported by the Wellcome Trust.

Table of Contents

CHAPTER 3

CHAPTER 4

CHAPTER 5

CHAPTER 6

List of Figures

List of Tables

Chapter 1

Introduction

In this thesis I will explore the properties of oligodendrocytes in the white matter of the mammalian brain. I will characterize their anatomy, basic electrophysiological properties and current response to neurotransmitters, and I will describe their response to simulated ischaemia, which mimics the causes of white matter diseases such as cerebral palsy, spinal cord injury and stroke. I will also report in less detail on the properties of the astrocytes that share the white matter with the oligodendrocytes, and on the response of neurons in the grey matter to simulated ischaemia.

1.1 The white matter – a historical view

In humans the white matter makes up half of the brain volume, with the other half being the grey matter (Schoenemann et al., 2005). During evolution brain size has increased, and the human brain is significantly larger than is expected for a primate of our size (Passingham, 1973; Rilling & Insel, 1999). Among primates, humans have the largest prefrontal cortex, an area thought to contribute to many particularly human characteristics like creative thinking, decision making, forward planning, working memory and language. With an increasing absolute amount of grey matter volume, the white matter should increase disproportionately to maintain the connectivity of neurons (Ringo, 1991). In fact, the white matter in human cortex is indeed disproportionately larger than is expected by comparison with the brains of smaller primates (Ringo, 1991). Despite the increasing importance of the white matter for maintaining the neuronal connectivity in our larger volume brains, if one looks back at the history of neuroscience it is understandable why the white matter has been given a lower priority for investigation compared to the grey matter.

First, the white matter is mainly populated by glial (*Greek*: *glue*) cells. This name was given to them by Virchow in 1856, when he named these cell *Nervenkitt,* i.e.

nerve-glue or nerve-putty (Somjen, 1988), as he thought they were there only to fill in the gaps between the neurons. Second, until recently there has been a general conception that glia are passive and inactive members of the brain, whereas the neurons in the grey matter are the working machinery of the brain.

However, some scientists did not share Virchow's views on the unimportance of glia: in 1886 Golgi suggested that glia feed metabolic substrates to neurons (Somjen, 1988), while Del Rio Hortega (1921, 1928) both named and classified oligodendrocytes and suggested that they were myelinating cells similar to Schwann cells in the peripheral nervous system (Wood & Bunge, 1984). Del Rio Hortega (1921) used silver-carbonate staining to show that oligodendrocyte processes were attached to the myelin (or ended in close vicinity to it). These findings were reaffirmed by Penfield in 1924, implying that oligodendrocytes do form myelin in the CNS (Wood & Bunge, 1984; Somjen, 1988).

Rio Del Hortega grouped oligodendrocytes into two classes: perineuronal (if the cell body was adjacent to a neuronal soma in the grey matter) and interfascicular (oligodendrocytes with somata among the myelinated axons in the white matter). He further classified them into four types depending on morphology (Wood & Bunge, 1984). This classification is still in use today, as it was confirmed by EM studies (Stensaas & Stensaas, 1968) and by light microscope images of dye-filled oligodendrocytes (Butt et al., 1995; Berry et al., 1995).

1.2 An overview of the function of oligodendrocytes

Oligodendrocytes produce myelin by tightly wrapping their cell membrane many times around the axons, generating a myelin sheath. This reduces the effective capacitance (and increases the resistance) of the axonal membrane, and hence less charge is needed to produce a depolarization. As a result, myelin increases the conduction velocity of the action potential (Bunge, 1968; Hille, 2001). One oligodendrocyte can myelinate up to 30 axons with 150-200μm long myelin sheaths, but it does not myelinate the same axon twice (Butt & Ransom, 1989; Ransom et al., 1991).

These myelin sheath segments, which are called internodes, are separated by an unmyelinated gap on the axon, which is named the node of Ranvier (see Fig. 1.1, at the end of the chapter), where voltage-gated sodium channels cluster in the axonal membrane. On each side of the node of Ranvier are so-called paranodes (where the myelin sheath has a looser structure) where potassium channels cluster in the axonal membrane (Salzer, 2003). This architecture allows the action potential to travel fast down the axon, by "jumping" between nodes. In addition to increasing the propagation speed of the action potential, oligodendrocytes have also been suggested to secrete neurotrophic factors that support neurons and increase their survival (Dai et al., 2003; Wilkins et al., 2003).

In diseases like multiple sclerosis (Zajicek & Compston, 1995; Skundric, 2005), periventricular leukomalacia (Kinney, 2005), spinal cord injury (Beattie et al., 2002), stroke (Dewar et al., 2003) and schizophrenia (Davis et al., 2003) oligodendrocytes get damaged. This causes a loss of neuronal function, as the action potential slows down or ceases altogether, resulting in movement disorders (spinal cord injury, cerebral palsy) or cognitive disorders (periventricular leukomalacia, schizophrenia).

Recent reports have suggested that neurotransmitters act on oligodendrocytes, both to control the cells' development and to damage them in disease (detailed descriptions are given later in this chapter). However, the neurotransmitter responses of oligodendrocytes have not been very well characterized, especially in comparison to what we know about neuronal responses to neurotransmitters. It is therefore of great interest to study further the neurotransmitter responses in these cells and explore their involvement in oligodendrocyte pathology: such studies form a major part of this thesis.

1.3 The development of oligodendrocytes

Oligodendrocyte development is controlled by a complex array of transcription factors and growth factors, but also by neurotransmitters. As a background to the experiments I have carried out on the neurotransmitter responses of oligodendrocytes, in this section I will review what is known about the development of oligodendrocytes.

1.3.1 The birth of oligodendrocytes

Most experiments done to understand the developmental origins of oligodendrocytes have been carried out in the spinal cord neuronal epithelium. In the ventral part of the spinal cord oligodendrocytes are generated at embryonic day (E) 14 in the rat (Pringle & Richardson, 1993; Yu et al., 1994) and at E12.5 in the mouse (Miller, 2002). There are two main streams of thought on how oligodendrocytes are generated; the first is based more on cell lineage studies in culture and the other more on studies of oligodendrocyte formation *in vivo*.

The first theory is that oligodendrocytes are generated from a glial-restricted progenitor cell (i.e. a cell that generates only glia). It is based on the finding that progenitor cells isolated from neonatal animals could generate two types of cell in culture, i.e. so-called type 2 astrocytes and oligodendrocytes (Raff et al., 1983a; Raff et al., 1983b). Consequently these cells were named O-2A progenitor cells. A possible precursor to these O-2A cells is another glial restricted precursor which, when isolated from the embryonic neuroepithelium, generates oligodendrocytes and two types of astrocyte (so called types 1 and type 2), and will not grow into neurons either in culture (Rao et al., 1998) or when transplanted into the rat brain (Herrera et al., 2001). These cells are found both ventrally and dorsally in the neuroepithelium, but the ventrally situated ones seem to be more prone to generate oligodendrocytes than the dorsal ones (Gregori et al., 2002; Fig. 1.2B).

The second theory is driven from the findings that oligodendrocytes are generated in a very restricted region of the ventricular zone in the spinal cord neuroepithelium (Pringle & Richardson, 1993; Yu et al., 1994), and that two oligodendrocyte specific transcription factors, Olig1 and 2 are involved in specifying an oligodendrocyte fate (Lu et al., 2000; Takebayashi et al., 2000; Zhou et al., 2000b). There is a specialised precursor domain in the ventral spinal cord, the pMN domain, that generates most of the oligodendrocytes in the CNS, but also generates motoneurons (Zhou et al., 2001; Zhou & Anderson, 2002; Lu et al., 2002; Takebayashi et al., 2002). Oligodendrocytes are generated in the pMN domain under the control of sonic hedgehog (Shh) signalling from the notochord and floor plate during the second wave of

cell genesis in the spine (Pringle et al., 1996), when Olig2 expression coincides with Nkx2.2 expression (Zhou et al., 2001). This seems to be a general mechanism for oligodendrocyte generation as most oligodendrocytes are generated ventrally in the spinal cord and in the hind-, mid- and fore-brain in a sonic hedgehog dependent manner (Tekki-Kessaris et al., 2001; Rowitch, 2004; Le et al., 2005). Sonic hedgehog induces expression of Olig2, which is required for generation of both motor neurons and oligodendrocytes (Zhou & Anderson, 2002; Lu et al., 2002; Takebayashi et al., 2002), indicating that oligodendrocytes and motor neurons share a common precursor cell (Fig. 1.2A). Once formed, spinal oligodendrocytes migrate dorsally to colonize spinal white matter tracts. Similarly, precursors formed in the basal forebrain (probably under the control of Shh) gives rise both to both GABAergic interneurons and to oligodendrocytes that migrate into the cerebral cortex (He et al., 2001). Astrocytes are generated in a separate region from oligodendrocytes; in the spinal cord astrocytes are generated in the p2 domain, which also generates ventral interneurons (Pringle et al., 1998; Zhou & Anderson, 2002; Lu et al., 2002). Recently it has been shown that there is also a small fraction of oligodendrocytes (15%) for which genesis is sonic hedgehog independent, which are generated in the dorsal region of the neural tube (Cai et al., 2005; Vallstedt et al., 2005; Fogarty et al., 2005). This dorsal oligodendrocyte generation seems to rely on fibroblast growth factor (FGF) signalling (Kessaris et al., 2004; Fogarty et al., 2005). Whether there is a functional difference between oligodendrocytes generated dorsally or ventrally is still unknown.

These two theories do not necessarily contradict each other as there might be a glial restricted precursor that potentially could become either an astrocyte or an oligodendrocyte, depending on the positional cues in its environment. This would allow these cells to generate oligodendrocytes in the pMN domain and astrocytes in the p2 domain (see review by Rowitch et al., 2002).

The oligodendrocyte precursor described by both theories (i.e. in culture or *in vivo*) is defined by its expression of several molecules: the ganglioside GT3 which is recognised by the antibody A2B5 (Eisenbarth et al., 1979), the PDGFα receptor (Pringle et al., 1992) and the chondroitin sulfate proteoglycan NG2 (Stallcup & Beasley, 1987;

Levine & Stallcup, 1987). In what follows, I will use a superscript + (or positive) to mean "labels positively with antibody against the named protein". It is commonly assumed that the O-2A precursors, A2B5$^+$ cells, PDGFα R$^+$ cells and NG2$^+$ cells are all the same cell type, since in culture these markers all label the same cell type. However, as will become clear in this thesis (see Chapter 3), *in vivo* they do not only recognize oligodendrocyte precursors. Nevertheless, for convenience, I will initially use these labels when talking about oligodendrocyte precursors.

1.3.2 Oligodendrocyte migration, proliferation and differentiation: effects of growth factors

After oligodendrocyte genesis, the precursor cells have to migrate large distances to reach their final destination, as well as proliferate and start to differentiate. The precursor oligodendrocyte (which expresses the markers A2B5, PDGFαR and NG2) differentiates first into an intermediate stage that expresses (with some overlap with the precursor markers) the lipid sulphatide O4 (Sommer & Schachner, 1981). It then differentiates further to a more mature stage expressing the cytosolic antigen RIP and galactosylceramide (GalC), before differentiating to a yet more mature stage expressing the myelin components myelin basic protein (MBP) and proteolipid protein (PLP). This stage marks the start of myelination, O4 expression is then lost, and finally myelin/oligodendrocyte glycoprotein (MOG) appears late in myelination (Fig. 1.3; Baumann & Pham-Dinh, 2001).

1.3.2.1 Migration

In the CNS, neuronal migration is controlled either by long range or short range attractants or repellents, and oligodendrocyte migration is no different (Tsai & Miller, 2002; Jarjour & Kennedy, 2004).

Oligodendrocyte precursor cells are highly motile and can travel long distances along the neural axis. For example in the optic nerve (Small et al., 1987) they migrate from the optic chiasm to the retina, repelled by netrin 1 secreted by cells in the optic chiasm (Sugimoto et al., 2001). Netrin1 also repels newly generated cells in the ventral

regions of the spinal cord (Tsai & Miller, 2002; Tsai et al., 2003), making them move away from their origin. The idea that oligodendrocytes migrate along axons has been disputed, since in the optic nerve without axons oligodendrocyte still migrate (Ueda et al., 1999), but migration along axons has been seen *in vivo* using time lapse imaging of oligodendrocyte precursors migrating parallel to unmyelinated axons in the corpus callosum (Kakita et al., 2003) and into the grey matter from the sub-ventricular zone (Kakita & Goldman, 1999). In addition to this imaging evidence for axonal guidance, various growth factors secreted from astrocytes or axons promote oligodendrocyte migration and proliferation or differentiation (Richardson et al., 1988; Noble et al., 1988; Barres & Raff, 1993; Barres & Raff, 1999). Effects on migration, proliferation and differentiation are interrelated, as agents that promote differentiation will reduce migration, and vice versa.

1.3.2.2 Proliferation and differentiation

There is a complex control exerted by growth factors and other molecules on the development of oligodendrocytes. However the main player in the control of migration, proliferation and survival of oligodendrocyte precursors is platelet-derived growth factor (PDGF) released by astrocytes (Raff et al., 1988; Richardson et al., 1988; Noble et al., 1988) and/or axons (Barres & Raff, 1993). PDGF acts on PDGFα receptors in oligodendrocyte precursors, to control the cells' proliferation, motility and the timing of their differentiation, both in culture (Raff et al., 1988; Richardson et al., 1988; Noble et al., 1988) and in vivo (Butt et al., 1997a). PDGF is also the main chemo-attractant for oligodendrocyte precursors (Armstrong et al., 1990). In addition, basic fibroblast growth factor (bFGF) increases the sensitivity of oligodendrocyte precursors to PDGF, by increasing the expression level of the PDGFα receptor in the precursors (McKinnon et al., 1990). In culture, the combination of bFGF and PDGF makes the oligodendrocytes migrate, but without PDGF they only proliferate, and if neither is present they will start to differentiate (McKinnon et al., 1991). This is also true *in vivo* as PDGF application in developing rats delays differentiation of the oligodendrocyte precursor (Butt et al., 1997b), and if the effects of bFGF are cancelled by expression of a dominant negative receptor, the oligodendrocytes will not migrate (Osterhout et al.,

1997). So these two growth factors keep the oligodendrocyte precursors in a proliferatory and migratory state. When an oligodendrocyte precursor differentiates into an immature oligodendrocyte, expressing the marker O4, it becomes less motile and also loses its PDGFα receptor and hence its proliferation signal (Barres & Raff, 1993; Fig. 1.3)

In addition to PDGF and bFGF, there are several other growth factors that are secreted that modulate oligodendrocyte development. For example, in culture and *in vivo*, ciliary neurotrophic factor (CNTF) promotes PDGF-induced proliferation (Barres et al., 1996). Furthermore, the oligodendrocyte precursors themselves secrete TGFβ, which inhibits proliferation and hence allows them to differentiate (McKinnon et al., 1993), but if bFGF is also present it opposes this effect of TGFβ (McKinnon et al., 1993). Interleukin 2 inhibits proliferation of oligodendrocyte precursors (Saneto et al., 1986; Knobler et al., 1988), as does insulin-like growth factor (IGF-1) since it promotes differentiation of the precursors (McMorris & Dubois-Dalcq, 1988; Wilson et al., 2003). On the other hand both epidermal growth factor (EGF) and TGFα suppress differentiation without affecting migration or proliferation (Sheng et al., 1989), as does fibroblast growth factor 2 (Goddard et al., 2001) which actually destroys myelin via activation of microglia and astrocytes (Goddard et al., 2002). Finally, it is worth noting that, even if oligodendrocyte precursor proliferation is increased, it does not necessarily have an effect on the final number of mature oligodendrocytes (Barres et al., 1996; Butt et al., 1997b) because there may be a corresponding increase in cell death that compensates for the larger number of cells generated (Fig. 1.3).

I will come back to some theories of how these growth factors influence oligodendrocyte development in section 1.3.3.2. However, oligodendrocyte development is not only controlled by a complicated soup of growth factors: various neurotransmitters, and potassium channel activity, have also been shown to have an effect. These effects are likely to mediate local control of oligodendrocyte development, while the growth factors mediate long range effects. In addition, integrins (reviewed by Baron et al., 2005), neuregulin and Notch-1/Jagged-1 signalling have been shown to mediate very localized effects on oligodendrocyte development (reviewed by Bozzali &

Wrabetz, 2004), but as they are not directly relevant to my work I will not discuss them in more detail.

1.3.3 Role of neurotransmitters and potassium currents in the development of oligodendrocytes

The number of mature myelinating oligodendrocytes produced needs to be matched to the number and length of the axons requiring myelination. One way to achieve this would be if factors were released locally from axons that controlled the proliferation and differentiation of oligodendrocytes. In this section I will review current ideas about how neurotransmitter and K^+ release from axons may contribute to this.

1.3.3.1 Axonal activity affects oligodendrocyte development

Perhaps unsurprisingly, since oligodendrocytes myelinate axons, an increase in the electrical activation of axons promotes oligodendrocyte proliferation and survival (Barres et al., 1993; Barres & Raff, 1993). In addition, oligodendrocytes migrate along axons (Small et al., 1987; Baulac et al., 1987; Kiernan & ffrench-Constant, 1993; Kakita et al., 2003) to reach their targets. If axonal electrical activity is inhibited with TTX, it disrupts glial development and myelination without affecting axons (Friedman & Shatz, 1990; Demerens et al., 1996), but see however Colello et al. (1995) who claimed that myelination was unaffected by electrical activity in axons, and suggested that the precursors already present at the age (P0) when they blocked electrical activity were sufficient to myelinate the axons present. In addition, an increase in axonal firing has been shown to promote differentiation of oligodendrocytes and increase myelination (Demerens et al., 1996; Stevens et al., 2002: Fig. 1.3).

A possible mechanism underlying these effects is that axons release substances when activated that influence oligodendrocyte development. Although PDGF may be one of these factors (Barres & Raff, 1993), there is increasing evidence for a role of smaller transmitter molecules, particularly glutamate and adenosine. Both frog sciatic nerve (Wheeler et al., 1966) and frog optic nerve axons (Weinreich & Hammerschlag, 1975) release preloaded radioactive glutamate in response to repetitive electrical stimulation, and so do spinal cord nerves (Dan et al., 1994). Moreover, axonal

stimulation, or application of the drug veratridine which generates action potentials, causes the calcium concentration to rise in optic nerve glial cells, and this is blocked by kynurenic acid (a non-specific glutamate receptor antagonist) but also by blocking glutamate transporters with dihydrokainate (Kriegler & Chiu, 1993; Chiu & Kriegler, 1994). The effect of the transporter blocker can be explained by the fact that axonal action potentials will increase the intracellular sodium concentration and the extracellular potassium concentration. This could make axonal glutamate transporters release glutamate by reversed operation of glutamate transporters, since uptake by glutamate transporters depends on there being a low intracellular sodium concentration and a low extracellular potassium concentration: when these concentrations rise, the transporters tend to release glutamate (Szatkowski et al., 1990). Interestingly, in neonatal optic nerve, axon stimulation increases the extracellular potassium level (from 5 to 20mM for 20Hz stimulation) more than in mature optic nerve (from 5mM to 11mM for 400Hz stimulation), and the increase in potassium concentration produced by a single stimulus was seven times higher in neonatal than in mature optic nerve (Connors et al., 1982). The change from the neonatal level of potassium accumulation to the mature level occurred within the first postnatal week, before myelination has begun (Foster et al., 1982), suggesting that the axonal physiology (and perhaps lack of K^+ buffering by astrocytes) facilitates more glutamate release from active axons at the time in development when oligodendrocytes start to become mature.

1.3.3.2 Effects of glutamate on proliferation and differentiation

If glutamate is released via reversed uptake, it could modulate oligodendrocyte development by activating glutamate receptors on oligodendrocytes or their precursors (Steinhauser et al., 1994; Patneau et al., 1994; Borges et al., 1994; Borges et al., 1995; Chvatal et al., 1995; Fig. 1.3 and Fig. 1.4). The properties of glutamate receptors are reviewed in section 1.4.2 below. As described in detail below (section 1.4.4.2), although it is generally believed at present that oligodendrocytes express AMPA/kainate receptors and not NMDA receptors, the data that I will present in this thesis show that this dogma is wrong (see Chapter 4). Several studies support a role for glutamate

receptors in controlling oligodendrocyte development. Firstly, activation of NMDA receptors on cultured oligodendrocyte precursor cells increased their migration rate and inhibiting their NMDA receptors decreased migration by 90%, while inhibiting AMPA receptors only reduced migration by 40% (Wang et al., 1996; Fig. 1.4). Secondly, glutamate acting through AMPA or kainate receptors on oligodendrocyte precursors decreases proliferation, as well as inhibiting the proliferative effects of PDGF and bFGF (Gallo et al., 1996; Yuan et al., 1998). In these studies, even though glutamate blocked proliferation, it did not seem to promote migration (contradicting the work of Wang et al., 1996) or differentiation (Gallo et al., 1996; Yuan et al., 1998). Interestingly, bFGF (but not PDGF) increases the expression of the GluR7, KA1 and KA2 subunits of kainate receptors and expression of the GluR4 subunit of AMPA receptors (Gallo et al., 1994; Chew et al., 1997), while PDGF increased GluR1 subunit expression, and both growth factors together increased even further the expression of GluR1 and augmented the AMPA-evoked current in oligodendrocyte precursors (Chew et al., 1997).

Glutamate-evoked inhibition of proliferation in oligodendrocyte precursors may serve to decrease the numbers of oligodendrocytes produced once oligodendrocytes arrive near axons releasing glutamate (Fig. 1.4). It is perhaps surprising that the growth factors that promote proliferation also increase the glutamate evoked current. However, to understand the possible roles of PDGF and glutamate released from axons it is necessary to know how far these messengers spread - conceivably PDGF signals spread further than glutamate (which is efficiently taken up) and act on oligodendrocytes some distance from active axons, increasing glutamate receptor expression so that proliferation is only turned off when the cells arrive near the axons and can sense the glutamate they are releasing.

Glutamate apparently blocks oligodendrocyte proliferation, both in culture and in brain slices, by raising the intracellular sodium concentration, and thus inhibiting potassium channels which are expressed in oligodendrocyte precursors but not in mature cells (Berger et al., 1991; Borges et al., 1994; Borges & Kettenmann, 1995; Gallo et al., 1996; Knutson et al., 1997; Yuan et al., 1998). The resulting inhibition of outward K^+ flux leads to a depolarization of the cells. Consistent with a role for K^+

channels in regulating proliferation, increased expression of the voltage-gated channel subunits Kv1.3 and Kv1.4 increases oligodendrocyte proliferation (Vautier et al., 2004), and PDGF (which also increases proliferation as described above) increases expression of outward rectifying potassium channels (Chittajallu et al., 2005). Moreover, the glutamate-evoked inhibition of proliferation is mimicked by tetraethylammonium ions, which block potassium channels, and is unaffected by calcium removal (Gallo et al., 1996; Knutson et al., 1997; Yuan et al., 1998), which rules out the possibility that the inhibition of proliferation is produced by oligodendrocyte depolarization leading to activation of voltage-gated Ca^{2+} channels and a Ca^{2+} influx. The dependence of glutamate's actions on Na^{+} entry is demonstrated by the fact that when applying glutamate (or kainate) with N-methyl-D-glucamine replacing extracellular Na^{+}, the glutamate-evoked inhibition of potassium outward current does not occur (Knutson et al., 1997). In addition, if the intracellular Na^{+} concentration is increased with veratridine, a similar inhibition of the outward potassium current and of oligodendrocyte proliferation is produced, even in the presence of PDGF and bFGF (Knutson et al., 1997; Yuan et al., 1998).

Apart from effects of glutamate mediated by K^{+} channel closure, when glutamate activates its receptors it will also increase the intracellular calcium concentration which may activate various enzymes. Activation of non-NMDA receptors on oligodendrocyte precursor cells leads to an increase in intracellular calcium concentration (Pende et al., 1994; Holtzclaw et al., 1995), that induces an increase in gene expression since it increases mRNA levels for nuclear messengers like immediate early genes (Pende et al., 1994). High intracellular calcium levels could also lead to an activation of protein kinase C, which inhibits proliferation and promotes differentiation and myelin basic protein expression (Baron et al., 1998).

1.3.3.3 Effects of other neurotransmitters on oligodendrocyte development

Glutamate is not the only neurotransmitter that could influence the development of oligodendrocytes. Adenosine has also been shown to be released by electrical stimulation of dorsal root ganglion axons and to activate adenosine receptors on

oligodendrocyte precursor cells. This decreases proliferation of the cells, and stimulates migration, differentiation and myelin formation (Stevens et al., 2002; Othman et al., 2003). Moreover, $GABA_A$ receptor activation in oligodendrocyte precursors has also been reported to block outward rectifying potassium channels (Pastor et al., 1995), which could lead to a reduction of proliferation as has been shown for glutamate (see above). The acetylcholine receptor M3 receptor is expressed in oligodendrocyte precursors and when activated it increases proliferation by activating the MAP kinase signalling pathway (Ragheb et al., 2001). Furthermore, histamine, norepinephrine, serotonin, angiotensin II, bradykinin, ATP and substance P have all been shown to increase the intracellular calcium concentration in oligodendrocyte precursors (Bernstein et al., 1996), which could also influence the development of the oligodendrocytes. Finally, activation of dopaminergic D3 receptors, which are expressed in precursor and immature oligodendrocytes (but not in mature cells), promotes differentiation of the precursor cells to become mature cells, but inhibits myelin formation by immature cells (Bongarzone et al., 1998; Fig. 1.4).

1.3.3.4 The role of oligodendrocyte potassium channels in myelination

Part of the inhibitory effect on myelination of blocking action potentials (Demerens et al., 1996) might involve a suppression of K^+ release by action potentials. The effect of an action potential evoked rise of $[K^+]_o$ on oligodendrocytes will depend on their membrane permeability to K^+. As described below, mature oligodendrocytes express inward rectifying potassium channels (Sontheimer et al., 1989; Borges et al., 1994) and blocking these channels with TEA reduces myelination without affecting axonal maturation and function (Shrager & Novakovic, 1995). Moreover, animals with the weakly inward rectifying K^+ channel subunit Kir4.1 knocked out show severe motor defects that can be related to a lack of myelin in these animal (Neusch et al., 2001). When the oligodendrocytes from these knock-out animals were cultured they showed no inward rectifying potassium channels, were highly depolarized, were morphologically immature, and did not produce myelin, unlike those from wild type animals (Neusch et al., 2001). If depolarization (produced by TEA or channel knock-out) suppresses myelination, one might expect K^+ release from axons to also suppress myelination, if the released K^+ depolarizes oligodendrocytes. In this case blocking action potentials

would reduce K^+ release and promote myelination, not inhibit it as is observed (Demerens et al., 1996). However, because of the $[K^+]_o$-dependence of the conductance of inward rectifier channels, a rise of $[K^+]_o$ can actually lead to more outward current and hence a hyperpolarization (Ishihara & Hiraoka, 1994), which would promote myelination. Blocking action potentials would then block K^+ release, cause depolarization and inhibit myelination.

1.4 Ion channel expression in oligodendrocytes

As oligodendrocytes express a large repertoire of potassium channels and neurotransmitter receptor channels (reviewed by Verkhratsky & Steinhauser, 2000), which can influence the cells' development and function as described above, I will review the general function and structure of potassium channels, glutamate and GABA receptors, and then review what is currently known about how the expression of each channel or receptor changes with oligodendrocyte development. This provides background information relevant to my description, in Chapters 3-5, of how I find oligodendrocyte membrane currents change with the development of the cells (Chapter 3), and how the cells respond to glutamate (Chapter 4) and GABA (Chapter 5).

1.4.1 Potassium channels

In general terms, potassium channels maintain a negative membrane potential. In neurons potassium channels help to terminate periods of intense activity and to lower the effectiveness of excitatory inputs to a cell, while in glial cells they help to transport excess extracellular potassium ions away from active neurons (Hille, 2001). There is a great diversity in potassium channels: the subunits making up these channels can be divided into three groups based on structural properties (Coetzee et al., 1999), as follows.

The first group comprises potassium channel subunits that have six transmembrane domains with a conserved so-called P (pore or H5) domain. These include the voltage-gated potassium channels activated by depolarization, like the Kv family which consists of eight subfamilies, as well as members of the KQT and eag

families, and the calcium-activated K^+ channels, which are made of the SK and slo subunit families (Coetzee et al., 1999). Among these groups, the voltage-gated K^+ channels can be further divided according to their electrophysiological properties, into fast delayed rectifiers (I_K), which are mainly made from the Kv class of subunit and make it possible for neurons to fire short and frequent axon potentials, slow delayed rectifier channels mainly made from the KQT and the eag subunit families, and transient outward current or A-type potassium channels (I_A). Four subunits assemble to form a functional channel.

The second group of subunits has two transmembrane domains with one pore domain, which are the components of the inward rectifying channels (Kir). Inward rectification means that these channels pass inward current (below the reversal potential) better than outward current (above the reversal potential) and in addition, as mentioned above, the conductance of the channel depends on the extracellular potassium concentration. This family consists of seven subfamilies, Kir1-Kir7, showing different degrees of inward rectification. Four subunits assemble to form a functional channel.

The third group is made of subunits with four transmembrane domains and two pore domains (P1 and P2): these channels have been called "leak" potassium channels and could be important in setting the resting potential, regulating cellular excitability and allowing uptake of potassium. These channels can be closed by second-messenger systems (reviewed by Coetzee et al., 1999; Hille, 2001). Because these subunits have two pore domains, only 2 subunits are needed to form a channel (Coetzee et al., 1999).

1.4.2 Glutamate receptors

A major part of the work described in this thesis involves the characterization of glutamate receptors present on oligodendrocytes (see Chapter 4). Glutamate receptors fall into two categories: ionotropic receptors (divided into AMPA, kainate and NMDA subtypes) and G protein coupled metabotropic receptors (mGluRs). Ionotropic glutamate receptors activate channels that are selective for cations, and are

approximately equally permeable to Na^+ and K^+. NMDA receptors also conduct Ca^{2+} ions, as do AMPA receptors that do not contain the GluR2 subunit (described below). NMDA receptors have a much lower EC_{50} for glutamate than AMPA receptors, around 1μM for prolonged exposure to glutamate (as occurs in ischaemia), versus tens of μM for AMPA receptors (Patneau & Mayer, 1990). Metabotropic glutamate receptors, like other G protein coupled receptors, activate various downstream enzyme systems including adenylate cyclase and phospholipase C, and will not be dealt with in depth here as they are not a major focus of this thesis.

AMPA receptors are composed of subunits named with the prefix GluR, of which four have been cloned, termed GluR1-GluR4. Similarly, five kainate receptor subunits called GluR5, GluR6, GluR7, KA1 and KA2 have been cloned. NMDA receptors need both glutamate and glycine present to be activated, and are composed of 4 subunits from a family named with the prefix NR. Of these, NR1 provides the glycine binding site, NR2A-D provide glutamate binding sites, and NR3A and B apparently do not bind glutamate. NMDA receptors subunits are often assembled from two glutamate binding subunits (i.e. NR2A-D) and two glycine binding NR1 subunits. Although it is thought that to assemble a functional receptor it is necessary to have two NR1 subunits, the NR2 subunits can either be identical or different. NMDA receptors made of only NR1 and NR3A/B subunits are unaffected by glutamate (because they lack an NR2 subunit to bind glutamate) but are activated by glycine (Chatterton et al., 2002). In addition, so-called δ1 and δ2 subunits have been cloned; these are orphan subunits that are structurally related to glutamate receptors, but do not appear to form functional channels. The channels are thought to be tetramers, with each subunit possessing three transmembrane domains and having an extracellular N-terminus and intracellular C-terminus (reviewed by: Dingledine et al., 1999; Cull-Candy & Leszkiewicz, 2004).

For most NMDA receptors (an exception will be described in Chapter 4) the pore of the NMDA receptor is almost completely blocked by Mg^{2+} at the resting potential of the cell, and the cell must be depolarised in order for the Mg^{2+} block to be removed to enable the channel to conduct ions (reviewed by Dingledine et al., 1999). However, the Mg^{2+}-sensitivity of the NMDA receptor depends on which NR2 or NR3

subunits are present in the receptors. Receptors made by co-expression of NR1 and a single NR2 subunit show a magnesium sensitivity sequence NR2A > NR2B > NR2C > NR2D (reviewed by Cull-Candy & Leszkiewicz, 2004), while NMDA receptors made of only NR1 and NR3A/B subunits have a relatively low magnesium sensitivity (Chatterton et al., 2002). The different subunits do not only differ in magnesium sensitivity but also in their kinetics of operation. For example receptors composed of NR1 and NR2A have a 50 fold faster decay of activation when glutamate is removed than do NR1/NR2D receptors. It has been shown that NMDA receptors with the subunit combinations NR1/NR2A/NR2B, NR1/NR2A/NR2C and NR1/NR2B/NR2C exist in CNS neurons and have properties different from those of receptors containing two identical NR2 subunits (reviewed by Cull-Candy & Leszkiewicz, 2004), but it remains to be seen whether other NR2 subunit combinations occur and, if so, how they would function. Furthermore, incorporating NR3 subunits into an NMDA receptor with 2 NR1 subunits and 1 NR2 subunit can decrease the magnesium sensitivity and calcium permeability of the receptor, and slightly increase the mean open time of the receptor (Sasaki et al., 2002); in addition NR3 expression decreases the surface expression of the NMDA receptors (Cull-Candy & Leszkiewicz, 2004).

1.4.3 GABA receptors

In Chapter 5 of this thesis I characterise how oligodendrocytes respond to the inhibitory amino acid GABA. Two different classes of receptor are activated by GABA. They are the ionotropic receptors, known as $GABA_A$ or $GABA_C$, and the G protein coupled receptors, known as $GABA_B$. I will focus mainly on the ionotropic receptors here, as they are most relevant to the experiments described in this thesis.

$GABA_{A,C}$ receptors are directly coupled to chloride channels. Binding of GABA opens the chloride channel allowing chloride to either to enter cells (if $E_{Cl} < V_{membrane}$), causing hyperpolarization, or to leave the cell (if $E_{Cl} > V_{membrane}$) causing depolarization (reviewed by Mehta & Ticku, 1999). The chloride reversal potential, E_{Cl}, depends on the internal chloride concentration, which is controlled mainly by the cation-chloride

co-transporters expressed by the cell and the chloride-bicarbonate exchanger. The Na^+-K^+-$2Cl^-$ co-transporter, NKCC1, which is expressed in oligodendrocytes, astrocytes and young neurons, transports Cl^- into the cell, making the chloride reversal potential more positive than the resting potential (Mehta & Ticku, 1999; Verkhratsky & Steinhauser, 2000). By contrast, the K^+-Cl^- co-transporter KCC2, which is expressed in mature neurons and in oligodendrocytes (Delpire, 2000; Malek et al., 2003) exports Cl^- from the cell, so the Cl^- reversal potential becomes more negative than the resting potential.

The inhibition/excitation induced by activation of $GABA_{A/C}$ receptors is rapid in onset and short lasting (on a tens of milliseconds timescale), whilst $GABA_B$ receptor inhibition has a delayed onset and is more prolonged (on the order of seconds). In addition to interacting with enzymes, $GABA_B$ receptors interact with K^+ and Ca^{2+} ion channels. For example postsynaptic neuronal $GABA_B$ receptors are coupled to K^+ channels, and their activation leads to the opening of K^+ channels and K^+ efflux, causing hyperpolarization of the postsynaptic cell, while presynaptic $GABA_B$ receptors inhibit presynaptic calcium channels causing a decrease in neurotransmitter release (reviewed by Mehta & Ticku, 1999)

In Chapter 5 I describe immunocytochemistry experiments examining the $GABA_A$ receptor subunits present in oligodendrocytes. $GABA_{A/C}$ receptors are made up of five subunits, with each subunit being composed of four transmembrane (TM) domains, a large extracellular N-terminus and a large intracellular loop between TM domains 3 and 4. There are a number of classes of $GABA_{A/C}$ receptor subunits, with each class containing multiple members: 6 α, 4 β, 3 γ, 1 δ, 1 ε, 1 π and 3 ρ subunits have currently been cloned (reviewed by: Mehta & Ticku, 1999; Sieghart et al., 1999). The ρ subunits only combine with each other and in doing so form $GABA_C$ receptors. $GABA_C$ receptors are predominantly expressed in the retina, although ρ subunits have been found both in the hippocampus and cerebellum (Boue-Grabot et al., 1998). The properties of $GABA_A$ receptors are determined by their subunit composition. Theoretically 151,887 $GABA_A$ receptors can be formed using all available subunit combinations, but studies using recombinant receptors have shown that those with properties similar to the ones expressed *in vivo* are mainly composed of α, β and γ

subunits (Sieghart et al., 1999). Indeed, antibody labelling of $GABA_A$ receptor clusters in neuronal membranes showed that the majority of receptors were composed of α, β and γ subunits (Sieghart et al., 1999), and the ratio of subunits within a receptor is thought to be 2α:2β:1γ (although the γ subunit can be replaced by an ε or π).

1.4.4 Changes in ion channel expression with oligodendrocyte development

1.4.4.1 Potassium and sodium channel expression

Oligodendrocytes express different membrane ion channels at different maturational stages. In culture, oligodendrocyte precursor cells express both TTX-sensitive voltage gated sodium channels, outward rectifying potassium channels and rapidly inactivating A type potassium channels (Sontheimer et al., 1989; Barres et al., 1990c; Berger et al., 1992a; Knutson et al., 1997; Schools et al., 2003). In addition, some of the outward rectifying potassium channels were calcium-activated (Sontheimer et al., 1989; Barres et al., 1990c). Oligodendrocyte precursors *in situ* have been reported to show an almost identical pattern of ion channel expression (Berger et al., 1991; Steinhauser et al., 1992; Chvatal et al., 1995; Žiak et al., 1998; Chittajallu et al., 2005), although I will show in chapter 3 that the situation is more complicated, and that not all "oligodendrocyte precursors" express the same channel types.

The channel expression has been reported to change with maturation: immature cells show less A type current and outward rectifying currents and an absence of voltage gated sodium current (Sontheimer et al., 1989; Berger et al., 1991; Steinhauser et al., 1992; Borges et al., 1994; Chvatal et al., 1995; Knutson et al., 1997; Bernard et al., 2001; Chittajallu et al., 2005). However, there is a larger component of inward rectifying K^+ current in the immature cells (which is also present in some precursor cells but to a lesser extent). Mature oligodendrocytes are also reported to have strong inward rectifying currents at very negative potentials, but also a time- and voltage-independent potassium conductance which was blocked by barium in the external solution (Chvatal et al., 1995; Gipson & Bordey, 2002). Hence, the mature oligodendrocytes show a more time-independent ohmic current-voltage relationship, but they do exhibit some slowly

decaying outward current at positive potentials (Soliven et al., 1988; Sontheimer et al., 1989; Berger et al., 1991; Steinhauser et al., 1992; Berger et al., 1992a; Borges et al., 1994; Chvatal et al., 1995). This slowly decaying current distinguishes oligodendrocytes from astrocytes, which show a very ohmic and time-independent current-voltage relationship (Steinhauser et al., 1992). This potassium channel expression in oligodendrocytes is seen across a large range of species, as the currents seen in cultured cells were from frogs, lambs, rats and mice.

The change in the K^+ channel expression of oligodendrocytes with maturation correlates with a decrease of membrane resistance with maturation (Soliven et al., 1988; Sontheimer et al., 1989), although the increased membrane area of the cells may also account for the lower resistance. Some report a hyperpolarization of the resting membrane potential with age (Knutson et al., 1997), but this may reflect less shunting by the seal between the electrode and the cell in the lower resistance older cells, and other studies show no change in resting membrane potential (Soliven et al., 1988; Sontheimer et al., 1989).

1.4.4.2 Glutamate receptor expression

Oligodendrocytes have been shown to respond to glutamate with the activation of a cation current, and in addition the ionotropic receptor agonists glutamate, AMPA and kainate, but not the mGluR agonist trans-APCD, have been reported to increase the intracellular calcium concentration in oligodendrocytes (Holtzclaw et al., 1995; Belachew et al., 1998a). Reports differ profoundly over how the glutamate response changes with oligodendrocyte maturation. On the one hand, it has been claimed that, in culture, the glutamate response is larger in precursor or immature cells than in mature oligodendrocytes (Borges et al., 1994). Alternatively, the glutamate-evoked current has been suggested not to differ significantly between precursor oligodendrocytes and mature oligodendrocytes (Berger et al., 1992c; Žiak et al., 1998). Finally, it has been reported that, in culture, the glutamate response in mature cells is larger than that in precursors (Patneau et al., 1994). This issue is important because glutamate-mediated damage to oligodendrocytes in periventricular leukomalacia is largely damage inflicted

on precursor or immature cells (see section 1.8 below), so this damage might be explained if glutamate receptor expression is particularly high at that developmental stage. In this thesis I will report experiments examining how the glutamate-evoked current (and the current evoked by glutamate release in simulated ischaemia) depends on the developmental stage of the oligodendrocyte.

Much of this thesis is devoted to defining which receptor types mediate glutamate's effects on oligodendrocytes, because knowing this is essential if damaging actions of glutamate on oligodendrocytes in neurological conditions are to be prevented. The glutamate-evoked currents in oligodendrocytes have previously been reported to be generated entirely by AMPA or kainate receptors, both in culture (Barres et al., 1990c; Patneau et al., 1994; Borges et al., 1994; Borges & Kettenmann, 1995; Gallo et al., 1996; Yuan et al., 1998) and in brain slices (Berger et al., 1992c). The metabotropic glutamate receptor agonist ACPD evoked neither a current nor a rise in intracellular calcium level (Berger et al., 1992c; Borges et al., 1994; Pende et al., 1994). Most importantly, NMDA is reported to generate no current in oligodendrocytes, either in culture (Barres et al., 1990c; Berger et al., 1992c; Patneau et al., 1994; Pende et al., 1994) or in brain slices (Barres et al., 1990b). However, there are some indications that NMDA receptors might be present. Wang et al. (1996) showed that O-2A cells, in culture, exhibit NMDA-evoked currents that are magnesium-dependent and are reduced with an NMDA antagonist. This finding is both supported and contradicted at the same time by a demonstration that spinal cord grey matter oligodendrocytes show NMDA-evoked currents, but only in mature oligodendrocytes and not in the precursor oligodendrocytes which one would expect to behave like the O-2A cells studied in culture (Žiak et al., 1998): essentially no NMDA responses were detected in white matter oligodendrocytes in that study.

Oligodendrocytes have been reported to express mRNA for the AMPA receptor subunits GluR2, 3 & 4, but not for GluR1 (Jensen & Chiu, 1993; Patneau et al., 1994; Yoshioka et al., 1996; Matute et al., 1997; Garcia-Barcina & Matute, 1998; Itoh et al., 2002), and for the kainate receptor subunits GluR6 & 7 and KA-1 & 2, but not for GluR5 (Jensen & Chiu, 1993; Patneau et al., 1994; Yoshioka et al., 1996; Garcia-

Barcina & Matute, 1996; Matute et al., 1997). Some of these mRNA studies found a slight change in subunit expression with maturation. Furthermore, when detecting AMPA/kainate subunits at the protein level with immunohistochemistry, no GluR2 subunit was found in the oligodendrocytes, but GluR3 and GluR4 were expressed (Li & Stys, 2000), and immunoprecipitation experiments demonstrated that GluR2 does not assemble with the other subunits (Puchalski et al., 1994). These data suggest that the AMPA receptors present may lack GluR2 and therefore be Ca^{2+}-permeable. There is a controversy as to whether message for NMDA receptor subunits is expressed in oligodendrocytes: Yoshioka et al., (1996) show that an oligodendrocytes precursor cell line expressed mRNA for NR1 and NR2D, but Matute and colleagues (1997) did not detect any message for NMDA receptor subunits in the optic nerve.

In summary, although there is good evidence for the presence of AMPA receptors in oligodendrocytes, the weight of evidence suggests an absence of NMDA receptors. This would imply that, unlike neurons which often die in neurological disorders as a result of an excessive Ca^{2+} influx through NMDA receptor channels, oligodendrocytes lack this death mechanism and may be damaged predominantly by a Ca^{2+} influx through GluR2-lacking AMPA receptors. The results I present in this thesis will challenge this idea.

1.4.4.3 GABA and other neurotransmitter receptor expression

GABA evokes a bicuculline-blocked current response in oligodendrocytes throughout their development (Pastor et al., 1995; Matute et al., 1997; Williamson et al., 1998). In addition, GABA has been shown to raise intracellular calcium concentration at all stages of the oligodendrocyte lineage (Kirchhoff & Kettenmann, 1992; Bernstein et al., 1996; Belachew et al., 1998a; Schmidt et al., 2000), suggesting that in unclamped cells the chloride reversal potential is above the resting potential so that GABA generates a depolarization. In fact, in perforated patch experiments (which avoid alteration of E_{Cl} by the patch pipette) GABA application causes depolarization in precursors (Lin & Bergles, 2004). Examining message for $GABA_A$ receptor subunits in precursor oligodendrocytes showed that they express mRNA for α2, α3, α4, α5, γ2, γ3

and to a lesser extent γ1, subunits, while δ subunits were not detected and β subunits were not tested for (Williamson et al., 1998).

Glycine also evokes a strychnine-sensitive Cl^- current in precursor oligodendrocytes; this response seems to be lost in immature cells but reappears in mature oligodendrocytes (Pastor et al., 1998). Glycine also increases the intracellular calcium level, as do histamine, norepinephrine, serotonin, angiotensin II, bradykinin, substance P and ATP, in oligodendrocyte precursor cells (Bernstein et al., 1996; Belachew et al., 1998a). In addition, adenosine increases intracellular calcium concentration, oligodendrocytes express mRNA for the A1, A2a, A2b and A3 subunits of adenosine receptors (Stevens et al., 2002), and the A1 receptor subunit has been detected at the protein level (Othman et al., 2003). Moreover, dopamine increases intracellular calcium concentration and oligodendrocytes at all maturational stages express mRNA for D3 dopamine receptors (Bongarzone et al., 1998). Oligodendrocytes also respond to acetylcholine and express mRNA for the muscarinic receptor subunits M3 and M4, and to a lower extent the M1, M2 and M5 subunits (Ragheb et al., 2001).

1.5 The heterogeneity of the $NG2^+$ cells

In this thesis I will provide evidence that $NG2^+$ cells in the white matter may fall into different classes. Since these cells have, until recently, all been thought to be oligodendrocyte precursors, here I will review what is known about this cell type. In the following I will deal only with the $NG2^+$ cells that are present in the parenchyma of the brain, ignoring the $NG2^+$ cells present on the vasculature (Hughes & Chan-Ling, 2004).

As described above in sections 1.3.1 and 1.3.2, the $NG2^+$ cells are conventionally thought to be oligodendrocyte precursor cells as they co-express PGDFαR (Nishiyama et al., 1996a; Nishiyama et al., 1996b), a marker for oligodendrocyte precursor cells (Pringle et al., 1992) and have similar membrane currents to oligodendrocyte precursors (reviewed by Stallcup, 2002). Around birth, $NG2^+$ cells are evenly distributed through the brain and spinal cord, and they proliferate and migrate to occupy both the grey and white matter (Dawson et al., 2000; Dawson et al., 2003). Eventually many of them

either mature into myelinating oligodendrocytes or undergo apoptosis (Barres & Raff, 1994; Trapp et al., 1997; Dawson et al., 2000). Although the number of these so-called oligodendrocyte progenitors declines as they mature, cells expressing NG2 are found in adult animals and are 5-9% of the total cell population in the adult brain. Such cells are found both in white and grey matter (Butt et al., 1999; Dawson et al., 2000; Mallon et al., 2002; Dawson et al., 2003), but with a 50% higher density in the white matter (Dawson et al., 2000; Dawson et al., 2003). Interestingly, the $NG2^+$ cells form the major population of dividing cells in the adult brain: up to 75% of BrdU labeled cells in the adult animal are $NG2^+$ (Dawson et al., 2000; Dawson et al., 2003).

The $NG2^+$ cells remaining in the adult are often defined to be adult oligodendrocyte precursors, which are postulated to be reserve cells that can replace damaged myelinating oligodendrocytes: indeed, in demyelinating diseases $NG2^+$ cells can proliferate and differentiate slowly into myelinating oligodendrocytes, which are thought to remyelinate axons (Cenci Di Bello et al., 1999; reviewed by Reynolds et al., 2002). Similarly, $NG2^+$ cells can proliferate in response to various CNS injuries like stab wounds, viral infections, kainate-induced lesion and stroke injuries (reviewed by Levine et al., 2001). The $NG2^+$ cells can also (like astrocytes) produce a protective glial scar as a response to injury and, in addition, the NG2 protein has been shown to be highly inhibitory for axonal growth and can prevent axons from growing over the glial scar (Chen et al., 2002).

However, despite the general acceptance of the notion that adult $NG2^+$ cells are oligodendrocyte precursors, it is notable that some $NG2^+$ cells are found in adult grey matter areas where there is little or no myelination (Levine & Card, 1987; Ong & Levine, 1999; Butt et al., 2005), raising the question of what their functional role is. Furthermore, some $NG2^+$ cells found in chronic MS lesions do not differentiate to myelinate demyelinated axons (Reynolds et al., 2002). The fact that it has yet to be shown directly that $NG2^+$ cells can remyelinate axons, the presence of $NG2^+$ cells in chronic MS lesions (reviewed by Levine et al., 2001; Butt et al., 2004), and the occurrence of glial scar formation in response to injury (which might be seen as a more astrocyte "behavior"), all raise the question of whether all of the $NG2^+$ cells are

oligodendrocyte precursors which transform into mature oligodendrocytes in pathological conditions.

In recent years, as more work has been done to characterize $NG2^+$ cells, more evidence has been provided that questions the homogeneous nature of the $NG2^+$ cells, and it seems that these cells are more complex and intriguing than previously thought. There seem to be some $NG2^+$ cells that become oligodendrocytes and others that do not. Some evidence indicating this heterogeneity is as follows. Firstly, oligodendrocytes need axons for survival (Barres et al., 1993) but, when the rat optic nerve is enucleated (to remove the retinal ganglion cell axons), although no oligodendrocytes develop the nerve still has $NG2^+$ cells (Greenwood & Butt, 2003). Moreover, in an Olig1/2 knockout mouse no oligodendrocytes develop, but some $NG2^+$ cells are present (Liu & Rao, 2004). Secondly, when EGFP is expressed under the control of the promoter for PLP (which is a myelin protein and only expressed in oligodendrocytes), there seem to be two populations of $NG2^+$ cells, one that expresses EGFP and one that does not (Mallon et al., 2002). This result indicates that there is a subset of $NG2^+$ cells that are not in the oligodendrocyte lineage. Interestingly, Terada and colleagues (2002) claim that precursor oligodendrocytes committed to the oligodendrocyte lineage express the tetraspanin protein CD9, and those that do not express it remain as adult $NG2^+$ cells, since (in $NG2^+$ cells) CD9 expression peaks in P10 animals (in the mid cortical region) at 41% of cells, but becomes less than 1% of cells by P90 (Berry et al., 2002; Terada et al., 2002). Moreover, in young animals almost all $NG2^+$ cells co-express PDGFαR, but in the adult only half of the $NG2^+$ cells do (Diers-Fenger et al., 2001). To further complicate the identity of the $NG2^+$ cells, it has been suggested that a subset of these cells could be astrocytic, as some cells expressing EGFP controlled by the GFAP promoter (an astrocyte marker) also express NG2 (Matthias et al., 2003) as well as GFAP mRNA (Zhou et al., 2000a). However, Schools et al. (2003) have later shown that although $NG2^+$ cells express the mRNA for GFAP they do not express the protein (i.e. they are not labeled by antibody to GFAP). To sum up: little is known about the identity of the $NG2^+$ cells other than that some of them are oligodendrocyte precursors, and perhaps a subset of them has another role.

Further supporting the idea of heterogeneity of the $NG2^+$ cells are the findings that some of these cells can develop into GABAergic neurons (Belachew et al., 2003; Aguirre et al., 2004; Dayer et al., 2005) and can share a common precursor with hippocampal (He et al., 2001) or neocortical (Dayer et al., 2005) interneurons. Differentiation into interneurons is seen when EGFP/$NG2^+$ cells are transplanted into the hippocampus (Belachew et al., 2003) and into the sub-ventricular zone (Aguirre et al., 2004) or by carrying out a cell fate analysis (Dayer et al., 2005). At least some $NG2^+$ cells also express some neuronal "behavior", as grey matter $NG2^+$ cells receive both glutamatergic and GABAergic synaptic inputs from neurons (Bergles et al., 2000; Lin & Bergles, 2004; Lin et al., 2005; Jabs et al., 2005). In addition, there is a significant electrophysiological difference between grey and white matter $NG2^+$ cells: white matter $NG2^+$ cells have a more positive membrane potential and lower cell capacitance, but a higher membrane resistance, and express less voltage-gated potassium and sodium channels (Chittajallu et al., 2004). As a result, some grey matter NG2 cells can generate depolarization-induced spikes that are like immature action potentials (Chittajallu et al., 2004).

$NG2^+$ cells in the grey matter wrap around synapses (Ong & Levine, 1999), presumably to sense neuronal activity. However, in the white matter, $NG2^+$ cells also contact neurons as they wrap around the nodes of Ranvier (Butt et al., 1999; Butt et al., 2005). From these results showing contact of NG2 cells with neurons, the name "synantocyte" has been suggested for some of the adult $NG2^+$ cells, these being the subset of $NG2^+$ cells that will not generate oligodendrocytes and are likely to be a newly defined set of glia (Butt et al., 2002; Butt et al., 2005). To further support this notion, recently it was shown that $NG2^+$ cells are needed at the node of Ranvier to prevent axons from sprouting at this point (Huang et al., 2005). This result may show one function of the non-oligodendrocyte $NG2^+$ cells.

1.6 Ion channel expression in astrocytes

Astrocytes are highly abundant glial cells, identified by their expression of the intermediate filament glial fibrillary acidic protein (GFAP), which have a variety of important functions in the CNS (reviewed by; Porter & McCarthy, 1997; Nedergaard et al., 2003; Ransom et al., 2003). They send processes to the blood vessels, where they induce capillary endothelial cells to make tight junctions and form the blood brain barrier, and they control arteriolar diameter to regulate blood flow (Peppiatt & Attwell, 2004). In the grey matter they control the extracellular potassium concentration to prevent hyperexcitability, and they surround neuronal synapses, where they respond to, and take up (Fig. 1.5), released neurotransmitter (Nedergaard et al., 2003; Ransom et al., 2003). They also control the supply of neurotransmitter to neurons, e.g. via the glutamate-glutamine cycle in which glutamate is taken up and converted to glutamine, before being passed to neurons for conversion back into transmitter glutamate (Marcaggi & Attwell, 2004). In the white matter they wrap around the nodes of Ranvier (Butt et al., 1994). In addition, astrocytes may "feed" neurons with energy substrates (glucose may be converted to lactate in astrocytes, which is passed to neurons for conversion to pyruvate and use in oxidative phosphorylation (Sibson et al., 2001; Chih et al., 2001b), and they have been implicated in water homeostasis and regulation of extracellular pH (Ransom et al., 2003; Simard & Nedergaard, 2004). Moreover they have been found to modulate neuronal synaptic transmission by releasing glutamate exocytotically (Bezzi et al., 2004), and to regulate neurogenesis in the adult brain, as well as giving birth to neurons in the developing brain (Nedergaard et al., 2003). Astrocytes are highly coupled via gap junctions, and can communicate with each other through Ca^{2+} signals, where waves of $[Ca^{2+}]$ elevation pass through the gap junctions (Nedergaard et al., 2003).

Mature astrocytes, and the majority of immature astrocytes, in situ, show a passive membrane current-voltage relationship generated by a voltage- and time-independent potassium conductance (Müller et al., 1994; Chvatal et al., 1995; Cotrina et al., 1998; Zhou et al., 2006): they do not express voltage-activated potassium or sodium channels. However, in the young animal, a subset of astrocytes expresses outward

rectifying potassium channels as well as K_A channels, and a few show expression of voltage-activated sodium channels, which however completely disappear as the cells mature (Chvatal et al., 1995; Zhou et al., 2006). This subset of immature astrocytes has been given the name complex cells, and they are labelled by antibodies not only to GFAP but also to NG2, but in the adult animal GFAP is never found with NG2 (Zhou et al., 2000a; Zhou et al., 2006). It is uncertain whether these cells should really be called astrocytes: perhaps they are only a transient stage of the $NG2^+$ cells when $NG2^+$ cells also produce GFAP protein. I will use the word astrocyte when referring to astrocytes with a "passive" I-V relation, as I would characterize the complex cells as being $NG2^+$ glia.

Astrocytes express both T and L type voltage-gated calcium channels (Barres et al., 1990a; Verkhratsky & Steinhauser, 2000) and chloride channels (Verkhratsky & Steinhauser, 2000). Moreover, they express quite a large repertoire of neurotransmitter receptors. Astrocytes express AMPA/kainate receptors both in the grey and white matter (Žiak et al., 1998; reviewed by Verkhratsky & Steinhauser, 2000), and metabotropic glutamate receptors (mGluR) (Kimelberg, 1995; Porter & McCarthy, 1997) and NMDA receptors in the grey matter (Müller et al., 1993; Žiak et al., 1998; Schipke et al., 2001). As in oligodendrocytes, the AMPA receptors in astrocytes lack the GluR2 subunit, so they are calcium permeable. However, even if the astrocyte AMPA receptors allow calcium through, and the astrocytes express NMDA receptors, these receptors do not make the astrocytes vulnerable to glutamate excitotoxicity as occurs in neurons and oligodendrocytes. This may be because the density of receptors is less than in neurons and oligodendrocytes. Astrocytes also express $GABA_A$ and $GABA_B$ receptors, both in grey and white matter, and (as in oligodendrocytes) activation of $GABA_A$ receptors causes depolarization produced by Cl^- efflux through $GABA_A$ receptor channels, because astrocytes express the $Na^+/K^+/2Cl^-$ co-transporter and the $Cl^-/HCO3^-$ exchanger that maintain a high intracellular concentration of chloride (reviewed by: Kimelberg, 1995; Porter & McCarthy, 1997; Verkhratsky & Steinhauser, 2000). Similarly they also express glycine receptors in the grey matter, which also generates a depolarization upon activation (Pastor et al., 1995; Verkhratsky & Steinhauser, 2000).

In addition, astrocytes also express, both in vitro and in situ, purinergic receptors (P1, P2, P2X, P2Y) (Kimelberg, 1995; Verkhratsky & Steinhauser, 2000), adrenaline, serotonin (5-HT_{1A}) and histamine (H_2 and H_3) receptors, and acetylcholine receptors (M_{1-4}) (reviewed by Porter & McCarthy, 1997). Moreover, astrocytes in vitro express also substance P, angiotensin II, somatostatin, bradykinin, neuropeptide Y and opioid (kappa and delta) receptors (Kimelberg, 1995; Porter & McCarthy, 1997). The function of all these neurotransmitter receptors on astrocytes is still uncertain.

1.7 Grey matter ischaemia

Part of this thesis addresses the effects of the rise of neurotransmitter concentration which occurs in brain ischaemia. As background to these experiments I will now review briefly what is known about brain ischaemia, starting with grey matter ischaemia as it has been the focus of more studies. White matter ischaemia is reviewed in the following section.

1.7.1 Overview of the effects of ischaemia on the brain

Ischaemia refers to a situation in which the blood supply (and hence the energy supply) to an organ are interrupted. Brain ischaemia, more commonly known as stroke, is one of the leading causes of death and disability in Europe and North America. Brain ischaemia can be divided into two categories of disorder. Firstly, global ischaemia occurs when the blood supply to the whole brain is cut-off, as occurs during cardiac arrest when the heart ceases to pump blood. Secondly, focal ischaemia occurs when the blood supply to a localised brain region is interrupted, as a result of a blood clot or vasospasm in the vessel supplying that region, or rupturing of the blood vessel due to high blood pressure.

Removing the blood supply to the brain deprives it of oxygen and glucose, the substrates for energy production. If the energy deprivation is severe enough then it leads to infarction, where all of the cells in the affected area die. With less severe energy

deprivation there is variability amongst cell types and regions of the brain as to how vulnerable they are to energy deprivation: neurons are the most vulnerable cell type, followed by oligodendrocytes, then astrocytes and finally endothelial cells (reviewed by Pulsinelli, 1985).

The severity of energy deprivation varies depending on the proximity of the cells to the occluded/burst blood vessel. In focal ischaemia the core of the ischaemic region is composed of cells surrounding the blood vessel, and is where the most severe energy deprivation and death occur. The penumbra of the ischaemic region is the area surrounding the core, where energy deprivation and subsequent cell death are not as severe, due to some oxygen and glucose reaching these cells from other nearby blood vessels (Lipton, 1999).

1.7.2 Ion gradient rundown caused by ischaemia

Ischaemia will block the production of ATP in the affected region, leading to inhibition of the Na^+-K^+-ATPase (and other ATP-dependent reactions). As a result a slow run down of transmembrane ion gradients occurs (Fig. 1.6), with $[K^+]_o$ rising slowly at first (Hansen, 1985). This induces an initial depolarisation, which can be followed by a longer lasting hyperpolarization produced by activation of Ca^{2+}-gated and ATP-gated K^+ channels (Jiang & Haddad, 1994; Nowicky & Duchen, 1998). After a few minutes, action potential evoked excitatory and inhibitory synaptic transmission are greatly reduced (Fujiwara et al., 1987; Leblond & Krnjevic, 1989), due to the actions of adenosine released from cells, as intracellular ATP (adenosine triphosphate) is broken down (Fowler, 1990; Katchman & Hershkowitz, 1993a). Adenosine acts on presynaptic A1 receptors and reduces action potential evoked glutamate release by inhibiting Ca^{2+} channel opening (Centonze et al., 2001). At this stage miniature excitatory and inhibitory postsynaptic currents are still present, and in fact increase in frequency (Katchman & Hershkowitz, 1993b; Fleidervish et al., 2001; Allen & Attwell, 2004) Finally, after a few minutes ischaemia, there is a sudden regenerative rundown of ion gradients, with $[K^+]_o$ rising by 50-60mM and $[Na^+]_o$ falling by the same amount

(Hansen, 1985). This depolarises neurons to around -20mV (Fig. 1.6); an event termed the anoxic depolarisation, which causes a loss of neuronal excitability (reviewed by Tanaka et al., 1997). The rise of $[K^+]_o$ and associated depolarisation also lead to Cl^- entry, and then water entry, which makes cells swell. On restoration of blood flow, as can occur if an occluding clot is digested, neurons recover to their pre-ischaemic resting membrane potential within half an hour of reperfusion (Xu & Pulsinelli, 1994; Xu & Pulsinelli, 1996).

1.7.3 Glutamate release in grey matter ischaemia

The majority of studies into neuronal dysfunction and death caused by ischaemia show the excitatory neurotransmitter glutamate to be the initial damage causing agent. This phenomenon is known as glutamate excitotoxicity and was first discovered in the retina (Olney, 1978). Early work by Choi and colleagues demonstrated that exposing cultured neurons to glutamate for 5 minutes caused them to die, with the amount of death increasing as the glutamate concentration was increased, and 100μM glutamate causing 60% of neurons to die (Choi et al., 1987; Fig. 1.7A). But does the concentration of extracellular glutamate reach 100μM during ischaemia? A number of *in vivo* studies recording the increase of extracellular neurotransmitter concentrations that occurs during ischaemia have demonstrated that $[glutamate]_o$ does increase to these levels. Figure 1.7B is an extract from a paper by (Satoh et al., 1999), where hippocampal extracellular glutamate levels were monitored by microdialysis during global anoxia (oxygen deprivation) in guinea pig. A few minutes after the onset of anoxia, extracellular glutamate levels rose sharply to 200μM. This sudden rise in glutamate concentration corresponds to the time of the anoxic depolarisation, as shown in Figure 1.6. The third piece of evidence linking glutamate to ischaemia-induced neuronal death comes from studies where the actions of glutamate have been blocked during ischaemia. Figure 1.7C is taken from a paper by O'Neill et al (2000), where the majority of ischaemia-induced cell death in the hippocampus was shown to be prevented in the presence of glutamate receptor antagonists.

1.7.4 Mechanisms of glutamate-evoked neuronal death

Experiments *in vitro* have shown that glutamate can cause neuronal death in two ways (reviewed by Zipfel et al., 2000). When glutamate activates its ionotropic receptors, the resulting cation influx and consequent depolarisation lead to a Cl^- influx into neurons, and thus (for osmotic reasons) a water influx. The resulting cell swelling can lead to a rapid glutamate- and Cl^--dependent necrotic death (Koh et al., 1990). More commonly, however, glutamate kills neurons more slowly by activating NMDA (*N*-methyl-D-aspartate) receptors, which allow calcium into the cell, increasing the intracellular calcium concentration to neurotoxic levels (Choi, 1988, Arundine et al., 2001). The $[Ca^{2+}]_i$ rise (Fig. 1.6) causes a lethal activation of Ca^{2+}-dependent proteases, lipases and endonucleases which digest the cells proteins, membranes and genetic material. In addition it can overload mitochondria with Ca^{2+}, depolarising them, reducing their energy production, and releasing cytochrome C, which activates the chain of proteolytic caspase enzymes to kill the cell by apoptosis (reviewed by Lipton, 1999). In animal models, block of NMDA receptors can be neuroprotective even after the initial ischaemic insult, indicating that excessive activation of these receptors is still occurring at a time when a therapeutic intervention could be made (Gill et al., 1988).

Thus, glutamate is released in large amounts during ischaemia and this glutamate is capable of inducing neuronal death. But how is the glutamate being released? Why do the glutamate transporters in Figure 1.5 not keep the glutamate concentration at a low level? Electrophysiological studies have shown that before the anoxic depolarisation a low level of glutamate release occurs from synaptic vesicles (Katchman & Hershkowitz, 1993b; Fleidervish et al., 2001), whilst after the anoxic depolarisation the change of ion gradients shown in Figure 1.6 leads to a large release of glutamate via reversal of glutamate transporters (Rossi et al., 2000), because the direction of operation of the transporters is determined by the prevailing transmembrane ion concentration and voltage gradients. Indeed, blocking release by glutamate transporters, or blocking glutamate receptors, both prevent the anoxic depolarisation

from occurring (Rossi et al., 2000), suggesting that the anoxic depolarisation is mainly caused by the accumulation of glutamate (rather than K^+) in the extracellular space.

1.7.5 Brain energy stores delaying glutamate release in ischaemia

Whether an anoxic depolarization (AD) occurs during transient ischaemia, and its time of occurrence, will be determined by how much stored energy the brain has to maintain ion gradients in the face of a temporary interruption of its energy supply. Brain ATP is largely derived from glucose: glycolysis is followed by oxidative phosphorylation in mitochondria (see chapter 8, Fig. 8.1). It has been suggested (but disputed: Chih et al., 2001b) that neuronal activity-evoked glycolysis (Pellerin et al., 1998; Magistretti & Pellerin, 1999) or almost all glycolysis (Sibson et al., 1998) is in glia, which export lactate to neurons as a substrate for their mitochondria. Since neurons consume most brain energy (Attwell & Laughlin, 2001), this lactate export might explain how the brain's main energy store (assumed to be glial glycogen: (Gruetter, 2003b; Brown, 2004) could sustain the activity of the neurons during energy deprivation, but no information is available on which CNS energy stores delay the occurrence of the AD. In Chapter 8 I examine which energy stores delay the rundown of ion gradients that leads to massive glutamate release in the grey matter of the brain.

1.8 White matter ischaemia

1.8.1 Glutamate also damages white matter cells in pathological conditions

The death of neurons in pathological conditions, which is mainly caused by a rise of extracellular glutamate concentration activating NMDA receptors, does not only occur in anoxia or ischaemia, but also in more chronic conditions such as Huntington's or Alzheimer's disease (Hynd et al., 2004). Glutamate can also damage white matter oligodendrocytes, in both acute and chronic diseases, including brain injury after pre- or perinatal infection or asphyxia or premature birth (periventricular leukomalacia, leading to cerebral palsy and cognitive deficits (Volpe, 2001)), spinal cord injury (Stys, 2004),

multiple sclerosis (Matute et al., 2001) and stroke (Dewar et al., 2003). In perinatal asphyxia and spinal cord injury glutamate is released in the white matter by the reversal of glutamate transporters in axons and oligodendrocytes as a result of ATP depletion (Li et al., 1999; Fern & Möller, 2000; Fig. 1.8A, B), i.e. a mechanism similar to that occurring in grey matter ischaemia (Rossi et al., 2000). In multiple sclerosis, the extracellular glutamate concentration may rise as a result of release by cystine-glutamate exchange in microglia/macrophages (Piani & Fontana, 1994), or because of increased glutamate production by glutaminase and reduced degradation by glutamate dehydrogenase and glutamine synthetase (Werner et al., 2001).

1.8.2 Glutamate-mediated damage to white matter is thought not to involve NMDA receptors

A major difference between the excitotoxic actions of glutamate on oligodendrocytes and on neurons is that, as noted above, oligodendrocytes are reported to lack NMDA receptors (Berger et al., 1992a; Patneau et al., 1994), and are thought to be damaged by glutamate acting either on calcium-permeable AMPA/kainate receptors (Volpe, 2001; Matute et al., 2001; Fig. 1.8A; Dewar et al., 2003; Stys, 2004) or by reversing cystine-glutamate exchange and depriving the cells of antioxidant protection (Oka et al., 1993). Consistent with a role for AMPA receptors in glutamate-mediated oligodendrocyte damage, blocking these receptors attenuates white matter injury in animal models of hypoxia/ischaemia (McDonald et al., 1998; Follett et al., 2000; Fern & Möller, 2000; Tekkök & Goldberg, 2001; Deng et al., 2003), spinal cord injury (Agrawal & Fehlings, 1997; Wrathall et al., 1997) and multiple sclerosis (Pitt et al., 2000; Smith et al., 2000). In addition, white matter damage in periventricular leukomalacia occurs at a time in development when a large proportion of oligodendrocytes are precursor and immature cells (Back et al., 2002) which, in culture, have been reported to show a higher expression than mature cells of AMPA/kainate receptors and downstream [Ca^{2+}] signalling (Itoh et al., 2002; Deng et al., 2003;

Rosenberg et al., 2003), although there are reports disputing this as described above in Section 1.4.4.2.

Despite the consensus view that glutamate damages white matter oligodendrocytes and their precursors by acting on AMPA/kainate receptors, there is some evidence that NMDA receptors may also play a role. NMDA receptor blockers slow the loss of white matter action potentials (Tekkök & Goldberg, 2001) and reduce white matter damage in ischaemia (Schäbitz et al., 2000) and in an animal model of multiple sclerosis (Wallström et al., 1996). In this thesis I have, therefore, re-examined the possible involvement of NMDA receptors in the pathology of oligodendrocytes (see Chapter 6).

1.9 The anatomy of the brain areas studied

In this section I review the basic properties, relevant to my thesis work, of the brain areas that were studied.

1.9.1 The structure of the cerebellum

In chapters 3-7 I report experiments carried out on white matter oligodendrocytes and astrocytes in the cerebellar white matter. The cerebellum is an additional "small brain", located at the rear of the brain. It is divided into a central vermis and two hemispheres each side of the vermis, but I recorded from cells located in the white matter of the vermis. The cerebellar vermis is composed of a number of folia, with each folium having the same general structure. Within each folium cells are arranged in three neuronal layers and a layer of white matter. First, the middle neuronal layer is the Purkinje cell layer: it is in the middle of the three neuronal layers and contains the somata of Purkinje cells and Bergman glial cells. Secondly, outside of the Purkinje cell layer (towards the pia) is the molecular layer, which contains Purkinje cell dendrites, inhibitory interneurons (basket and stellate cells), the axons of granule cells, $NG2^+$ cells, and the processes of the Bergman glia cells (in developing animals, till about P18, there is also a layer of developing granule cells just below the surface of the

folium). Thirdly, below the Purkinje cells is the granular layer, which is composed of excitatory granule cells and inhibitory Golgi cells, as well as $NG2^+$ cells and astrocytes. Finally, beneath the granular layer lies the white matter containing efferent and afferent axons, oligodendrocytes, astrocytes and microglia. In addition, there are also the deep cerebellar nuclei which lie deep in the central white matter (Fig. 1.9).

The cerebellum receives sensory input, and inputs from the cortex and other parts of the motor system, to coordinate ongoing movements and participate in motor planning. There are two main systems of afferent fibres to the cerebellum: (1) inputs from the inferior olive which are excitatory (using glutamate as a transmitter) and synapse onto cells in the deep cerebellar nuclei and Purkinje cells via climbing fibres; (2) from various spinal and cranial nerves the mossy fibres send synapses both to the deep cerebellar nuclei and to granule cells. The efferents are only from the Purkinje cells: they are all inhibitory (using GABA as a transmitter) and synapse onto cells in the deep cerebellar nuclei, which then send the main output of the cerebellum as excitatory inputs to various parts of the motor system (reviewed by Blumenfeld, 2002). The cerebellar oligodendrocytes that I record from in the experiments of this thesis may therefore myelinate excitatory axons (mossy fibres), inhibitory axons (Purkinje cell axons) or perhaps both (Fig. 1.9).

Cerebellar oligodendrocytes develop in the fourth ventricle and migrate via the superior medullary velum to the cerebellum (Reynolds & Wilkin, 1988). The oligodendrocytes develop temporally from the base of the cerebellum to the top of the folia (Reynolds & Wilkin, 1988). However, Levine and Card show that $NG2^+$ cells appear scattered around the cerebellum around E16, reaching their peak density around p7 (the day that I tended to use for studying precursor cells in the cerebellum) and then develop equally throughout the cerebellum (Levine & Card, 1987; Levine et al., 1993). The cerebellum myelinates somewhat later than other brain structures, which makes it optimal for studying different developmental stages of oligodendrocytes in the same animal (Hamano et al., 1998).

1.9.2 The structure of the corpus callosum

In chapters 3 and 4 I report experiments on white matter oligodendrocytes studied in the corpus callosum. The corpus callosum is a thick band of fibres located between the cerebral hemispheres, connecting the left and right hemispheres (Fig. 1.10). The main components of the corpus callosum are oligodendrocytes and axons, then astrocytes, microglia and $NG2^+$ cells (Peters et al., 1991). The main neuronal fibres crossing the corpus callosum are axons of the pyramidal cells located in cortical layers II/III and V, all of which are excitatory (Kumar & Huguenard, 2001). Although most of the fibres in the corpus callosum are excitatory, there are a few inhibitory fibres as well, but in young animals the contribution of inhibitory fibres is higher than in the adult (Gonchar et al., 1995; Kimura & Baughman, 1997).

The corpus callosum was studied in addition to the cerebellum for two reasons. First, I wanted to be sure that the results obtained in cerebellum were likely to hold for other brain regions. Secondly, the corpus callosum is an area which is thinned in severe periventricular leukomalacia (Fedrizzi et al., 1996; Coley & Hogan, 1997), so I wanted to be sure that potentially damaging neurotransmitter receptors demonstrated to exist in cerebellar oligodendrocytes are also present in this more clinically relevant area. The corpus callosum is fully myelinated a week before the cerebellum (Hamano et al., 1998), which makes it good for studying more mature oligodendrocytes than in the cerebellum.

1.9.3 The structure of the hippocampus

In chapter 8, I recorded from pyramidal cells in layer CA1 of the hippocampus, because these cells have previously been most intensively studied in experiments mimicking ischaemia. The pyramidal cells are well studied in this regard because they are particularly vulnerable to ischaemic injury as a result of the large number of NMDA receptors that they express.

The hippocampus is involved in the formation of memories; studies on patients who have had their hippocampi removed show them to be incapable of forming new

long term memories (anterograde amnesia). The hippocampus has a curved structure and lies beneath the cerebral cortex, and its structure and connections are shown in Figure 1.11. The main excitatory cell types in the hippocampus are pyramidal neurons, which make up the pyramidal cell layer, and granule cells, which form the bulk of the dentate gyrus. The pyramidal cell layer is 3-6 cells deep and extends around the outside of the hippocampus in a C-shape. The cells closest to the dentate gyrus have large cell bodies and are called CA3 (Cornu Ammonis region 3) cells, and the cells more distal to the dentate gyrus with smaller cell bodies are called CA1 cells. Pyramidal neurons have extensively branched dendritic trees, with a small basal dendrite (which projects into the stratum oriens) and a larger apical dendrite (which projects through the stratum radiatum into the stratum lacunosum-moleculare). There are three main classes of inhibitory interneurons which have their cell bodies within or near the pyramidal cell layer and project to CA1 cells. These are axo-axonic cells, which synapse onto the initial segment of pyramidal neurons, basket cells, which synapse onto the pyramidal neuron somata, and bistratified cells, which synapse onto the apical and basal dendrites of pyramidal neurons. CA1 pyramidal neurons receive excitatory inputs from CA3 pyramidal neurons via the Schaffer collaterals in the stratum radiatum and stratum oriens, and from projection neurons from cortical and sub-cortical regions(reviewed by Johnston & Amaral, 2004).

1.10 Summary of the aims of this thesis

The main part of this thesis describes experiments investigating the electrophysiological properties and neurotransmitter receptor expression of white matter oligodendrocytes, and the response of these cells to anoxic/ischaemic conditions. In addition, I describe experiments investigating the energy stores present in grey matter which delay neurotransmitter release during ischaemia. The organisation of the description of the experiments is as follows.

- The experiments in Chapter 3 investigate the morphology, protein expression, and electrophysiology of oligodendrocytes at all developmental stages, and also of astrocytes. The aim was to be able to define the developmental stage of cells

by their electrophysiological and morphological properties, as well as to identify whether the $NG2^+$ cells are homogenous or heterogeneous.

- The experiments in Chapters 4 & 5 investigate neurotransmitter receptor expression in white matter oligodendrocytes using electrophysiology and immunohistochemistry. Chapter 4 looks at what glutamate receptors are expressed, and their properties, at different developmental stages of the oligodendrocytes. Chapter 5 looks at what GABA receptors are expressed in oligodendrocytes at different developmental stages, as well as investigating the response to various other neurotransmitters which have been reported to affect oligodendrocytes. At the end of both chapters the properties of different classes of $NG2^+$ cell are further investigated.
- The experiments in Chapter 6 investigate the effect of ischaemia on precursor and mature oligodendrocytes. They look into the mechanisms that are involved in the generation of an inward current evoked by ischaemia, which may possibly lead to the cells' death. At the end of the chapter the differences in response of the different classes of $NG2^+$ cells are investigated.
- Experiments in Chapter 7 investigate spontaneous synaptic activity in $NG2^+$ cells in cerebellar white matter. The aims were to characterize what neurotransmitter generates them and to determine whether the spontaneous events were affected by ischaemia.
- Experiments in Chapter 8 investigate the ability of different types of metabolic inhibition to induce an anoxic depolarisation in hippocampal tissue, comparing the effect of chemical inhibition of glycolysis and oxidative phosphorylation either separately or together, and comparing this with the effect of oxygen and glucose deprivation alone. The aim was to understand which energy reserves delay the neurotransmitter release which generates the anoxic depolarisation.

The results of each chapter are assessed in a Discussion section within each chapter. Chapter 9 provides a more global discussion of the work I have done, and suggests further experiments for the future

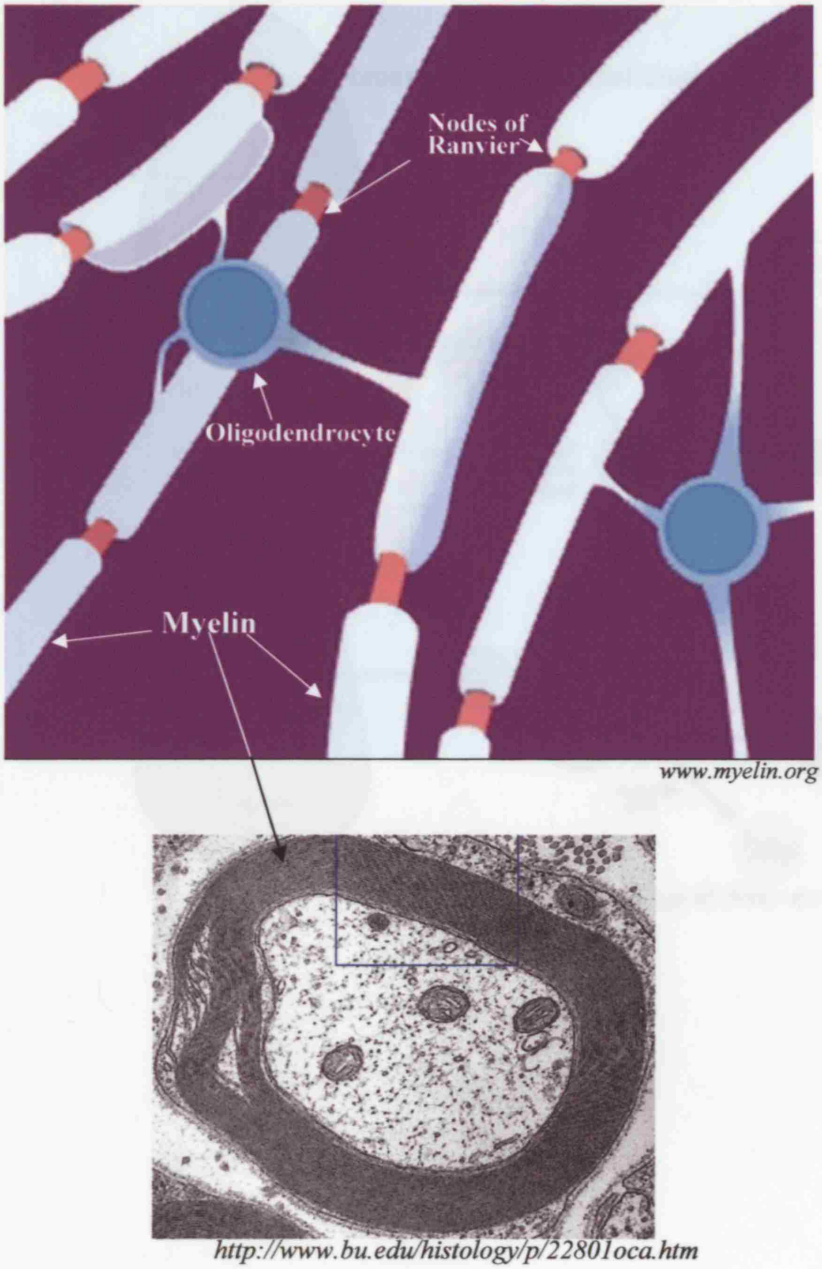

Figure 1.1 Schematic diagram of oligodendrocytes and myelin. **A** A schematic diagram of the white matter, showing an oligodendrocyte myelinating many axons, and the nodes of Ranvier. **B** An electron microscope picture of a cross section of a myelinated fibre. Within the boxed area many parallel membrane layers comprise the compact myelin around the axon.

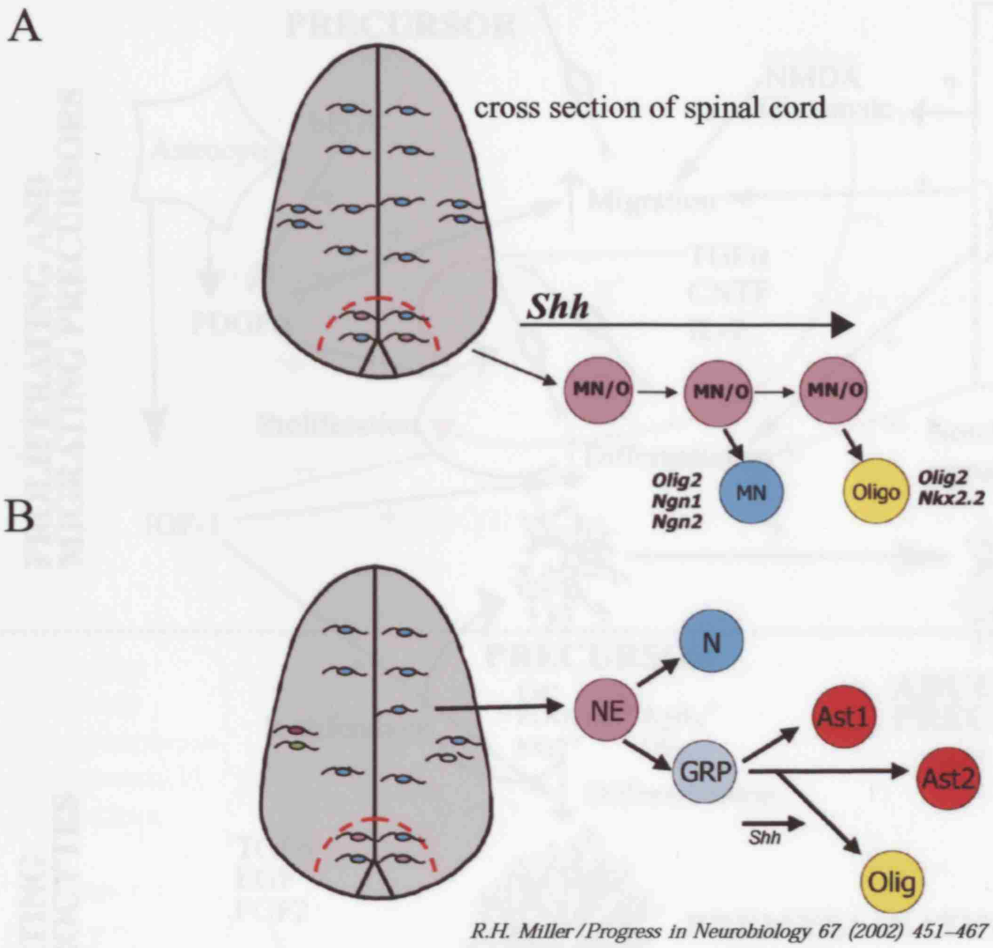

Figure 1.2 Diagram of the two theories regarding oligodendrocyte generation. **A** Neuroepithelial cells in the vental spinal cord (red line) are induced by sonic hedgehog to become motor neuron/oligodendrocyte precursor (MN/O) cells. Expression of the transcription factors Olig2 and neurogenin (ngn) in these cells results in motor neuron specification (MN). During the second wave of cellular genesis when neurogenin signalling goes down, Nkx2.2 expression goes up and its co-expression with Olig2 results in oligodendrocyte precursor genesis (Oligo). **B** The second theory, where neuroepithelial (NE) cells become specified either as neuronal precursors (N) or glial restricted precursors (GRP). In both theories, oligodendrocytes are preferentially generated from the ventral regions, influenced by local Shh signalling.

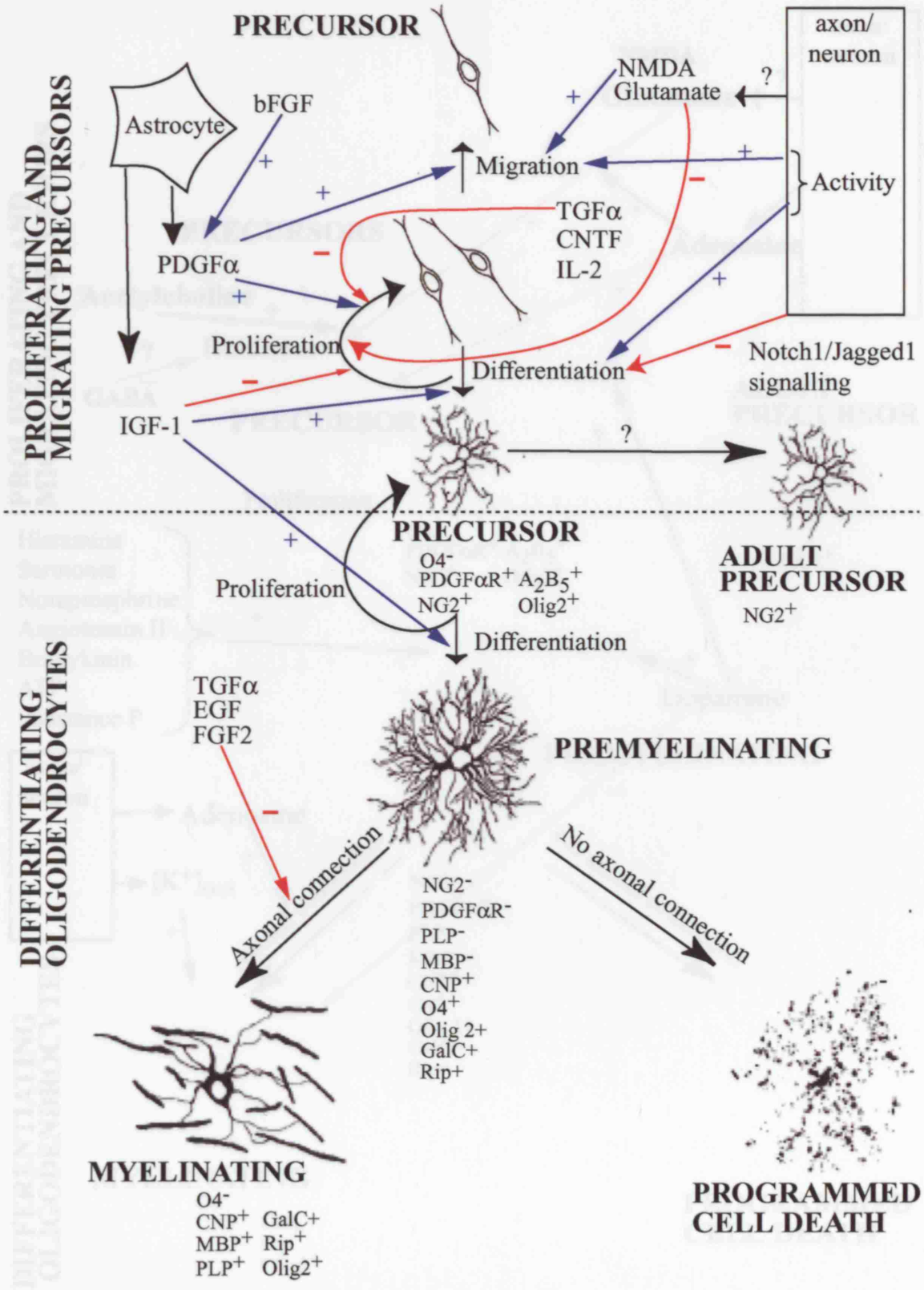

Figure 1.3 Summary diagram of growth factor regulation of oligodendrocyte development. Blue lines indicate positive effects whereas red lines indicate inhibition. Above the dashed line cells are precursors; below the line they are differentiating or mature. Question marks indicate uncertainty over the signalling involved. Beneath each cell stage I indicate the markers that are expressed at that stage.

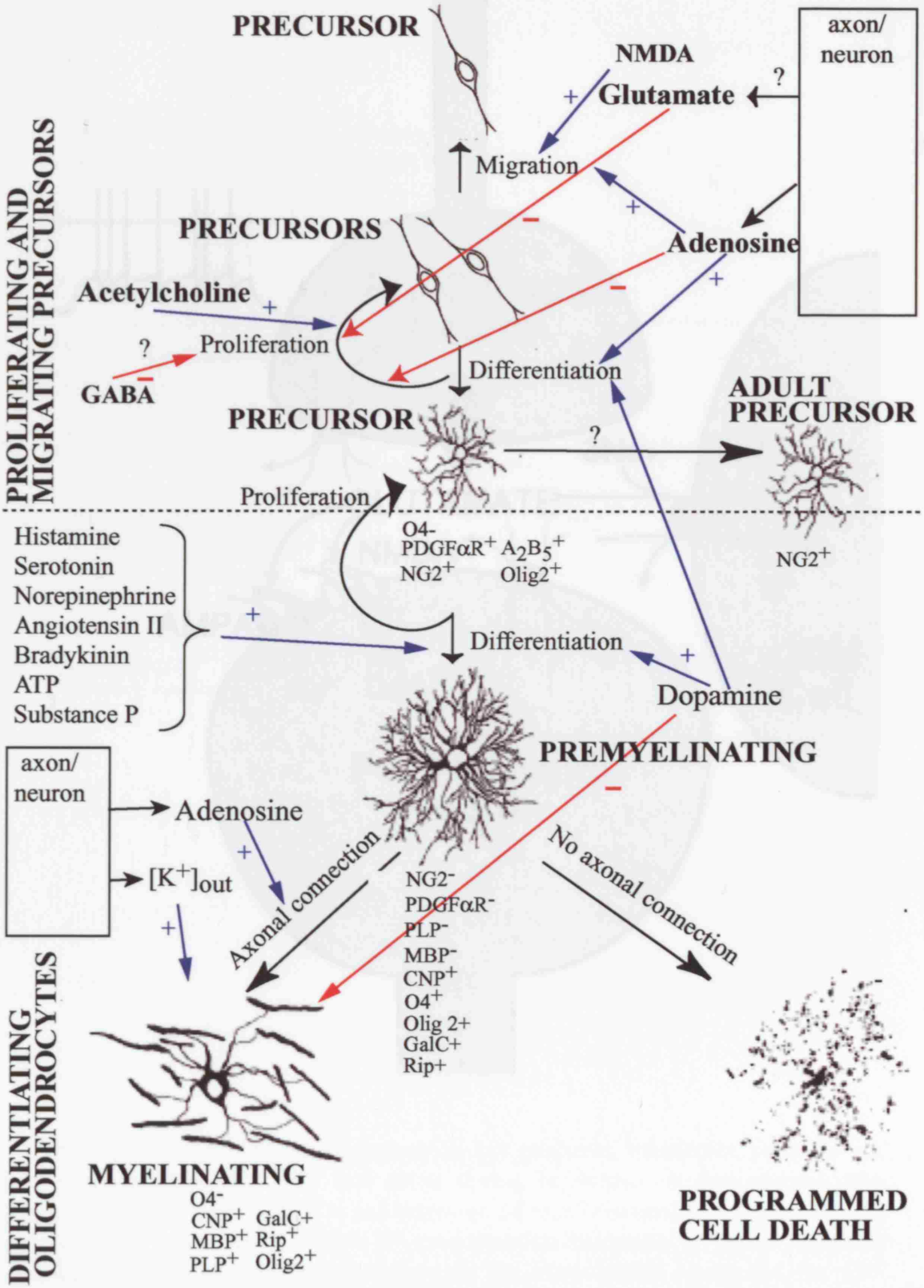

Figure 1.4 Summary diagram of neurotransmitter regulation of oligodendrocyte development. Blue lines indicate positive effects whereas red lines indicate inhibition. Above the dashed line cells are precursors; below the line they are differentiating or mature. Question marks indicate uncertainty over the signalling involved. Beneath each cell stage I indicate the markers that are expressed at that stage.

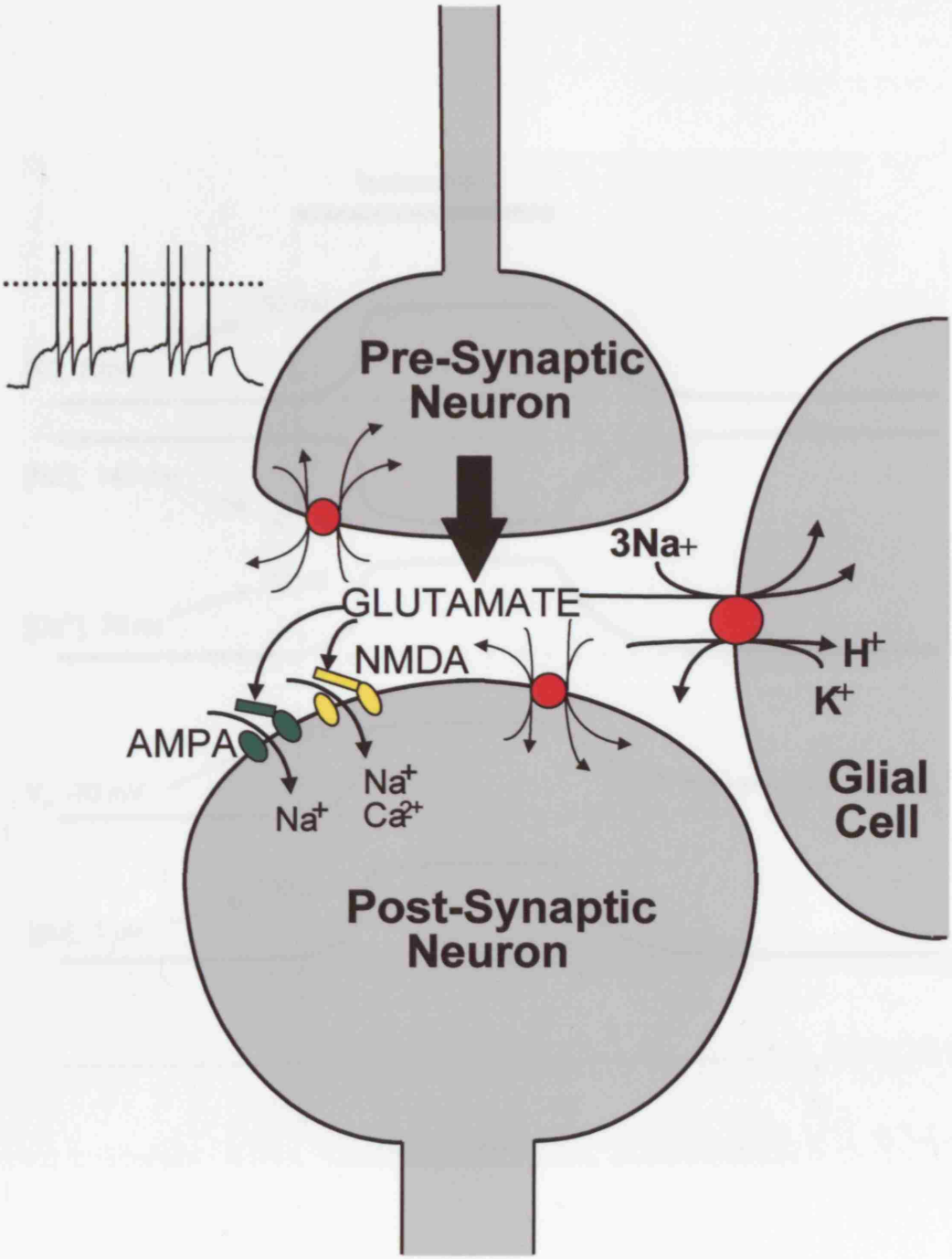

Figure 1.5 Schematic diagram of an excitatory synapse, showing glutamate release by the presynaptic neuron in response to action potentials (inset at top left), postsynaptic receptors that the glutamate acts on, and glutamate uptake by glial cells and neurons.

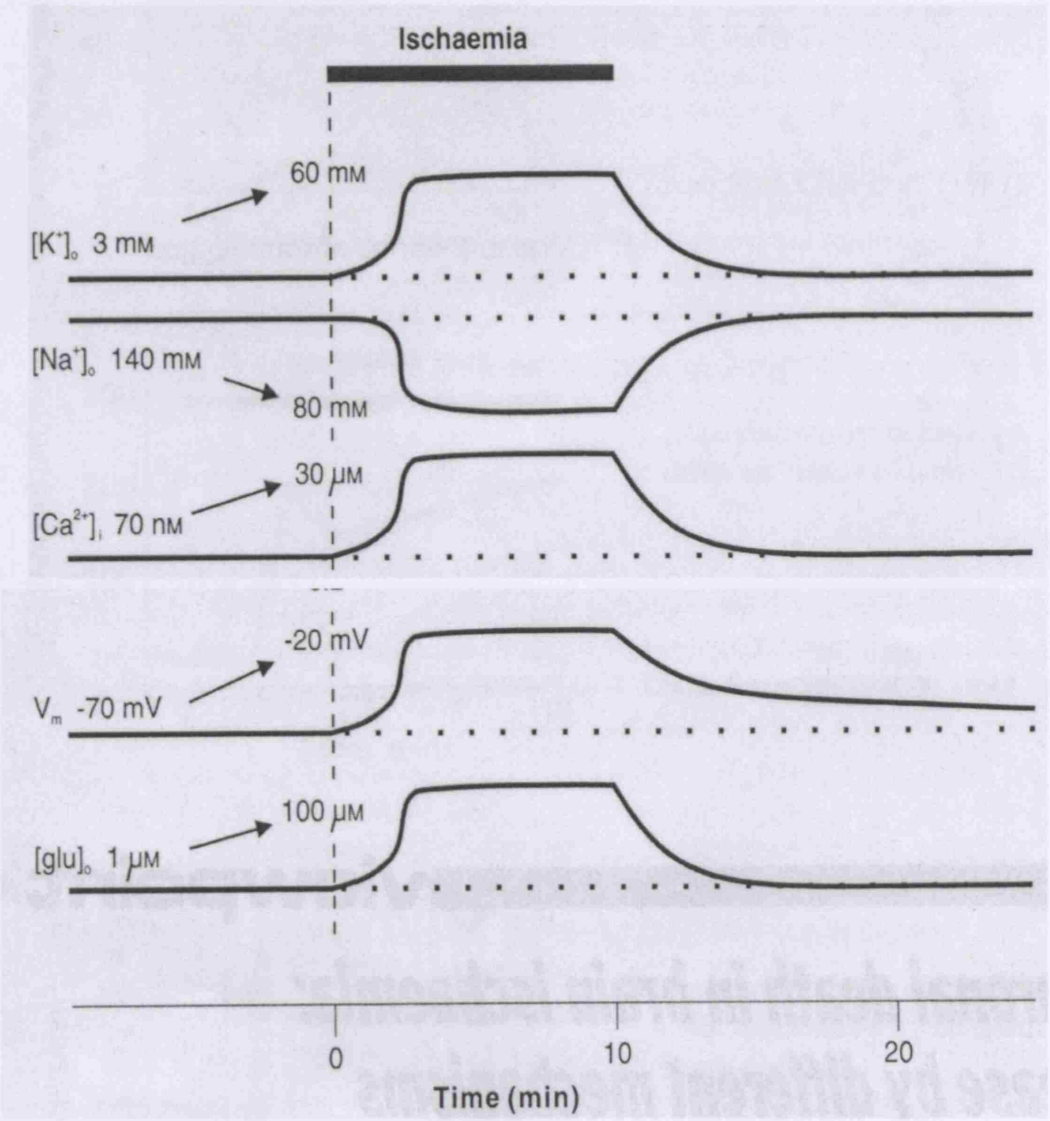

Figure 1.6 Summary of the alterations in ion gradients, membrane potential and extracellular glutamate level that occur during ischaemia. A few minutes after ischaemia is induced, there is a redistribution of ions between the intracellular and extracellular compartments. The K^+ concentration increases in the extracellular space, the Na^+ concentration decreases in the extracellular space and the Ca^{2+} concentration increases inside cells. At the same time as this redistribution of ions occurs, neurons depolarise from -70mV to -20mV, and this is coincident with a large increase in the extracellular glutamate concentration. In addition to these changes the extra- and intracellular pH go acid by up to 1 unit. From Szatkowski and Attwell (1994).

A

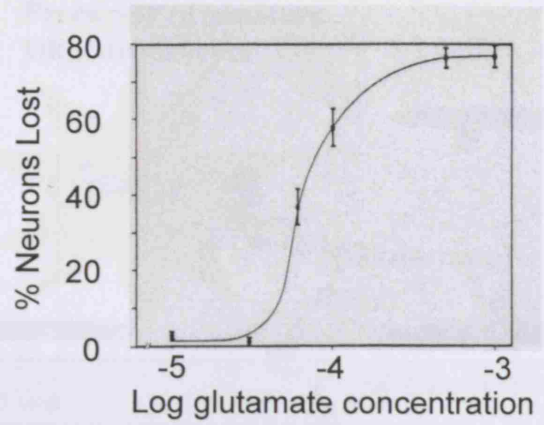

Glutamate kills neurons

Taken from Choi et al. (1987)

B

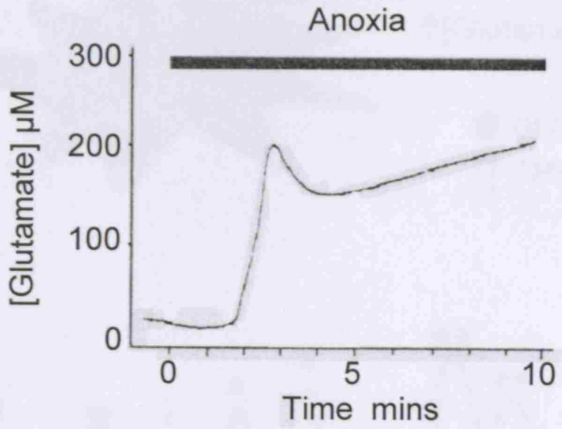

Anoxia/ischaemia causes a dramatic rise in $[Glutamate]_o$

Taken from Satoh et al. 1999

C

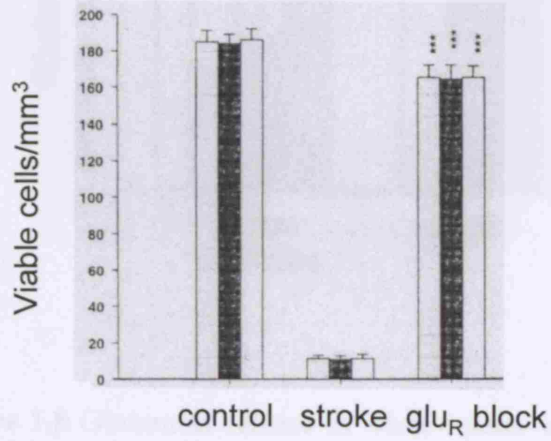

Glutamate receptor antagonists block ischaemia-evoked death

Taken from O'Neill et al. 2000

Figure 1.7 Glutamate is a major agent of death during ischaemia. **A** Application of glutamate to cultured cortical neurons for 5 minutes induces death in a dose-dependent manner, with 100µM glutamate killing 60% of cells (cell death was measured 24 hours later). **B** Microdialysis experiment showing that glutamate is released into the extracellular space during *in vivo* hippocampal anoxia, and the concentration peaks at 200µM which is high enough to induce the death of most neurons. **C** Applying glutamate receptor antagonists during *in vivo* hippocampal ischaemia protects neurons from cell death. The three bars for each condition represent different animals.

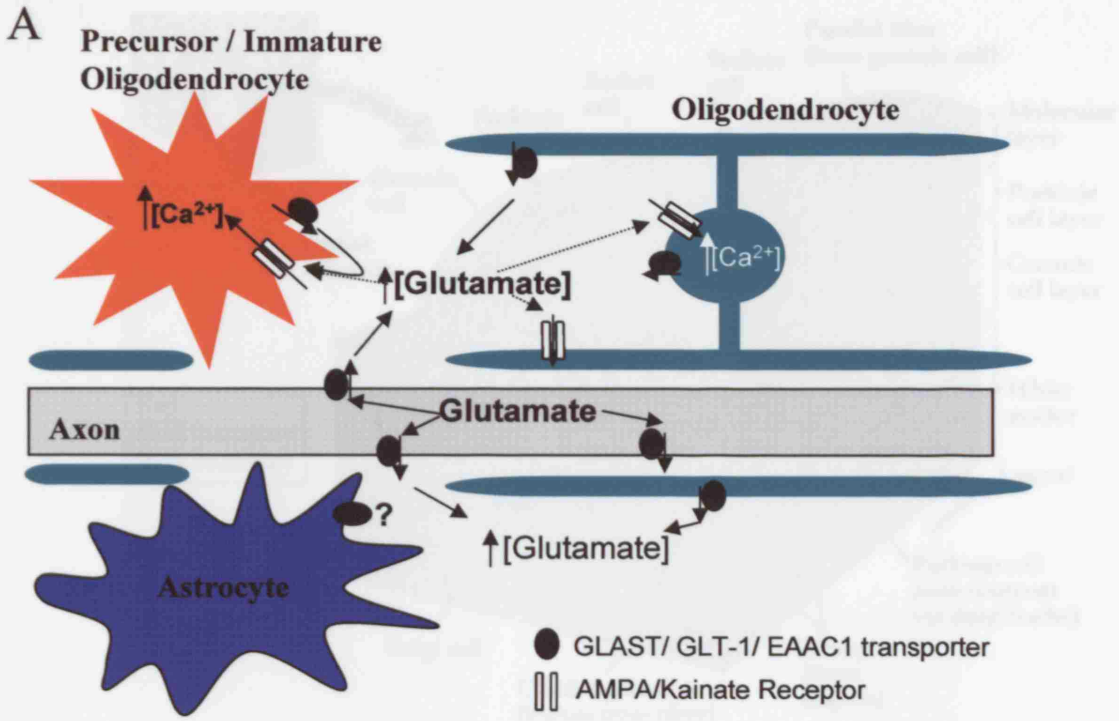

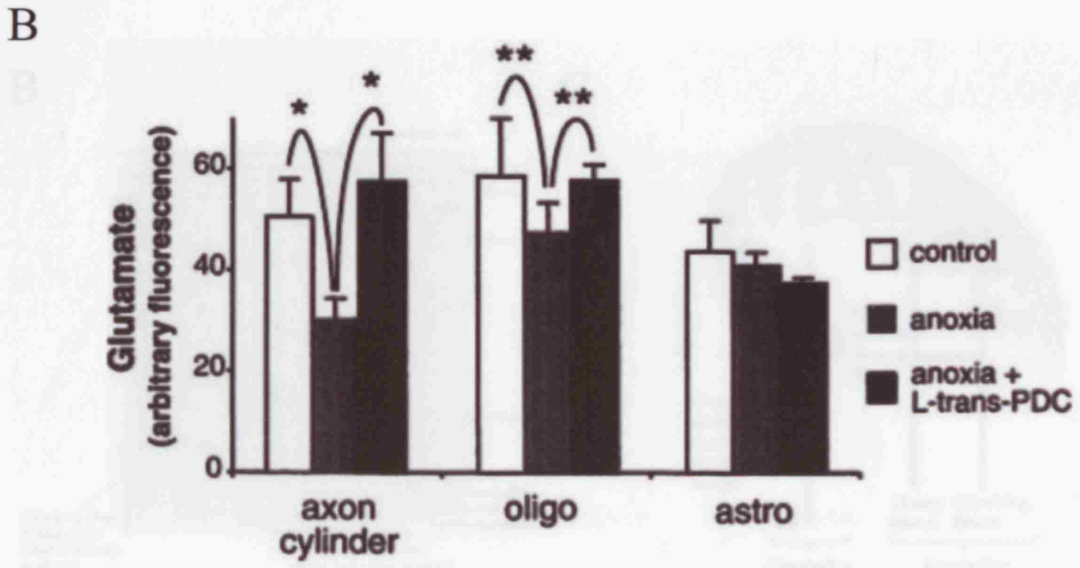

Taken from Li et al. (1999)

Figure 1.8 Glutamate release in white matter ischaemia. **A** Schematic diagram of glutamate release from axons and oligodendrocytes, via reversed uptake, in the white matter. The glutamate activates glutamate receptors, which are conventionally thought to be calcium-permeable AMPA receptors (see text) which allow calcium to enter and reach too high a concentration in both precursor and mature oligodendrocytes. **B** Immunohistochemical measurements of glutamate concentration in spinal cord axons, oligodendrocytes and astrocytes during anoxia. Glutamate is lost from axons and oligodendrocytes (but not astrocytes) and this loss is prevented by preloading with the glutamate transport inhibitor PDC, implying that glutamate is released into the extracellular space via reversed glutamate uptake.

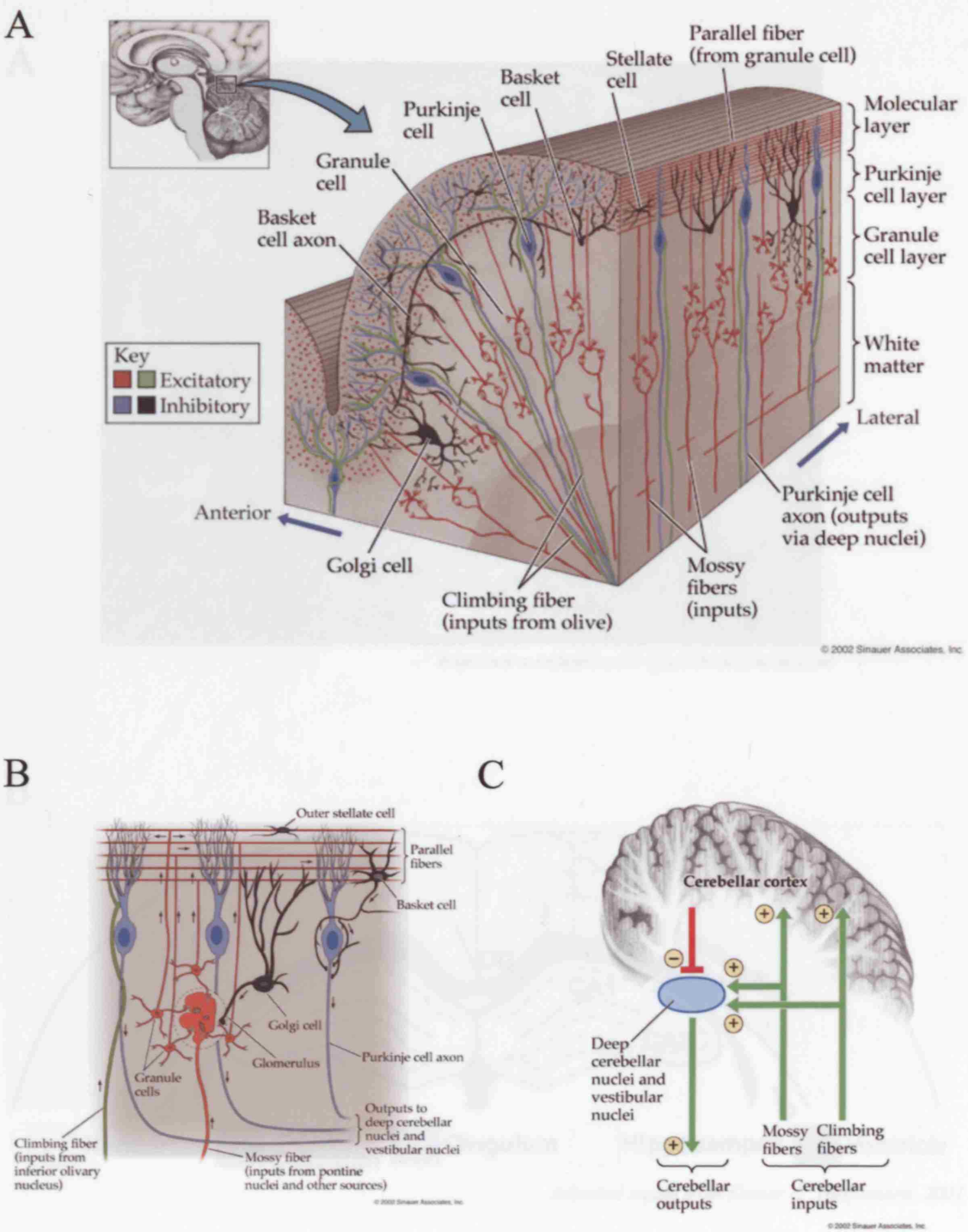

Images are taken from Chapter 15, Cerebellum; In Neuroanatomy Through Clinical Cases by Blumenfeld 2002

Figure 1.9 Structure of the cerebellum. **A** Three dimensional view of a cerebellar folium, showing the three neuronal layers and the white matter. **B** A more detailed view of the cells found in the three neuronal layers, their synapses and input and output connections. **C** A general view of the inputs and outputs of the cerebellum.

A

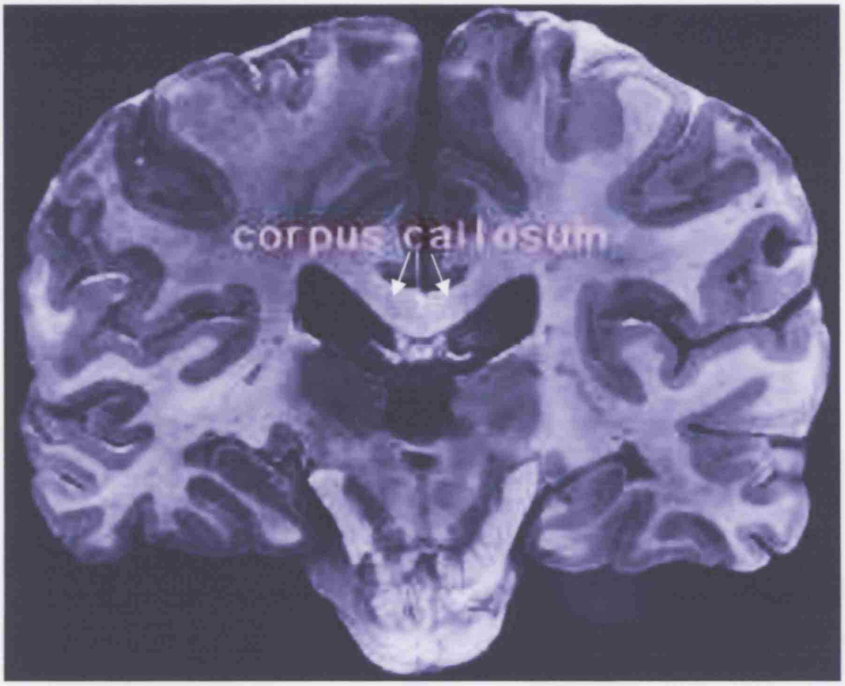

http://www.indiana.edu/~pietsch/callosum.html

B

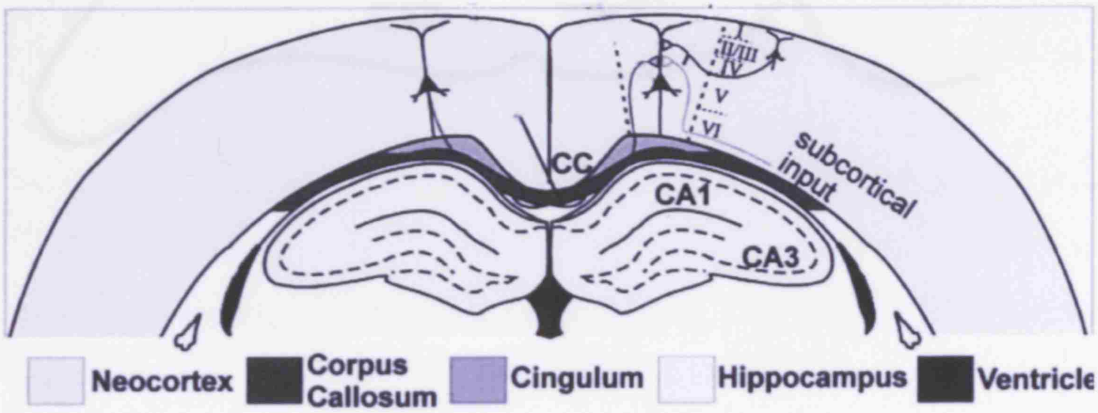

Adjusted image from Kumar & Huguenard, 2001

Figure 1.10 Structure of the corpus callosum. **A** MRI image of the corpus callosum **B** A schematic diagram of the corpus callosum and the pathway of the main fibres passing through it (as described in the text).

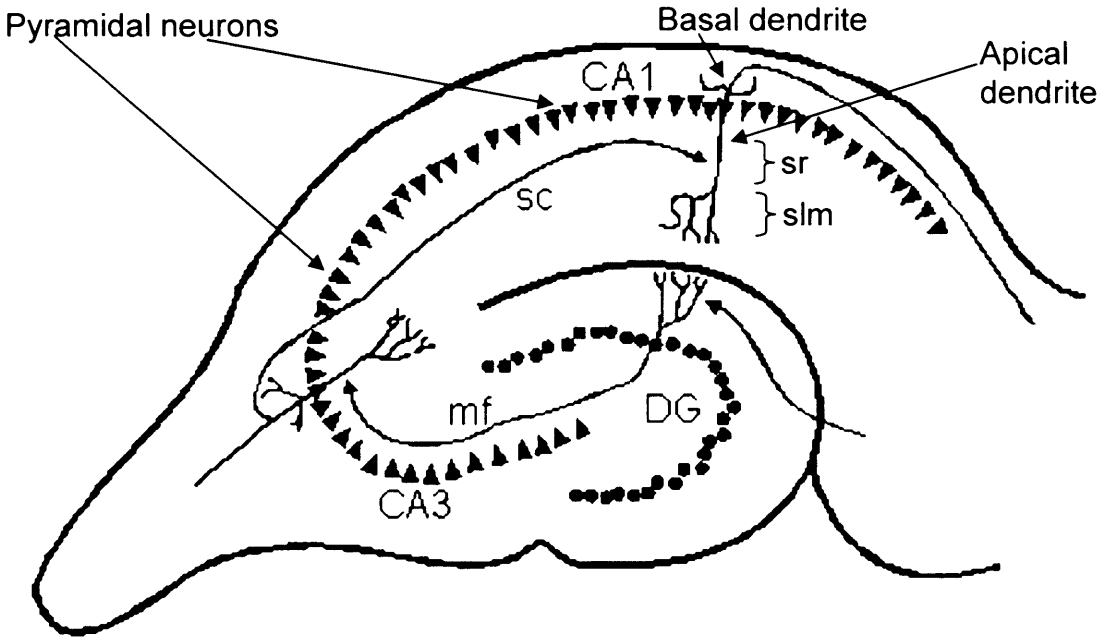

Figure 1.11 Diagram of the hippocampus and inputs to area CA1 of the hippocampus. Mossy fibres (mf) project from the dentate gyrus (DG) to CA3 pyramidal neurons. Schaffer collaterals (sc) project from CA3 pyramidal neurons to CA1 pyramidal neurons. CA1 pyramidal neurons have 2 dendritic trees, smaller basal dendrites that are located in the stratum oriens, and larger apical dendrites that pass first through the stratum radiatum (sr) and then into the stratum lacunosum-moleculare (slm).

Chapter 2

Methods

This chapter explains the general methods used for experiments throughout the thesis. Further details of the specific methods used are provided in each results chapter.

2.1 Cell preparation

2.1.1 Preparation of cerebellar slices

Sprague-Dawley rats, aged postnatal day 7-28 (P17-P28), were used for the preparation of the cerebellar brain slices employed for the experiments in chapters 3-6. Animals were killed by cervical dislocation followed by decapitation, and the head was immediately immersed in ice-cold oxygenated slicing medium, composed of (in mM): NaCl 126, $NaHCO_3$ 24, NaH_2PO_4 1, KCl 2.5, $CaCl_2$ 2.5, $MgCl_2$ 2, D-glucose 10 (gassed with 95% O_2/5% CO_2), pH 7.4, and containing 1mM kynurenic acid to block glutamate receptors during the slicing process. The scalp was removed and the skull was opened by cutting between the eyes, followed by lateral cuts on either side of the head from the anterior to the posterior. The excised region of the skull was lifted with forceps, and the whole brain was quickly removed and placed in ice-cold oxygenated slicing medium. To obtain parasagittal slices of the cerebellar vermis, cuts were made through the inferior colliculus and spinal cord (to separate the cerebellum from the rest of the brain) and the cerebellar hemispheres on either side of the vermis were removed (to isolate the vermis). The cerebellar block was mounted on one of the cut surfaces on the stage of a vibrating tissue slicer (Vibratome) using Superglue and mechanically stabilised using an agar block attached to the Vibratome stage; in the case of young animals (P7) an extra agar block was glued to the stage as a base for the brain. The cerebellum was immersed in ice-cold oxygenated slicing medium throughout the cutting process. Sagittal slices of the cerebellar vermis, 225 μm thick, were cut and placed in oxygenated slicing medium

at room temperature until used for recording, less than 9 hours after the animal was killed. At the time of the experiment a slice was placed in the recording chamber and held in place by a "harp", made of a parallel array of nylon threads (separated from each other by 0.5-1.0 mm) strung on a platinum frame.

2.1.2 Preparation of hippocampal slices

Sprague-Dawley rats, aged postnatal day 12 or 28 (P12 and P28), were used for the preparation of the hippocampal brain slices used in chapter 8. An animal was sacrificed and the brain was removed as described in section 2.1.1. To obtain transverse sections of the hippocampus, the hemispheres of the brain were separated by cutting down the longitudinal fissure. Each hemisphere was placed on its cut medial surface, and a small section of the frontal lobe was removed to provide a flat surface by which to attach the hemisphere to the slicing stage, and to ensure that hippocampal slices were prepared in the transverse plane. Each hemisphere was mounted on the stage of a vibrating tissue slicer (Vibratome) using Superglue and mechanically stabilised using an agar block attached to the Vibratome stage. The hemispheres were immersed in ice-cold oxygenated slicing medium throughout the cutting process. Slices of the whole hemisphere, 225 μm thick, including the hippocampus, were made and placed in oxygenated slicing medium at 34°C for 30 minutes. The slices were then kept at room temperature until they were used for recording (less than 9 hours after the animal was killed). At the time of the experiment a slice was placed in the recording chamber and held in place by a "harp" (see above).

2.1.3 Preparation of corpus callosum slices

Sprague-Dawley rats, aged postnatal day 12 (P12), were used for the preparation of corpus callosum brain slices studied in chapter 4. An animal was sacrificed and the brain was removed as described in section 2.1.1. To obtain coronal sections of the corpus callosum, the cerebellum was removed from the brain to provide a flat surface by which to attach the hemisphere to the slicing stage, and to ensure that corpus

callosum slices were prepared in the coronal plane. In addition, a small part of the frontal lobe was cut off, to speed up the slicing procedure. The forebrain was then mounted on the stage of a vibrating tissue slicer (Vibratome) using Superglue and mechanically stabilised using an agar block attached to the Vibratome stage. The brain was immersed in ice-cold oxygenated slicing medium throughout the cutting process. Slices of the whole two hemispheres, 225 μm thick, including the corpus callosum, were made and placed in oxygenated slicing medium at room temperature. The slices were then kept at room temperature until they were used for recording (less than 9 hours after the animal was killed). At the time of the experiment a slice was placed in the recording chamber and held in place by a "harp" (see above).

2.2 Standard solutions used and model system for ischaemia

In general I used a HEPES-based external solution for drug application experiments at room temperature, and a bicarbonate-based external solution for ischaemia experiments and some drug application experiments at 33°C. Internal (i.e. pipette) solutions were either Cs- or K^+-based. The recipes for each experiment are given in the following chapters.

To mimic brain ischaemia *in vitro*, I inhibited glycolytic and mitochondrial ATP production by removing glucose and O_2, but I needed to use metabolic blockers as well (Reiner et al., 1990), because in open recording chambers oxygen from the room air can rapidly diffuse through the solution to the tissue, preventing true inhibition of oxidative phosphorylation as would occur *in vivo*. In chapters 6 and 8, energy deprivation was simulated by replacing 10mM glucose with 7mM sucrose and/or bubbling with 95% N_2/5% CO_2, and (except for some experiments in chapter 8) glycolysis was blocked with iodoacetate (2mM) and oxidative phosphorylation was blocked with antimycin (25-100μM) and/or rotenone (100μM) or NaCN (1mM). A detailed analysis of the efficacy of different metabolic blockers is presented in Chapter 8.

2.3 Dye filling and cell identification

In whole cell recording experiments in chapters 3-7, a fixable fluorescent Lucifer yellow dye was added to the pipette filling. The dye diffused into the cell (see section 2.9) and hence revealed the cell's morphology and its gap junctional network. Using the filter set for Lucifer yellow (see Table 2.3) on the microscope, this allows immediate cell identification by morphology during whole cell recordings. In addition, each cell was marked onto a map of the cerebellum or corpus callosum, to simplify the later search for the cell in the confocal microscope and to document any differences in cell properties between regions. After recording from the slice, the slice was fixed in 4% paraformaldehyde in phosphate buffered saline (PBS) for an hour at room temperature with slight agitation. Then the slice was washed three times for 15 minutes each wash in 0.1M PBS. After the wash the slice was kept in the fridge (with 0.05% NaN_3 added to the 01M PBS solution) until being mounted on a slide for confocal imaging of the Lucifer yellow fluorescence to fully record the cell's morphology, or being used for immunohistochemistry to identify the type of cell recorded using cell specific markers (see section 2.11).

2.4 Mechanical and optical set-up

Slice experiments (Fig. 2.1) were carried out on a set-up equipped with an Olympus BX51WI upright microscope, with a fixed stage and microscope-moving table, or on a fixed stage Zeiss Axioscop, upright microscope. Slices were continuously perfused with oxygenated external solution in the recording chamber, via an inlet connected to a peristaltic pump (flow rate 6-10ml/min) or gravity fed from 150ml syringes (flow rate 2-6 ml/min). Slices were viewed using a 40x water immersion objective with differential interference contrast (DIC) optics. Both microscopes were equipped with a halogen lamp and filter sets for viewing Lucifer yellow filled cells (Lucifer yellow excitation: 428nm, and emission: 540 nm).

2.5 Pipettes and electrical set-up

Patch pipettes were made from thick-walled filament-containing borosilicate glass capillaries (outer diameter 1.5 mm, inner diameter 0.86 mm, type GC150F-10 from World Precision Instruments), and they were produced using a two step vertical puller (Narishige PC-10). Pipettes were filled with the appropriate intracellular solution (see individual Results chapters for the internal solution composition).

The recording electrode was inserted into the pipette holder of a patch-clamp headstage (Axopatch CV202AU, Axon Instruments), which was attached to and moved by an electric micro-manipulator (SMI, Luigs and Neumann). The electrode had either a resistance of 4.3-6 MΩ (chapters 3-7) or 2.3-4 MΩ (chapter 8) when placed in the bath. An Ag/AgCl pellet (or, in experiments using cyanide (chapter 8) which reacts with AgCl electrodes (Rajantie & Williams, 2001), a 4M-NaCl filled Agar bridge to prevent changes of bath electrode potential) was placed in the recording chamber to serve as the bath electrode. In Chapter 8, inputs to CA1 pyramidal neurons were electrically stimulated, by placing a glass pipette filled with extracellular solution close to the CA3 region of the hippocampus. Membrane currents were recorded with either an Axopatch 200A or 200B amplifier (filtered at 10 kHz), and stored via a digital data recorder (PCM701ES, Sony) on video tape. Data were also stored directly onto a personal computer (using pClamp 8 or pClamp9, following digitisation with a Digidata 1200, Axon Instruments) at a sampling rate appropriate for each experiment, as well as being stored to a computer using Axoscope sampling at 1 kHz. Additionally, all data were recorded continuously using a chart recorder. Most data were analysed directly from the chart record; but some of the data was analysed off-line using Clampfit 8 or Clampfit 9 (Axon Instruments).

2.6 Patch-clamp recordings

All recordings were performed in the conventional whole cell configuration (Hamill et al., 1981; Edwards et al., 1989). The general principle of the patch-clamp technique is to obtain a high resistance seal (usually 1-10 GΩ) between the cell

membrane and the tip of the glass patch pipette. A gigohm-seal is obtained by attaching the pipette onto the cell surface and sucking gently (Fig. 2.2A). The chances of formation of a gigohm-seal are increased by applying positive pressure to the pipette before contacting the cell to keep the pipette tip clean, to prevent the attachment of any debris flowing in the bath solution or of tissue when entering the slice (for a description of slice patching see Edwards et al., 1989).

After formation of a high resistance seal in the cell-attached mode, and compensation of the pipette capacitance transient (see below for details of capacity transients), further suction is applied to the pipette to rupture the membrane patch below the pipette tip to achieve a low resistance access to the cell's interior. In this conventional whole-cell patch-clamp mode, the cell interior is in direct contact with the pipette interior (Fig. 2.2B). Ions of the cytoplasm will diffuse into the pipette, and vice versa, resulting in the cell becoming dialysed within minutes after the membrane patch is broken (see Section 2.7 for estimates of the time needed for this to occur). In this way the composition of the intracellular solution can be controlled by the pipette solution.

Owing to the different composition of the pipette solution and the bath solution, a junction potential exists at the end of the electrode before sealing onto the cell, which is not present when the pipette solution has filled the cell in whole-cell mode (Fig. 2.2B). For the pipette solutions used in the majority of my experiments, with $[Cl^-]_i$ = $[Cl^-]_o$, correcting for this potential adds a voltage of about -3mV to the apparent potential (Fenwick et al., 1982).

2.7 Series resistance

Pipette series resistance is the resistance between the cell's interior and the pipette's interior when in the whole-cell patch-clamp configuration, and can be measured as outlined below, in Section 2.8. A low series resistance (in the range of 1-10MΩ) implies a good electrical and diffusion pathway into the cell. A good diffusion pathway is essential for the efficient exchange of molecules between the pipette and the cell. A good electrical pathway to the cell interior is important because current flowing

between the pipette and the cytoplasm will result in a voltage drop across the pipette tip, the value of which depends on the series resistance and the size of the current. A high series resistance or large current flow will result in a high voltage drop, and the apparent membrane potential is the sum of the real membrane potential, in the soma, plus the voltage drop. Series resistance compensation (typically 50-70%) was employed to minimise such voltage errors.

For experiments on oligodendrocytes in Chapters 4-7, the pipette series resistance was typically 4-12 MΩ with 60% compensation. For a typical glutamate or NMDA-evoked current at the resting potential of ~200pA, this will lead a negligible voltage error of 0.8-2.4 mV. For voltage steps to positive potentials, in some cells outward currents of ~ 1nA were evoked, and these will cause a voltage error of 4-12mV (the cell will be less depolarized than the command potential). This was neglected for the I-V data in chapter 3, since no quantitative analysis of these currents was performed, but was corrected for in providing the I-V relations for drug-evoked response.

Series resistance also presents a problem in Chapter 8, where recordings of the anoxic depolarisation in CA1 pyramidal neurons are described. In whole-cell mode the series resistance (R_s) was compensated from an average of 5MΩ to 2MΩ. The current flowing at the peak of the anoxic depolarisation averaged 6nA and from the equation,

$$V_{error}=IR_s \qquad (2.1)$$

this will give a voltage error of 12mV at the time of the anoxic depolarisation. All cells were clamped at an apparent holding potential of -33mV, meaning that at the time of the anoxic depolarisation the actual membrane potential was 12mV more positive, at -21mV. This leads to the size of the anoxic depolarisation current being underestimated, as the voltage of the cell is closer to the reversal potential of the anoxic depolarisation (shown to be +10mV by (Hamann et al., 2002) so the driving force for cation entry into the cell is reduced.

The effect of these voltage errors can be corrected for with the method employed by (Hamann et al., 2002). The voltage-dependence of the current flowing at the time of the anoxic depolarisation was approximated by an ohmic relation (ignoring for simplicity the slight outward rectification produced by the contribution of Mg^{2+}-

blockable NMDA receptors (Rossi et al., 2000), which will reduce the effect of series resistance voltage errors, and ignoring the small current flowing before ischaemia):

$$I = G \times (V - V_{rev}) \tag{2.2}$$

where I is the measured current flowing, G is the conductance generating the anoxic depolarisation current, V is the true membrane potential and V_{rev} is the reversal potential of the anoxic depolarisation. If R_s is the series resistance,

$$V = V_c - IR_s \tag{2.3}$$

where V_c is the command potential (i.e. desired holding potential), and from equations 2.2 and 2.3

$$I = G \times \frac{(V_c - V_{rev})}{(1 + GR_s)} \tag{2.4}$$

Defining the current which would flow in the absence of R_s errors (i.e. with V fixed at V_c) as

$$I_c = G \times (V_c - V_{rev}) \tag{2.5}$$

equation 2.5 becomes:

$$I = \frac{I_c}{1 + (I_c R_s)/(V_c - V_{rev})} \tag{2.6}$$

and thus:

$$I_c = \frac{I}{1 - (IR_s)/(V_c - V_{rev})} \tag{2.7}$$

In Chapter 8 of this thesis the amplitudes of anoxic depolarisation currents were compared following various drug treatments during ischaemia. A t-test was performed to see whether there was a significant difference between the amplitudes (uncorrected for series resistance errors) after the different treatments, and in cases where the p-value was on the border of significance (i.e. close to p=0.05) the analysis summarised in equation 2.7 was applied to correct for series resistance errors. In practice the amplitude of the anoxic depolarisation current was underestimated by 20% as a result of R_s errors, but recalculating the peak current to compensate for these errors did not alter the significance of results

2.8 Capacity transient analysis and voltage non-uniformity

By analysing the current response to a voltage step, it is possible to measure the pipette series resistance and to assess whether the cell is uniformly voltage clamped. I will consider two cases: first a spatially compact voltage-uniform cell, and then a cell with long processes (like the oligodendrocytes studied in chapters 4-7, or the pyramidal cells studied in chapter 8) where the voltage is non-uniform. The membrane acts as a capacitor and resistor connected in parallel, and the series resistance is in series with these (Figs. 2.2, 2.3 & 2.4). The current flow, I, through this circuit in response to a voltage step, V_s, is (Tessier-Lavigne et al., 1988):

$$I(t) = \left(\frac{V_s}{R_m + R_s}\right) \cdot \left(1 + \frac{R_m \cdot e^{-t/\tau}}{R_s}\right) \qquad (2.8)$$

where t is the time after the onset of the voltage step, R_m is the membrane resistance, R_s is the series resistance, and τ , the decay time constant of the current transient, is:

$$\tau = C_m \cdot \frac{R_s \cdot R_m}{R_s + R_m} \qquad (2.9)$$

At the onset of the voltage step, at t = 0, the capacitor is uncharged and the voltage across it is zero. Consequently, just as the voltage step is applied, the voltage across the series resistance is the applied voltage step, and the initial current flowing allows calculation of the series resistance as:

$$R_s = \frac{V_s}{I(t = 0)} \qquad (2.10)$$

At steady state, i.e. $t = \infty$, the capacitor is fully charged and no current flows through it. The membrane resistance can then be calculated from the voltage step and the current at $t = \infty$:

$$R_m = \frac{V_s}{I(t = \infty)} - R_s \qquad (2.11)$$

Substituting R_s from equation 2.10 gives:

$$R_m = V_s \cdot \frac{I(t = 0) - I(t = \infty)}{I(t = 0) \cdot I(t = \infty)} \qquad (2.12)$$

The membrane capacitance can be calculated by rearranging equation 2.9 to give:

$$C_m = \tau \cdot \frac{R_s + R_m}{R_s \cdot R_m} \tag{2.13}$$

Substituting R_s from equation 2.10 and R_m from equation 2.12 gives:

$$C_m = \tau \cdot \frac{I(t=0)^2}{V_s \cdot \left(I(t=0) - I(t=\infty)\right)} \tag{2.14}$$

The time constant, τ, was obtained by fitting the current transient with a single exponential using Clampfit. An example of a fitted capacity transient for an electrically compact cell is shown in Figure 2.3. The current change at t=0 was obtained by extrapolating this exponential back to the time of the voltage step.

This analysis assumes that the cell is isopotential, and predicts a monoexponential decay of the capacity current. This is the case for electrically compact cells such as the small oligodendrocyte precursors. For cells with complex morphology, however, the resistance of the processes or dendrites makes the cell non-uniform in voltage, and the capacity current decays as the sum of 2 or more exponentials (Fig. 2.4). Nevertheless, from the argument preceding equation 2.10, just at the moment the voltage step is applied, the cell capacitance is uncharged, so all the applied voltage step appears across the pipette series resistance, and this R_s can be calculated from equation 2.10.

The non-spherical shape of either oligodendrocytes, with thin and long processes, or CA1 pyramidal cells, with a soma and 2 large branching dendritic trees, may cause a lack of uniformity of the voltage. The degree of non-uniformity in neurons has been analysed by Major (1993), who has shown that voltage control at most dendritic sites in CA1 pyramidal neurons is extremely poor. A similar problem might be expected to occur in the long processes of mature oligodendrocytes. For situations where I needed to control the voltage accurately (for example, when determining the current-voltage relationship of the NMDA-evoked current in chapter 4), I used spatially compact oligodendrocyte precursor cells. The voltage non-uniformity in morphologically complex cells can also introduce a problem when measuring synaptic

currents (as in Chapter 7), where distal synaptic inputs are filtered and smoothed before they reach the recording site in the cell soma.

2.9 Diffusion of substances from the pipette into the cell

During whole-cell patch-clamping the intracellular ion composition is controlled by the pipette solution. Knowing the time needed for equilibration of the concentration in the pipette and cell interior is useful when filling cells with dye, or replacing intracellular K^+ with Cs^+ to improve voltage uniformity. The time needed for a substance to diffuse into the cell from the patch-pipette can be estimated as follows. The diffusive flux, J, of a substance along the x axis (from the pipette into the cell) is given by:

$$J = - D \cdot A \cdot \frac{dC}{dx} \tag{2.15}$$

where D is the diffusion coefficient of the substance, A is the area available for diffusion, C is the concentration of the substance at point x and dC/dx is the concentration gradient of C in the x direction. Assuming the end of the pipette to be an idealised barrier of width w and area A, equation 2.15 becomes:

$$J = D \cdot A \cdot \frac{C_{pipette} - C_{cell}}{w} \tag{2.16}$$

with $C_{pipette}$ being the concentration of the substance in the pipette and C_{cell} being the concentration of the substance in the cell. For a cell of volume V_{cell}, the amount of substance in the cell is $V_{cell}.C_{cell}$. The diffusive flux, J, tends to increase the total amount of substance in the cell, so:

$$J = \frac{d(V_{cell} \cdot C_{cell})}{dt} \tag{2.17}$$

From equations 2.16 and 2.17, the rate of increase of the substance's concentration in the cell is given by:

$$\frac{d(V_{cell} \cdot C_{cell})}{dt} = D \cdot A \cdot \frac{C_{pipette} - C_{cell}}{w} \tag{2.18}$$

The pipette series resistance across the barrier is:

$$R_s = \frac{\rho \cdot w}{A} \tag{2.19}$$

where ρ is the resistivity of the pipette solution. Putting equation (2.19) into equation (2.18) gives:

$$V_{cell} \cdot \frac{dC_{cell}}{dt} = \frac{D \cdot \rho}{R_s} \cdot (C_{pipette} - C_{cell}) \tag{2.20}$$

or, since $C_{pipette}$ is constant:

$$\frac{d(C_{cell} - C_{pipette})}{dt} = - \frac{D \cdot \rho}{V_{cell} \cdot R_s} \cdot (C_{cell} - C_{pipette}) \tag{2.21}$$

Rearranging and integrating, this gives:

$$\int_0^t \frac{1}{(C_{cell} - C_{pipette})} \cdot d(C_{cell} - C_{pipette}) = - \frac{D \cdot \rho}{V_{cell} \cdot R_s} \cdot \int_0^t dt \tag{2.22}$$

which gives:

$$\log_e \left(\frac{(C_{cell} - C_{pipette})_t}{(C_{cell} - C_{pipette})_0} \right) = - \frac{D \cdot \rho}{V_{cell} \cdot R_s} \cdot (t - 0) \tag{2.23}$$

and this gives:

$$\frac{(C_{cell} - C_{pipette})_t}{(C_{cell} - C_{pipette})_0} = e^{- \frac{D \cdot \rho}{V_{cell} \cdot R_s} \cdot t} \tag{2.24}$$

If $C_{cell} = 0$ at $t = 0$, rearranging gives:

$$(C_{cell} - C_{pipette})_t = - C_{pipette} \cdot e^{- \frac{D \cdot \rho}{V_{cell} \cdot R_s} \cdot t} \tag{2.25}$$

Thus, the concentration of the substance in the cell, C_{cell}, approaches the concentration of the substance in the pipette, $C_{pipette}$, exponentially:

$$C_{cell}(t) = C_{pipette} \cdot \left(1 - e^{- t/\tau} \right) \tag{2.26}$$

with a time constant of:

$$\tau = \frac{V_{cell} \cdot R_s}{D \cdot \rho} \tag{2.27}$$

For a typical mature oligodendrocyte of a volume 2887.2 ± 807.9 μm^3 (calculated from anatomical measurements by Marta et al. (2003) and sizes from my confocal images of filled mature oligodendrocytes), with the series resistance of 10 MΩ, a diffusion

coefficient of 10^{-9} m^2s^{-1} (typical for small cations like Na^+, K^+ and Cl^-) and a resistivity of 0.1 Ωm, predicts a time constant for equilibration of small ions in the cell of ~ 289s (or from 208 to 370s using the s.e.m. values for the volume estimate).

This is the time taken for ions to diffuse from the pipette into the cell, assuming that the cell is well mixed. An estimate of the time it takes for substances to diffuse throughout the cell is given by equation 2.28,

$$t = x^2 / 2D \tag{2.28}$$

where x is the distance of diffusion and D the diffusion coefficient, as above. For ions to diffuse down a 200μm process within the cell, around 20 seconds is required. Thus, the time taken for diffusion within the cell is much less than the time taken for diffusion into the cell.

2.10 Field potential recordings

Non-invasive recording of the time of the ischaemia-induced anoxic depolarisation was carried out, in the experiments of Chapter 8, by recording the extracellular field potential with an electrode (filled with external solution) placed in the pyramidal cell apical dendrite layer. The electrode was connected to the patch clamp and current-clamped to 0pA, and the change in voltage recorded. At the time of the anoxic depolarisation the rise of $[K^+]_o$ leads to a sudden negative shift of the extracellular potential (Rader and Lanthorn, 1989), due to the entrance of cations into cells making the extracellular space more negative.

2.11 Immunohistochemistry

Immunohistochemistry was used either to identify recorded cells or to study the receptor subunits present in brain sections.

2.11.1 Tissue sections

Sprague-Dawley rats, at postnatal day 12 (P12), were used for the preparation of cerebellar and corpus callosum brain slices. An animal was sacrificed, and the brain was removed as described in section 2.1.1. Either part of the cerebellum or a brain volume including the corpus callosum were prepared as described in sections 2.1.1 and 2.1.3, and was then immersed in 4% paraformaldehyde in phosphate buffered saline and left overnight in the fridge. For larger brain regions, slight agitation for an hour prior to the placing in the fridge gave better fixation of the tissue. The brain sample was then washed three times (each time for half an hour) at room temperature in phosphate buffered saline, with slight agitation, and was then prepared for slicing as described in sections 2.1.1 and 2.1.3, except that sections were made 50-100 μm thick and slicing was done at room temperature in 0.1M PBS.

2.11.2 Antibody labelling

Sections either from fixed recorded slices (225μm thick) or fixed sectioned slices (50-100μm thick) were first treated with a blocking and permeabilizing solution, containing 10% goat serum (or donkey serum, when goat primary antibodies were used), 0.05% Triton X-100, 0.05% NaN_3 and 0.1M PBS (for O4 sulfatide primary antibody Triton was omitted from the solution), for 4-6 hrs at room temperature with slight agitation. This was then followed by an incubation with a primary antibody (see table 2.1 for information on antibodies and concentrations) in phosphate buffered saline containing 0.05% NaN_3 for 12-18 hrs at room temperature with slight agitation. Then, slices were washed three times for 20 min with 0.1M PBS. To reveal labelling with primary antibody, a secondary antibody was used which was appropriate for the species that the primary antibody was raised in. Secondary antibodies were conjugated to a fluorophore molecule (see table 2.2). The slices were incubated in secondary antibody (for type and concentration see table 2.2), diluted in 0.1M PBS containing 0.05% NaN_3, for 8 hrs at room temperature with slight agitation, then the slices were washed 3 times for 20 min. Slices were then either mounted on a microscope slide or stained again for

the second primary antibody (when doing double labelling experiments), by using the protocol described above except that the blocking and permeabilizing step was omitted. In some cases the slices were also incubated for 10 min at room temperature with 300nM DAPI (Molecular Probes) diluted in 0.1M PBS, to reveal cell nuclei.

Three types of control experiment were done for the antibody labelling. First, I always tested the effect of omitting the primary antibody. Second, when available, a blocking peptide was incubated with the primary antibody (at 10 times the antibody concentration, for 8 hours at room temperature with light agitation) prior to the normal protocol for incubation of the antibody with the tissue. Third, a normal rabbit or mouse IgG (not raised against anything, from Vector) was used to further check for unspecific staining (it was used at the same concentration as the primary antibody and the normal labelling protocol was followed). When dual labelling was carried out, an extra control was added to the protocol: not only did I test the effect of omitting both antibodies and just adding the two secondary antibodies, but I also incubated slices with just one of the two primary antibodies, but with both secondaries (this was done for each primary used). In this way, I could make sure that there were no interactions between the second secondary antibody and the first primary antibody or vice versa.

All slices were finally mounted on a microscope slide (BDH) with Citifluor (glycerol/PBS, Citifluor), covered with a 0.17mm thick glass cover slip, and sealed with nail varnish (Boots, UK).

2.11.3 Confocal imaging and set up

All fixed slices were imaged in a confocal laser scanning microscope (LSM) . The confocal microscope was either a Zeiss LSM 510 inverted microscope or a Zeiss LSM Pascal upright microscope. For high resolution images a 63x oil DIC objective was used; for low magnification images a 10x DIC objective was used.

All imaging with multiple wavelengths was done with sequential scans at the different wavelengths, even if there was a good separation between the excitation and emission wavelengths on the fluorescence signals, in order to minimise "bleed through"

from one signal to the other. The argon laser line 488nm was used to excite FITC and Alexa 488 fluorophore containing antibodies (see table 2.3 for excitation and emission wavelengths, and filters used) and the 458nm laser line of the argon laser was used for Lucifer yellow detection (see table 2.3). The HeNe laser 543nm line was used for rhodamine, Alexa 555 and Cy3 fluorophore containing antibodies, and the 633nm line (only available on the LSM 510 microscope) was used for Cy5 and Alexa 568 containing secondary antibodies. The ultraviolet laser 364nm line of the LSM 510, or the 405nm diode line 405 of the LSM Pascal was used for detection of DAPI.

Scanning was done in x-y and z directions, and averaged 2-4 times depending on the signal. The size of the z stack depended largely on the depth of the cell of interest, ranging from 15-90μm, taken in 0.2μm sections. Gain and offset were initially set for each image depending on the signal being detected, and those settings were then held constant for the control slices. Projections of images were done in LSM Examiner software, and control slices were treated in the same way with respect to brightness and contrast adjustments.

2.12 Western blotting

Sprague-Dawley rats, at postnatal day 12 (P12), were used for the preparation of optic nerve and corpus callosum. The optic nerve and corpus callosum were dissected and immediately put into Eppendorf bottles containing 2% SDS (sodium dodecyl sulphate), in distilled water. The brain specimens were then sonicated until fully dissolved. They were then added to a sample buffer (comprising 80mM Tris-HCl at pH 6.8, 100mM dithiotreitol, 10% glycerol, 2% SDS and 0.1% bromophenol blue) in two dilutions (3x and 10x) and loaded on to an SDS-PAGE gel with running buffer (25mM Tris, 250mM glycine (pH 8.3, 0.1% SDS) and left to run overnight, at room temperature. Then the SDS-PAGE gel was placed against pre-wetted nitrocellulose membrane with three pieces of Whatman 3MM filter paper on each side, forming a "sandwich" which was placed in a BioRad western blot cassette. This procedure was carried out with all components wet with transfer buffer (50mM Tris, 380mM glycine,

0.1% SDS and 20% methanol). Transfer was carried out in a BioRad Western blotting apparatus with transfer buffer, at 300mA for 3 hours. After transfer, the nitrocellulose membrane was stained with 0.1% Ponceu S in 5% acetic acid, and the positions of protein lanes and molecular weight markers were marked with a pencil. The membrane was blocked with: 4% Marvel milk in 0.01% Tween-20 and 0.1M PBS solution for 4 hrs at room temperature with slight agitation. Primary antibodies (mouse anti-MBP (1:650, Chemicon), rabbit anti-NG2 (1:500, Chemicon), mouse anti-NR1 (1:500, Chemicon), rabbit anti-NR1 (1:1000, Chemicon) were then added and left to incubate overnight at 4°C with slight agitation. The excess antibodies were washed off three times for 10 min in the milk solution, followed by a wash in solution containing only 0.1M PBS. Secondary antibodies coupled to horse radish peroxidase (HRP) were added: these were donkey anti–rabbit (1:5000, Chemicon) and goat anti-mouse (1:5000, Chemicon). They were left to react with the primary antibodies for an hour at room temperature. The membrane was then again washed four times in milk solution for 10 min each time. The secondary antibodies were detected by application of SuperSignal West Pico chemiluminescent substrate for HRP. In a dark room, an exposure film was then placed down on top of the membrane for a minute and then the film was removed and developed.

2.13 Data analysis and statistics

Data are presented as mean $\pm$ s.e.m. and the significance of changes was normally assessed with 2-tailed Student's t-tests. T-tests were either paired, as when analysing whether events within the same group of cells had altered over time or with a drug treatment, or unpaired, as when comparing whether the mean responses of different groups of cells were significantly different. Prior to applying an unpaired t-test, an F-test was applied to address whether the two sets of data had significantly different variance or not (i.e. heteroscedastic or homoscedastic). When the data did not follow a Gaussian distribution, I used the non-parametric Mann-Whitney test. When comparing three groups, instead of two, a one-way ANOVA was used followed by a

Tukey post hoc test. In addition, a Chi-squared test was used when comparing the ratio of occurrence of events between groups of cells, and Yates' correction for continuity was applied due to the small size of the sample groups.

Primary Antibody	Immunogen	Labels	Dilution	Supplier
Myelin Basic Protein (MBP)	Mouse IgG Rat IgG	Mature oligodendrocytes	1:100	Chemicon
O4 Sulfatide	Mouse IgM	Immature oligodendrocytes	1:40	Chemicon
NG2	Rabbit, poly Ig	Oligodendrocyte precursors*	1:200	Chemicon
NG2	Guinea pig poly Ig		1:100	Dr.Stallcup
GFAP	Rabbit Poly Ig	Astrocytes	1:500	DAKO
Olig 2	Rabbit poly Ig	All oligodendrocytes	1:20000	Dr. Rowitch
Ankyrin	Mouse IgG	Nodes of Ranvier	1:100	Chemicon
NMDA receptor subunits	Mouse IgG	NR1 subunits	1:100	Chemicon
	Rabbit poly Ig	NR2A subunits	1:50	Chemicon
	Rabbit poly Ig	NR2B subunits	1:50	Chemicon
	Mouse IgG	NR3A/3B subunits	1:50	Chemicon
	Goat IgG	NR2D subunits	1:100	Santa Cruz
	Goat IgG	NR2C subunits	1:100	Santa Cruz
GABA receptor subunits	Rabbit poly Ig	β_2 subunits	1:100	Novus biological
	Rabbit poly Ig	α_2 subunits	1:250	Novus biological
	Rabbit poly Ig	β_3 subunits	1:100	Novus biological
	Rabbit poly Ig	γ_2 subunits	1:250	Alpha diagnostic
	Rabbit poly Ig	α_1 subunits	1:100	Upstate
	Goat IgG	β_1 subunits	1:50	Santa Cruz
	Goat IgG	β_3 subunits	1:50	Santa Cruz
	Mouse IgG	$\beta_{2,3}$ subunits	1:100	Chemicon

Table 2.1 List of primary antibodies used for the experiments presented in this thesis, their dilution and supplier.

Secondary Antibody	Anti	Fluorophore	Excitation Wavelength (nm)	Emission Wavelength (nm)	Dilution	Supplier
Goat	mouse IgG	Rhodamine	540	580	1:300	Chemicon
		FITC	490	525		
	mouse IgM Fab fragment	Rhodamine	540	580	1:150	
		FITC	490	525		
	Rabbit	Rhodamine	540	580	1:1500	
	Rabbit	Alexa 555	553	569	1:200	Molecular probes
	Rat IgG	Cy3	553	575	1:400	Jackson laboratories
	Mouse IgG	FITC	490	525	1:100	
	Guinea Pig	FITC	490	525	1:100	
	Guinea Pig	Cy5	651	674	1:100	
Donkey	Goat IgG	FITC	490	525	1:200	Molecular probes

Table 2.2 List of secondary antibodies for the experiments presented in this thesis, their dilution and supplier.

Fluorophore	Excitation Wavelength (nm)	Emission Wavelength (nm)	Laser	Excitation Line (nm)	Emission Filter (nm)
Rhodamine	540	580	HeNe Laser	543	LP 560
Alexa 555	553	569			
Cy3	553	575			
Cy5	651	674		633	LP650
FITC	490	525	Argon Laser	488	BP505-530
Lucifer Yellow	428	540		458	BP505-600
DAPI	360	460	Diode	405	LP 420
	360	460	UV	364	LP 385 BP 385-470

Table 2.3 List of various fluorophores used, along with their peak excitation and emission wavelengths. In addition, the table gives information on what laser, and laser line were used for confocal imaging as well as the filters used.

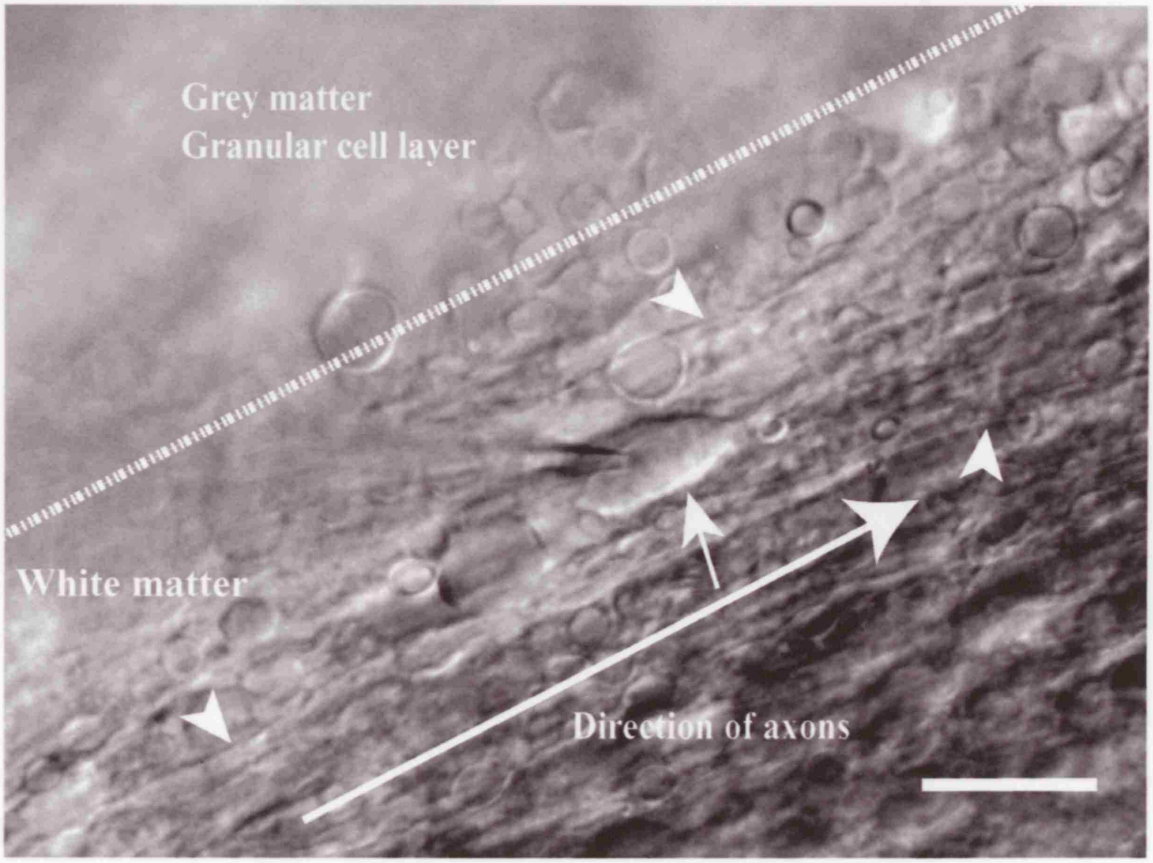

Figure 2.1 Whole-cell clamped oligodendrocyte in the white matter of a cerebellar slice, visualized with DIC optics. Many parallel axons (two of which are indicated with arrowheads) run in the direction indicated by the long arrow. The electrode is attached to an oligodendrocyte soma (small arrow). These somata tended to be oval, and to lack visible processes (although processes are in fact present, as seen for the dye-filled cells presented later in this thesis). Scale bar 20 μm.

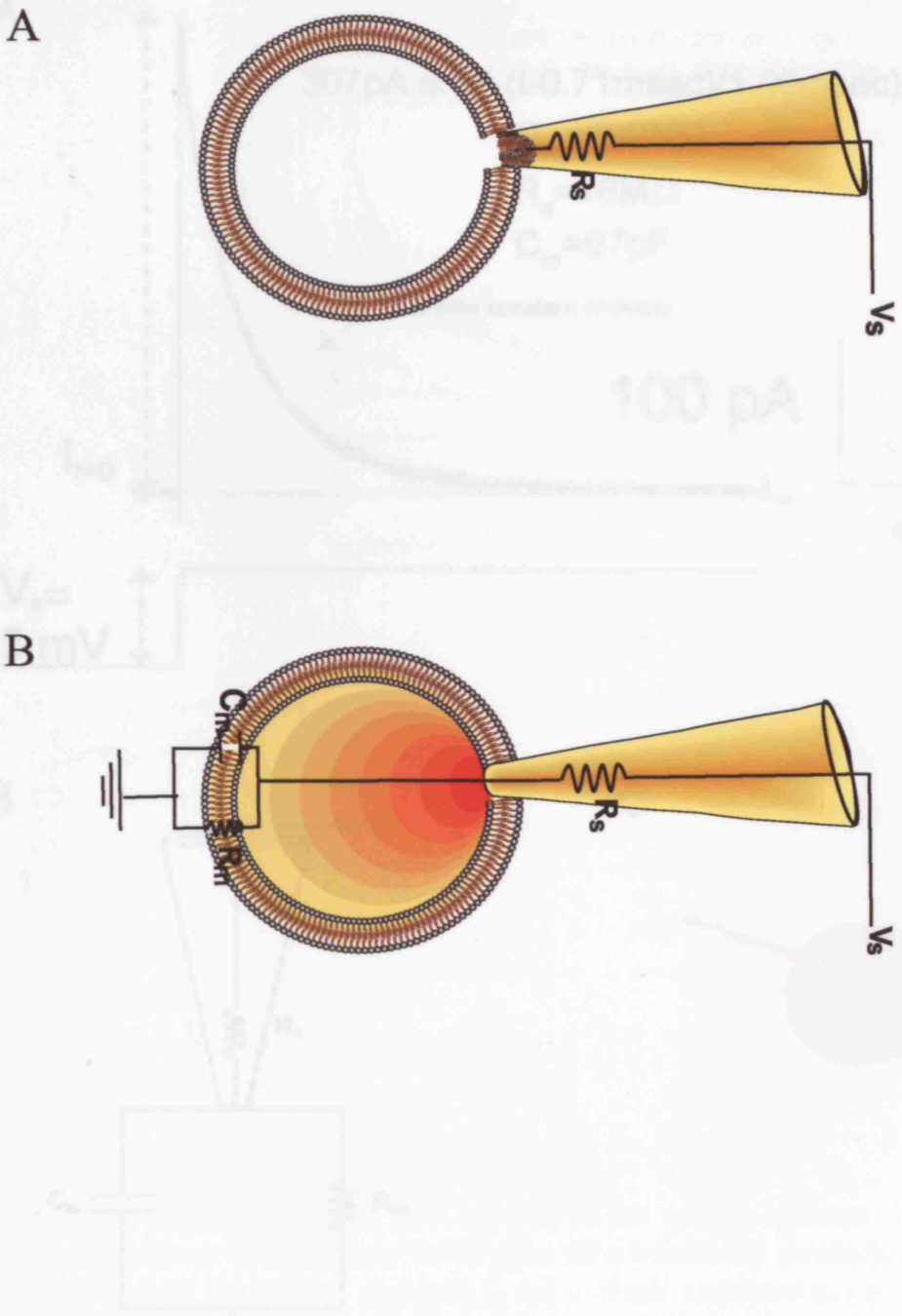

Figure 2.2 Diagrammatic representations of patch clamp configurations and the electrical circuit diagram of the pipette and cell. **A** Seal formation, where the patch pipette is attached to the outside of the cell membrane. Very little current flows through the cell, as the membrane attached to the pipette forms a high resistance. However a small current will flow through the seal with the membrane and across the high resistance patch. **B** Whole-cell configuration, where the patch of membrane under the pipette is ruptured, producing a current pathway between the pipette and the cell that is freely permeable to all molecules present within the pipette, leading inevitably to dialysis of the cell with the contents of the pipette. Here current can flow through the cell and the membrane voltage or current can now be clamped and controlled by an amplifier. Vs is a step of voltage applied to the pipette, Cm is the capacitance of the cell membrane. Rs is the series resistance of the pipette and Rm is the resistance of the membrane.

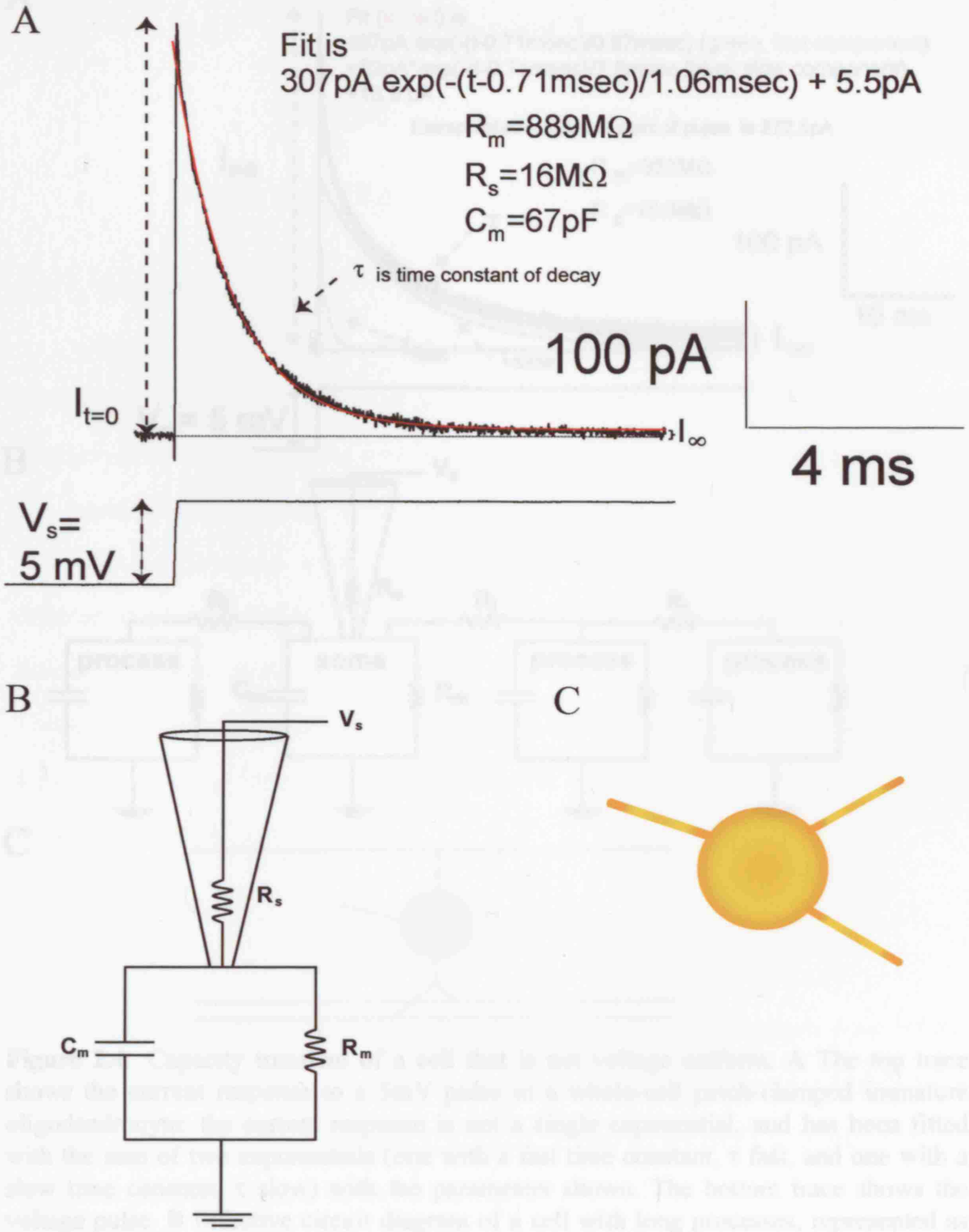

Figure 2.3 Measurement of capacitance of a spatially compact cell. **A** The top trace shows the current response to a 5mV pulse in a whole-cell patch-clamped spatially compact precursor oligodendrocyte. The bottom trace shows the applied voltage step, V_S. **B** Cell membrane circuit of a cell that is spatially compact, so that its capacity transient can be fitted with a single decaying exponential. **C** A schematic diagram of a spatially compact precursor oligodendrocyte, with short processes. Measuring the capacitance: the current just after the onset of the voltage step, $I_{t=0}$ is found by extrapolating from fitting the decay with a single exponential. The fit gives a $I_{t=0}$ of 307.5 pA, a steady state current I_∞ of 5.4 pA and a decay time constant, τ of 1.06 ms. This implies a series resistance of 16 MΩ (from equation 2.10), while equation 2.12 gives a membrane resistance of 889 MΩ and from equation 2.13 the membrane capacitance was found to be 67pF.

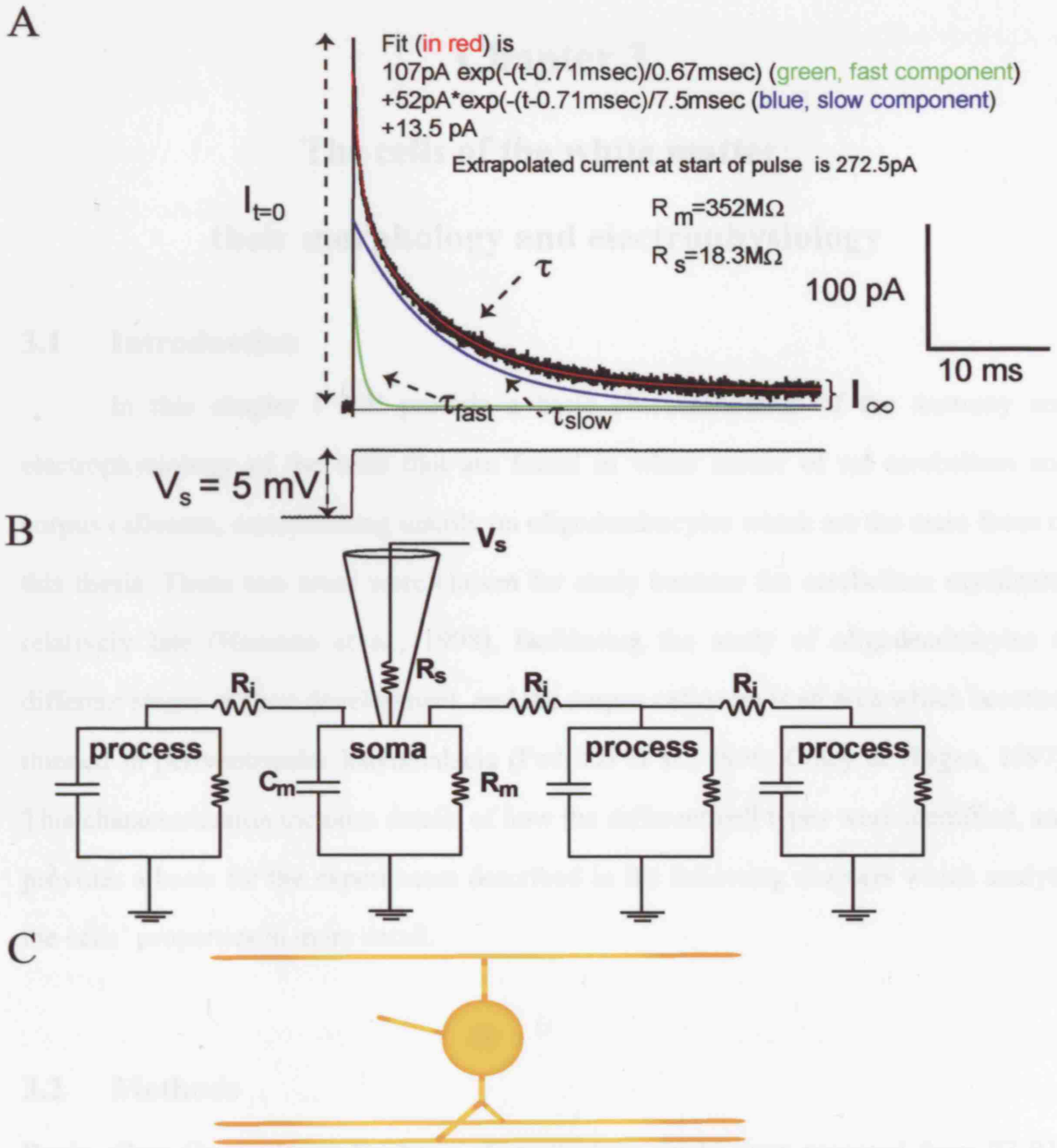

Figure 2.4 Capacity transient of a cell that is not voltage uniform. **A** The top trace shows the current response to a 5mV pulse in a whole-cell patch-clamped immature oligodendrocyte: the current response is not a single exponential, and has been fitted with the sum of two exponentials (one with a fast time constant, τ fast, and one with a slow time constant, τ slow) with the parameters shown. The bottom trace shows the voltage pulse. **B** Effective circuit diagram of a cell with long processes, represented as electrical RC compartments in addition to the soma, which result in the membrane potential being non-uniform. Ri is the intracellular resistance along the cell processes. This circuit would generate a multi-exponential capacity transient. **C** A schematic diagram of an immature or mature oligodendrocyte, showing the processes that generate the distant electrical compartments in B. To measure the series resistance the current at the time of the pulse (0.71 msec in the example above, but denoted $I_{t=0}$) is found by extrapolation after fitting the decay with the sum of two exponentials. The fit gives an $I_{t=0}$ of 172.5 pA, I_∞ of 13.5 pA and two exponentials with amplitudes and time constants as shown in A. The value of $I_{t=0}$ gives a series resistance of 18.3 MΩ (from equation 2.10), and equation 2.12 gives a membrane resistance of 352 MΩ. It is not possible to calculate the capacitances of the different compartments nor the values of the resistances along the processes.

Chapter 3

The cells of the white matter:

their morphology and electrophysiology

3.1 Introduction

In this chapter I will provide a basic characterization of the anatomy and electrophysiology of the cells that are found in white matter of rat cerebellum and corpus callosum, concentrating mainly on oligodendrocytes which are the main focus of this thesis. These two areas were chosen for study because the cerebellum myelinates relatively late (Hamano et al., 1998), facilitating the study of oligodendrocytes at different stages of their development, and the corpus callosum is an area which becomes thinned in periventricular leukomalacia (Fedrizzi et al., 1996; Coley & Hogan, 1997). This characterization includes details of how the different cell types were identified, and provides a basis for the experiments described in the following chapters which analyse the cells' properties in more detail.

3.2 Methods

Brain slices Cerebellar or forebrain slices (225μm thick) were prepared from P7-P14 rats as described in Section 2.1. Slices were superfused at 24±1°C with HEPES-buffered solution, containing (mM): 144 NaCl, 2.5 KCl, 2 $MgCl_2$, 10 HEPES, 1 NaH_2PO_4, 2.5 $CaCl_2$, 10 glucose, pH adjusted to 7.4 with NaOH.

Recording & cell identification White matter cells (avoiding the cerebellar nuclei when working on cerebellar slices, since these contain neurons) were whole-cell clamped with pipettes containing a K^+-based solution comprising (mM): 130 KCl, 4 NaCl, 0.5 $CaCl_2$, 10 HEPES, 10 EGTA, 2 MgATP, 0.5 Na_2GTP, K-Lucifer yellow 2, pH set to 7.2 with KOH; or a Cs^+-based solution, comprising (mM): 130 CsCl, 4 NaCl, 0.5 $CaCl_2$, 10 HEPES, 10 BAPTA, 2 MgATP, 0.5 Na_2GTP, K-Lucifer yellow 2, pH set to 7.2 with CsOH. The series resistance was 8-20MΩ, before 60% compensation. Cells

were identified from dye-fill morphology and antibody labelling, using the methods of Sections 2.3 & 2.11 as described in detail below. Electrode junction potentials were compensated for, and I-V relations were from responses to 200 msec voltage steps.

Antibody labelling is described in detail in chapter 2, section 2.11.

Statistics These are described in chapter 2, section 2.13.

3.3 Results

3.3.1 The white matter

To determine the prevalence of the major classes of cell present in the white matter of cerebellum and corpus callosum, I labelled the white matter with antibodies against Olig2 (a transcription factor present in all stages of the oligodendrocyte lineage), myelin basic protein (MBP, expressed in mature myelinating oligodendrocytes), the lipid sulphatide O4 (expressed in immature oligodendrocytes), the proteoglycan NG2 (present in precursor oligodendrocytes, but also in vascular cells which were excluded from the following analysis), and glial fibrillary acidic protein (GFAP, an intermediate filament specific to astrocytes). At the same time, DAPI was used to mark the nuclei of all cells, so that the percentage of all cells labelled with each marker could be determined, and antibody to ankrin G (which helps to cluster voltage-gated Na^+ channels at the nodes of Ranvier) was used to define the position of Ranvier nodes. Throughout the following text, positive labelling for a marker will be indicated by the superscript suffix "+" after the label, and an absence of labelling will be denoted by the suffix "-".

Labelling for Olig2 and GFAP showed that the cerebellar white matter at postnatal day p12 in rodents is mainly populated by $Olig2^+$ oligodendrocyte lineage cells, which were 50.7±2.1% of 1220 cells counted, and $GFAP^+$ astrocytes (28.7±4.1% of 249 cells, Fig. 3.1). The remaining 20.6 % of cells are likely to be mainly microglia and astrocytes that do not express GFAP (Walz, 2000; Kimelberg, 2004). In addition, some of the unaccounted for 20.6% of cells are $NG2^+$ but $Olig2^-$ cells found in the white matter, as described below in section 3.3.3 in this chapter.

The marker GFAP, which labels the majority of astrocytes, labels the cerebellum quite uniformly (Fig. 3.2A, B) but the astrocytes are more aligned in the white matter compared to the scattered staining in the grey matter (except for the very distinct pattern reflecting labelling of the aligned processes of Bergmann glia in the molecular layer: Fig. 3.2A, B). The oligodendrocyte lineage marker Olig2 stains the white matter heavily in the cerebellum and marks out beautifully the boundaries of the white matter tracts. However there is some staining in the grey matter, indicating that there are oligodendrocyte lineage cell bodies in the grey matter as well (Fig. 3.2C, D).

By using markers for oligodendrocytes at different developmental stages, I investigated the different distribution and morphology of precursor, immature and mature oligodendrocytes. The precursor marker NG2 interestingly labels not only the white matter but also the grey matter (Fig. 3.2E, F). Although some of these $NG2^+$ cells are associated with the vasculature and are not related to oligodendrocytes, the majority are scattered throughout the neuropil and are distant from the blood vessels. These grey matter $NG2^+$ cells could have the role of being a reserve cell to replace mature oligodendrocytes if they become damaged, as has previously been thought (Cenci Di Bello et al., 1999; reviewed by Reynolds et al., 2002), but is now disputed (Butt et al., 2005). The staining seen with the O4 antibody, which marks immature oligodendrocytes, is more confined within the white matter tracts (Fig. 3.2G, H), and almost no labelling is detectable in the grey matter. The myelin marker MBP, which labels mature oligodendrocytes, is even more confined to the white matter (Fig. 3.2I, J). However MBP^+ processes stretch from the white matter tract far into the grey matter, presumably reflecting the fact that axons are myelinated as they pass into the grey matter (Fig. 3.2I, J). At least some of the myelinating processes seen with MBP labelling at this developmental stage are mature, as labelling with ankyrin G shows quite distinct labelling of the nodes (Fig. 3.2K).

The corpus callosum shows somewhat different labelling with Olig2 and MBP compared to the cerebellum (Fig. 3.3). First, the Olig2 labelling is not well spatially defined, and is fairly uniform throughout both grey and white matter. However, in the white matter the $Olig2^+$ cell bodies tend to be aligned in a row (similar to a string of

pearls), whereas in the grey matter the Olig2$^+$ cell bodies are more scattered (Fig. 3.3 A, B). Secondly, the MBP$^+$ processes are not all aligned in a single direction, as in the cerebellum, but in addition to the general orientation of processes across the corpus callosum, there are also MBP$^+$ processes perpendicular to this direction, presumably reflecting the direction of the axon tracts that they are myelinating. As in the cerebellum there are processes that stretch out into the grey matter, consistent with axons being myelinated some distance into the grey matter. Most notable, however, is the presence of apparently flat patches of MBP$^+$ processes scattered around in the grey matter (Fig. 3.3C, D).

3.3.2 The morphology and electrophysiology of oligodendrocytes

To characterise in detail the morphology of individual oligodendrocytes, these cells were whole-cell voltage clamped at different developmental stages. By including Lucifer yellow in the pipette, which diffuses into the cell and all its processes, the morphology of the cell could be studied and the cell type could be identified. In addition, the presence of Lucifer yellow in the cell allowed me to find the cell again when (after fixation) investigating the cell's protein expression using the antibodies described above and in Section 2.3).

Oligodendrocyte morphology and electrophysiology varies with developmental stage (Figs. 3.4 to 3.6, all the cells of which are from cerebellar white matter). Precursor oligodendrocytes were identified by their simple morphology, i.e. short processes not aligned to axons in the white matter, and their NG2 protein expression (Figs. 3.4A, B, & 3.6A, C). All 15 cells with this morphology, that NG2 antibody was applied to, showed expression of NG2. Immature cells had one or more processes aligned with the axons in the white matter and more than one process that was not aligned with the axons (Figs. 3.4C & 3.6E, G). These non-aligned processes are presumably still growing, and seeking out axons to myelinate (or retracting after unsuccessful myelination). Immature cells were also identified by their O4 expression (Fig. 3.4C). All 6 cells with immature morphology that were tested showed labelling for O4. Mature oligodendrocytes had all

their processes aligned with the axons in the white matter tract (Fig. 3.4D, Fig. 3.6I, K), and expressed MBP (Fig. 3.4D). All 17 cells tested with mature morphology showed expression of MBP.

In addition to the developmental changes of oligodendrocyte morphology and protein expression, there was also a developmental change in the expression of voltage-gated ion channels, although these changes were more complicated than has been portrayed in the earlier literature (see Section 1.4.4.1 for a review). As Figure 3.6 shows, the response of the cells to positive and negative voltage steps could either be ohmic or could show time-dependence produced by voltage-gated channels (described in more detail below). There was a general tendency for the membrane resistance near the resting potential to decrease ($p<0.001$) with maturation (Fig. 3.5A, for which maturation state was defined from the morphology revealed by Lucifer filling), which is similar to what has been reported before (Soliven et al., 1988; Sontheimer et al., 1989). The resting potential was approximately -60mV (-57.5$\pm$2.9mV in 37 mature cells, although without shunting by the electrode seal it would be slightly more negative), which is similar to the membrane potential that Soliven et al. (1988) and Chvatal et al. (1995) reported, but more positive than what Gipson and Bordey (2002) found.

To test more objectively how the electrophysiological characteristics of the cell changed with morphology and hence maturation, I invented a morphology index. The index takes into account several aspects of the organization of the processes of the cells, bearing in mind that as cells become more mature they align their processes more with the axons they are myelinating, and extend their processes along the axon till they reach the node of Ranvier where the next oligodendrocyte will start. Thus maturity can be considered as being related to the length (measured in the direction of the axons), L, of the field of processes put out by the cell, and inversely related to the width, W, of the field of processes (Fig. 3.5C), as more mature cells tend to have long processes with few processes extending perpendicular to the axons, while the precursors have a more "round" field of processes (i.e. with the same length and width). More mature cells also tend to have more processes aligned with axons, and fewer processes that are unaligned and seeking axons to myelinate. Therefore I counted the number of processes parallel to

the axons in the white matter (denoted P) and number of the processes that were not parallel to the axons (denoted S for "seeking"). These parameters were then combined to produce an index that would be large for mature cells and small for precursors, by defining

Morphology Index = $(L/W)\cdot(P+1)/(S+1)$

(the extra value of 1 being added to P and S to ensure that neither ever became zero). I then plotted the membrane resistance at -63mV against this index, which showed a negative correlation (Fig. 3.5B) similar to that seen in Figure 3.5A when stage of maturity was judged simply by looking at the Lucifer fill morphology. Given that it is extremely laborious to label every recorded cell with antibodies to define its developmental stage, this index can be used as a substitute to detect developmental changes in oligodendrocytes.

An interesting aspect of Figure 3.6 is that at each developmental stage not all the cells have the same electrical properties. Comparing the two mature cells shown, while the current-voltage (I-V) relation of Figure 3.6L is ohmic, which resembles what is expected for the time- and voltage-independent potassium conductance reported for mature oligodendrocytes (Chvatal et al., 1995; Gipson & Bordey, 2002), that of Figure 3.6J shows a sag in the current at positive potentials probably produced by a transient potassium conductance (or activation of an inward current). A similar range of behaviour is seen for immature cells. Looking at the I-V relation of Figure 3.6F, it looks remarkably like that of Figure 3.6J except that it has less current flowing at each potential because the input resistance is higher, while the I-V relation of Figure 3.6H is similar to that of Figure 3.6L, as it is ohmic but with a higher input resistance (see Fig. 3.5A for the change of input resistance with maturation). However, the most dramatic difference in current-voltage relations is between the two precursor cells shown. The I-V relation of Figure 3.6D is similar to the ohmic relation seen in the immature and mature cells of Figure 3.6H, L, except with a much higher input resistance. By contrast, the I-V relation of Figure 3.6B is remarkable as at depolarized potentials it shows both a transient inward current and an outward rectifying current, like the ones that have been reported before both in situ (Berger et al., 1991; Steinhauser et al., 1992; Chvatal et al.,

1995; Žiak et al., 1998; Chittajallu et al., 2005) and in culture (Sontheimer et al., 1989; Barres et al., 1990c; Berger et al., 1992a; Knutson et al., 1997; Schools et al., 2003) for precursor oligodendrocytes.

3.3.3 Two different NG2 expressing cells in cerebellar white matter

Analysing this difference in current-voltage relation in the precursors in more detail (Fig. 3.7) it became clear that the $NG2^+$ cells are not a homogenous group of cells, and they fall into two distinct classes expressing one of two sets of ion channels. One type of $NG2^+$ cell generates a large transient inward current when the membrane potential is stepped to depolarizing potentials (Fig. 3.7A), which is similar to the voltage-gated sodium channel current seen in neurons, and this transient inward current is followed by an outward rectifying current. The other type of $NG2^+$ cell shows neither the transient inward current nor the outward rectifying current (Fig. 3.7B). The transient inward current was abolished in the presence of 1μM tetrodotoxin (TTX, which blocks voltage-gated sodium channels, Fig. 3.8A, B), indicating that it is indeed mediated by Na^+ channels.

The 15 $NG2^+$ cells recorded from fell into two classes, those which expressed sodium currents and those which didn't. When the mean I-V relations of the two types of cell were plotted, they showed that, although the two types did not differ in input resistance near the resting potential ($p=0.19$, Fig. 3.10A), the cells expressing voltage-gated Na^+ channels generated a much larger change ($p=0.001$) in the outward current with increasing voltage at positive potentials than those which lack the voltage-gated Na^+ channels. The mean I-V relations with Cs^+ in the pipette are shown in Figure 3.9A. Seven cells without sodium currents (not tested for NG2 expression, but with precursor morphology) were labelled with antibody for Olig2 and all were found to be Olig2 positive: the I-V relation of these selected cells was similar to that for cells without sodium current that were $NG2^+$ (Fig. 3.9A). The larger increase in outward current at positive potentials seen in the sodium channel expressing precursors, compared to those which did not express voltage-gated sodium channels, was even bigger if K^+ was

present in the intracellular pipette instead of Cs^+ (Fig. 3.9B), as is expected if this current is carried by K^+ channels that do not pass Cs^+ so well as K^+. The slope resistance at positive potentials, with intracellular K^+, is quantified in Figure 3.10B.

The two classes of precursors did not differ in membrane resistance near the resting potential (Fig. 3.10A; p=0.19), length of the field encompassed by their processes (p=0.18), width of the process field (p=0.36), or size of the cell body (p=0.11, Fig. 3.10C), however they did differ significantly in their value of morphology index (Fig. 3.10D, p=0.03). The difference in morphology index reflected mainly the fact that cells lacking Na^+ current displayed a slight increase in number (P) of processes arranged parallel to the axons relative to the number (S) of "seeking" processes arranged not parallel to the axons, and the cells lacking Na^+ current had a higher number of "seeking" processes compared to the cells lacking Na^+ current. Another difference between the two cell classes was that the sodium current expressing cells also showed spontaneous synaptic activity: these observations will be discussed in detail in Chapter 7.

Since there are two classes of NG2 cell as defined electrophysiologically, I looked at whether all $NG2^+$ cells express Olig2, to check whether all $NG2^+$ cells are in the oligodendrocyte lineage. Interestingly, not all $NG2^+$ cells were $Olig2^+$ in the white matter of the cerebellum: 82% were $Olig2^+$ and so are presumably oligodendrocyte precursors, while 18% did not express Olig2 and might therefore be suspected of not being (or no longer being) in the oligodendrocyte lineage (Fig. 3.11A, B, E). Looking at the granular layer of the cerebellum, a larger fraction (40%) of the $NG2^+$ cells were $Olig2^-$ than in the white matter (Fig. 3.11C, E), while on the other hand all $NG2^+$ cells in the molecular layer were $Olig2^+$ (Fig. 3.11D, E). These results suggest that there may be more than one role of NG2 cells and further work is needed to determine the exact role of these cells in the white matter and grey matter.

It has been reported that $NG2^+$ cells wrap their processes around nodes of Ranvier (Butt et al., 1999), perhaps suggesting that they respond to passing action potentials (Bergles et al., 2000) or assist the propagation of the action potential. Figure 3.12 shows a $NG2^+$ cell wrapping around a process of an immature oligodendrocyte

filled with Lucifer yellow, raising the possibility that NG2 cells might somehow also assist maturation of oligodendrocytes or myelination.

3.3.4 The morphology and electrophysiology of white matter astrocytes

From the cell counts shown in Figure 3.1, astrocytes (defined as $GFAP^+$ cells, i.e. ignoring any $GFAP^-$ astrocytes) are the second most numerous cell type in the cerebellar white matter, comprising 28.7±4.1% of all cells. Astrocytes tended to have a quite different morphology to oligodendrocytes, with numerous branching processes not necessarily aligned to the axons of the white matter (Fig. 3.13A, B). Another typical feature of astrocytes was that often they were dye coupled to each other ($GFAP^+$ cells) and to other $GFAP^-$ cells (Fig. 3.13B). By contrast such dye coupling was almost never observed for oligodendrocytes. Astrocytes, whether coupled or not coupled, had ohmic I-V relations (Fig. 3.13C, D). Their mean input resistance was 156±76MΩ (n=8) when studied with Cs in the pipette.

3.4 Discussion

The data presented here show that there is little ambiguity in identifying the different types of cell present in the white matter. Astrocytes are quite distinguishable from oligodendrocytes, both from their morphology and electrophysiology, as well as from their expression of specific markers. Cells at different stages of the oligodendrocyte lineage also differ in morphology and electrophysiology, allowing them to be confidently identified and the properties of each developmental stage to be analysed.

Previously $NG2^+$ glia were thought to be oligodendrocyte precursor cells, and their presence in the adult animal was thought to indicate that they could function as a reserve cell which could proliferate and replace mature oligodendrocytes if the latter became damaged in conditions like stroke, spinal cord injury or multiple sclerosis (Cenci Di Bello et al., 1999; Levine et al., 2001; Reynolds et al., 2002). However, it is

now becoming clear that they are probably two distinct cell types which both happen to express NG2. As I have shown in this chapter, there are two types of $NG2^+$ cell with different electrophysiological properties and somewhat different morphology. In addition, 18% of $NG2^+$ cells in the white matter are not labelled by the oligodendrocyte marker Olig2 and 40% were $Olig2^-$ in the granular layer. This result supports the findings of Mallon et al. (2002) who demonstrated two populations of $NG2^+$ cells in the grey matter of the cortex, one population in the oligodendrocyte lineage (slightly less than half of the $NG2^+$ cells) which expressed the PLP gene and another population apparently not of the oligodendrocyte lineage as it did not express the PLP gene.

My data show that all the cells that I tested which lacked voltage-gated sodium current were $Olig2^+$, but this does not imply that cells *with* Na^+ current are $Olig2^-$ because (by chance) I did not successfully label any Na^+ current-expressing cells for Olig2. My results showing two types of NG2 cell in white matter, one of which expresses neuronal-like voltage-gated Na^+ channels, differ somewhat from previous findings. Chittajallu et al. (2004) previously found $NG2^+$ cells expressing voltage-gated Na^+ current, with $NG2^+$ cells in the grey matter expressing more voltage-gated Na^+ current than those in white matter. In addition, Aguirre et al. (2004) showed that some $EGFP^+/NG2^+$ cells transplanted into the hippocampus generated GABAergic interneurons (rather than oligodendrocytes) with voltage-gated Na^+ current, and similarly Dayer et al. (2005) found that some GABAergic interneurons in the grey matter may be derived from $NG2^+$ cells, both of which reports might suggest that, in grey matter at least, $NG2^+$ cells with voltage-gated Na^+ current are destined to become neurons. However, cells expressing voltage-gated Na^+ channels have previously been defined to be oligodendrocyte precursors in situ in the grey (Berger et al., 1991; Steinhauser et al., 1992; Chvatal et al., 1995; Žiak et al., 1998; Chittajallu et al., 2005) and white matter (Chittajallu et al., 2004) and oligodendrocyte precursors in culture also show voltage-gated Na^+ currents (Sontheimer et al., 1989; Barres et al., 1990c; Berger et al., 1992a; Knutson et al., 1997; Schools et al., 2003). In contrast, the $NG2^+$ cells I find that are both $Olig2^+$ and $NG2^+$ showed no voltage-dependent potassium or sodium current, and such a cell has not been described before in the literature: even though

Chittajallu et al. (2004), showed that white matter $NG2^+$ cells had less outward rectifying current and less sodium current then grey matter ones, they still expressed some voltage-gated currents, but the ohmic $NG2^+$ cells that I recorded from did not.

From Figure 3.6 it is noticeable that there is an overall gain in inward current at negative potentials as the oligodendrocytes mature, which has been reported previously (Sontheimer et al., 1989; Berger et al., 1991; Steinhauser et al., 1992; Borges et al., 1994; Chvatal et al., 1995; Knutson et al., 1997; Bernard et al., 2001; Gipson & Bordey, 2002; Chittajallu et al., 2005), as well as a gain in the slowly decaying potassium current seen at positive potentials in immature and mature cells (Chvatal et al., 1995; Gipson & Bordey, 2002). On the other hand, the heterogeneity in the current-voltage relationship at each developmental stage has not been previously reported. From Figure 3.6 is clear that there are almost two sets of "oligodendrocytes" for each maturation stage. Further study is needed to characterize this difference in more detail and try to characterize better the current-voltage relationship in these cells.

Having characterized the basic morphological and electrophysiological properties of the cells in the white matter, in the following chapters I will document their responses to neurotransmitters and simulated ischaemia.

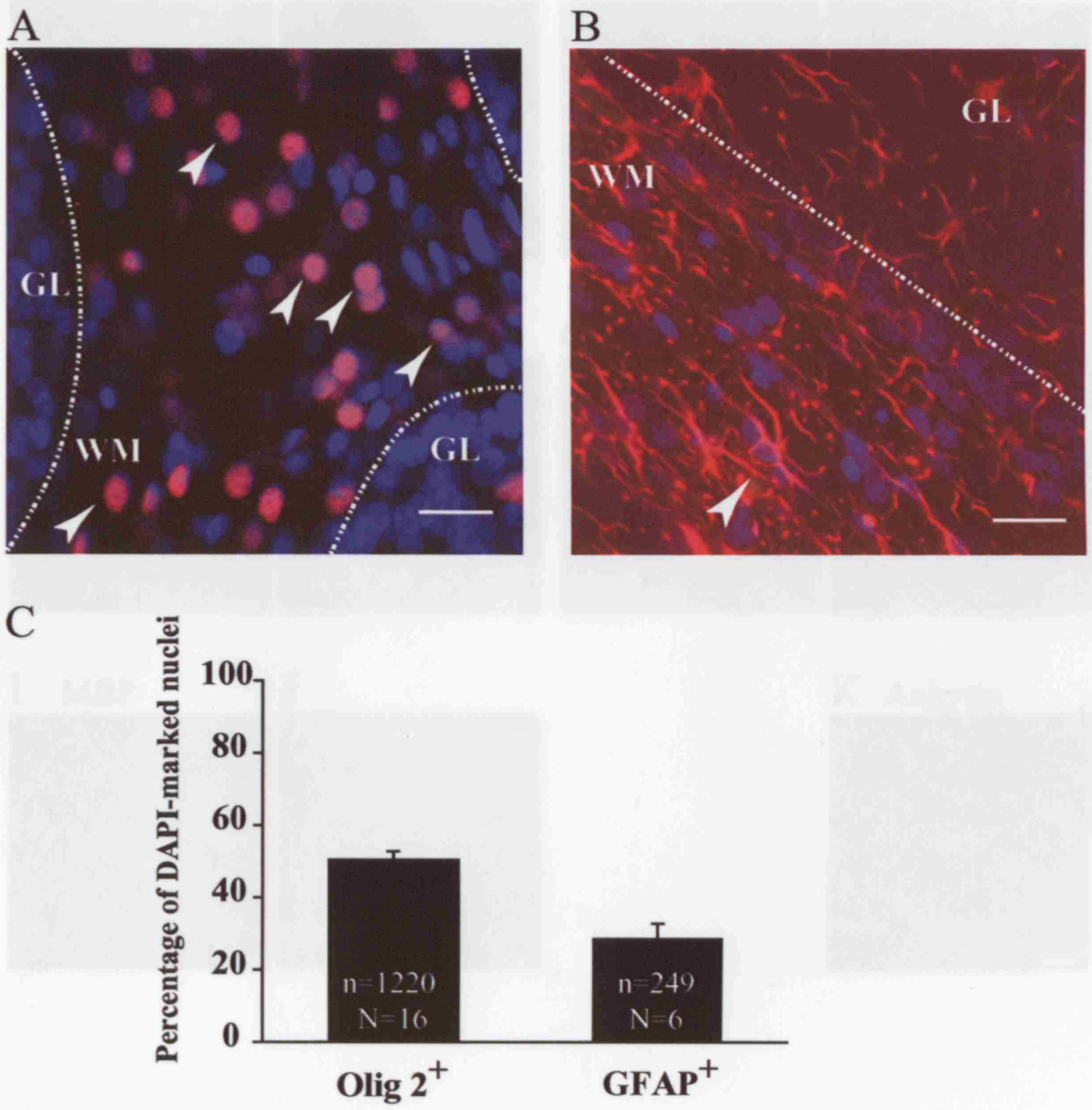

Figure 3.1 Numbers of oligodendrocytes and astrocytes in the cerebellar white matter. **A** Cerebellar slice stained with Olig2 (red, to mark oligodendrocytes) and DAPI (blue, stains cell nuclei); overlap of labelling is purple when both wavelengths are emitted at a similar intensity. **B** Cerebellar slice, stained with GFAP (red, stains astrocytes) and DAPI (blue, stains cell nuclei). Here there is no overlap of labelling as GFAP stains the cytoplasm and processes but not the cell nuclei. An astrocyte is defined when the GFAP staining wraps around a DAPI stained nucleus. Arrowheads show an example of such co-localization. **C** Mean ratios of number of oligodendrocytes to total number of DAPI labelled nuclei, and of number of astrocytes to total number of DAPI labelled nuclei. N is the number of 145µm square areas counted; n is the number of DAPI labelled cells counted. WM white matter, GL granular layer. Scale bar is 20µm.

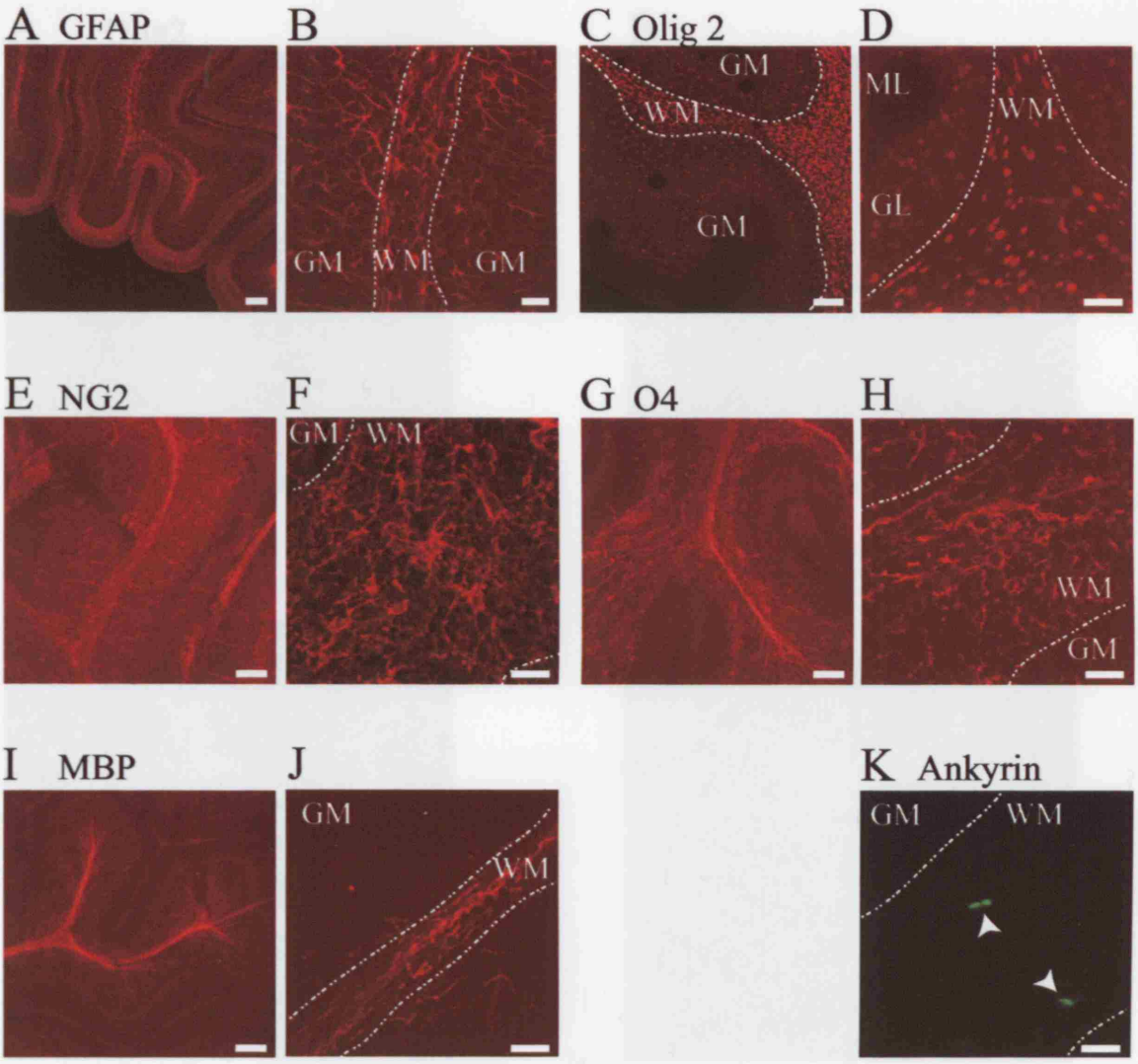

Figure 3.2 Cells in the white matter of the cerebellum at P12. **A** Low magnification view of GFAP staining. **B** High power view of A, where the GFAP staining is seen in the white matter. **C** Low magnification view of Olig2 staining. **D** A higher magnification view of C, where individual cells in the white matter are more visible. **E** Low magnification view of NG2 staining. **F** A higher power view of E, where the NG2 staining is seen in the white matter. **G** Low magnification view of O4 staining. **H** Higher magnification of G, where the O4 staining is seen in the white matter. **I** Low magnification view of MBP staining. **J** Higher magnification view of I, where the MBP staining is seen in the white matter. **K** High magnification view of ankyrin stained white matter, showing two nodes of Ranvier (arrowheads). A,C,E,G,I: scale bars 100μm; B,D,F,H,I,K: scale bars 20μm.

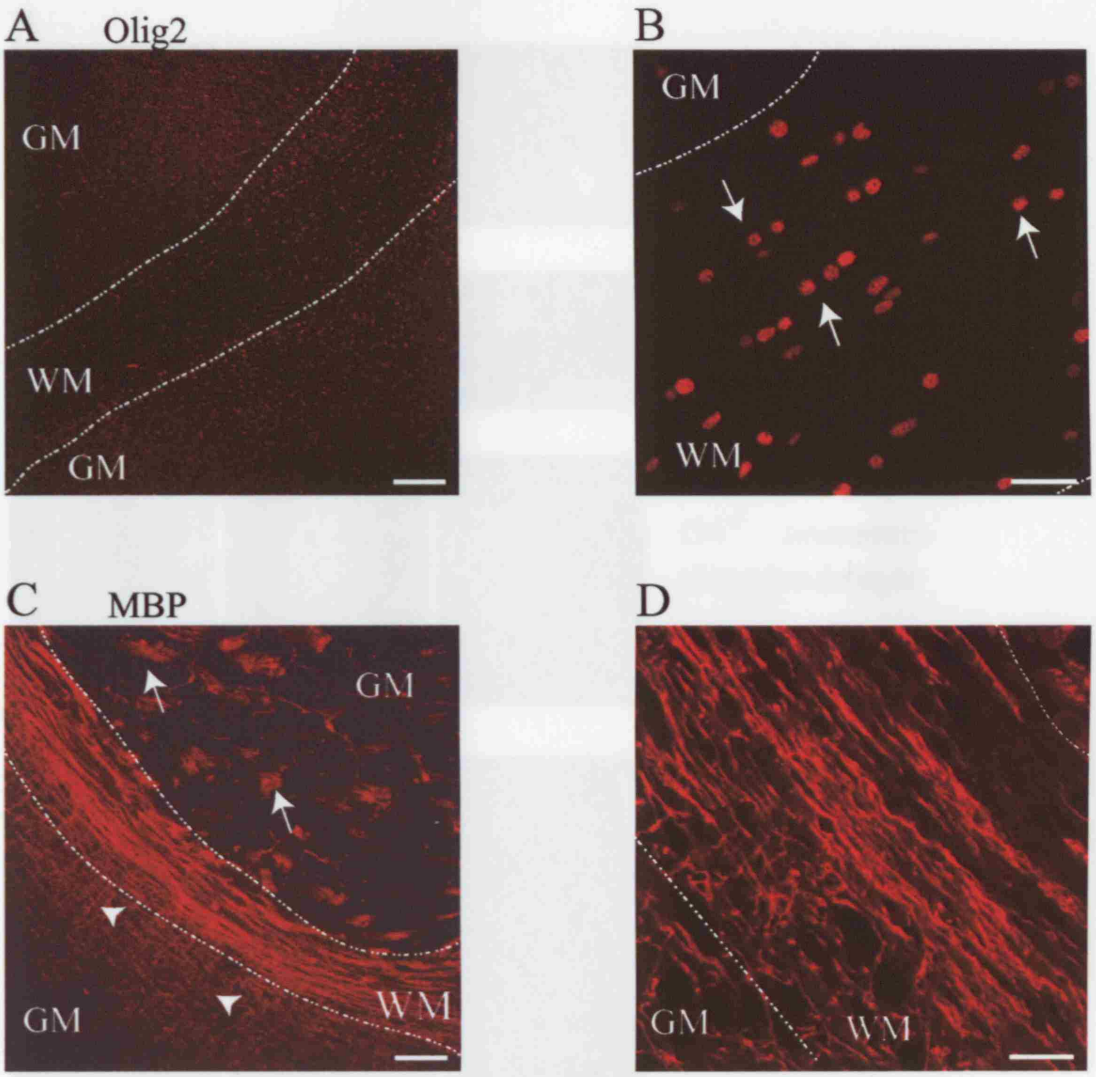

Figure 3.3 Oligodendrocyte-specific markers in the corpus callosum. **A** Olig2 staining: oligodendrocyte cell bodies are not just found in the white matter, but are scattered around the grey matter as well. **B** High magnification view of the white matter in A; notice how the Olig2 positive cell bodies line up in a row (arrows). **C** A low magnification view of corpus callosum stained for MBP; notice the patches of MBP positive staining in the grey matter (arrows) and how the myelinating processes reach far into the grey matter (arrow heads). **D** A higher magnification of C, showing MBP positive cell processes in the white matter. A & C scale bars 100μm, B & D scale bars 20μm. GM, grey matter, WM, white matter.

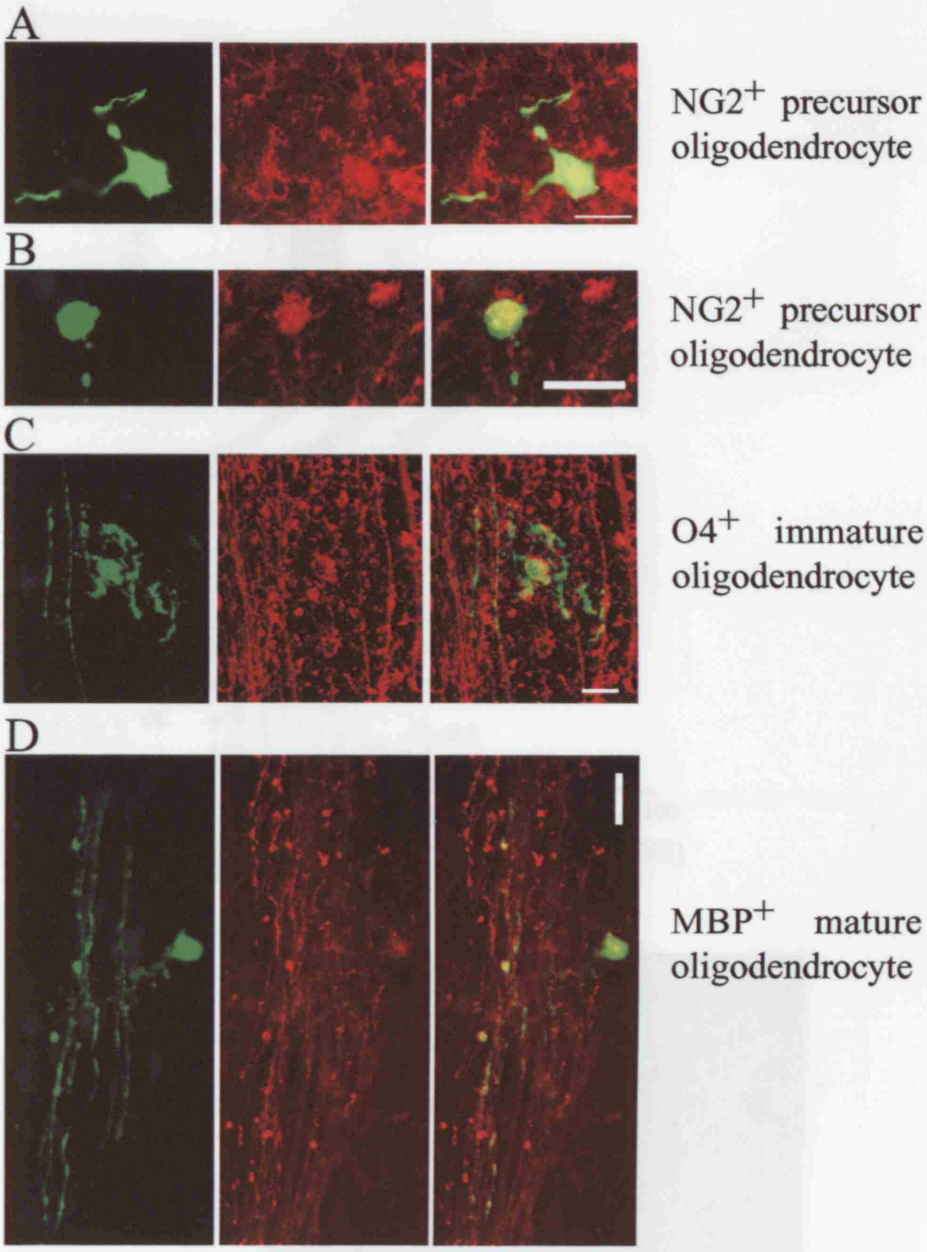

Figure 3.4 Identification of Lucifer yellow filled cells (green) with specific antibodies against proteins expressed at different oligodendrocyte developmental stages (red). **A** & **B** Cells with precursor morphology (green) stained positive for NG2 (see overlay). **C** Cell with immature oligodendrocyte morphology (green) stained positive for O4, notice that some processes are parallel (to axons) and others are not. **D** Cell with mature oligodendrocyte morphology (green) stained positive for MBP. Notice that all its processes are parallel to the axons in the white matter. Scale bar is 20µm.

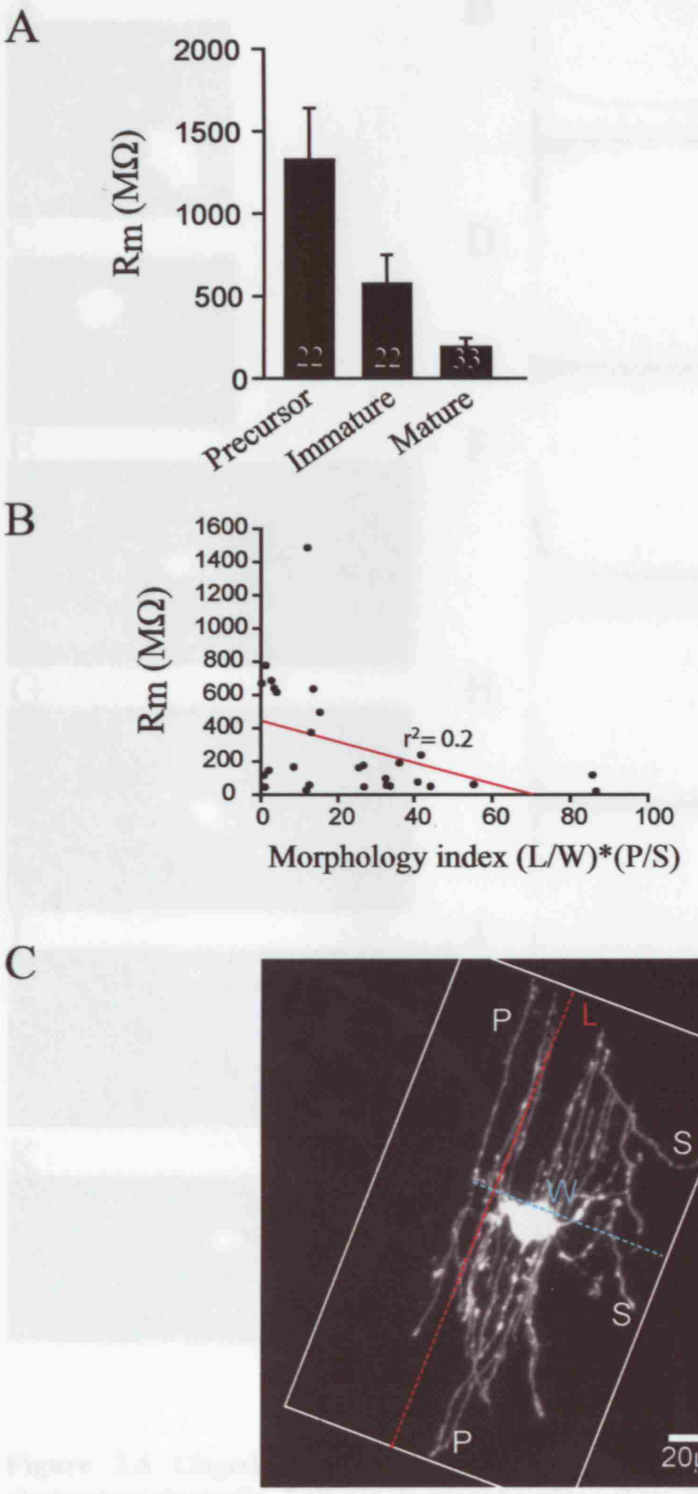

Figure 3.5 Correlation of electrophysiological changes with morphological development. **A** Input resistance decreases significantly with development ($p<0.001$ comparing mature with precursor or immature cells). **B** Membrane resistance decreases with increasing morphology index (defined in text); red line shows linear regression. **C** Example of how the cell length and width were measured. The cell shown is an immature cell as it has some processes "seeking" axons to myelinate (S), as well as parallel processes (P). Length is measured between the furthest distant points of the cell, along the longest axis of the field of processes (white box), as indicated by the red line. The width is measured between the furthest points in the perpendicular direction (blue line).

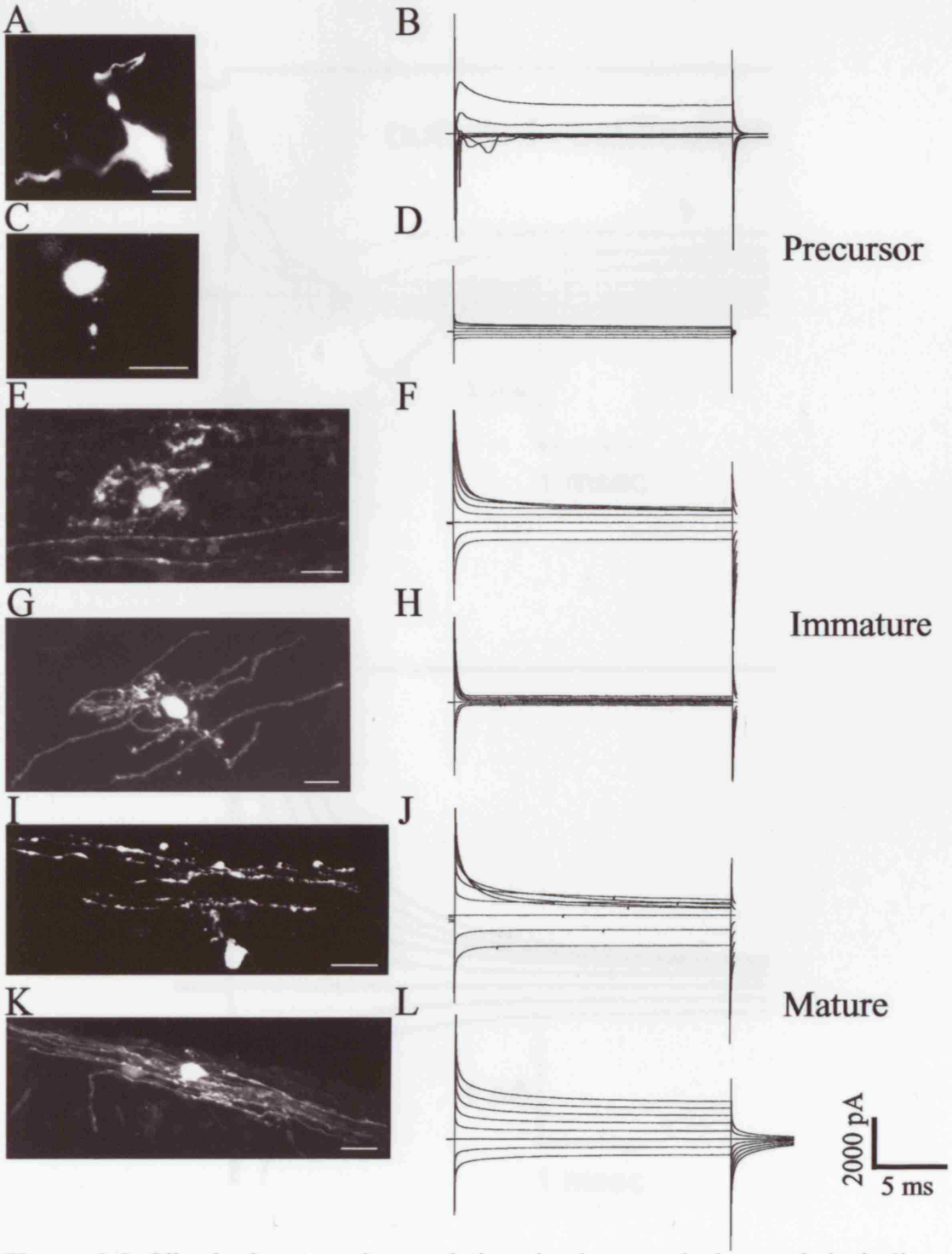

Figure 3.6 Oligodendrocytes change during development both morphologically and electrophysiologically. Left panels show Lucifer yellow fills of cells; right panels show current response of cells to 20mV voltage steps (from a holding potential of -63mV) ranging between -103 and +37mV. **A** & **C** Lucifer yellow filled cells showing precursor morphology but with different voltage gated channel expression. **B** Precursor from A has both voltage-gated sodium and potassium channels, generating a transient inward and a sustained outward current respectively. **D** The precursor shown in B shows a fairly time-independent response to voltage steps (after the capacity transient) but with some sag of outward current at positive potentials. **E** & **G** Cells showing immature morphology, but with different input resistance. **F** The cell in E shows lower input resistance and some sag of outward current evoked by positive potentials. **H** The cell in G has a higher input resistance and no time-dependent current. **I** & **K** Cells with mature morphology, but expressing somewhat different channels. **J** The cell in I shows a sag of outward current at positive potentials. **L** The cell in K is ohmic at all potentials, similar to H but with a lower input resistance. Scale bar is 20μm.

A

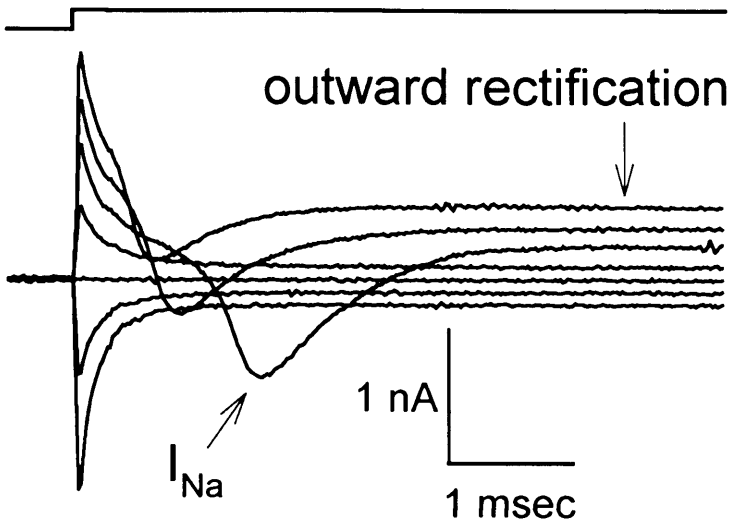

B

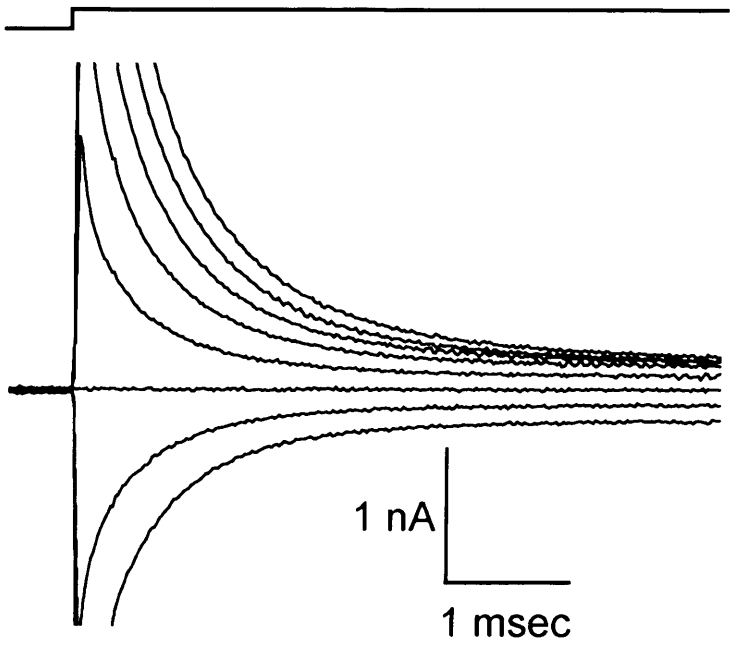

Figure 3.7 The two types of precursor oligodendrocyte current-voltage relationship. **A** A precursor showing voltage-gated sodium current and outward rectifying potassium current. **B** A precursor showing no outward rectifying current and no sodium current.

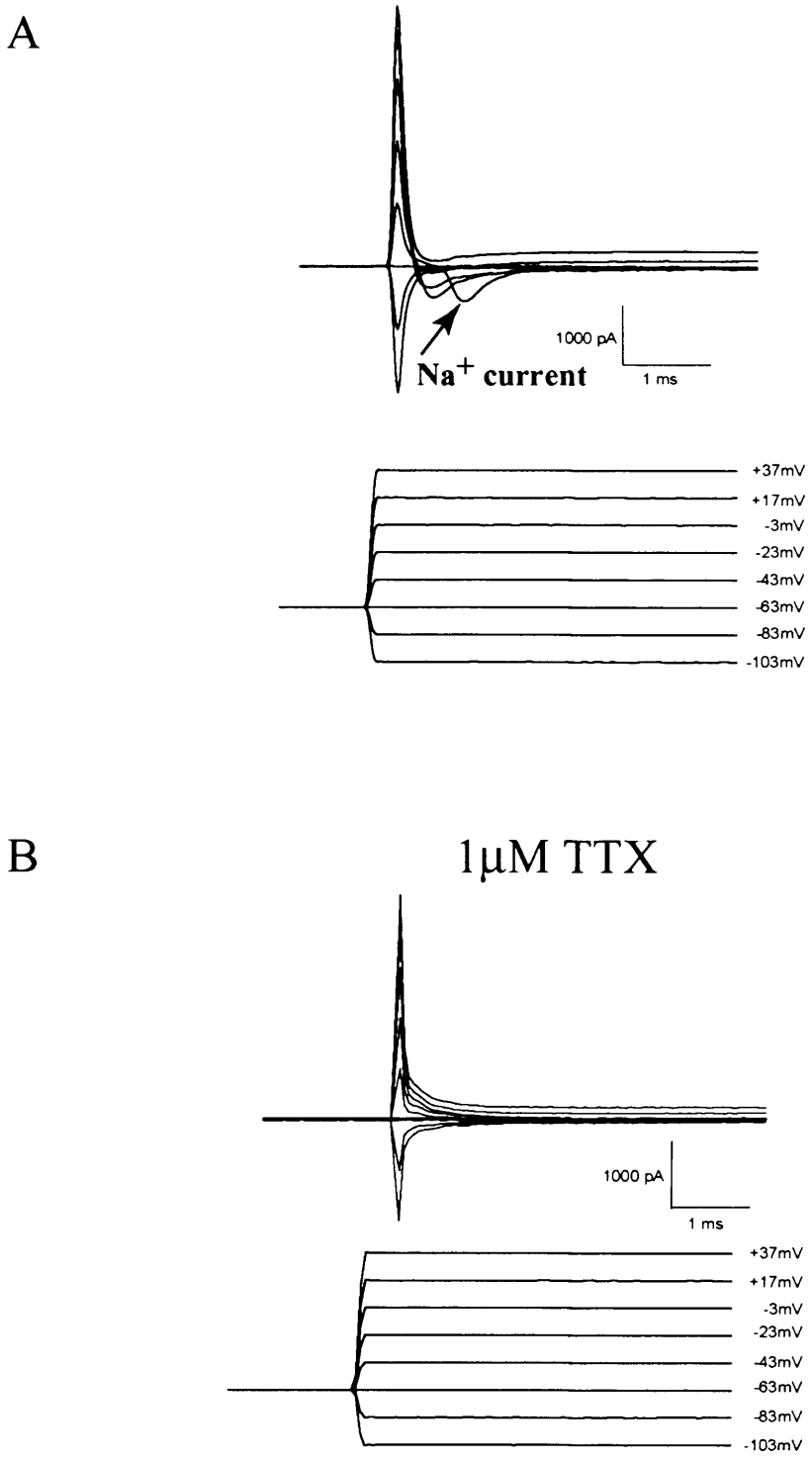

Figure 3.8 In the subtype of oligodendrocyte precursor that expresses voltage-gated sodium channels, TTX blocks the channels. **A** Response of a precursor oligodendrocyte to voltage steps in 20mV increments from a holding potential of -63mV, showing large voltage-gated inward currents at depolarizing potentials. **B** Same cell as in A, but in the presence of 1μM TTX: the large inward current is abolished.

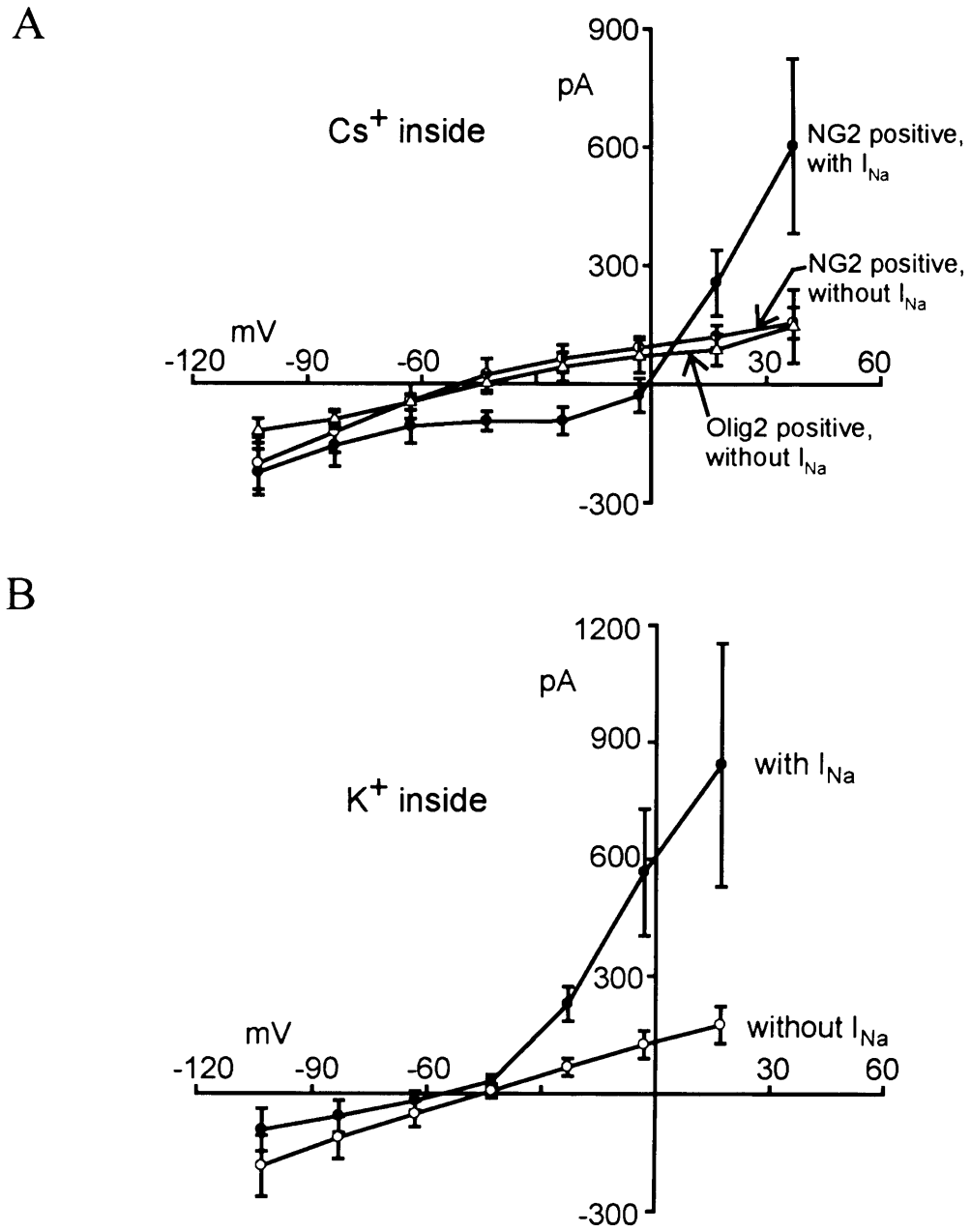

Figure 3.9 Electrophysiological differences between subtypes of precursor cell. **A** Data for cells labelled after recording with antibody against NG2 proteoglycan or Olig2 transcription factor. Mean steady-state current-voltage relationship (with Cs^+ in the pipette) for NG2 positive precursors that showed a voltage-gated Na^+ current (5 cells), NG2 positive cells that showed no Na^+ current (9 cells), and Olig2 positive cells (5 cells, none of which showed any Na^+ current). **B** Data for cells studied with K^+ in the pipette, which were not labelled with antibodies, but were defined by whether they expressed (7 cells) or did not express (11 cells) a voltage-gated Na^+ current. Whether with K^+ or Cs^+ in the pipette, the cells expressing Na^+ current showed more outward rectification at positive potentials.

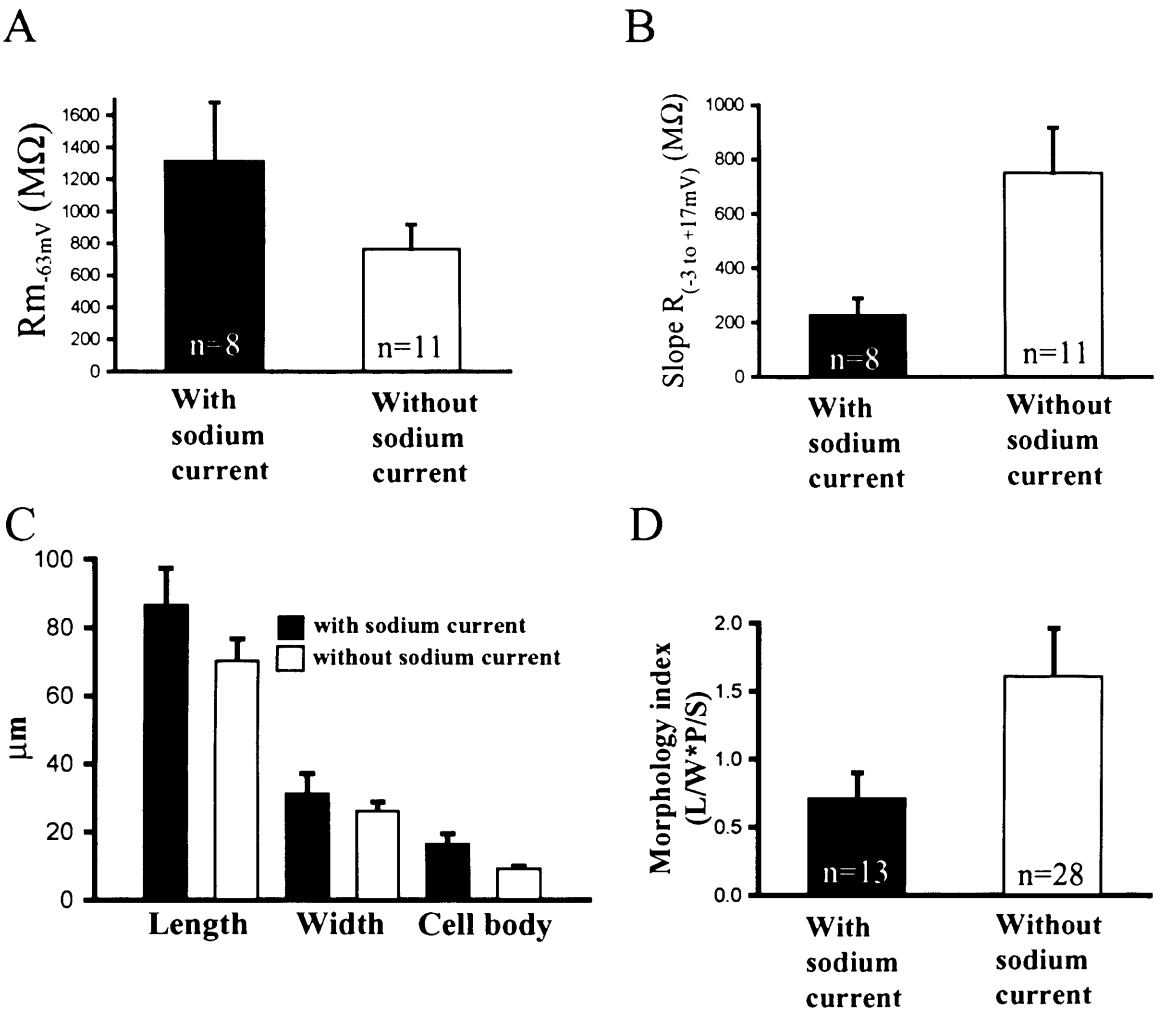

Figure 3.10 Electrophysiological and morphological differences between the two types of precursor. **A** Mean membrane resistance at -63mV in the two types of precursor is not significantly different (p=0.19). **B** Precursors with voltage-gated sodium channels have a lower slope resistance between -3mV and +17mV than cells lacking sodium channels (p=0.01). Both A and B were for cells using the K^+-based internal solution. **C** The two precursors did not differ significantly in the length of the area encompassed by their processes (L in the formula for morphology index: see text), the width (W) of the area encompassed by their processes, or the diameter of their cell body. **D** However, there is significant morphological difference (p=0.03) between the two precursors, according to the morphology index (see text for a definition of this index). This mainly arose from a higher ratio of parallel (P) to "seeking" (S) processes for the cells without a sodium current. C and D include cells studied with Cs^+ or K^+ in the pipette.

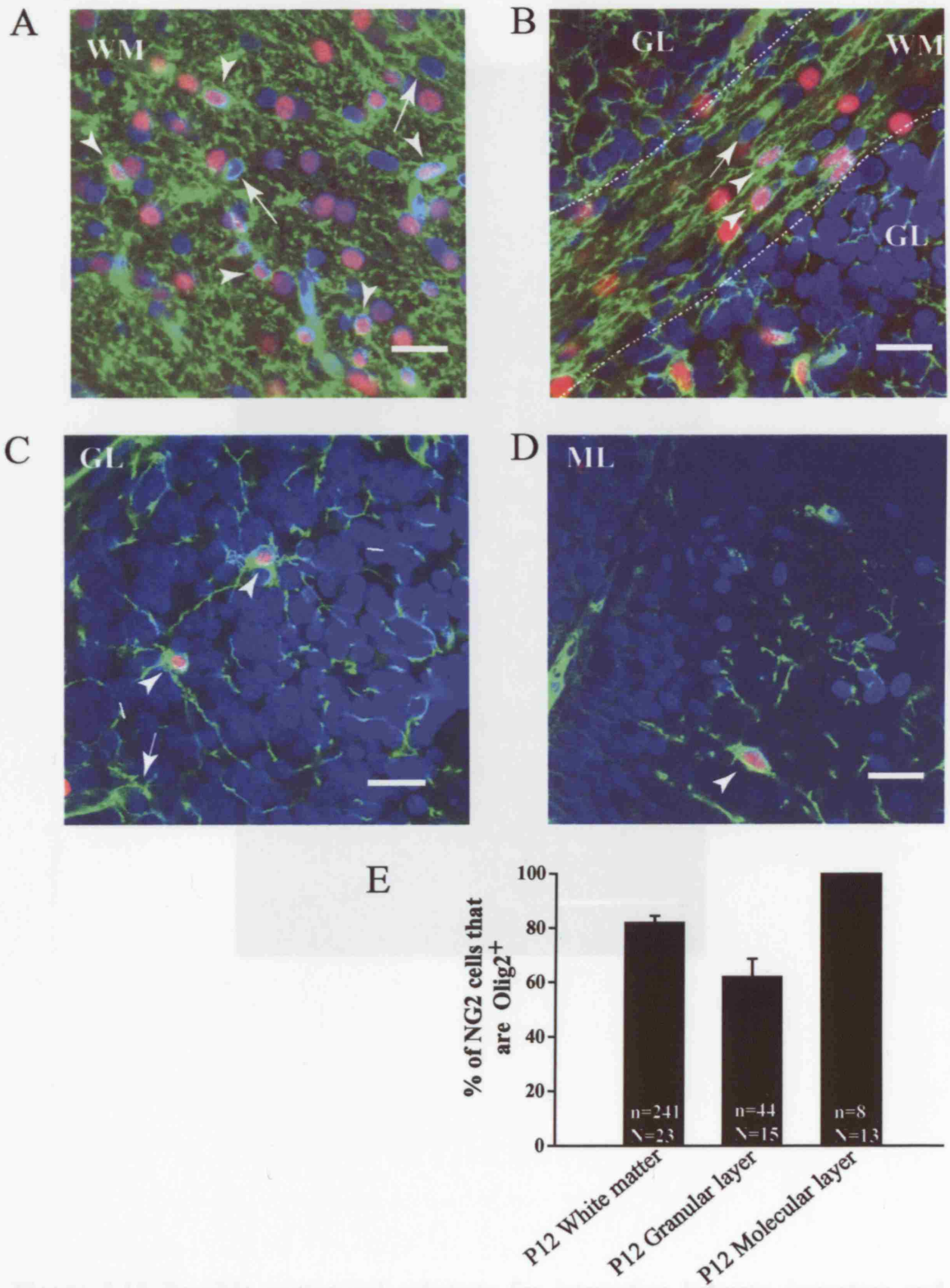

Figure 3.11 Not all NG2$^+$ cells are Olig2 positive. **A**, **B** NG2 (green) and Olig2 (red) staining of the white matter (WM) in the cerebellum, with DAPI (blue) to identify cell nuclei. Arrowheads indicate where NG2 and Olig2 are colocalized; arrows show cells that are NG2 positive but are Olig2 negative. **C** Labelling in the granular layer (GL). **D** Labelling in the molecular layer (ML). E The percentage of NG2 positive cells that are Olig2 positive in the cerebellum at p12. For each area, n is the number of cells counted and N is the number of 145 µm square areas in which counting was done. Scale bar 20µm.

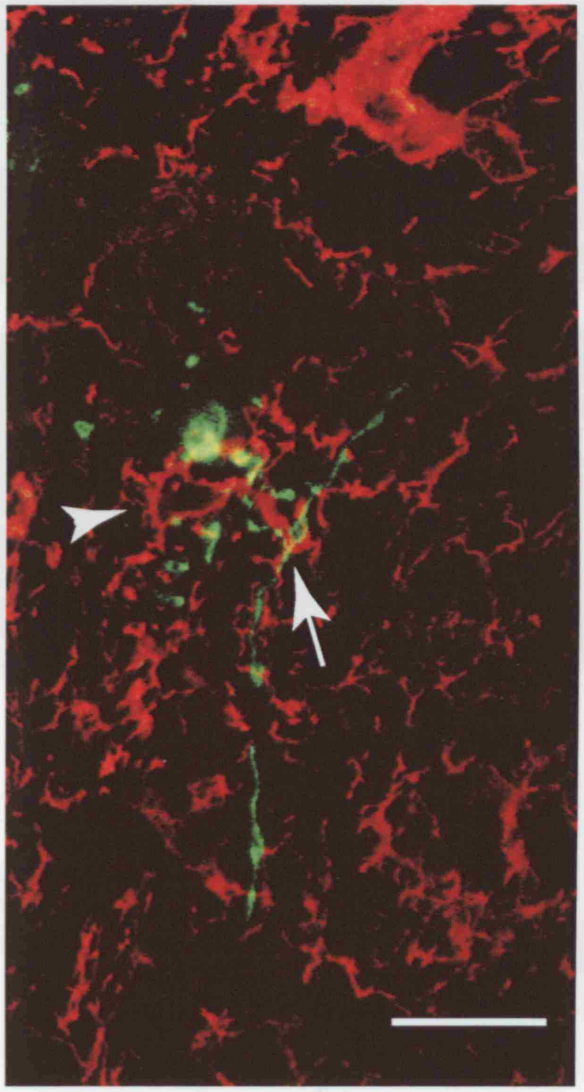

Figure 3.12 Possible anatomical substrate for interaction between immature and precursor oligodendrocytes: an NG2 positive cell wrapping around a process of an immature oligodendrocyte. Picture shows NG2 staining (red) in the white matter of the cerebellum, and a Lucifer yellow filled immature cell (green). Arrowhead points at a cell stained for NG2 and arrow points at the point where the NG2 cell wraps around the process of the immature oligodendrocyte. Scale bar 20μm.

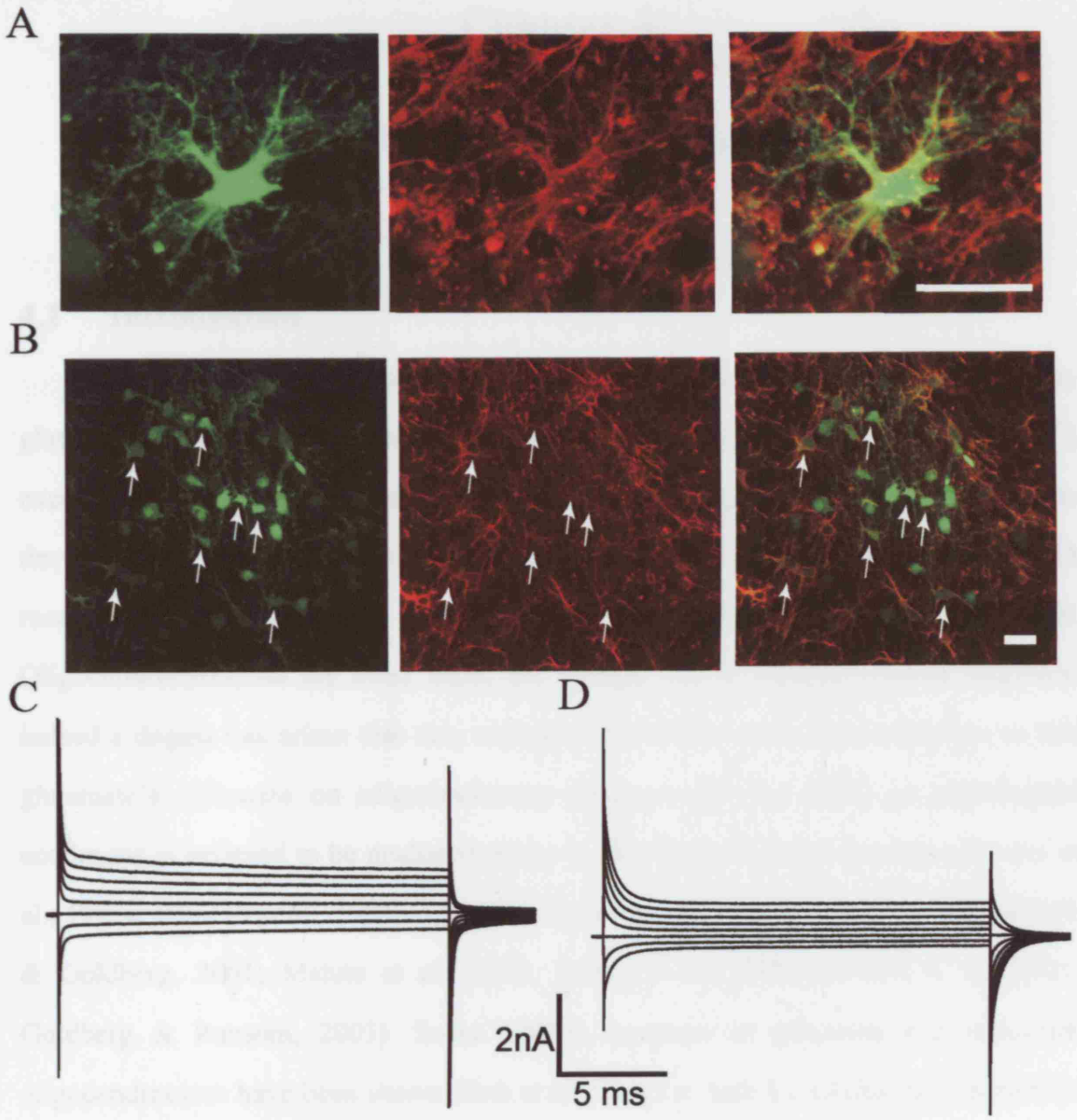

Figure 3.13 Astrocyte morphology and electrophysiology. **A, B** Lucifer yellow (green) filled astrocytes with either no detectable dye coupling (**A**) or extensive dye coupling (**B**). Pictures also show labelling for GFAP (red), so that where GFAP and Lucifer overlap it appears yellow in the overlay. In **B** the arrows show cell bodies clearly labelled for GFAP (arrows). **C** The membrane current-voltage relationship of the cell in **A**, showing the response to 20mV steps from -63mV (ranging from -103mV to +37mV). **D** The membrane current-voltage relationship of the cell in **B**. Scale bar 20μm.

Chapter 4

Glutamate signalling to oligodendrocytes

4.1 Introduction

As described in Chapter 1, excitotoxicity in neurons is mainly generated by glutamate acting on NMDA receptors, allowing Ca^{2+} to enter the cell and raise $[Ca^{2+}]_i$ excessively (Choi, 1988). Furthermore, synaptic strength changes contributing to developmental "wiring" of the neuronal network are also generated in part by NMDA receptors (Collingridge & Bliss, 1995; Herlenius & Lagercrantz, 2004). Oligodendrocytes, on the other hand, are thought not to express NMDA receptors, indeed a dogma has arisen that they express only AMPA and kainate receptors so that glutamate's influence on oligodendrocyte development and death in pathological conditions is believed to be mediated solely by AMPA and kainate receptors (Berger et al., 1992a; Patneau et al., 1994; Stys, 1998; Follett et al., 2000; Pitt et al., 2000; Tekkök & Goldberg, 2001; Matute et al., 2002; Dewar et al., 2003; Groom et al., 2003; Goldberg & Ransom, 2003). Some AMPA receptors in precursor and immature oligodendrocytes have been shown (Itoh et al., 2002) to lack the GluR2 subunit (which is the subunit that makes AMPA receptors calcium impermeable). Thus, when glutamate levels are high, calcium entry through these receptors can lead to calcium overload in oligodendrocytes (Matute et al., 1997).

In spite of the generally held view that calcium-permeable AMPA/KA receptors mediate glutamate's destructive effects on oligodendrocytes, there is some evidence for NMDA receptors in cultured oligodendrocyte precursor cells (Wang et al., 1996) and in spinal grey (but not white) matter (Žiak et al., 1998) oligodendrocytes. Furthermore, NMDA receptor blockers slow the loss of white matter action potentials and reduce white matter damage in ischaemia (Schäbitz et al., 2000; Tekkök & Goldberg, 2001)

and in a model of multiple sclerosis (Wallström et al., 1996). I have, therefore, re-examined which receptors mediate glutamate's actions on oligodendrocytes.

4.2 Methods

Brain slices As described in detail in Chapter 2, cerebellar or forebrain slices were prepared from P7-P14 rats. Slices were superfused at 24±1°C with HEPES-buffered solution, containing (mM): 144 NaCl, 2.5 KCl, 2 $MgCl_2$, 10 HEPES, 1 NaH_2PO_4, 2.5 $CaCl_2$, 10 glucose, 0.1 glycine (to activate the NMDA receptor glycine site), strychnine 0.005 (to block glycine receptors), pH adjusted to 7.4 with NaOH. Omitting glycine or adding D-serine did not affect the NMDA receptor mediated current (see text below). Sometimes Mg^{2+} was omitted (as described below).

Recording & cell identification White matter cells (avoiding the cerebellar nuclei) were whole-cell clamped with pipettes containing a K^+-based solution (for glutamate application) comprising (mM) 130 KCl, 4 NaCl, 0.5 $CaCl_2$, 10 HEPES, 10 EGTA, 2 MgATP, 0.5 Na_2GTP, K-Lucifer yellow 2, pH set to 7.2 with KOH, or a Cs^+-based solution (for NMDA application), comprising (mM) 130 CsCl, 4 NaCl, 0.5 $CaCl_2$, 10 HEPES, 10 BAPTA, 2 MgATP, 0.5 Na_2GTP, K-Lucifer yellow 2, pH set to 7.2 with CsOH. Series resistance was 8-20 MΩ, before 60% compensation. Cells were identified from dye-fill morphology and antibody labelling (see Sections 2.3 & 2.11).

Antibody labelling This is described in detail in chapter 2, section 2.11.

Western blotting This is described in chapter 2, section 2.12.

Post-embedding electron microscopic immunocytochemistry This work was done by my collaborator Linda H. Bergersen. Cerebellar tissue from adult rats (250-300g) was prepared as previously described (Landsend et al., 1997). Antibodies to GFAP (Sigma, 0.5μg/ml) and NMDA NR1 subunits (a gift from R. Wenthold, 0.1μg/ml) were detected with goat anti-rabbit immunoglobulin coupled to 10nm gold particles (GAR10; British BioCell International, Cardiff). Gold particle density was quantified by point counting using an overlay screen (Landsend et al., 1997): to include the majority of particles representing membrane-situated antigenic sites, immunogold particle centres and screen

points within 20nm of membranes were recorded. Particle density over mitochondria in mossy fibre terminals and axon cytoplasm was negligible (see Fig. 4.8E), showing insignificant non-specific background.

Statistics These are described in chapter 2, section 2.13.

4.3 Results

4.3.1 NMDA and AMPA/KA receptors mediate glutamate-evoked currents in oligodendrocytes

At all developmental stages, cerebellar white matter oligodendrocytes responded to glutamate (100μM) with an inward current at -63mV (Fig. 4.1A). The glutamate-evoked current tended to be larger in mature oligodendrocytes (Fig. 4.1A, B). The size of the glutamate response did not differ significantly between cerebellar lobules (at least 2 cells recorded from for each lobule, p=0.4; data not shown). The glutamate-evoked current was not affected by 1μM TTX (p=0.4, Fig. 4.1C, D), showing that axonal action potentials generated by glutamate acting on neurons did not contribute to the current recorded in the oligodendrocytes (e.g. by releasing K^+). (This concentration of TTX is sufficient to block axonal action potentials since it blocked synaptic input from axons to oligodendrocyte precursor cells, as described in Chapter 7). The current was potentiated when the local glutamate concentration was raised by blocking glutamate transporters with TBOA (p=0.016; Fig. 4.1C, D). D-AP5, MK-801 and NBQX all reduced the glutamate-evoked current (Fig. 4.1E, F), suggesting the presence of both NMDA and AMPA/kainate receptors in oligodendrocytes. Blockers of metabotropic glutamate receptors had no effect on the glutamate-evoked current (Fig. 4.1F).

4.3.2 The response of oligodendrocytes to glutamate analogues

NMDA (60μM) evoked an inward current in precursor, immature and mature cerebellar oligodendrocytes (Fig. 4.2A, B). The NMDA-evoked current was largest in mature cells (Fig. 4.2B, p=0.042 compared with precursors), although the increased

membrane area of mature cells may result in the current density being lower. In both corpus callosum (Fig. 4.2C, D) and cerebellum (Fig. 4.2E, F) oligodendrocytes the current evoked by 60mM NMDA was comparable in size (at -63mV in 0mM Mg^{2+}) to the current produced by AMPA (20μM) or kainate (30μM: these agonist concentrations were chosen to be approximately twice the EC_{50} measured for NMDA, AMPA and kainate receptors in neurons). The response to NMDA was much larger than that produced by the metabotropic glutamate receptor agonist (1S, 3R)-ACPD (100μM).

The NMDA-evoked current ran down with time (Fig. 4.3), decreasing by about 35% over 20 mins. Because this rundown was approximately linear with time (Fig. 4.3), for pharmacological studies (Fig. 4.4) the current in drugs was quantified relative to the average of equally spaced preceding and following control responses. The current was blocked by D-AP5 (Fig. 4.4A, C), as expected for NMDA receptors (p values for the effects of TTX and the agents described below are given in the legend to Fig. 4.4). It was unaffected by TTX, like the response to glutamate, ruling out the possibility that NMDA generated a current by evoking action potentials in neurons (Fig. 4.4B, C). The current was also unaffected by NBQX, strychnine or bicuculline (Fig. 4.4C), ruling out an indirect action via AMPA/kainate, glycine or $GABA_A$ receptors. Finally, the current was not significantly affected (p=0.072) when glycine (100μM, with strychnine 5μM) was present, implying that the NMDA receptors' glycine-binding sites are well activated by endogenous glycine or D-serine.

4.3.3 NMDA receptor mediated currents in oligodendrocytes are only weakly blocked by Mg^{2+}

Changing from Mg^{2+}-free superfusion solution to solution containing 2mM Mg^{2+} decreased the NMDA-evoked current at -63mV approximately 3 to 4-fold, independent of developmental age (Fig. 4.5A, B). This decrease is much less than is found for most neurons (Kirson et al., 1999), or for most cloned NMDA receptors (Kuner & Schoepfer, 1996), which show a 60-fold reduction for receptors comprising NR1 and NR2A or 2B subunits and a 20-fold reduction for receptors comprising NR1

and NR2C or 2D subunits. However, the decrease seen in oligodendrocytes is comparable to that seen for cloned receptors comprising NR1, NR2A and NR3A subunits (Sasaki et al., 2002; see arrow in Fig. 4.5B)

In precursor oligodendrocytes the NMDA-evoked current reversed around 0mV (Fig. 4.5C), and in 2mM Mg^{2+} the I-V relation showed a region of negative slope which was similar to, but less marked than, that produced by Mg^{2+}-block of neuronal NMDA receptor channels. In mature oligodendrocytes, however, the I-V relation often failed to reverse at positive potentials (data not shown). This may reflect the NMDA receptors being electrotonically distant from the soma in the cell processes (see below). Alternatively, the Na^{+} entry produced by NMDA receptor activation may lead to block of a K^{+} current in the cell (Borges & Kettenmann, 1995).

4.3.4 Effects of drugs reported to have subunit-selective effects on NMDA receptors

Ifenprodil (10μM), which blocks NMDA receptors containing NR2B subunits (Williams, 2001), had no effect on the NMDA-evoked current (Fig. 4.4C). Neither pregnenolone sulphate (100μM), which potentiates NR1/NR2A and NR1/NR2B receptors by 60-82% but inhibits NR1/NR2C and NR1/NR2D receptors by 32% (Malayev et al., 2002), nor D-cycloserine (1mM) which potentiates NR1/NR2C receptors but inhibits NR1/2A and NR12B receptors (Sheinin et al., 2001), nor D-serine (100μM, in the absence of glycine), which potentiates receptors lacking NR3 subunits but inhibits NR3-containing receptors (Chatterton et al., 2002), had a significant effect on the current (Fig. 4.4C). This suggests the presence of a subunit (perhaps NR3) which suppresses the modulatory actions of drugs which act selectively on particular NR2 subunits, or the presence of a combination of subunits (e.g. NR1/NR2A/NR2C or NR1/NR2/NR3, or a mix of receptors containing different subunit combinations) that these agents modulate in opposite directions.

4.3.5 NMDA receptors are present in myelinating processes

To investigate the localization, and possible subunit composition of the NMDA receptors mediating the currents presented above, I investigated the labelling of cerebellar white matter by antibodies to different NMDA receptor subunits. Labelling of the myelinating processes, and of some cell bodies, of oligodendrocytes was seen using antibodies to NR2C (Fig. 4.6A, B) and, more weakly, NR2D (Fig. 4.6C, D), and this labelling was abolished by omitting the primary antibody, or by preabsorption of the antibody with the peptide to which it was raised. Strong labelling was also seen for NR1 subunits (Fig. 4.6E) and NR3 subunits (Fig. 4.6G), and weaker labelling was seen for NR2B (Fig. 4.6F) and NR2A (Fig. 4.6H), and all this labelling was abolished by omitting the primary antibody. NR1 labelling co-localized with labelling for myelin basic protein in mature cells (Fig. 4.7A). In a Lucifer yellow filled, recorded cell, for which the slice was fixed after recording, NR1 antibody labelled the recorded cell (Fig. 4.7B, done in 3 cells). Double labelling showed partial co-localization of NR1 and NR2C subunits, and of NR3 and NR2C subunits in oligodendrocyte processes (Fig. 4.7 C and D). These data, the lack of ifenprodil block, and the weak Mg^{2+}-block of the NMDA-evoked current, suggest that oligodendrocyte NMDA receptors contain at least NR1, NR2C and NR3 subunits.

Post-embedding electron microscopic immunochemistry (carried out by my collaborator Linda H. Bergersen in Oslo) showed that NR1 subunits were present in the myelinating processes of mature cerebellar oligodendrocytes (Fig. 4.8 A-C), in the outer- and innermost membranes and also within the myelin (perhaps remaining there from earlier in development). Disproving the possibility that antibody associates non-specifically with myelin, GFAP antibody was found to label astrocyte fibrils as expected but not to label myelinating processes (data not shown). By quantifying the immunogold particles in the myelin and in the postsynaptic densities of mossy fibre-granule cell (Fig. 4.8D) and parallel fibre-Purkinje cell synapses, it was found that the density of NMDA receptors throughout the myelin is as high as at the mossy fibre to granule cell synapse (Fig. 4.8E). The density of particles in the outer membrane of the myelin (where the receptors may sense glutamate released from surrounding cells)

tended (p=0.064) to be larger than that in the innermost membrane (where the receptors may sense glutamate released from the axon), but both were similar to the average density measured over all of the myelin (36.4±8.3, 17.7±4.3 and 33.6±4.5 particles/μm^2 respectively).

Western blotting of tissue solubilized from the optic nerve and corpus callosum showed also that NR1 subunits are present in both white matter areas (Fig. 4.9). Although these experiments do not demonstrate that NMDA receptors are present in oligodendrocytes, as opposed to being in astrocytes or being transported down axons, they are support the notion that NMDA receptors are present in white matter regions.

4.3.6 The two classes of $NG2^+$ cells differ in their glutamate-evoked responses

As described in chapter 3, the precursor oligodendrocytes (or $NG2^+$ cells) seem to fall into different classes with differing electrophysiology, morphology and Olig2 expression. The most easily detected difference between $NG2^+$ cell types is that some express voltage-gated Na^+ channels and some do not. To further explore differences between these cell types, I analysed their glutamate responses with respect to voltage-gated Na^+ channel expression.

Glutamate (100μM) evoked an inward current in both types of $NG2^+$ cell, but the size of the current differed significantly (p=0.014) according to whether the cells expressed voltage-gated Na^+ channels or not. In the $NG2^+$ cells expressing voltage-gated Na^+ channels, 100μM glutamate evoked a 4.4-fold larger inward current at -63mV (Fig. 4.10A). Furthermore, the NMDA-evoked responses also differed (Fig. 4.10B, C). In 2mM Mg^{2+} solution (Fig. 4.10B) 60μM NMDA evoked a 9-fold larger current in the $NG2^+$ cells expressing voltage-gated Na^+ channels (although this was not significantly larger because of the small number of cells studied), while in 0mM Mg^{2+} (Fig. 4.10C) NMDA evoked a 3-fold larger inward current in the cells that expressed voltage-gated sodium channels (significantly larger, p=0.001).

4.3.7 Astrocytes also express AMPA and NMDA receptors

To further explore the properties of white matter astrocytes, I looked at their current responses to agonists for NMDA and AMPA receptors. The $GFAP^+$ cells in the cerebellar white matter responded both to 60μM NMDA and to 20μM AMPA. In 0mM Mg^{2+}, the NMDA-evoked responses were always larger than the AMPA ones (5 times larger on average: Fig. 4.11). In five cells the effect of 1μM TTX on the NMDA response was investigated: it had no significant effect on the current evoked by NMDA ($p=0.33$), although the mean current was reduced by 28% (data not shown). This indicates that, like white matter oligodendrocytes, astrocytes express both NMDA and AMPA receptors that can be activated by glutamate. However, more experiments are needed to characterize these responses further.

4.4 Discussion

In this chapter I have shown that oligodendrocytes at all developmental stages respond to glutamate and this response is mediated by both AMPA/kainate and NMDA receptors. Here I will discuss the immediate implications of the data reported in this chapter. A more broad discussion in Chapter 9 will relate these results to data in the other chapters, and suggest experiments to advance the work started here.

4.4.1 Oligodendrocytes express functional NMDA receptors

I have shown that, contrary to most previous reports, oligodendrocytes express functional NMDA receptors. The NMDA-evoked currents that I observe cannot be produced by an agent released secondarily as a result of NMDA evoking action potentials in neuronal axons because they are unaffected by TTX (at a concentration, 1μM, which blocks synaptic transmission from axons to oligodendrocyte precursors, as described in chapter 7). In addition, to rule out indirect effects of NMDA, mediated by other transmitters, I showed that the NMDA-evoked current is unaffected by block of non-NMDA, $GABA_A$, or glycine receptors (Fig. 4.4), and oligodendrocytes do not show a significant current in response to application of the mGluR agonist ACPD (Fig. 4.2),

noradrenaline, dopamine, histamine, 5-HT, ATP, adenosine or ACh (see chapter 5). Antibody labelling (Fig. 4.6 & Fig. 4.7) and the voltage-dependence of the current (Fig 4.5C) show that oligodendrocytes themselves express NMDA receptors. Previous work which failed to detect NMDA receptor currents in oligodendrocytes was partly on cultured cells (Patneau et al., 1994), and may be explained by a down-regulation of NMDA receptor expression in culture. My data (Fig. 4.2C, D) contradict the absence of NMDA-evoked currents reported in oligodendrocytes in corpus callosum slices (Berger et al., 1992a).

Oligodendrocyte NMDA receptor currents occur both in cerebellum and corpus callosum (Fig. 4.2), and NMDA receptor subunits are detected in oligodendrocytes by immunocytochemistry in cerebellum and corpus callosum, and they are detected with Western blot in optic nerve and corpus callosum (Fig. 4.9). These data suggest that NMDA receptor expression may be a general property of white matter oligodendrocytes. Although my electrophysiological recordings are from precursor, immature and mature oligodendrocytes in P7-P14 rats, and need to be extended to adult animals, electron microscopy also shows NMDA receptor subunits in oligodendrocytes of adult rats (Fig. 4.8).

4.4.2 Oligodendrocyte NMDA receptors show weak Mg^{2+} block

The weak block by Mg^{2+} that I find for the oligodendrocyte NMDA receptors (Fig. 4.5), together with the immunocytochemistry presented in Figures 4.6 and 4.7, suggests that they may contain NR1, NR2C and NR3 subunits. Although the subunit composition of the receptors currently remains uncertain, it allows these receptors (unlike those in neurons) to generate a significant current even at the resting potential in physiological [Mg^{2+}].

4.4.3 Quantification of the effect of blockers on glutamate responses

The incomplete block of the glutamate-evoked current by D-AP5 and NBQX in Figure 4.1E, F reflects the high glutamate concentration used relative to the EC_{50} of NMDA receptors, and the fact that AP5 is a competitive blocker. For the data with 2mM Mg in Figure 4.1F, 50μM AP5 is estimated to block (neuronal) NMDA receptors

by only 39% (for 100μM glutamate, from equations 1 and 2 of Benveniste & Mayer (1991), using K_i=1.93μM from Benveniste & Mayer (1991) and K_d = K_{glu} = 1.1μM from Patneau & Mayer (1990)), while 25μM NBQX is estimated to block (neuronal) AMPA receptors by >99% (from the K_i of 0.1μM derived in Diamond & Jahr (1997), and the 2-site kinetic scheme and steady state K_d for glutamate of 9μM from Benveniste & Mayer (1991)). By contrast, when 50μM AP5 is used to block the response to 60μM NMDA in Figure 4.4A, C, it essentially abolishes the response: this reflects the fact that the NMDA concentration used is only twice the EC_{50} for NMDA, whereas 100μM glutamate is 40-fold higher than the EC_{50} for glutamate. If the 19% percentage block by AP5 seen in 2mM Mg in Figure 4.1F is scaled up by the factor of 2.56 (100%/39%) expected from the analysis above, to obtain the block that would occur if NMDA receptors were fully blocked, then the fractional contribution of NMDA receptors to the total glutamate-evoked current becomes 48% in 2mM Mg, which, when added to the 35% blocked by NBQX in Figure 4.1F, accounts for 83% of the glutamate-evoked current (experimental variability and minor differences in parameters between the neuronal NMDA receptors of Benveniste & Mayer (1991) and the oligodendrocyte receptors studied here could easily account for the remaining 17% of the current). Figure 4.1 E, F also show data employing 200μM, rather than 50μM AP5. Analysis as above indicates that this should block NMDA receptor currents by 78% (for 100μM glutamate). In zero Mg^{2+} solution I found that this blocked the 100μM glutamate-evoked current by 54% (Fig. 4.1F), while 25μM NBQX blocked the current by 26% (the fraction blocked by NBQX is lower than in 2mM Mg because the NMDA receptor-mediated current is 4-fold larger). As above, if I multiply the observed block of 54% by 100%/78%, to obtain the block that would occur if NMDA receptors were fully blocked, I get 69% which, when added to the 26% block by NBQX, gives 95% of the current. Again I can conclude that no other current contributes significantly to the glutamate-evoked current. Consistent with this, mGluR blockers did not reduce the glutamate-evoked current (Fig. 4.1F).

4.4.4 Glutamate responses differ between the two classes of $NG2^+$ cells

Glutamate and NMDA responses differed significantly between the classes of $NG2^+$ cell which did or did not express voltage-gated sodium channels, further suggesting that these cells are different and may have a different role in the white matter. One type of $NG2^+$ cell may serve as a reserve cell to provide more oligodendrocytes for myelination (i.e. it may be an oligodendrocyte precursor cell), while the other may be a separate cell type with unknown function (see Butt et al., 2002; Butt et al., 2005, for review).

4.4.5 Astrocytes also express receptors for AMPA and NMDA

Like oligodendrocytes in the white matter, astrocytes responded both to AMPA and NMDA. AMPA receptors have been well characterized previously in grey and white matter astrocytes (as reviewed by Porter & McCarthy, 1997). Although less well-known, NMDA responses in astrocytes and related radial glia have previously been shown in cerebellar Bergmann glia (Müller et al., 1993), retinal Müller cells (Puro et al., 1996), spinal cord grey matter (Žiak et al., 1998), and neocortex (Schipke et al., 2001). Further work is needed to determine whether astrocyte NMDA receptors have a weak Mg^{2+}-block like oligodendrocytes.

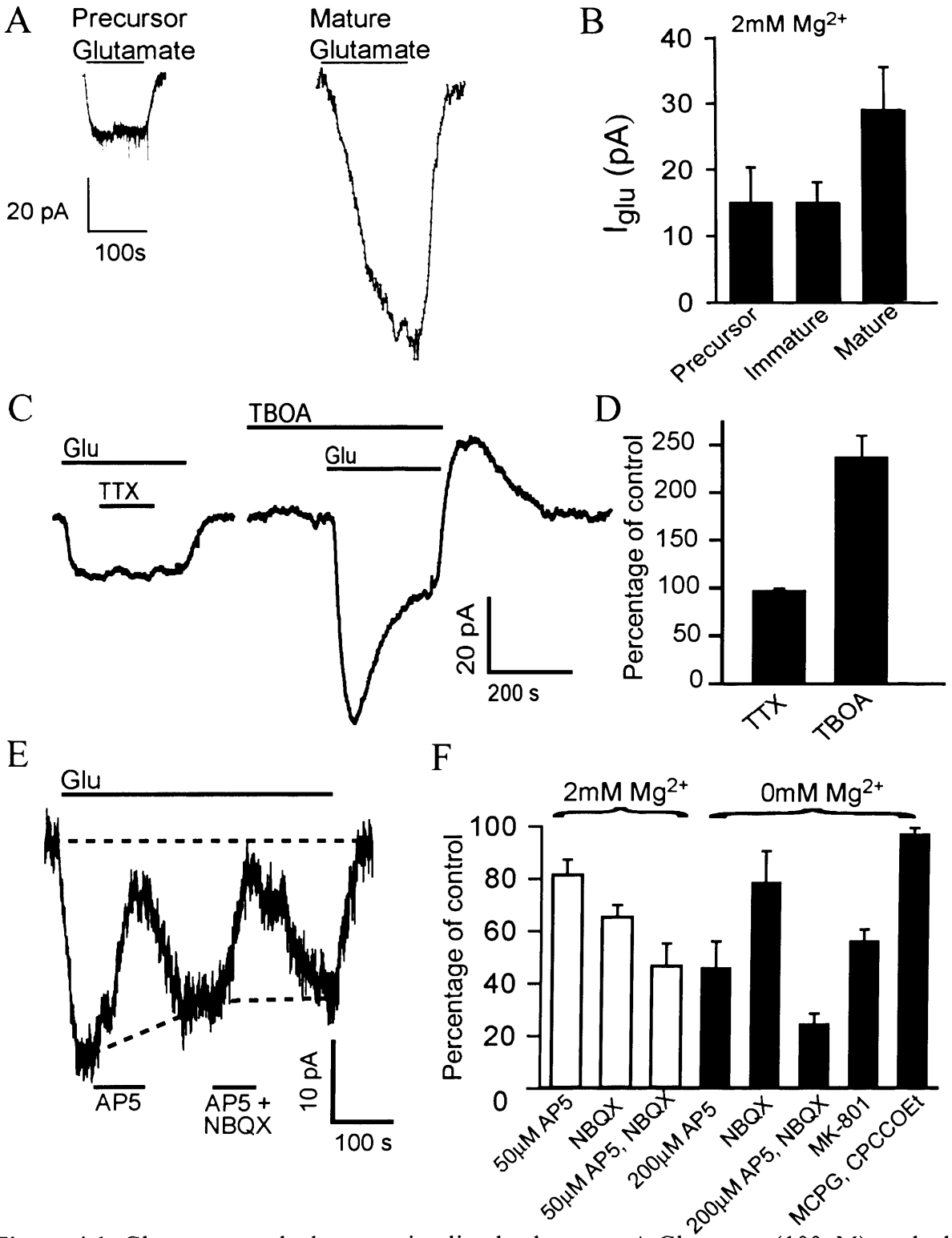

Figure 4.1 Glutamate-evoked current in oligodendrocytes. **A** Glutamate (100μM) evoked an inward current (at -63mV, 24°C) at developmental stages from precursor cells through to mature cells: left trace, precursor cell; right trace, mature cell. **B** Mean data from all maturation stages: mature cells (n=33) tended to show a larger glutamate-evoked current than precursor (p=0.11, n=22) and immature (p=0.14, n=22) cells, although the differences were not significant. **C** Effect of TTX and TBOA on the glutamate-evoked current in a mature cell. **D** Mean effect of TTX (n=5) and TBOA (n=4). **E** Effect of 200μM D-AP5 and 25μM NBQX in 0mM Mg^{2+} (in a mature cell). **F** Current remaining in 2mM Mg^{2+} (n=7) in 50μM AP5 (p=0.02), 25μM NBQX (p=0.0003), and AP5+NBQX (p=0.0008); and also in 0mM Mg^{2+} (n=4-6) in 200μM AP5 (p=0.01), 25μM NBQX (p=0.16), AP5+NBQX (0.0003), 10μM MK-801 (p=0.002 and 1mM MCPG plus 200μM CPCCOEt (mGluR blockers: p=0.25).

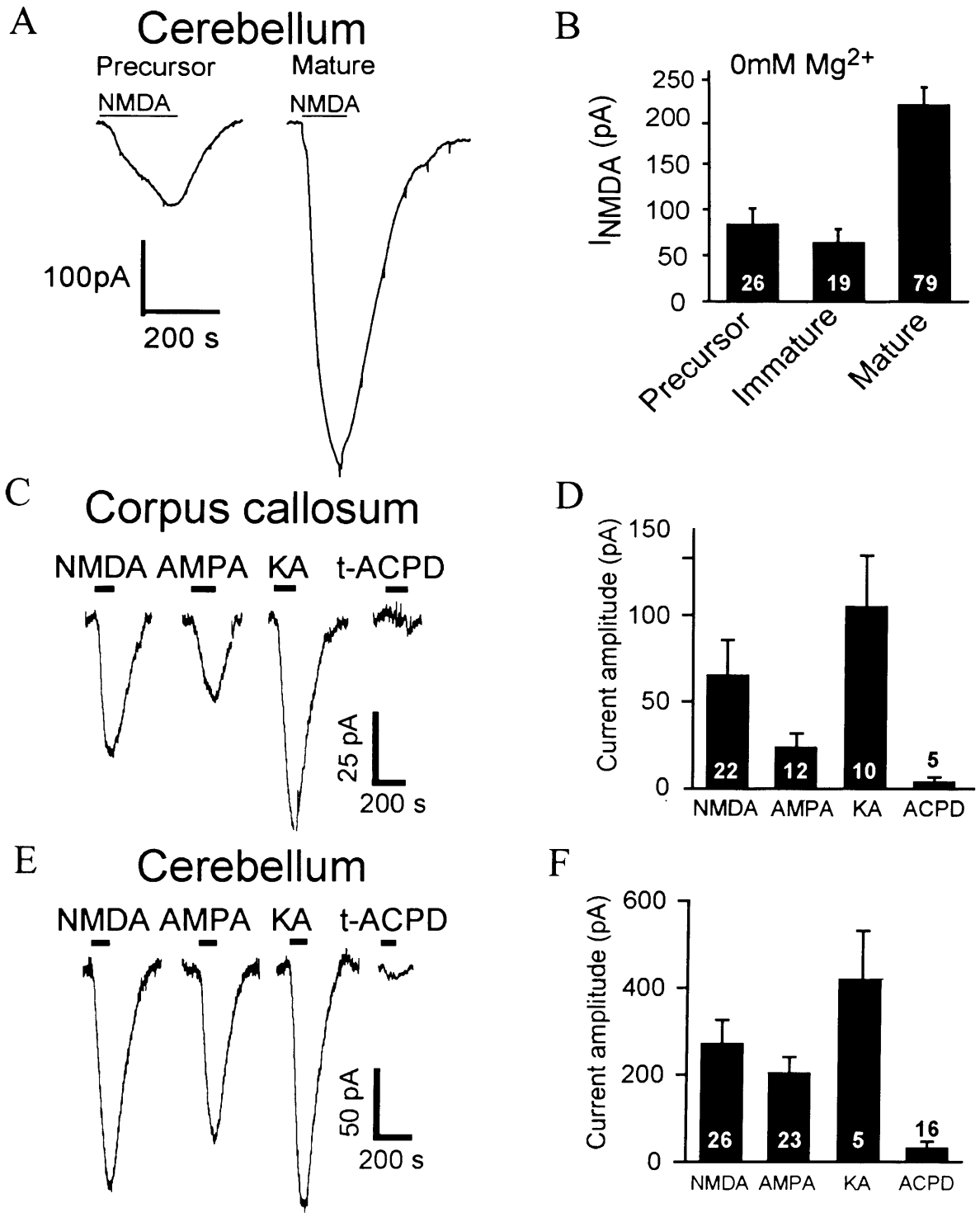

Figure 4.2 The components of the glutamate-evoked current in oligodendrocytes. **A** NMDA (60μM, in 0mM Mg^{2+}) evoked an inward current at all developmental stages of cerebellar oligodendrocytes (left trace: precursor cell; right trace: mature cell). **B** Mean data from all maturation stages: mature cells (n=79) had a significantly larger (p=0.010) NMDA-evoked current than precursor (p=0.042, n=26) and immature (p=0.059, n=19) cells. **C** Response of mature corpus callosum oligodendrocyte to 60μM NMDA, 20μM AMPA, 30μM kainate (KA) and 100μM trans-ACPD (all in 0mM Mg^{2+}). **D** Mean peak current in C for NMDA (n=22 cells), AMPA (n=12), KA (n=10) and ACPD (n=5). **E** Responses of mature cerebellar oligodendrocyte in 0mM Mg^{2+}. **F** Mean current in E for NMDA (n=26 cells), AMPA (n=23), KA (n=5) and ACPD (n=16). Holding potential was -63mV, 24°C.

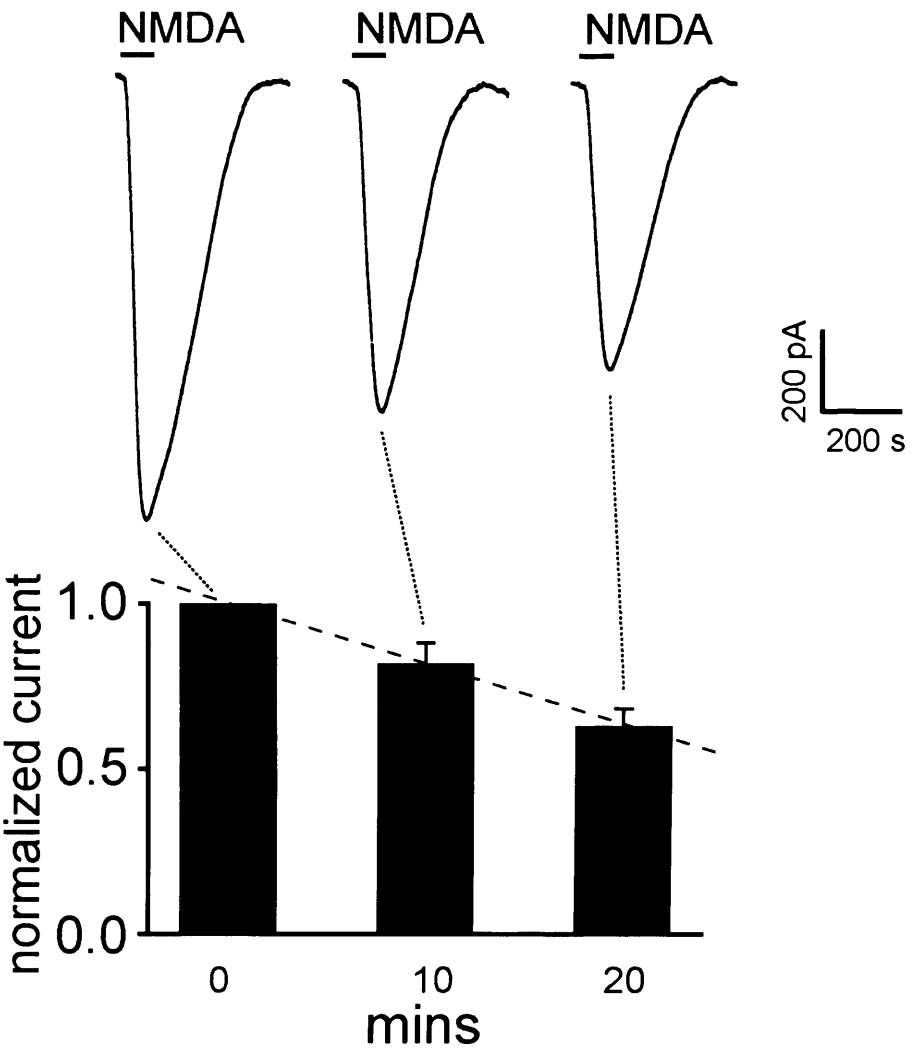

Figure 4.3 The rundown of the NMDA-evoked current in cerebellar oligodendrocytes. NMDA (60μM) responses run down linearly with time (dashed line) during repeated (1/10 mins) applications. Top, specimen cell; bottom bar chart, normalized data from 10 cells. Holding potential was -63mV, 24°C.

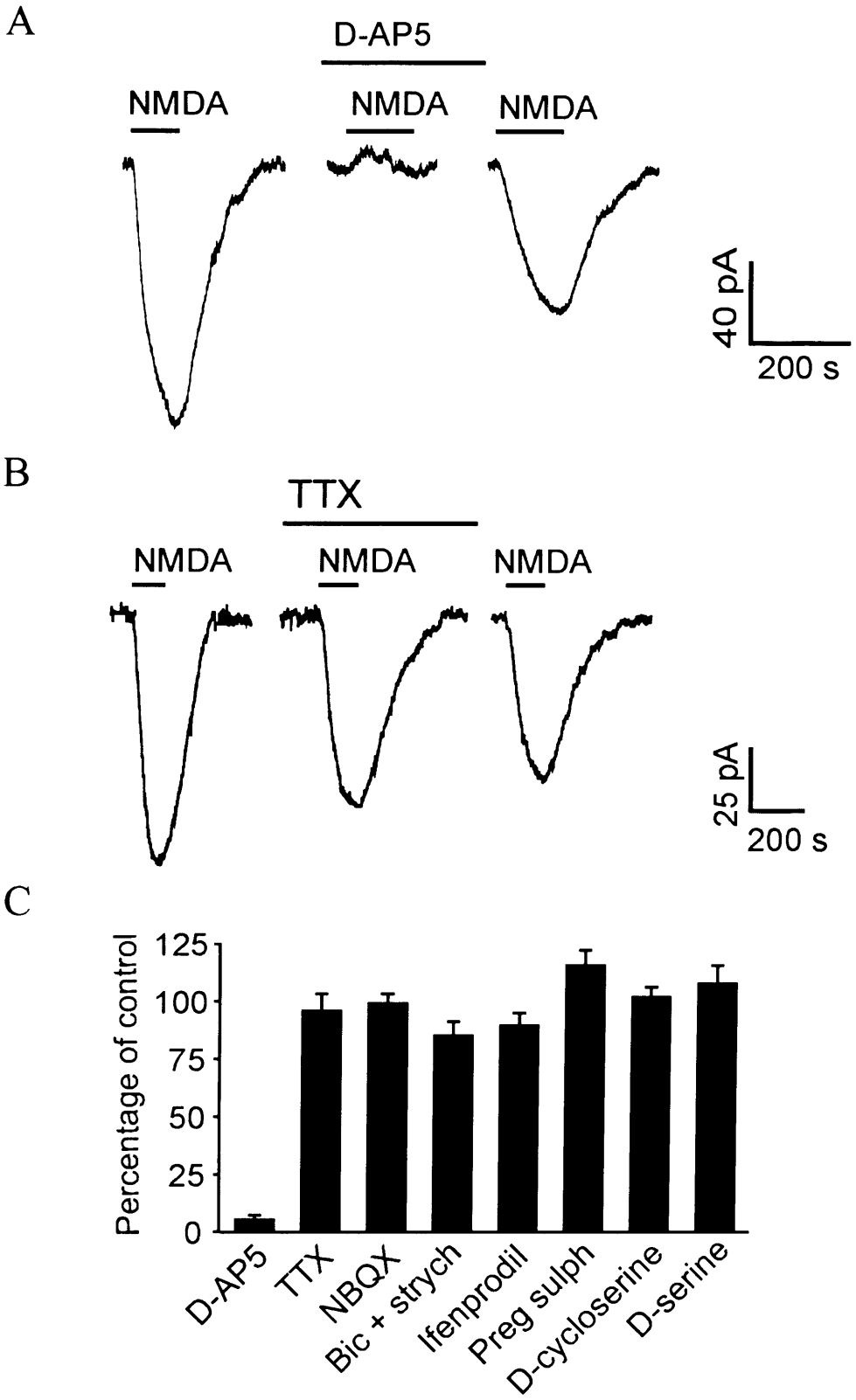

Figure 4.4 Characteristics of the NMDA-evoked current in oligodendrocytes. **A** Effect of D-AP5 (50 μM). **B** Effect of TTX (1 μM). **C** The mean effect of 50 μM D-AP5 (16 cells, $p=10^{-18}$), 1 μM TTX (5 cells, p=0.64), 25 μM NBQX (4 cells, p=0.96), 5 μM strychnine plus 20 μM bicuculline (16 cells, p=0.14), ifenprodil (10 μM, 3 cells, p=0.18), pregnenolone sulphate (100 μM, 4 cells, p=0.085), D-cycloserine (1mM, 3 cells, p=0.6) and D-serine (100 μM, 5 cells, p=0.34) on NMDA-evoked current at -63mV, in the presence of 100 μM glycine and 5 μM strychnine (except for D-cycloserine, D-serine in C); 60 μM NMDA; 24°C.

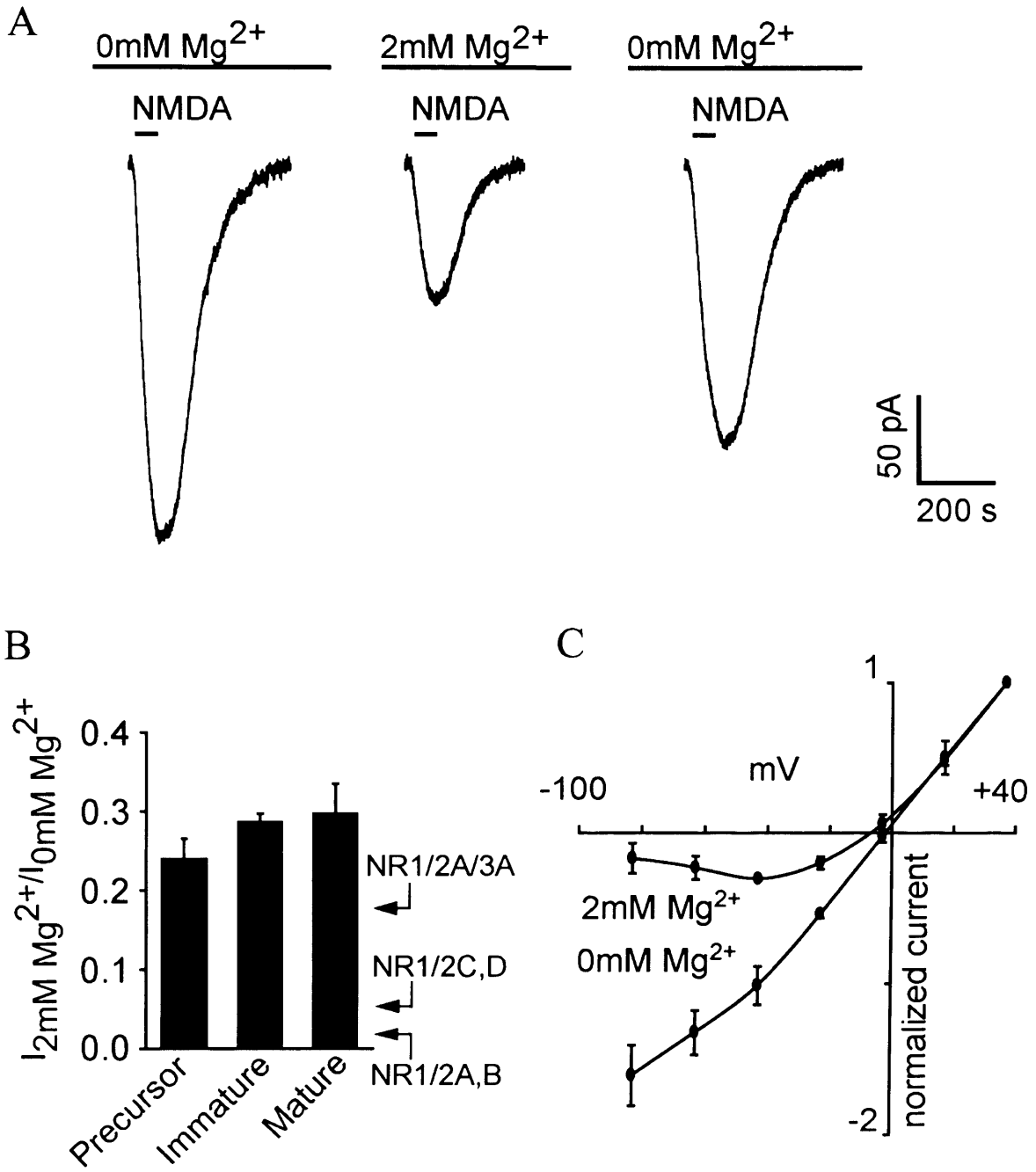

Figure 4.5 Oligodendrocyte NMDA receptors are only weakly Mg^{2+}-blocked. **A** NMDA response in a mature oligodendrocyte in 0mM, 2mM and 0mM Mg^{2+} again. **B** Fraction of NMDA-evoked current remaining in 2mM Mg^{2+} in 4 precursor, 6 immature and 9 mature cells (insignificantly different, p=0.51). Arrows: values for NR1 with NR2A or 2B, with 2C or 2D, or with 2A and 3A (Kuner & Schoepfer, 1996; Sasaki et al., 2002). **C** Mean normalized I-V relation for NMDA-evoked current in precursor cells, two cells in 0mM and three different cells in 2mM Mg^{2+}. Experiments were done on cerebellar oligodendrocytes with 100μM glycine and 5μM strychnine, 60μM NMDA; at 24°C, and -63mV (except for data in C).

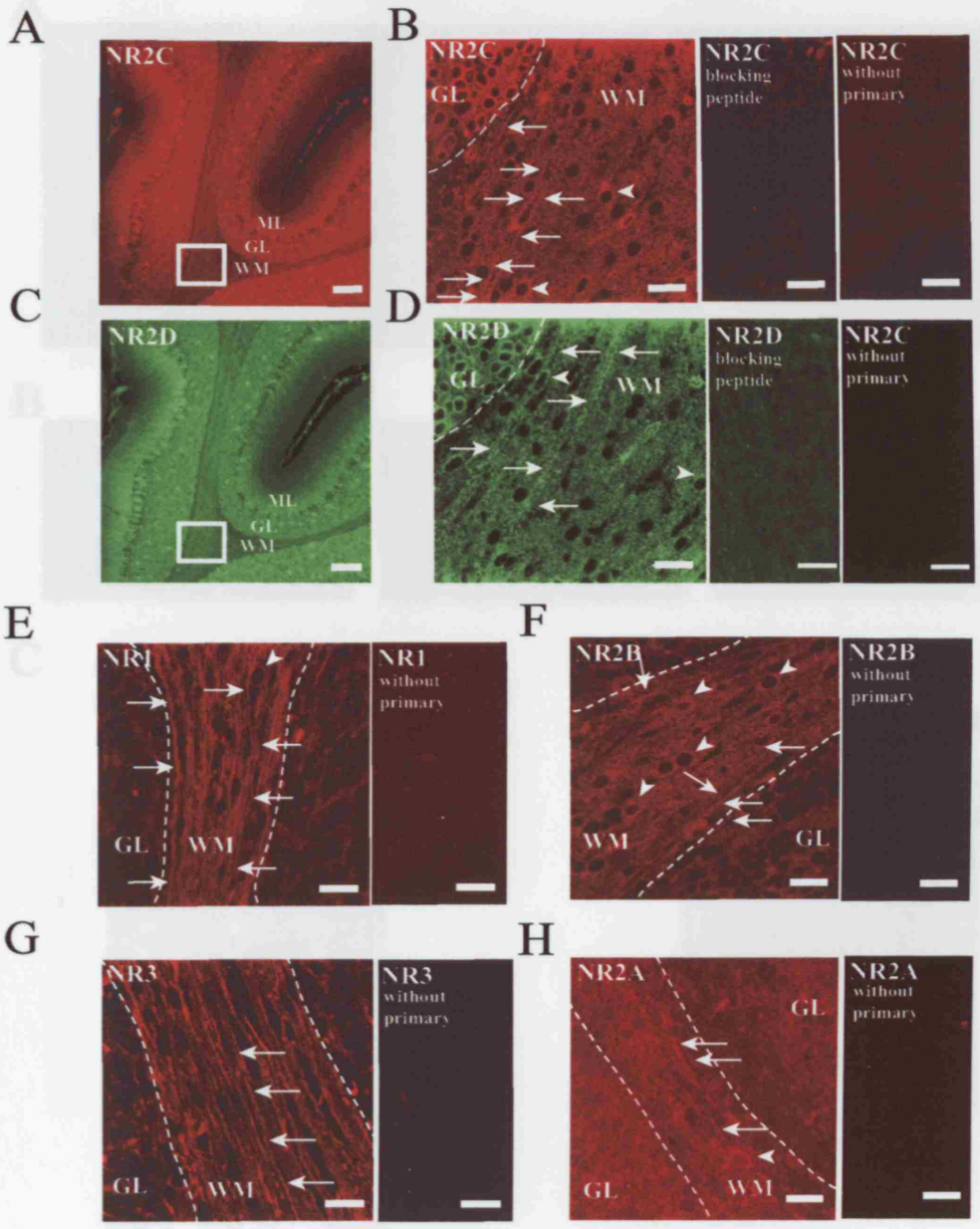

Figure 4.6 Antibody labeling of oligodendrocyte NMDA receptors. **A** Cerebellar cortex labelled with NR2C antibody. **B** High power view of box in A, together with panels showing abolition of labelling after peptide preabsorption of the antibody or omitting the primary antibody. WM, white matter, GL granular layer, ML molecular layer. Arrows: oligodendrocyte process; arrow heads: oligodendrocyte soma. **C** Cerebellar cortex labelled with NR2D antibody. **D** High power view of box in C, together with panels showing abolition of labelling after peptide preabsorption of the antibody or omitting the primary antibody. **E** Oligodendrocyte processes labelling with NR1 antibody, and control panel showing that labelling is abolished by omitting the primary antibody. **F** Oligodendrocyte processes labelling weakly with NR2B antibody, together with control panel showing that the labelling is abolished by omitting the primary antibody. **G** & **H** Like E and F but for NR3 and NR2A antibody labelling. Scale bars: 100 μm in A & C, 20 μm in B, D-H.

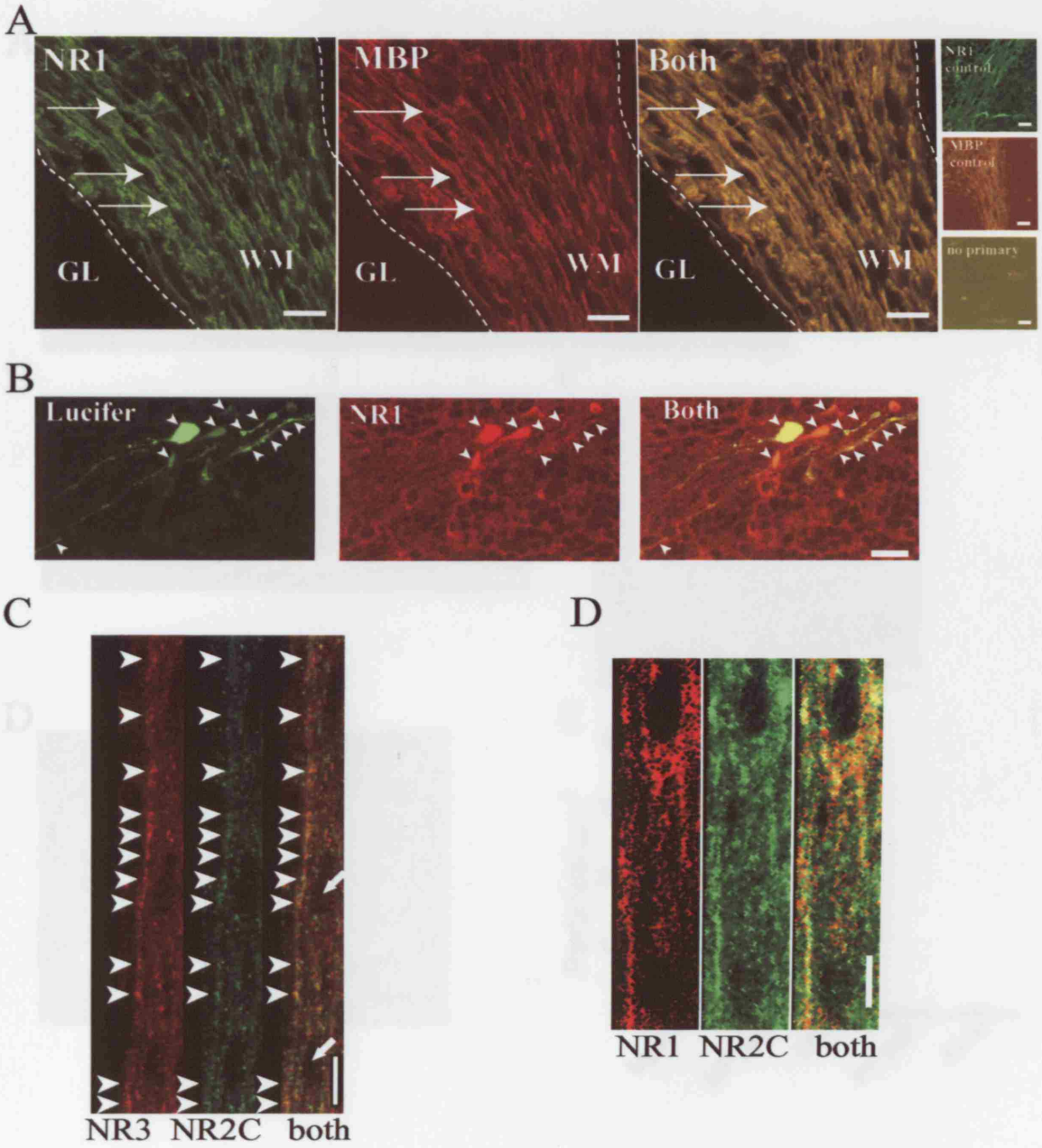

Figure 4.7 Co-localization of NMDA receptors. **A** Co-localization (yellow) of NR1 labelling (green) with MBP labelling (red) in the cerebellar white matter. Small images on the right show controls: the NR1 antibody or the MBP antibody alone with both secondaries, and both secondaries without any primary antibody. Scale bar 20μm. WM, white matter, GL granular layer, arrows show colocalization in processes. **B** Images of Lucifer fill of a recorded oligodendrocyte, NR1 labelling of the slice, and an overlay of both. Arrow heads show where processes of the cell label for NR1. Scale bar 20μm. **C** Colocalization (yellow) of NR3 (red) and NR2C subunits (green) in the myelinating processes of mature cerebellar oligodendrocytes. Arrow heads indicate points of high colocalization on one particular process. Dark areas indicated with arrows are cell nuclei. Scale bar 10μm. **D** Colocalization (yellow) of NR1 (red) and NR2C subunits (green) in myelinating processes and around the soma (arrow shows nucleus) of cerebellar oligodendrocytes. Arrow heads indicate points of high colocalization on two particular processes. Scale bar 5μm.

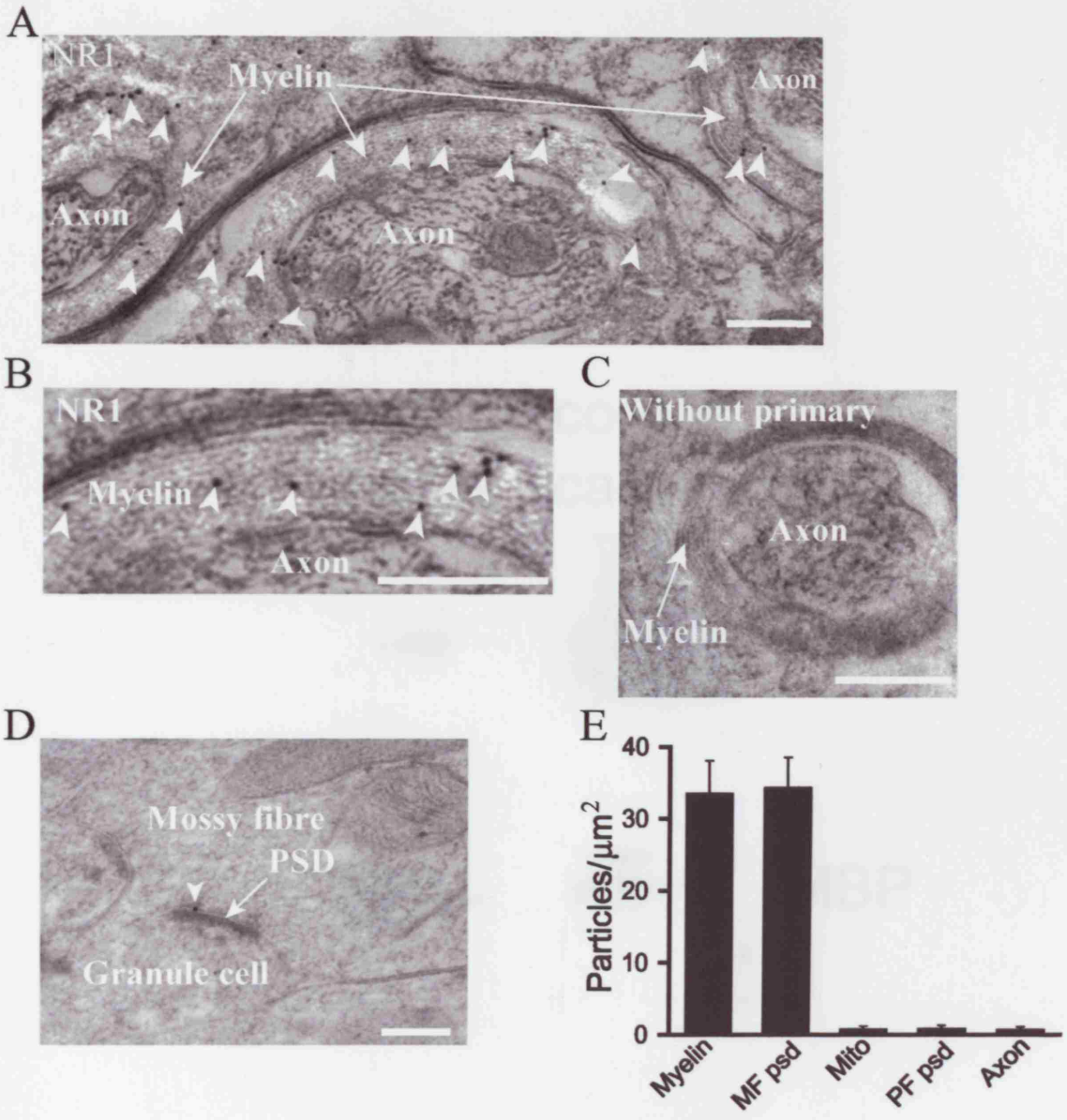

Figure 4.8 NR1 subunit of the NMDA receptor is found in the myelin. **A** Immunogold (black dots, arrowheads, Wenthold NR1 antibody) labelling cerebellar myelin. **B** Enlarged view of myelin in A: each black dot is a gold particle attached to NR1 antibody. **C** No labelling was seen with primary antibody omitted. **D** Mossy fibre terminal postsynaptic density (PSD) labelling. **E** Gold particle density in cerebellum over myelin (17 sheaths), mossy fibre synapse (MF psd, n=20), parallel fibre-Purkinje synapse (PF psd, n=26, this synapse express no NMDA receptors), mitochondria in mossy fibre terminal (Mito, n=30), and axon cytoplasm (Axon, n=17). Scale bars 0.25 µm. Shown with permission from Linda Bergersen.

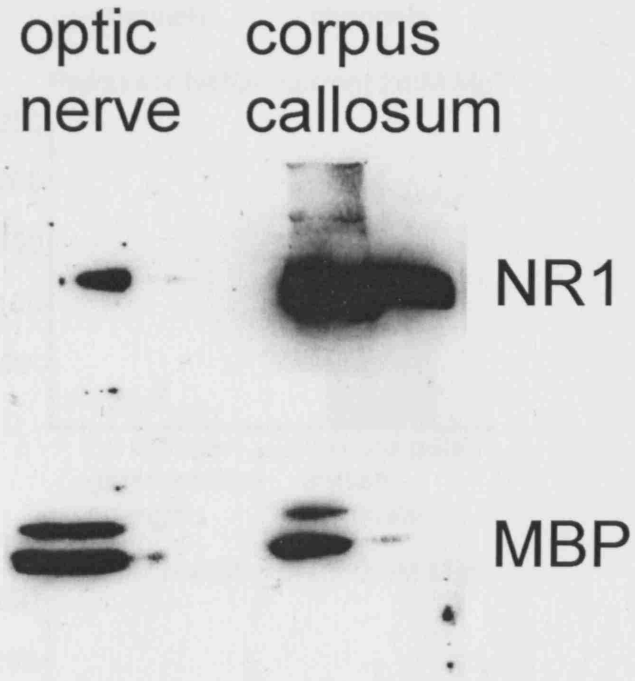

Figure 4.9 NR1 is present with MBP in both optic nerve and corpus callosum. Western blot of the NR1 subunit and myelin basic protein (MBP) in tissue solubilized from both white matter areas.

A

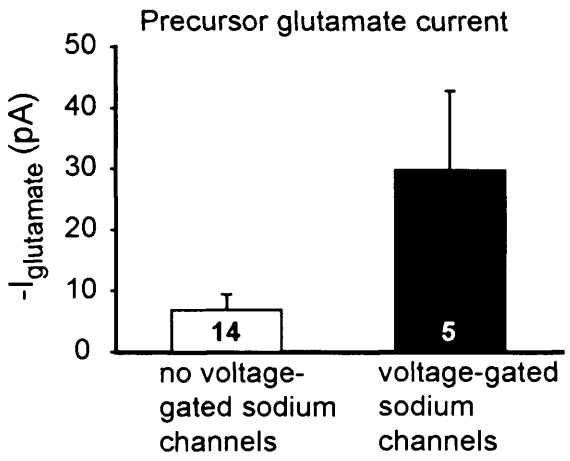

B

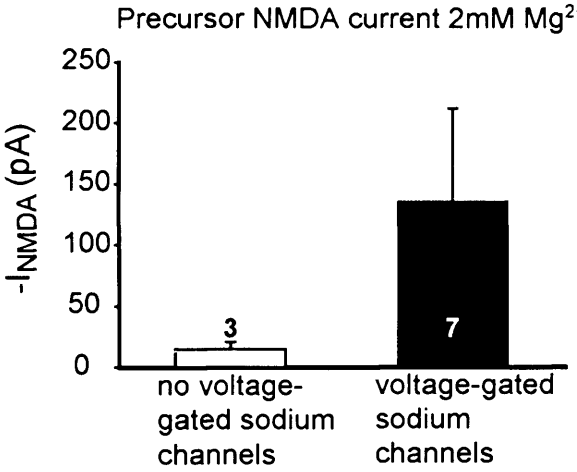

C

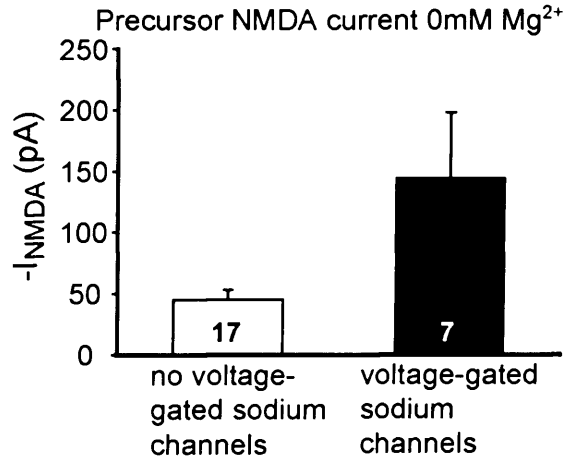

Figure 4.10 The two types of $NG2^+$ cell differ in their glutamate and NMDA responses. **A** Mean glutamate (100μM) evoked current at -63mV in precursors that either do not express voltage-gated sodium channels (n=14) or that do express sodium channels (n=5); significantly different, p=0.014. **B** Mean NMDA (60μM) evoked current at -63mV in the presence of 2mM Mg^{2+} in precursors that do not express voltage-gated sodium channels (n=3) or that do express sodium channels (n=7), not significantly different, p=0.34. **C** Mean NMDA (60μM) evoked current in the absence of Mg^{2+} in precursors that do not express voltage-gated sodium channels (n=17) or that do express sodium channels (n=7), significantly different, p=0.001.

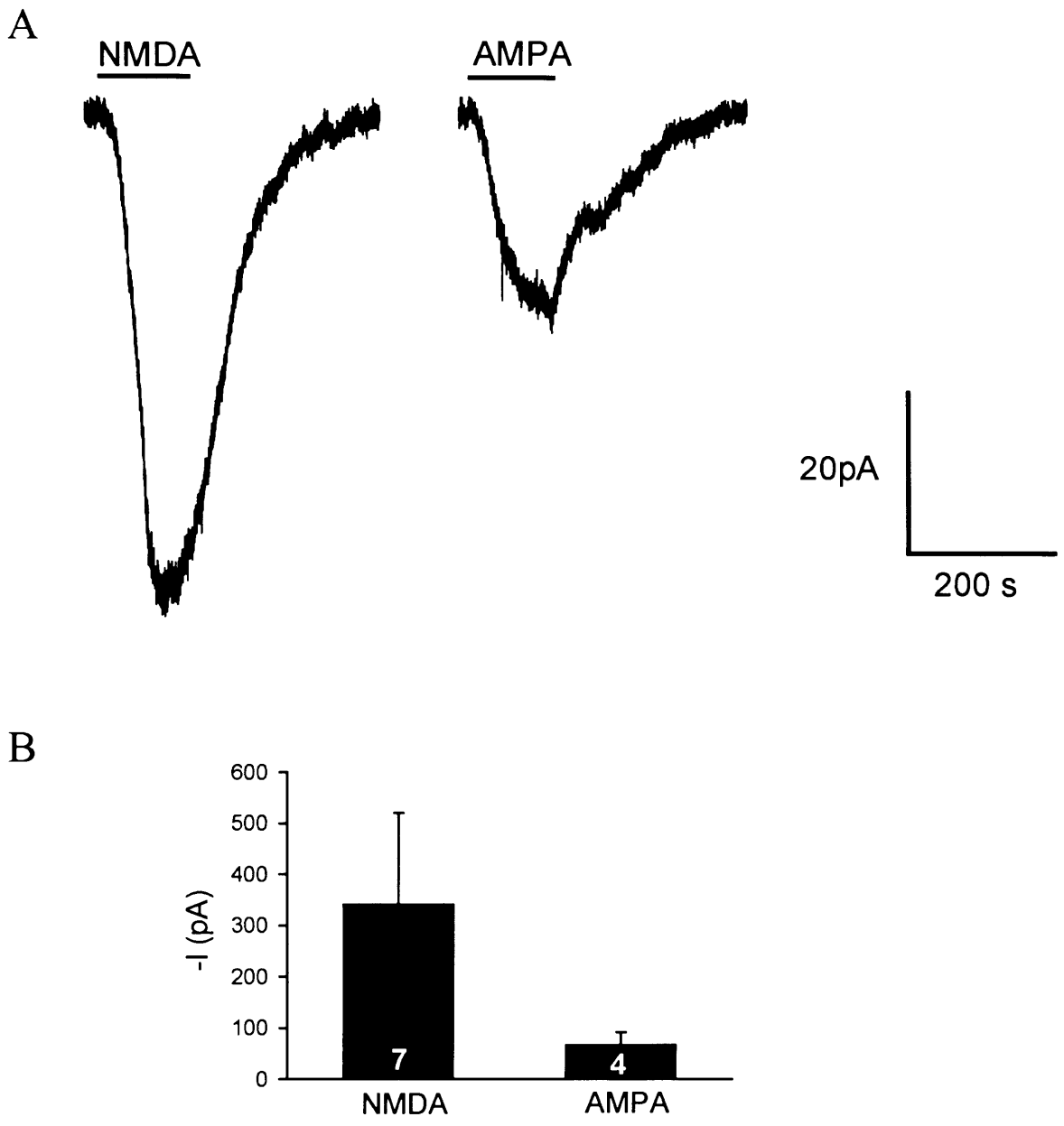

Figure 4.11 White matter astrocytes express NMDA and AMPA receptors **A** NMDA and AMPA responses at -63mV in the same astrocyte (0mM Mg^{2+}) **B** Mean response to NMDA (7 cells) and AMPA (4 cells) in cerebellar white matter astrocytes. All in cerebellar white matter, -63mV, 24°C.

Chapter 5

Signalling to oligodendrocytes by GABA and other neurotransmitters

The previous chapter characterized in detail the responses of oligodendrocytes to glutamate. Now I will look at the actions on oligodendrocytes of the major inhibitory neurotransmitter GABA, and of various other transmitters that are found in the brain, all of which have been suggested to act on oligodendrocytes (see Chapter 1).

5.1 Introduction

Neurotransmitters play a role in controlling the development of neurons, for example by regulating cell growth, proliferation and migration, as well as gene expression and synapse formation (Pearce et al., 1987; Rabacchi et al., 1992; Komuro & Rakic, 1993; LoTurco et al., 1995; Gu & Spitzer, 1995; Dolmetsch et al., 1998; Li et al., 1998). The development of oligodendrocytes is no different: effects of glutamate on oligodendrocyte development have been characterized as described in section 1.3.3. Moreover oligodendrocytes also express receptors for GABA (Barres et al., 1990c; Kettenmann et al., 1991; Butt & Tutton, 1992), glycine (Belachew et al., 1998b), acetylcholine (Rogers et al., 2001), adenosine (Vartanian et al., 1986; Stevens et al., 2002), ATP (Takeda et al., 1995), serotonin (Karschin et al., 1994), histamine (Takeda et al., 1995), dopamine (Bongarzone et al., 1998; Rosin et al., 2005) and melatonin (Husson et al., 2002). Little is known about the functional role of these receptors in oligodendrocytes, however it is likely that they play some role in the cells' development, perhaps controlling proliferation, maturation and myelination, as well as mediating the response of the cells to neurotransmitter released from axons or from other surrounding cells. Furthermore, just as glutamate receptors play a role in damaging oligodendrocytes in pathological conditions (see Chapters 1 and 6), it is possible that other neurotransmitter receptors on these cells may exacerbate or reduce damage to oligodendrocytes in white matter diseases. For example dopamine receptors have been suggested to reduce oligodendrocyte damage caused by glutamate or energy deprivation (Rosin et al., 2005), GABA may similarly reduce glutamatergic effects on oligodendrocyte precursors (Lin & Bergles, 2004, and see chapter 6), and melatonin

reduces oxidative damage to white matter after activation of glutamate receptors or ischaemia (Husson et al., 2002; Lee et al., 2005). It is important, therefore, to understand how oligodendrocytes respond to a range of neurotransmitters.

5.2 Methods

Brain slices Cerebellar slices (225μm thick) were prepared from P7-P14 rats as described in Section 2.1. Slices were superfused at 24±1°C with HEPES-buffered solution, containing (mM): 144 NaCl, 2.5 KCl, 2 $MgCl_2$, 10 HEPES, 1 NaH_2PO_4, 2.5 $CaCl_2$, 10 glucose, pH adjusted to 7.4 with NaOH, or at 33±1°C with bicarbonate-buffered Ringer's solution, composed of (in mM): NaCl 126, $NaHCO_3$ 24, NaH_2PO_4 1, KCl 2.5, $CaCl_2$ 2.5, $MgCl_2$ 2, D-glucose 10 (gassed with 95% O_2/5% CO_2), pH 7.4.

Recording & cell identification White matter cells were whole-cell clamped, as in chapter 3, with pipettes containing a CsCl-based solution, comprising (mM): 130 CsCl, 4 NaCl, 0.5 $CaCl_2$, 10 HEPES, 10 BAPTA, 2 MgATP, 0.5 Na_2GTP, K-Lucifer yellow 2, pH set to 7.3 with CsOH (E_{Cl} = 0mV), or a Cs-gluconate-based solution, comprising (mM): 130 Cs-gluconate, 4 NaCl, 0.5 $CaCl_2$, 10 HEPES, 10 BAPTA, 4 MgATP, 0.5 Na_2GTP, 2 K-Lucifer yellow, pH set to 7.3 (E_{Cl} = -86mV).

Antibody labelling is described in detail in chapter 2, section 2.11.

5.3 Results

5.3.1 GABA evokes a current in cerebellar white matter oligodendrocytes

Precursor oligodendrocytes have been reported to respond to GABA with either a Cl^- influx through $GABA_A$ receptor channels (Berger et al., 1992b; Williamson et al., 1998; Belachew et al., 1998a) or with an elevation of intracellular calcium concentration (Bernstein et al., 1996; Belachew et al., 1998a). These GABA-evoked responses have been reported to disappear with oligodendrocyte maturation (Kirchhoff & Kettenmann, 1992). However, in the optic nerve, mature oligodendrocytes have been shown respond to GABA (Butt & Tutton, 1992). To further investigate GABA responses throughout oligodendrocyte development, I used whole-cell voltage clamping (as in chapter 4) to record GABA-evoked responses in cerebellar white matter oligodendrocytes. In addition, by including Lucifer yellow in the pipette I could identify the cell I recorded from and its maturational stage, as described in detail in section 2.3 and 2.11.

Oligodendrocytes at all developmental stages responded to GABA (100μM), with an inward current at -63mV, when the chloride reversal potential was 0mV (Fig. 5.1). The GABA-evoked current increased significantly (p=0.0008) with maturation (Fig. 5.1A, B), contradicting the suggestion of Kirchhoff & Kettenmann (1992) that GABA responses are larger in precursors. To test whether the GABA responses are generated by conventional anion channels, I studied precursor oligodendrocytes, since these are more spatially compact and likely to be better voltage-clamped and to have their intracellular ion concentrations better controlled by dialysis from the whole-cell pipette. When the chloride reversal potential was set to -87mV, in three precursor cells the GABA-evoked current reversed at -61±2.7mV (Fig. 5.1C, these data are corrected for the -14mV junction potential of the Cs-gluconate internal solution) and GABA evoked a large outward current at -44mV (Fig. 5.1A).

Since GABA receptors are not just permeable to chloride but also to bicarbonate (Fatima-Shad & Barry, 1993), the GABA reversal potential is set by the receptor's relative permeability to these two ions and the ions' concentrations in the extracellular and intracellular solutions, as described by equation 5.1.

$$E_{GABA\,rev} = 61mV \cdot \log_e \frac{[Cl]_i + \frac{P_{HCO_3}}{P_{Cl}} \cdot [HCO_3]_i}{[Cl]_o + \frac{P_{HCO_3}}{P_{Cl}} \cdot [HCO_3]_o} \qquad (5.1)$$

where 61mV is the value of RT/F (with R the gas constant, T the absolute temperature, and F the Faraday) at the temperature of 33°C used here. The investigation of the GABA reversal potential was done in bicarbonate Ringer's, with 24mM extracellular bicarbonate concentration at pH 7.4, and an internal solution with pH set to 7.3. Now bicarbonate reacts with H^+ to form CO_2, so that

$[H]_o \cdot [HCO_3]_o = K[CO_2]_o$

where K is the equilibrium constant for the overall reaction. A similar equation can be written for the intracellular concentrations:

$[H]_i \cdot [HCO_3]_i = K[CO_2]_i$.

Assuming that CO_2 is freely permeable across the cell membrane, so that $[CO_2]_o = [CO_2]_i$, then

$[H]_i \cdot [HCO_3]_i = [H]_o \cdot [HCO_3]_o$ or $[HCO_3]_i = [H]_o \cdot [HCO_3]_o / [H]_i$

Thus, the intracellular bicarbonate concentration should be 19mM, given that the external pH is 7.4 and the internal pH is 7.3 (and ignoring diffusion of CO_2 and HCO_3

out of the cell into the patch pipette where there was no HCO_3^-). Assuming the permeability ratio of Cl and HCO_3 for the GABA receptors to be 0.44 (Fatima-Shad & Barry, 1993) one can calculate the predicted reversal potential for GABA using equation 5.1. Putting all the values into equation 5.1 gives a predicted GABA reversal potential of -64mV which is close to the observed reversal potential of -61mV in the precursors.

5.3.2 $GABA_A$ receptors mediate the GABA-evoked current in oligodendrocytes

To determine which GABA receptor mediates the GABA-evoked current in oligodendrocytes, I used selective pharmacological agents to either mimic or block the current recorded in response to GABA application, and immunohistochemistry to identify the specific subunits expressed in the white matter.

The GABA-evoked current in oligodendrocytes was significantly ($p=7.8\cdot10^{-9}$) reduced (by 74±2.3%) by the $GABA_A$ receptor antagonist bicuculline (20μM) (Fig. 5.2A, D), whereas the $GABA_B$ receptor antagonist CPG 35348 (50μM) did not reduce the GABA-evoked current at all (Fig. 5.2B, D), and the $GABA_B$ agonist baclofen (40μM) generated no current in the oligodendrocytes (n=8, data not shown). These data suggest that $GABA_A$ receptors mediate the GABA-evoked current.

The lack of complete abolition of the GABA-evoked current by the $GABA_A$ receptor antagonist bicuculline probably reflects the fact that bicuculline is a competitive antagonist at the $GABA_A$ receptor and that 20μM bicuculline is simply not a high enough concentration to completely block the current evoked by 100μM GABA, rather than the presence of bicuculline-insensitive $GABA_C$ receptors (which I did not test for, but which have been reported to be absent in cultured oligodendrocytes: Williamson et al., 1998). This can be seen as follows. I can calculate the percentage block expected to be produced theoretically by 20μM bicuculline in the presence of 100μM GABA, using the equations for competitive inhibition and assuming that GABA and bicuculline act with similar values of K_m at the receptors on oligodendrocytes as on neuronal receptors. The Hill coefficient for GABA acting on neuronal receptors has been found to be 0.99 (Jonas et al., 1998), suggesting a dose response curve with the form:

$$\frac{I}{I_{max}} = \frac{[GABA]}{([GABA + K_d)} \qquad (5.2)$$

where the EC_{50} for GABA is K_d = 7μM (Fujimoto et al., 1995). However, with the competitive inhibitor bicuculline present, equation 5.2 becomes:

$$\frac{I}{I_{max}} = \frac{[GABA]}{[GABA] + K_d\left(1 + \frac{[Bicuculline]}{K_{i\ (bicuculline)}}\right)} \qquad (5.3)$$

where the K_i for bicuculline blocking $GABA_A$ receptors is ~1μM for neuronal receptors (Takahashi et al., 1994). Putting in all the values gives I/I_{max} = 0.935 in the absence of bicuculline or 0.405 when [bicuculline] = 20μM. The predicted inhibition by bicuculline is therefore 1-(0.405/0.935) or 57%, thus one can not expect 100% inhibition using 20μM bicuculline in the presence of 100μM GABA. I found 74% inhibition (Fig. 5.2), which is slightly higher than expected from the calculation, but this difference could easily be explained by a small difference in the K_d values for GABA and bicuculline binding to neuronal and oligodendrocyte receptors. A greater inhibition than is calculated from the concentration applied to the surface of the slice would also occur if some of the GABA applied is taken up by GABA transporters in the slice, leading to a lower [GABA] near the cells and hence a greater block by bicuculline.

The glutamate antagonists NBQX (25μM) and AP5 (50μM) did not have any effect on the GABA-evoked current (Fig. 5.2C, D). This rules out the possibility that the GABA-evoked current seen in oligodendrocytes is a secondary effect of GABA mediated via glutamate receptors, which might occur, for example, if GABA acts on another cell that in turn releases glutamate which then evokes an inward current in the recorded oligodendrocyte.

To investigate what $GABA_A$ receptor subunits are expressed in the white matter, I used specific antibodies against different subunits. In the cerebellum both the α_1 and α_2 subunits are present in the white matter, where α_1 labels both the processes and the membranes of the cell bodies (Fig. 5.3A), but the α_2 subunits seem to label more the processes than the cell bodies (Fig. 5.3B). Omitting the primary antibody abolished the labelling (data not shown). When looking at the β subunit expression, only the antibody to β_1 gave strong staining and, like the α_2 antibody, it preferably labelled the processes relative to the cell bodies (Fig. 5.3C). Further, the β_3 subunit labelled some of the processes in the white matter but not as strongly as β_1 (Fig. 5.3D). However, the β_2 subunit did not label the white matter at all, although it did label the granule cell layer. Similar labelling to that seen with the β_2 antibody was seen when using an antibody recognizing both β_2 and β_3 subunits (Fig. 5.3F), which must imply that this antibody

binds only weakly to β_3 subunits. Finally, antibody to the γ_2 subunit labelled the white matter and labelled primarily the cell processes (Fig. 5.3E).

From the immunohistochemistry data above it is likely that the oligodendrocytes' $GABA_A$ receptors include α_1 and/or α_2, β_1 and γ_2 subunits in their composition. However, I cannot exclude the possibility that $GABA_C$ receptors formed of ρ subunits make a minor contribution to the current evoked by GABA.

5.3.3 Testing for endogenous GABA release

To test the potential for physiological or pathological activation of oligodendrocyte GABA receptors, I applied nipecotic acid (100μM): a protocol previously used by Solis & Nicoll (1992) to probe the effects of endogenous GABA release in hippocampal grey matter. This agent can raise the extracellular GABA concentration in two separate ways. First, it is a blocker (Borden, 1996) of the GAT-1, GAT-2 and GAT-3 GABA transporters which are present in white matter (at least in optic nerve: Howd et al., 1997). If GABA is being released exocytotically in the white matter (Lin & Bergles, 2004), inhibition of GABA uptake should promote its action on oligodendrocyte $GABA_A$ receptors. Secondly, because nipecotic acid can be (slowly) transported by GABA transporters, it evokes release of GABA by heteroexchange on the transporter (Solis & Nicoll, 1992). This is a process by which the transporter mediates exchange of extracellular nipecotic acid for intracellular GABA, without the transporter going through a whole transport cycle. Release of GABA in this way would mimic the release of GABA expected to occur by reversed uptake (Allen et al., 2004a) when ion gradients run down in conditions of energy deprivation (see Section 1.7.2).

Nipecotic acid (100μM) induced a small $GABA_A$ receptor mediated inward current (5.5±1.8pA, p=0.04, in eight out of 13 cells), which was 17 times smaller than the peak current evoked by an application of 100μM GABA to the same cells (Fig. 5.4A). This small current induced by nipecotic acid was blocked by 79±10% in four cells out of the eight by 10μM GABAzine, a $GABA_A$ receptor antagonist (Fig. 5.4B, including all eight cells in the mean gives 45±14% block). The low success rate for GABAzine blocking the current may reflect the very small amplitude of the current, making it difficult to detect above baseline fluctuations, so that in some cells an inward current drift may have been erroneously attributed to an effect of nipecotic acid.

5.3.4 GABA evokes an indistinguishable current in the two classes of $NG2^+$ cell

To further investigate the difference between the two classes of $NG2^+$ cell which were characterized in the preceding chapters (see Section 3.3.3), i.e. those that express sodium channels and those which do not, I investigated whether their GABA-evoked responses differed. The GABA responses of eight $NG2^+$ cells were recorded, six of which did and two of which did not express sodium channels. Although the low number of cells studied makes a firm conclusion uncertain,, it appears likely that the GABA-evoked current does not differ between the two classes of $NG2^+$ cell (Fig. 5.4A), because the mean current in the two types is similar, yet the two cells that did not express sodium channels had both the lowest and the highest recorded current.

5.3.5 Glycine, acetylcholine and purinergic signalling to oligodendrocytes

Like GABA, glycine has been reported to induce an elevation of the intracellular calcium concentration (Belachew et al., 2000) and an inward current in some oligodendrocytes in culture and in spinal cord (Pastor et al., 1995; Belachew et al., 1998a). Acetylcholine generates an inward current in cultured precursor oligodendrocytes (Belachew et al., 1998a) and it is thought that proliferation of oligodendrocyte precursors is increased by activation of muscarinic receptor which stimulate the MAPK pathway (Ragheb et al., 2001). On the other hand, in culture, adenosine inhibits proliferation and promotes both maturation and myelination (Stevens et al., 2002; Othman et al., 2003). To further test the effects of these and other transmitters on oligodendrocytes *in situ* in brain slices, I applied them to mature cerebellar white matter oligodendrocytes.

In mature oligodendrocytes, with E_{Cl}=0mV, glycine (100μM) generated an inward current (39±21pA) in two out of nine cells tested (response rate of 22%), with an overall mean including the non-responsive cells of 8.6±6.7pA (Fig. 5.5A, B, C). D-Serine (100μM) did not generate a current in any oligodendrocyte tested (Fig. 5.5D) and neither did acetylcholine (100μM, Fig. 5.5E).

There are several studies showing that adenosine (Schmidt et al., 2000; Stevens et al., 2002; Othman et al., 2003) and ATP (Takeda et al., 1995; Schmidt et al., 2000) increase intracellular calcium levels in oligodendrocytes. However, when these agents were applied to mature oligodendrocytes, in a slice, neither adenosine (100μM. Fig. 5.6A) nor ATP (100μM, applied in presence of an ectonucleotidase inhibitor (ARL

67156, 100μM) to reduce breakdown to adenosine and ADP) generated any detectable current change in the nine oligodendrocytes tested.

My results document only the effect of these neurotransmitters on the membrane current of the cell, and do not rule out the possibility that these transmitters act on mature oligodendrocytes by increasing the intracellular calcium concentration.

5.3.6 Effect of amine transmitters on oligodendrocyte membrane current

Serotonin has been reported to evoke an inward current in cultured precursor oligodendrocytes (Belachew et al., 1998a), and noradrenaline, serotonin and histamine increase the intracellular calcium concentration (Bernstein et al., 1996). Moreover, in mature oligodendrocytes, serotonin can inhibit inward rectifying potassium channels by acting on G protein coupled receptors (Karschin et al., 1994). Oligodendrocytes also express dopamine receptors, activation of which decreases oligodendrocyte differentiation *in vitro* (Bongarzone et al., 1998).

None of the 5 amines tested, i.e. noradrenaline (10μM, n=8), dopamine (100μM, n=10), serotonin (100μM, n=10), melatonin (100μM, n=5) and histamine (100μM, n=5), generated a current change in the oligodendrocytes. However it is possible they might generate an intracellular [calcium] elevation without activating ion channels.

5.4 Discussion

5.4.1 GABA evokes a current through $GABA_A$ receptor channels in oligodendrocytes at all developmental stages

In this chapter, I have shown that mature oligodendrocytes respond to GABA, contrary to the suggestion of Kirchhoff & Kettenmann (1992), but supporting findings from Butt & Tutton (1992) showing mature oligodendrocytes responding to GABA. The GABA response is mediated through $GABA_A$ receptors, as has previously been reported (Kirchhoff & Kettenmann, 1992; Berger et al., 1992d; Pastor et al., 1995; Williamson et al., 1998), as it is blocked with bicuculline and the GABA-evoked current reverses close to the predicted GABA reversal potential. On the other hand, no effect on the membrane current of activating or blocking $GABA_B$ receptors was found, even though it has been claimed that oligodendrocytes express these receptors (Fern et al., 1995b). However, as $GABA_B$ receptors are G-protein coupled I cannot rule out the

possibility that, by whole-cell clamping, I am washing out some factor that they need for activation.

Based on the fact that functional GABA receptors are pentamers, comprised of two α subunits, two β subunits, and an additional subunit that is normally γ_2 (reviewed by Wafford, 2005), my immunohistochemical data suggest that the $GABA_A$ receptors expressed in the oligodendrocytes are likely to have a subunit composition including α_1 and/or α_2 subunits, two β_1 subunits (or perhaps one β_1 and one β_3), and one γ_2 subunit.

5.4.2 Glycine, acetylcholine, purinergic input and amines

I showed that glycine evoked an inward current in 22% of cells, which is lower than the 45% reported by Pastor et al. (1995) in grey matter oligodendrocytes. Perhaps this is a regional difference, however it does not seem as though glycine is playing a major role in the function of cerebellar white matter oligodendrocytes.

Even though I did not detect any current responses to acetylcholine, adenosine, ATP, noradrenaline, dopamine, serotonin, histamine or melatonin, it does not exclude the possibility of these transmitters playing a role in oligodendrocyte development or function. Since all of these transmitters can activate G-protein coupled receptors, which could alter intracellular $[Ca^{2+}]$, cAMP or IP_3 concentrations without altering membrane current, I might not detect activation of these receptors by simply recording the membrane current with whole cell clamping. Further experiments are therefore needed to assess such possible effects of these neurotransmitters on oligodendrocytes.

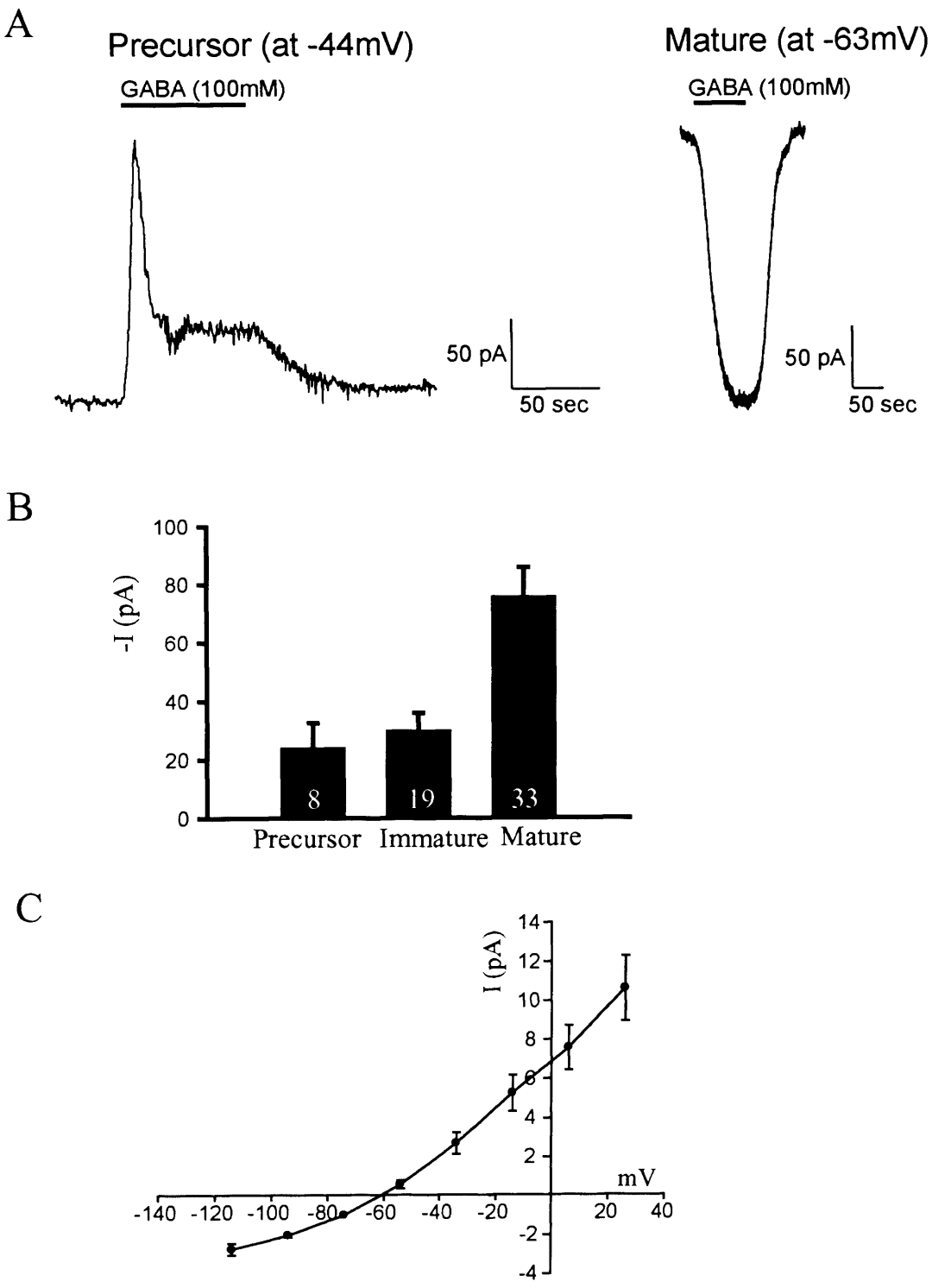

Figure 5.1 GABA-evoked currents in oligodendrocytes. **A** GABA (100μM) evokes an outward current at -44mV in a precursor oligodendrocyte (with E_{Cl}=-87mV) and an inward current at -63mV in a mature oligodendrocyte (with E_{Cl}= 0mV). **B** The mean GABA-evoked current at -63mV (with E_{Cl}=0mV) increased significantly (p=0.0008) with maturation. **C** Current-voltage relation for GABA-evoked current in 3 precursor cells (normalised to 1 at -63mV), showing that the current reverses at -61mV (with E_{Cl} = -87mV, but in HCO_3^--buffered solution).

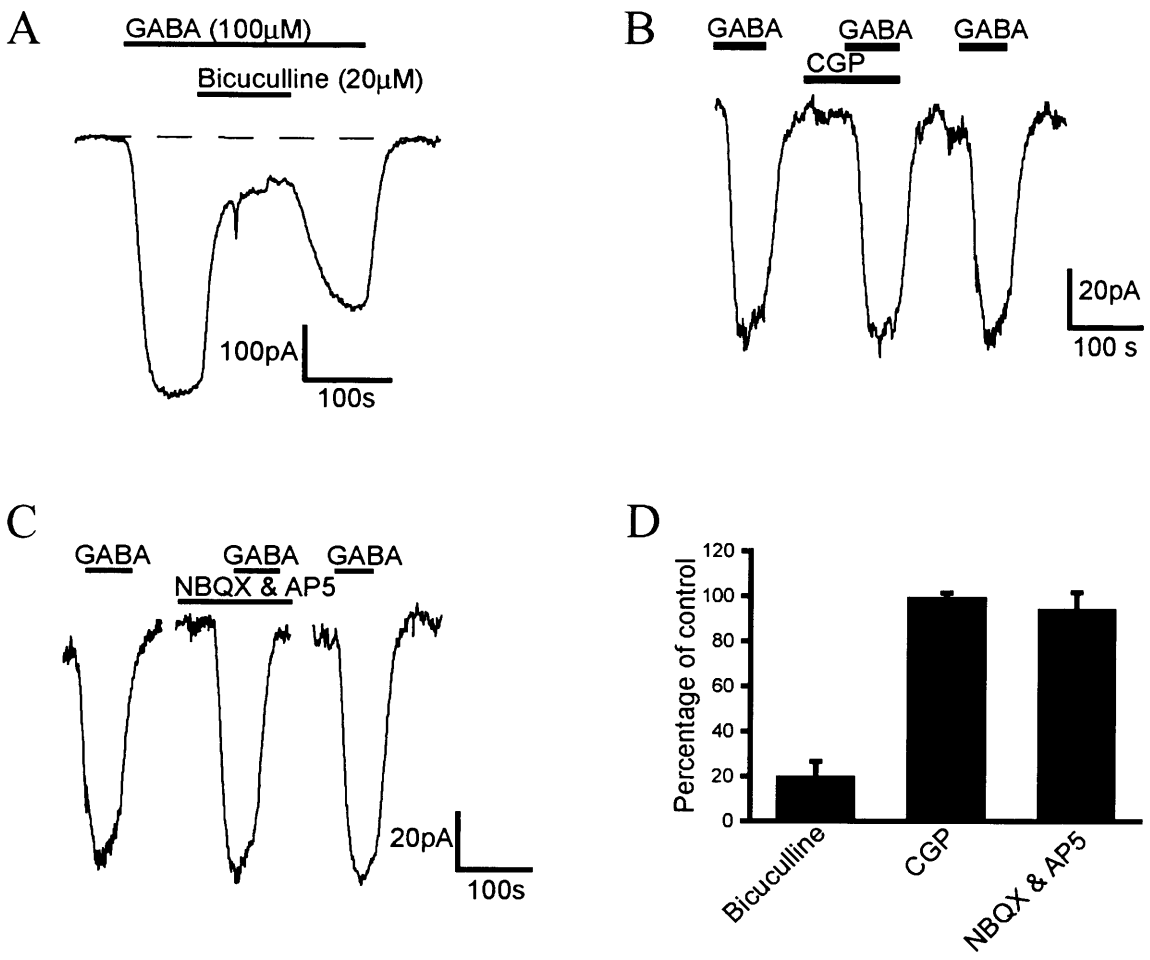

Figure 5.2 The GABA-evoked current is mediated by $GABA_A$ receptors. **A** The $GABA_A$ receptor antagonist bicuculline (20μM) blocks the GABA (100μM) evoked current (bicuculline alone generated no current change). **B** The $GABA_B$ receptor antagonist CGP 35348 (50μM) did not reduce the GABA (100μM) evoked current. **C** The glutamate antagonists NBQX (25μM) and AP5 (50μM) did not have any effect on the GABA (100μM) evoked current. **D** The mean effect on the GABA-evoked current (at -80mV, with E_{Cl} = -60mV) of: 20μM bicuculline (9 cells, p=0.008), 50μM CPG 35348 (6 cells, p=0.74), and 25μM NBQX & 50μM AP5 (4 cells, p=0.21).

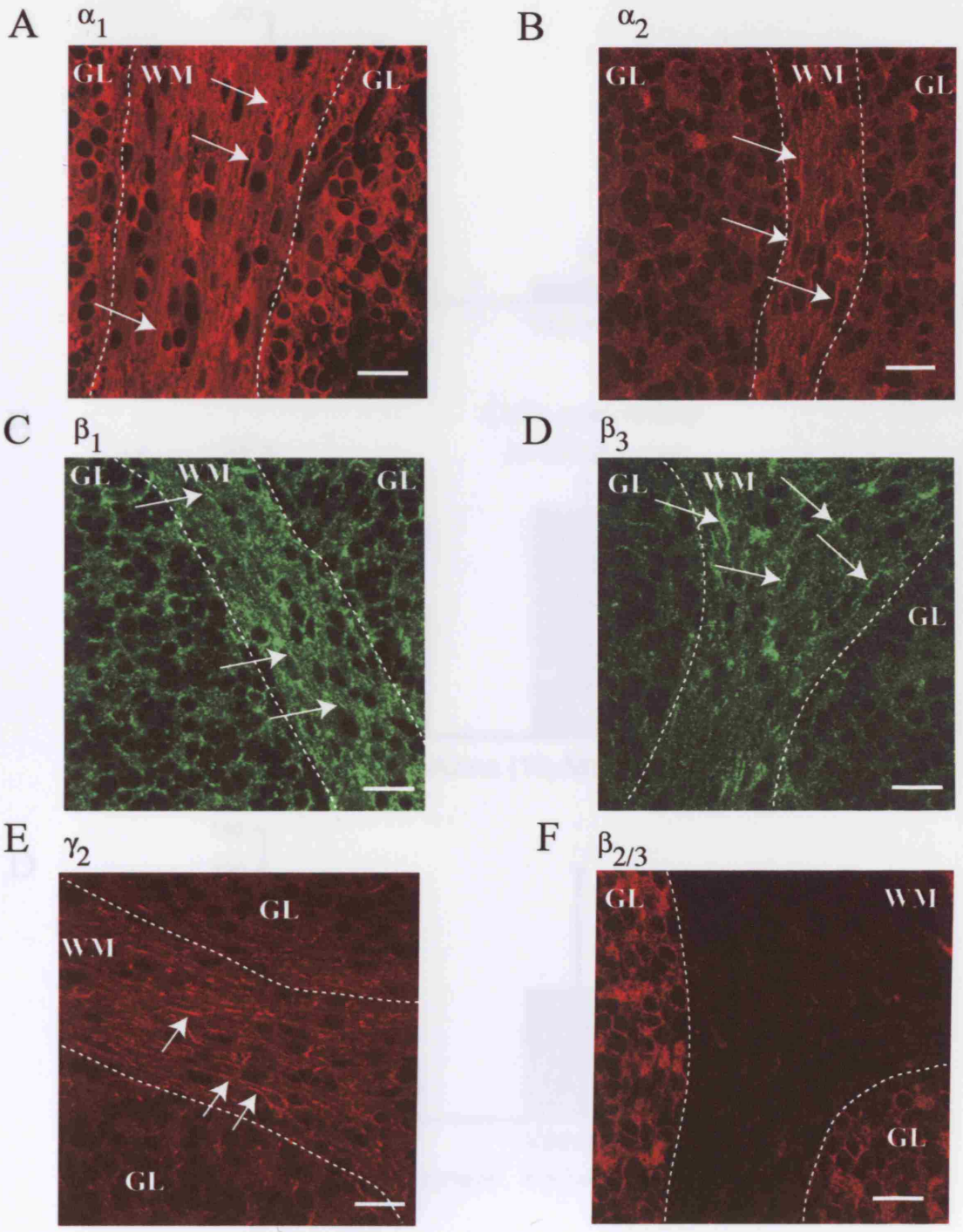

Figure 5.3 Antibody labelling of white matter GABA receptor subunits. Antibodies against the α_1 (**A**), α_2 (**B**), β_1 (**C**), β_3 (**D**) and γ_2 (**E**) subunits of the GABA receptor labelled cells in the white matter. Arrows point at labelled processes in the white matter. **F** The antibody against $\beta_{2/3}$ subunits (and that for β_2, not shown) did not label any cell in the white matter, but did label the cerebellar grey matter. Scale bar 20µm. WM, white matter; GL, granular cell layer.

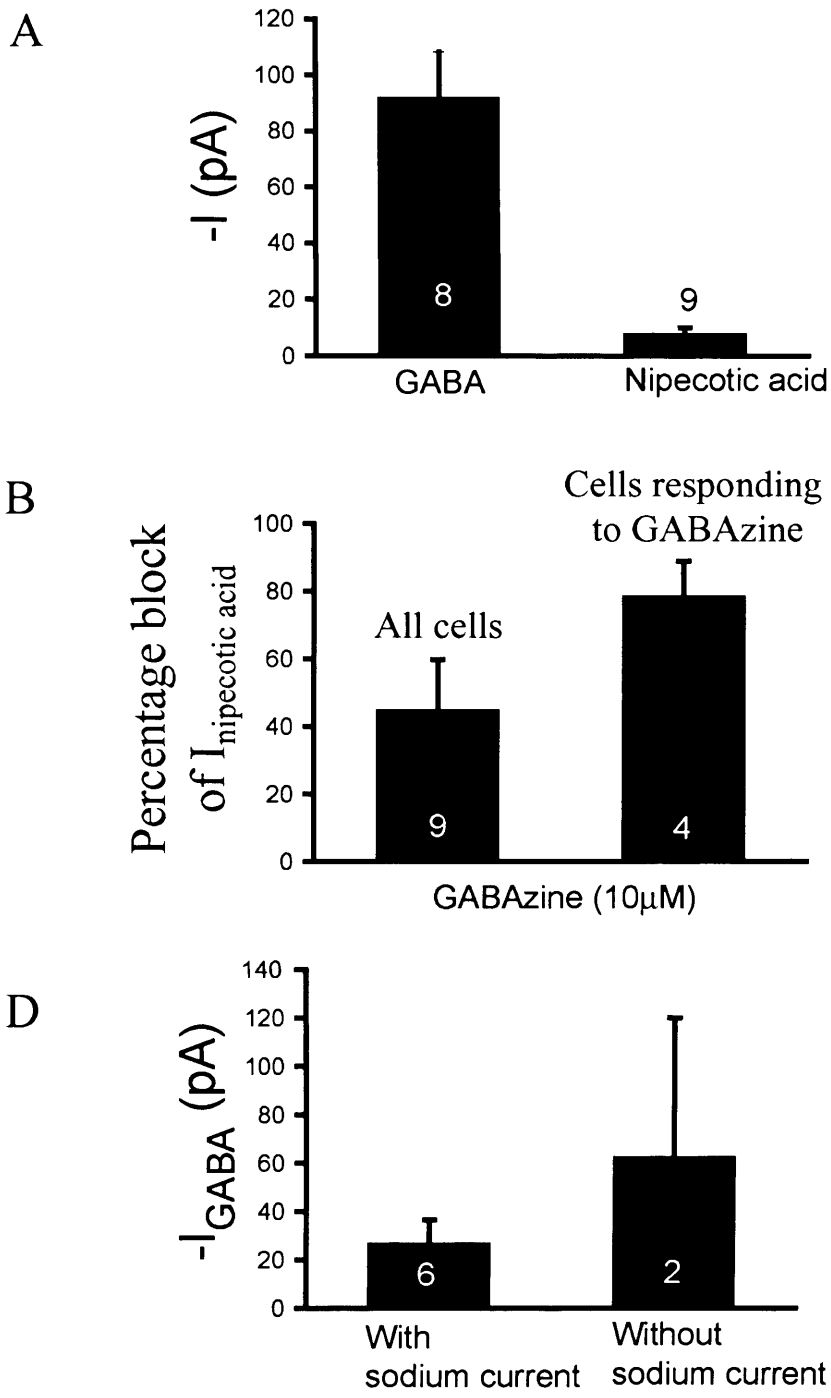

Figure 5.4 Test of the potential for endogenous GABA to act on oligodendrocytes, and comparison of the effect of exogenous GABA on the two types of $NG2^+$ cell. **A** GABA (100 μM) evoked a larger inward current (with E_{Cl}=0mV) in oligodendrocytes than was evoked by the GABA concentration rise produced by nipecotic acid (100 μM). **B** GABAzine (10 μM) reduced the current evoked by nipecotic acid in only 4 cells out of the 9 that responded to nipecotic acid application: the left bar shows pooled data for the effect of GABAzine on all 9 cells, while the right bar shows the effect of GABAzine on the 4 responsive cells. **C** The response to 100 μM GABA of the two types of $NG2^+$ cell is not significantly different. All at -63mV.

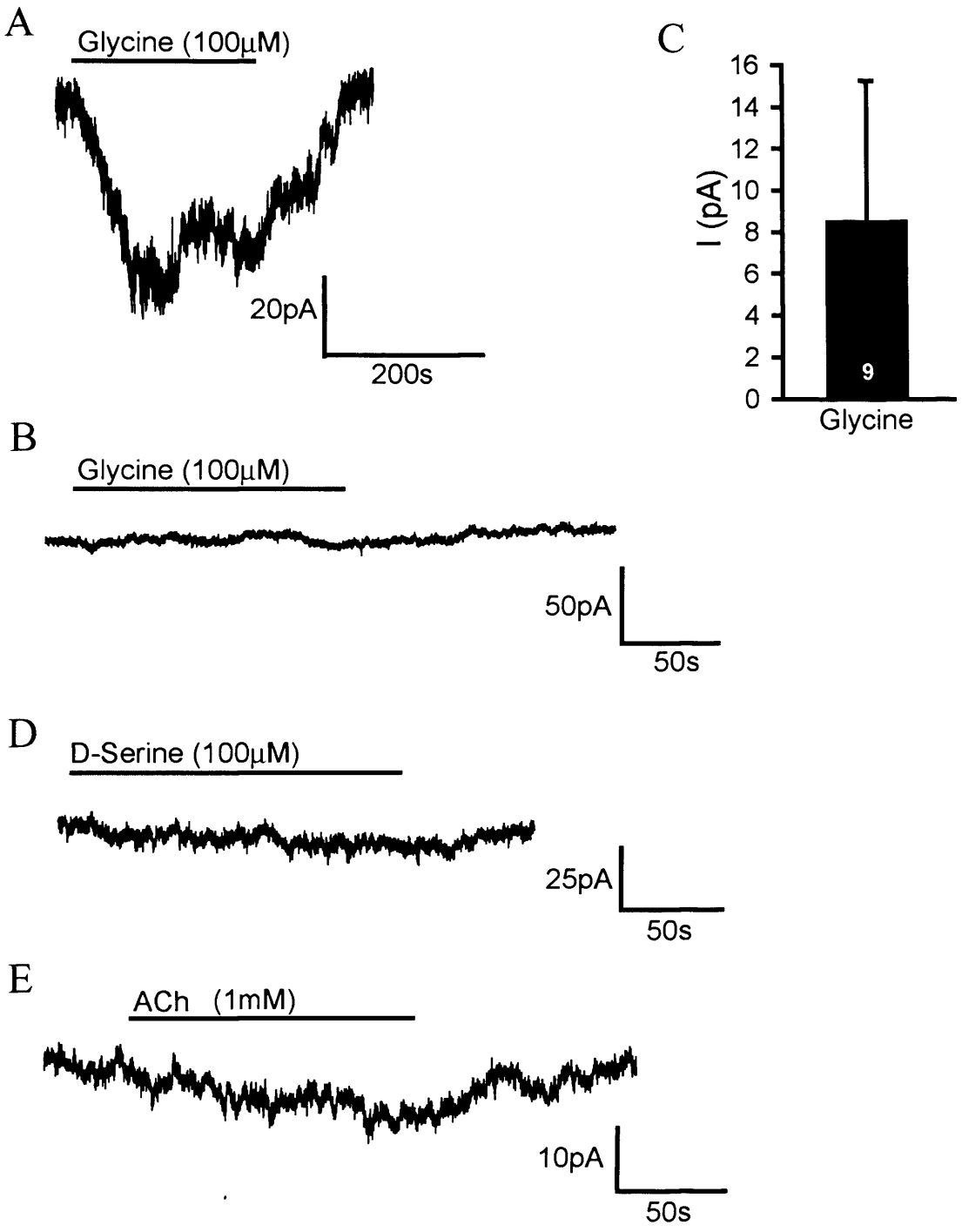

Figure 5.5 Glycine, D-serine and acetylcholine responses in oligodendrocytes. **A, B** Glycine (100μM) evoked a current in 2 out of 9 oligodendrocytes tested (A shows specimen response), but did not evoke a current in 7 out of 9 oligodendrocytes tested (B shows specimen response). **C** Mean glycine evoked current in all 9 cells tested. **D** 100μM D-serine did not evoke a current in oligodendrocytes (n=4), nor did 1mM acetylcholine (**E**). Holding potential was -63mV, E_{Cl}=0mV.

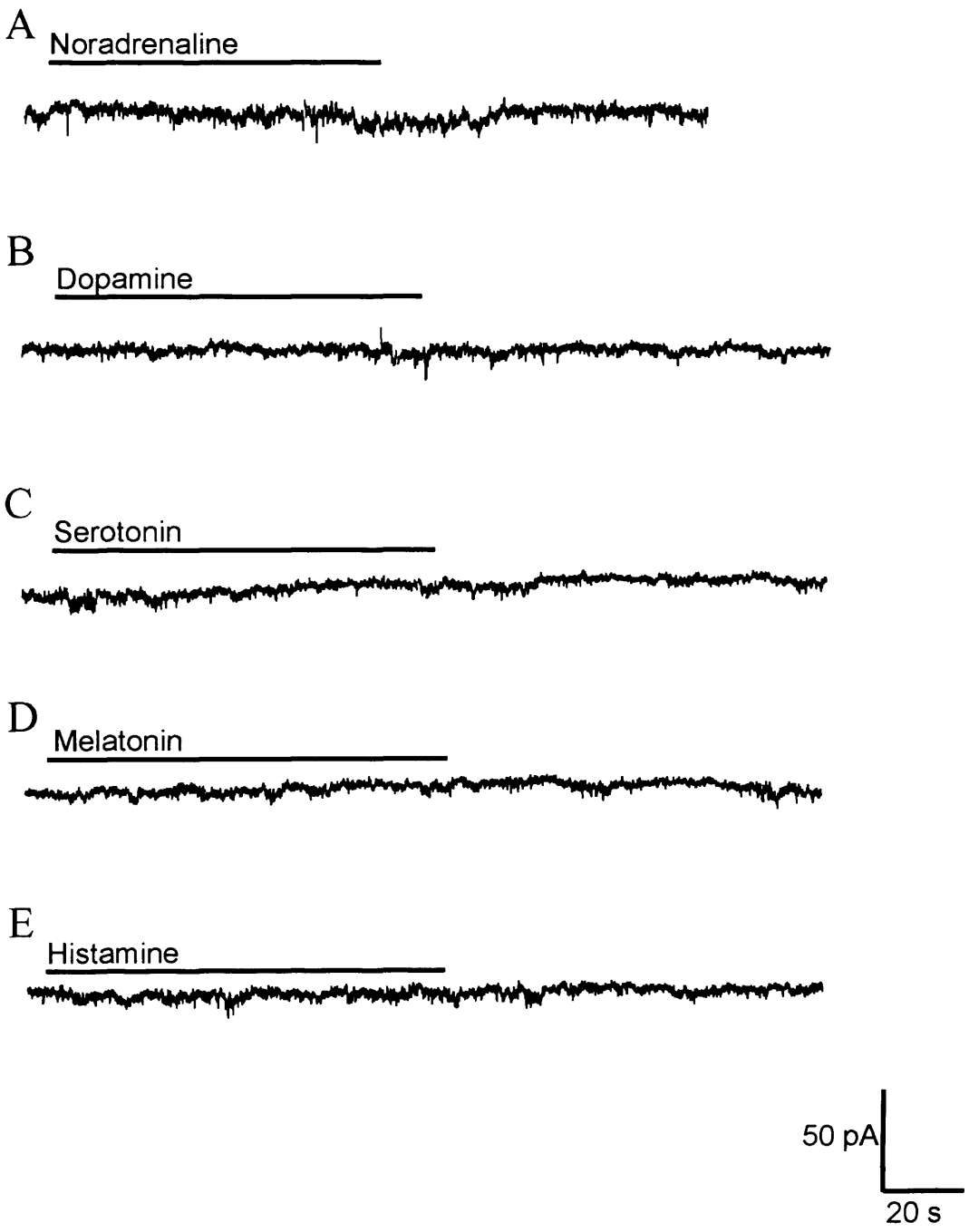

Figure 5.6 Amines do not generate a current response in oligodendrocytes. **A** 10μM noradrenaline (8 cells), **B** 100μM dopamine (10 cells), **C** 100μM serotonin (10 cells), **D** 100μM melatonin (5 cells) and **E** 100μM histamine (5 cells) did not evoke any current in the oligodendrocytes. Holding potential -63mV, E_{Cl}=0mV.

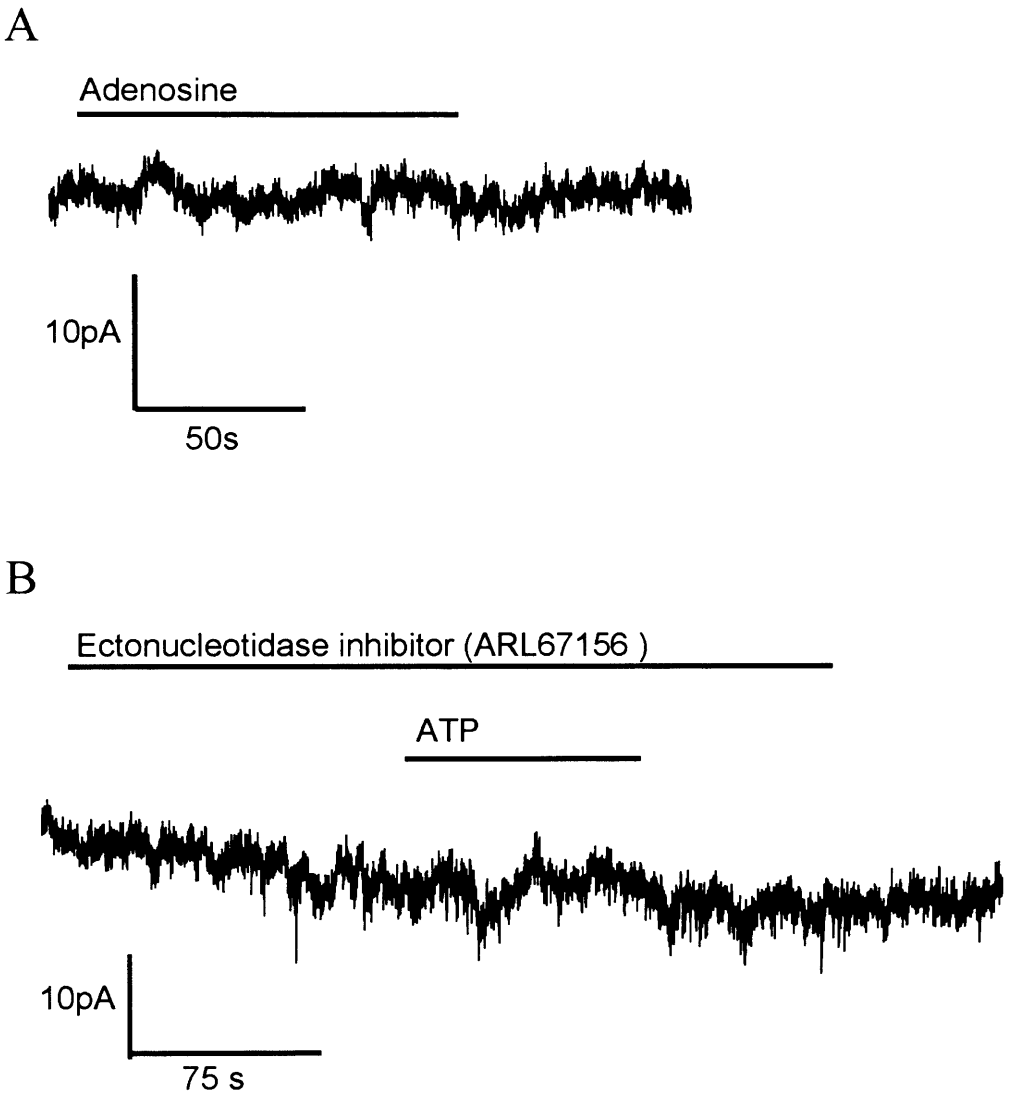

Figure 5.7 Adenosine and ATP do not generate a current in oligodendrocytes. **A** 100μM adenosine (9 cells) did not evoke any current in oligodendrocytes. **B** 100μM ectonucleotidase inhibitor ARL67156 did not generate a current nor did 100μM ATP (9 cells) applied in the presence of the inhibitor. Holding potential -63mV, E_{Cl}=0mV.

Chapter 6

White matter ischaemia

6.1 Introduction

In this chapter I will describe experiments investigating the electrical response of oligodendrocytes to simulated ischaemia, which mimics the occurrence of stroke, spinal cord injury or the conditions causing periventricular leukomalacia *in vivo*. A major aim was to investigate whether there is activation of the oligodendrocytes' glutamate and GABA receptors (described in chapters 4 & 5 of this thesis) during ischaemia since, as described in Chapter 1, there is evidence that in pathological conditions activation of glutamate receptors, at least, plays a role in damaging the cells.

6.2 Methods

Brain slices Cerebellar or corpus callosum slices (225μm thick) were prepared from P7-P14 rats as described in Section 2.1. Slices were superfused at 33±1°C with bicarbonate Ringer's solution, composed of (in mM): NaCl 126, $NaHCO_3$ 24, NaH_2PO_4 1, KCl 2.5, $CaCl_2$ 2.5, $MgCl_2$ 2, D-glucose 10 (gassed with 95% O_2/5% CO_2), pH 7.4.

Recording White matter cells were whole-cell clamped, as in chapter 3, with pipettes containing a CsCl-based solution, comprising (mM): 130 CsCl, 4 NaCl, 0.5 $CaCl_2$, 10 HEPES, 10 BAPTA, 2 MgATP, 0.5 Na_2GTP, K-Lucifer yellow 2, pH set to 7.3 with CsOH (E_{Cl} = 0mV) or a Cs-gluconate-based solution, comprising (mM): 130 Cs-gluconate, 4 NaCl, 0.5 $CaCl_2$, 10 HEPES, 10 BAPTA, 4 MgATP, 0.5 Na_2GTP, 2 K-Lucifer yellow, pH set to 7.3 (E_{Cl} = -87mV, or E_{Cl} = -60mV with 120mM Cs-gluconate and 10mM CsCl replacing 130mM Cs-gluconate).

Statistics These are described in chapter 2, section 2.13.

6.3 Results

6.3.1 Energy deprivation induces an inward current in oligodendrocytes

To mimic the energy deprivation which occurs in perinatal asphyxia, in stroke, or after blood vessel damage in spinal cord injury, I replaced external O_2 by N_2, replaced external glucose by 7mM sucrose, added 2mM iodoacetate to block glycolysis, and added either 100μM rotenone or 25μM antimycin to block oxidative phosphorylation. (Chapter 8 describes experiments comparing the effects of various combinations of metabolic blockers on CNS grey matter, which justifies this combination of blocking agents). This simulated ischaemia solution evoked a slowly developing inward current in both the precursor and the mature oligodendrocytes (Fig. 6.1, data recorded with an internal solution for which E_{Cl} = 0mV, see Methods). In 2mM Mg^{2+}, for 14 mature cells the peak inward current occurred after 6.7±2.0 mins and was 199±39 pA, while in 8 precursors it occurred after 13±1 mins and was 275±78 pA (Fig. 6.1A). Although the size of the peak ischaemia-evoked current did not differ significantly between the mature and the precursor oligodendrocytes (p=0.3), the time for the current to reach its peak was significantly shorter in the mature cells (p=0.01). On the other hand, when Mg^{2+} was absent from the extracellular solution (to maximise any current generated by NMDA receptors at the holding potential of -63mV), the time to peak current was similar in the mature cells and the precursors (9.2±0.9 mins and 11±2 mins respectively, p=0.4), but the precursors generated much less current than in 2mM Mg^{2+} (Fig. 6.1 A, C, 44±9pA, p=0.02), while the size of the current generated in mature cells (172±58pA) was unaffected by magnesium (p=0.2). There was a significant difference (p=0.004) in the size of the peak current between the mature and precursors in zero-Mg^{2+} solution (Fig. 6.1A).

6.3.2 Ischaemia activates oligodendrocyte AMPA and NMDA receptors

Antagonists to AMPA/kainate or NMDA receptors (NBQX and D-AP5) reduced the ischaemia-evoked current in both precursor and mature oligodendrocytes (Fig. 6.1B, C), demonstrating that the ischaemia-induced inward current was generated partly by a

rise of extracellular glutamate concentration, which activates both AMPA/kainate and NMDA receptors. In 2mM Mg^{2+} solution adding both NBQX and D-AP5 together reduced the inward current generated in ischaemia by 38% (Fig. 6.2A, C).

The relative contribution of NMDA and AMPA/kainate receptors to the glutamate-mediated current varied between cells, and was quantified in 0mM Mg^{2+} solution to make the NMDA receptor component more accurately measurable (*in vivo* Mg^{2+}-block would reduce the NMDA receptor component of the current by about a factor of 4 (see Chapter 4) but the depolarization of the cells produced by the ischaemia-evoked inward current would reduce the Mg^{2+}-block). Figure 6.2C, D summarizes the block by NBQX and D-AP5 of the ischaemia-evoked current in precursor and mature oligodendrocytes, giving the block both as a percentage of the ischaemia-evoked inward current (Fig. 6.2C) and as an absolute current (Fig. 6.2D). The NMDA receptor mediated current was usually similar to that mediated by AMPA/kainate receptors (Fig. 6.1C), but in some cells NMDA receptors mediated the majority of the current (Fig. 6.2B): on average in precursors D-AP5 blocked ~30% of the ischaemia induced current, while NBQX decreased the current by ~20% (Fig. 6.1C).

In mature oligodendrocytes the fraction of the inward current that was generated by glutamate was significantly ($p=0.04$) smaller than in precursor cells (compare Fig. 6.1B with Fig. 6.1C): the combination of D-AP5 and NBQX reduced the current by 16% (significantly reduced, $p=0.003$, Fig. 6.2C). However, although the fraction of the ischaemia-evoked inward current that was mediated by glutamate was less in mature than in precursor cells, because the magnitude of the ischaemia-evoked current was larger in mature cells in 0mM Mg^{2+} (Fig. 6.1A), the absolute size of the glutamate mediated current was similar in precursor and mature cells (Fig. 6.2D). This similarity of size suggests, in fact, that less glutamate is being released around mature cells in ischaemia, because they show a larger current response to exogenously applied glutamate (~2-fold larger in 2mM Mg^{2+}) and NMDA (~2.8-fold larger in 0mM Mg^{2+}) than do precursor cells (see Figs. 4.1A, B and 4.2A, B) presumably because they express a larger total number of glutamate receptors than do precursors.

All the simulated ischaemia experiments above were done in the cerebellar white matter, but it is the periventricular white matter which gets thinned in perinatal asphyxia, so I carried out some ischaemia experiments on the corpus callosum to test whether the responses found in the cerebellum are of general relevance and not specific to the cerebellum. I recorded from four mature cells in 0mM Mg^{2+} in the corpus callosum and in all of them simulated ischaemia induced an inward current with a similar time to peak (8.6±0.9 mins, p=0.7 compared with cerebellum) and similar size (Fig. 6.3) as for the mature oligodendrocytes in the cerebellum. As in cerebellar oligodendrocytes, D-AP5 blocked some of the ischaemia-evoked current (Fig. 6.3A, C).

These results, and those of Salter & Fern (2005) where they show that NMDA receptors are activated in optic nerve oligodendrocytes during ischaemia, allow me to conclude that in most white matter regions NMDA receptors are activated in ischaemia. This suggests that by blocking AMPA and NMDA receptors damage to the oligodendrocytes and their precursors could be reduced.

6.3.3 Simulated ischaemia evoked similar responses in the two classes of $NG2^+$ cells

Since the two classes of $NG2^+$ cells differed significantly in both their glutamate and NMDA responses (see section 4.3.6 for more detail), I analysed their responses to simulated ischaemia to determine whether they depended on whether the cells expressed voltage-gated Na^+ channels or not.

In both the $NG2^+$ cells expressing voltage-gated Na^+ channels and those that did not express Na^+ channels, simulated ischaemia generated an inward current with a similar time to peak, i.e. 12.9±0.6 and 13.4±0.1 mins in 2mM Mg^{2+} (p=0.9) and 10.3±0.7 and 13.7±4.4 mins in 0mM Mg^{2+} (p=0.5), respectively. Furthermore, the inward current generated in ischaemia (either with or without magnesium) was not significantly different between the two classes of $NG2^+$ cell (Fig. 6.4A, C). In addition, applying the glutamate receptor blockers NBQX and D-AP5 together reduced the current to a similar extent (Fig. 6.4B, D). Although the $NG2^+$ cells expressing voltage-

gated Na^+ channels have at least a 3-fold larger response to exogenously applied NMDA than cells lacking Na^+ channels (see section 4.3.6, Fig. 4.10B, C), activation of NMDA receptors in ischaemia in these two cell types was not significantly different either in 2mM Mg^{2+} ($p=0.47$, Fig. 6.5A) or in the absence of magnesium ($p=0.06$, Fig. 6.5C; the low number of cells studied makes it hard to come to a reliable conclusion on this point, however). The AMPA receptor activation in simulated ischaemia was also similar in the two cell classes (Fig. 6.5 B, D).

In $NG2^+$ cells which exhibited a voltage-gated Na^+ current, the inward current generated in simulated ischaemia included a significant contribution from rapid synaptic current-like events (see Fig. 6.2A, B, and Fig. 6.6A), which greatly increased in frequency early in ischaemia. These events are further analysed in chapter 7 of this thesis.

6.3.4 Oligodendrocyte $GABA_A$ receptors are activated in ischaemia

In both the grey and the white matter there is an increase in the extracellular GABA concentration during ischaemia (Shimada et al., 1993). In grey matter GABA release is either thought to be beneficial in ischaemia, as it will decrease the neuronal depolarization caused by glutamate, or thought to be harmful as it can cause cell damage resulting from an influx of Cl^- ions though $GABA_A$ receptors inducing cellular swelling (Inglefield & Schwartz-Bloom, 1998; Allen et al., 2004b). In the white matter, GABA acting on $GABA_A$ receptors has been reported to decrease action potential conduction in the spinal cord during ischaemia (Lee et al., 1993), but Fern et al. (1995b) reported the contrary, as they claimed that GABA ameliorated action potential conduction loss in optic nerve ischaemia by acting through $GABA_B$ receptors. Because of this discrepancy, and because oligodendrocytes respond to GABA which might be released in the white matter by GABA transporters, as shown in chapter 5, I looked at whether oligodendrocyte $GABA_A$ receptors are activated in simulated ischaemia. To test this I examined the effect of applying 10μM GABAzine: a concentration which

completely blocks the tonic activation of high affinity $\alpha_6\delta$ subunit containing $GABA_A$ receptors in cerebellar granule cells (Rossi et al., 2003).

Simulating ischaemia in five mature oligodendrocytes with E_{Cl} set at 0mV generated an inward current at -63mV as described above, and 10μM GABAzine reduced the current (Fig. 6.7A shows raw data in 2mM Mg^{2+}). The mean reduction of the inward current occurring in 5 cells in 0mM Mg^{2+} was 14±1% (p=0.0004, Fig. 6.6C white bar). This block is similar to the reduction produced by the combined application of AMPA and NMDA receptor antagonists in Figure 6.2. Setting the reversal potential for chloride more negative, at -87mV (see Methods), did not affect the size of the ischaemia-evoked inward current in mature oligodendrocytes (recorded now at a slightly more negative potential, -74mV instead of -64mV; see right two bars in (Fig. 6.6B). Interestingly, with this internal solution, which one might expect to lead to GABA producing an outward Cl^- current at -74mV, which GABAzine should block and thus generate an inward current shift, I found that GABAzine still reduced the ischaemia-evoked inward current (by 11±2%, Fig. 6.6C).

These results from mature oligodendrocytes indicate that $GABA_A$ receptors are activated during ischaemia. There are two possible explanations for why GABAzine reduced the inward current instead of increasing it, when E_{Cl} was set to -87mV and the cell was held at -74mV. Firstly, as explained in section 5.3.1, the bicarbonate permeability of the $GABA_A$ receptor could lead to the reversal potential for the net current through $GABA_A$ receptors being -64mV when E_{Cl} is set to -87mV, so that these receptors would generate an inward current at the holding potential of -74mV. Secondly, the mature cells are probably not well voltage clamped and perhaps their intracellular $[Cl^-]$ is not well controlled by dialysis from the pipette either (as described in chapter 2, sections 2.8 and 2.9), so even with E_{Cl} set below the holding potential at the soma where the pipette is attached, it may be above the membrane potential in the cells' processes. I therefore turned to precursor oligodendrocytes, as they are better voltage clamped and dialysed, to further study the activation of GABA receptors during ischaemia.

Precursor oligodendrocytes were clamped with one of two internal solutions with different chloride concentrations, so the chloride reversal potential was either E_{Cl} = -60mV or -87mV. Precursors clamped with the E_{Cl}=-60mV internal, held at -40mV showed a larger inward current in ischaemia (209±64pA in 4 cells) than those clamped with the E_{Cl}=-87mV internal and held at -44mV (61±20pA in 3 cells; Fig. 6.6B). The tendency (p=0.11) towards a smaller inward current in the precursor cells when E_{Cl} was -87mV may occur because, with the more negative Cl^- reversal potential (and essentially the same holding potential), there is a larger driving force for Cl^- entry when $GABA_A$ receptors are activated. Thus, more Cl^- ions will enter the cell, generating an outward current component which reduces the net inward current generated in ischaemia. GABAzine (10μM) had little effect on the ischaemia-evoked current (increased by 3±3%) in cells clamped with E_{Cl}=-60mV and held at -40mV, but in the cells clamped with E_{Cl} = -87mV and held at -44mV, it increased the inward current by 31±16% (see Fig. 6.6A). The reason for this difference between the two internals, when in both cases the cells were held at a membrane potential above the reversal potential for chloride, may reflect the fact that GABA receptors are also permeable to bicarbonate (as described above and in chapter 5). By using equation 5.1 to calculate the reversal potential for $GABA_A$ receptors, one finds that the reversal potential for the internal solution with E_{Cl}=-60mV is -48mV, which is quite close to the holding potential of -40mV so that not much current change mediated by $GABA_A$ receptors is expected. In contrast, for the internal with E_{Cl}=-87mV the predicted reversal potential is -64mV which is well above the holding potential of -44mV, so that Cl^- ions should enter the cell when $GABA_A$ receptors are activated and reduce the ischaemia-evoked inward current, and when the receptors are blocked the inward current should increase. Since this was exactly what happened, this is again consistent with $GABA_A$ receptors being activated in ischaemia in oligodendrocytes.

6.3.5 The ischaemia-induced inward current in oligodendrocytes is not generated via TRP channels

The data for 0mM Mg^{2+} in Figure 6.2C suggest that, for precursor and mature cells, only about 50% and 16% (respectively) of the inward ischaemia-evoked current can be accounted for by glutamate activating NMDA and AMPA/kainate receptors. Although $GABA_A$ receptor activation may generate some of the remaining current, I considered it worth testing for other possible contributions to the ischaemia-evoked current. TRP channels and voltage-gated Ca^{2+} channels seemed likely candidates.

There are six protein families that make up the mammalian TRP cation channel super-family, some of which are permeable to calcium. Almost all the TRP channel subunits are expressed in the mammalian central nervous system (reviewed by Moran et al., 2004), and one member of this family, the TRPM7 channel, has been shown to play a role in excitotoxic neuronal death, as it allows calcium to enter the cells and reach a toxic concentration even in the presence of glutamate receptor blockers (Aarts et al., 2003). In addition, it has been suggested that voltage-gated calcium channels get activated in white matter ischaemia and hence cause excitotoxic death of oligodendrocytes and astrocytes (Fern et al., 1995a).

I investigated the role of TRP and voltage-gated calcium channels in oligodendrocyte ischaemia by using lanthanum (La^{3+}) which inhibits current flow through TRPM7 channels (Runnels et al., 2001), and also blocks some other TRP family members (TRPM4, M1, V6, V5, V4 and C7, (TRPM4, M1, V6, V5, V4 and C7, reviewed by Clapham et al., 2001). Furthermore, lanthanum also blocks voltage-gated calcium channels (Hille, 2001).

Simulated ischaemia activated an inward current in five mature oligodendrocytes that was unaffected by 200μM La^{3+} (reduced by 0.3±0.3%, Fig. 6.7A, C). These results indicate that neither TRP channels nor voltage-gated calcium channels contribute a large fraction of the ischaemia-evoked inward current during white matter ischaemia. These findings support the finding of Fern and Möller (2000) that the intracellular calcium rise in oligodendrocytes, in culture, during simulated ischaemia was unaffected by La^{3+} and was mainly due to glutamate activating its receptors.

6.3.6 TTX does not affect the ischaemia-induced current in oligodendrocytes.

To explore the possibility that neuronal depolarization and hence propagation of action potentials was a major contributor to the generation of the inward current seen in oligodendrocytes during simulated ischaemia, I applied TTX to the slice, both during the generation of the inward current when ischaemia solution had been applied for some time, and throughout the whole experiment mimicking ischaemia.

In seven precursor cells (in 0mM Mg^{2+}) 1μM TTX reduced the ischaemia-evoked inward current by 15±13% (not significant, p=0.36, Fig. 6.7C). Out of these 7 cells, there was only one cell where TTX seemed to block the generation of the ischaemia induced current (shown in Fig. 6.6A) and in five precursors it did not have any effect on the development of the inward current (Fig. 6.7B). Furthermore, in two cells I had 1μM TTX present during the whole period of simulated ischaemia and with TTX present ischaemia still generated a similar size inward current as without TTX (data not shown due to the low number of cells studied). It seems likely from these data that neuronal excitation is not contributing significantly to the generation of the ischaemia-induced inward current in oligodendrocytes. Further experiments are needed to understand the why in some precursors the ischaemic current was affected by TTX but in other precursors it was insensitive to TTX.

6.4 Discussion

6.4.1 The ischaemia-evoked inward current in oligodendrocytes

Precursor and immature oligodendrocytes have been shown to be more vulnerable to ischaemia than mature cells (Back et al., 2002; Deng et al., 2003). Simulated ischaemia induced a similar magnitude of inward current in mature and precursor oligodendrocytes (in physiological solution containing 2mM Mg^{2+}, Fig. 6.1). Since the precursors have a smaller surface area (as seen from the morphology of the two cell stages shown in chapter 3), the ischaemia-induced inward current should produce more cation accumulation, and subsequent water accumulation by osmosis, which might induce more damage to these cells.

6.4.2 Activation of NMDA receptors in white matter ischaemia

I have shown that both AMPA and NMDA receptors get activated in oligodendrocytes during simulated ischaemia (Figs. 6.1, 6.2). This is the first electrical recording of the activation of oligodendrocyte glutamate receptors during (simulated) ischaemia. The main new result is that, contrary to previous findings (Matute et al., 1997; McDonald et al., 1998), I found that NMDA receptors are activated in oligodendrocytes during ischaemia, and in precursors these receptors can be responsible for the majority of the ischaemia-evoked current (Fig. 6.2B). NMDA receptors also get activated in mature cells, consistent with the findings of Schäbitz et al. (2000) who showed that NMDA receptor blockers ameliorated ischaemic damage to myelin and axons in the white matter.

The higher affinity of NMDA receptors, relative to AMPA receptors, will make them more likely to be activated in those neurodegenerative disorders involving a prolonged but small rise of extracellular glutamate concentration, as may occur in multiple sclerosis. Thus, oligodendrocyte NMDA receptors could contribute to causing the white matter damage which occurs when the extracellular glutamate concentration is raised in pre-/perinatal asphyxia, spinal cord injury, multiple sclerosis and stroke (Volpe, 2001; Matute et al., 2001; Dewar et al., 2003; Stys, 2004).

Even though the 13% block of the ischaemia evoked inward current by the NMDA receptor blocker D-AP5 (50μM) seen in mature oligodendrocytes is not as large as the 30% block seen in the precursors (Fig. 6.2C), the effect of activating NMDA receptors in mature cells may be particularly deleterious because the receptors' location in the myelinating processes of oligodendrocytes (see Fig. 4.8A, B in chapter 4) is associated with a high surface membrane to intracellular volume ratio and even a small Ca^{2+} or Na^{+} influx through NMDA receptor channels is expected to produce a large change of $[Ca^{2+}]_i$ or $[Na^{+}]_i$. This, together with the fact that the Mg^{2+}-block of the receptors is relatively weak (see chapter 4 for details), presumably accounts for the particularly deleterious effects that NMDA receptor activation has on oligodendrocyte processes during ischaemia even in physiological $[Mg^{2+}]$ (Salter & Fern, 2005). Synergy of the rise of $[Ca^{2+}]_i$ produced by activation of both AMPA/kainate and NMDA

receptors might explain why NMDA receptor blockers slow the loss of white matter action potentials (Tekkök & Goldberg, 2001) and reduce white matter damage in hypoxia/ischaemia (Schäbitz et al., 2000) and in an animal model of multiple sclerosis (Wallström et al., 1996). The rise of $[Na^+]_i$ produced by NMDA receptors will help to slow or reverse Na^+/Ca^{2+} exchange (Li et al., 2000) and thus increase the rise of $[Ca^{2+}]_i$. Thus, specific reduction of NMDA receptor function in oligodendrocytes might be beneficial during the onset of a disorder in which a rise of extracellular glutamate concentration causes oligodendrocyte damage. However, once the oligodendrocyte damage has occurred, then potentiating (rather than blocking) oligodendrocyte NMDA receptors may be a better therapeutic strategy if the migration of oligodendrocyte precursors into a damaged area depends on activation of oligodendrocyte NMDA receptors (Wang et al., 1996).

6.4.3 Activation of oligodendrocyte $GABA_A$ receptors in simulated ischaemia

I have shown that oligodendrocyte $GABA_A$ receptors are activated during simulated ischaemia (Figs. 6.6, 6.7). Depending on the exact value of E_{Cl} in precursor oligodendrocytes (see section 6.3.4), activation of $GABA_A$ receptors may decrease the depolarization of oligodendrocytes evoked by ischaemia (which could perhaps reduce damage to these cells), whereas in mature oligodendrocytes activation of $GABA_A$ receptors always produced an inward current regardless of the value of $[Cl^-]$ in the patch pipette and would tend to increase oligodendrocyte depolarization during ischaemia. This is consistent with a previous report that $GABA_A$ receptors are activated during ischaemia in the spinal cord and increase the damage produced by ischaemia (Sakatani et al., 1991). Furthermore it has been shown that oligodendrocytes have a high internal chloride concentration so activation of $GABA_A$ receptors will depolarize the cell (Kirchhoff & Kettenmann, 1992; Lin & Bergles, 2004). Interestingly, endogenous GABA release has been found to ameliorate recovery of the action potential in the optic nerve after anoxia, however that effect was found to be generated by $GABA_B$ receptors (Fern et al., 1995b).

6.4.4 The component of the ischaemia-evoked current that is not mediated by glutamate and GABA receptors

Further experiments are needed to fully characterize the mechanisms involved in generating the inward current seen in oligodendrocytes during simulated ischaemia. The data for 0mM Mg^{2+} in Figure 6.2C suggest that, for precursor and mature cells, only about 50% and 16% (respectively) of the inward ischaemia-evoked current can be accounted for by glutamate activating NMDA and AMPA/kainate receptors. In mature cells with E_{Cl}=0, a further 14% of the current is generated by activation of $GABA_A$ receptors (section 6.3.4), but I have not carried out corresponding experiments (in 0mM Mg^{2+} with E_{Cl}=0mV) on precursors. Thus, in mature cells around 30% of the inward current is due to GABA and glutamate release, and it would be interesting to know what generates the remaining 70% of the current. My experiments with La^{3+} suggest that it is not due to calcium entry through TRPM7 channels or voltage gated calcium channels, and it was quite insensitive to TTX. It would be interesting to examine the role of oxidative stress during ischaemia in oligodendrocytes, as it has been suggested as a mechanism causing damage to the cells (Oka et al., 1993; Deng et al., 2003; Cai et al., 2005)

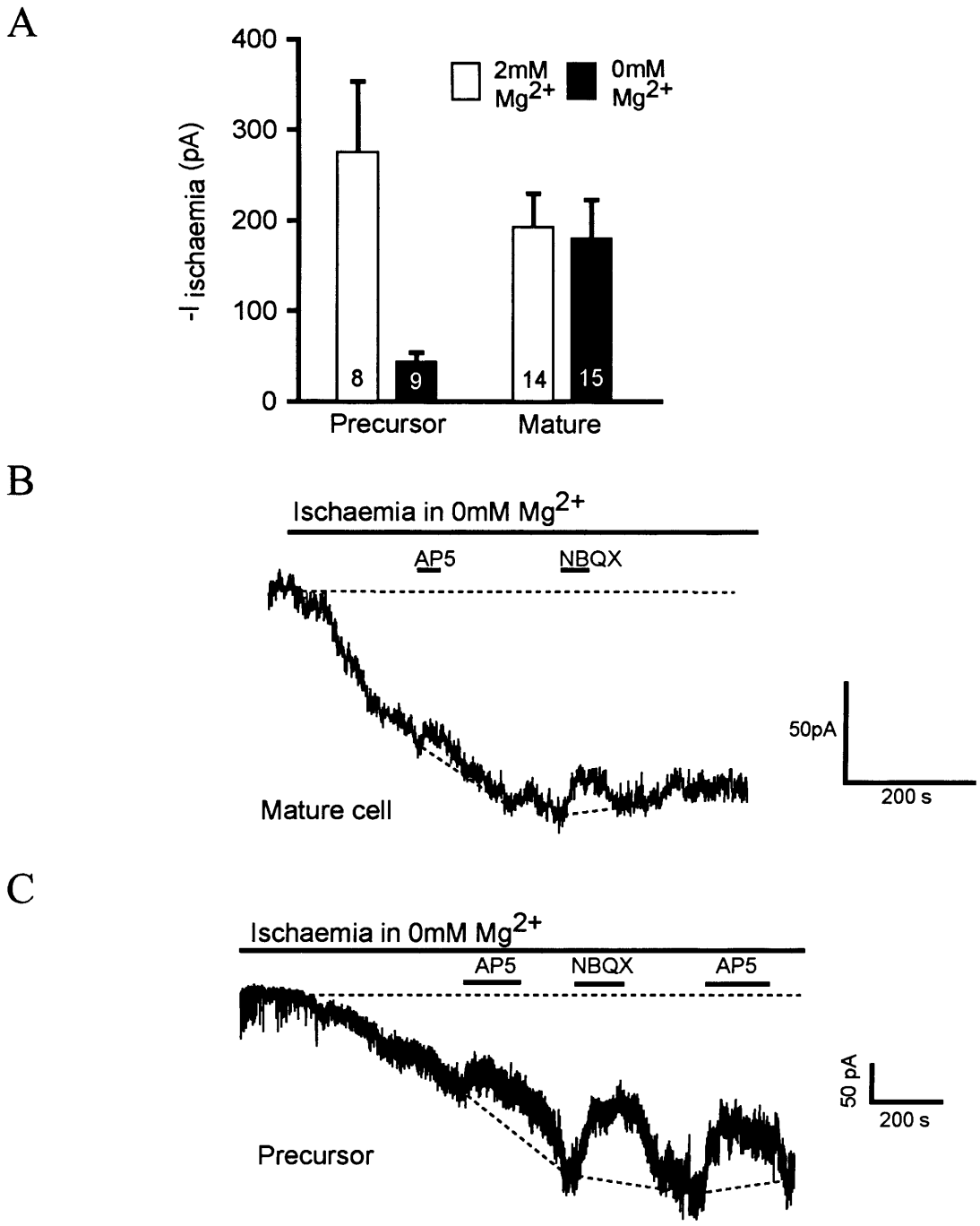

Figure 6.1 Metabolic inhibition in the white matter generates an inward current in oligodendrocytes at all developmental stages, that is mediated partly by glutamate receptors. **A** Ischaemia-evoked inward current in precursor and mature oligodendrocytes (peak inward current at -63mV after ~13 or ~7 mins simulated ischaemia in precursor or mature cells respectively). In 2mM Mg^{2+} the inward current did not differ significantly ($p=0.29$) between precursors and mature cells. However, in 0mM Mg^{2+} precursors showed much less current response to ischaemia than mature cells ($p=0.004$). In addition, the current response of precursors in 2mM Mg^{2+} and 0mM Mg^{2+} differed significantly ($p=0.02$), while that of mature cells did not. **B** Response to simulated ischaemia in a mature oligodendrocyte (in 0mM Mg^{2+}). The ischaemia-induced current is reduced with glutamate receptor blockers (50μM AP5, $p=0.010$ & 25μM NBQX, $p=0.048$). **C** Response to simulated ischaemia in a precursor oligodendrocyte (in 0mM Mg^{2+}). The ischaemia induced current is reduced with glutamate receptor blockers (50μM AP5, $p=0.016$ & 25μM NBQX, $p=0.020$).

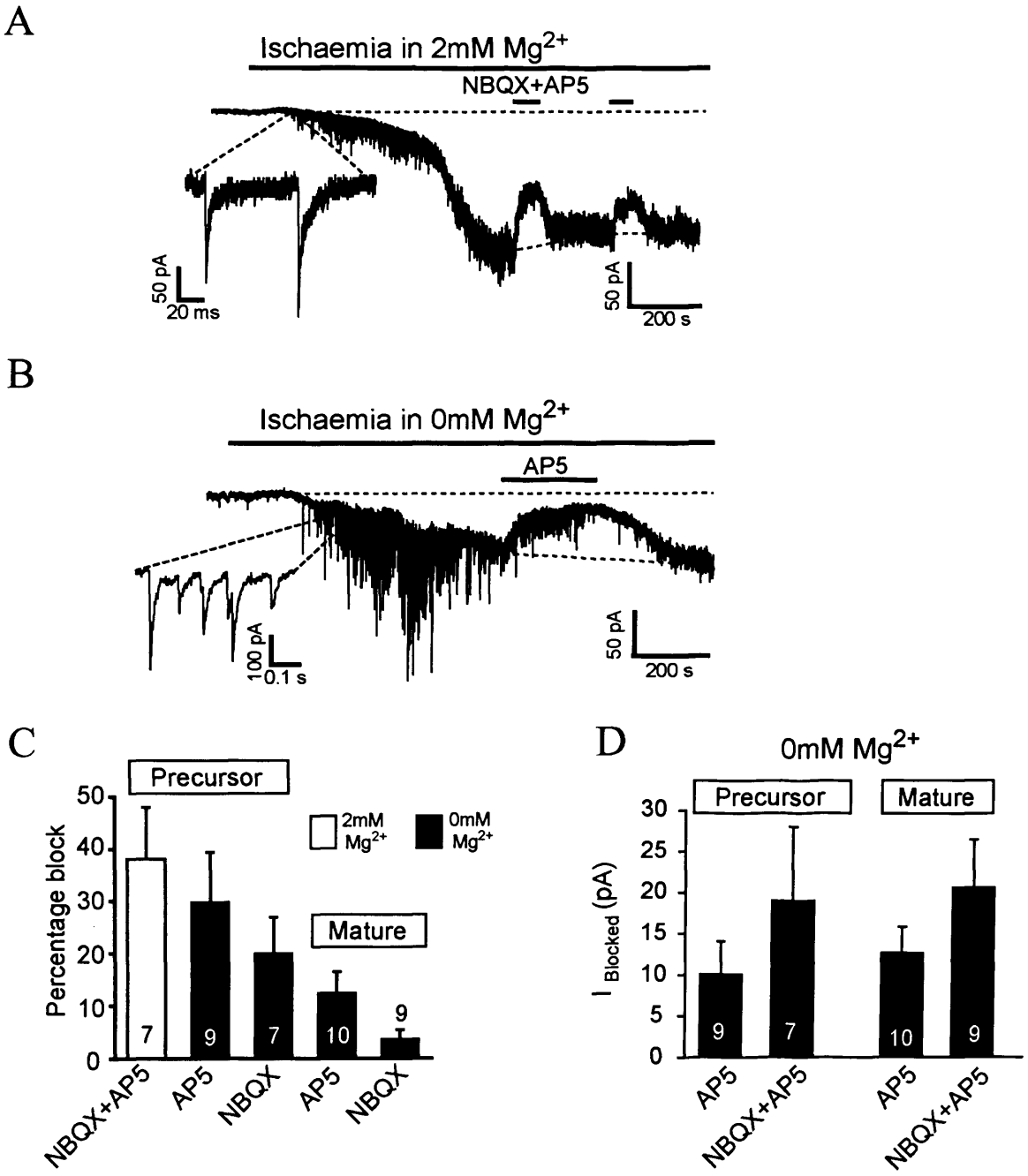

Figure 6.2 The relative contribution of AMPA and NMDA receptors to the ischaemia-evoked current. **A** Ischaemia-evoked current in an oligodendrocyte precursor (in 2mM Mg^{2+}) is reduced by NBQX (25 μM) plus D-AP5 (50 μM). Inset: ischaemia-induced synaptic-like currents. **B** Precursor response (0mM Mg^{2+}) showing dramatic transient increase in synaptic current activity (inset), and most inward current mediated by NMDA receptors. **C** Fractional block of inward current: in 2mM Mg^{2+} by D-AP5 plus NBQX in 7 precursors, and in 0mM Mg^{2+} by D-AP5 or NBQX in precursor cells (9 for D-AP5, 7 for NBQX) and in mature cells (10 for D-AP5, 10 for NBQX): p= 0.098 comparing D-AP5 effect in precursors and mature cells; p=0.019 comparing NBQX effect in precursors and mature cells. **D** Absolute current blocked by either NBQX and D-AP5 together or by D-AP5 alone, in precursor and mature cells (in 0mM Mg^{2+}); p= 0.31 comparing D-AP5 effect in precursors and mature cells; p=0.67 comparing NBQX + D-AP5 effect in precursors and mature cells. All cerebellum, -63mV, 33°C, number of cells is shown in the bars.

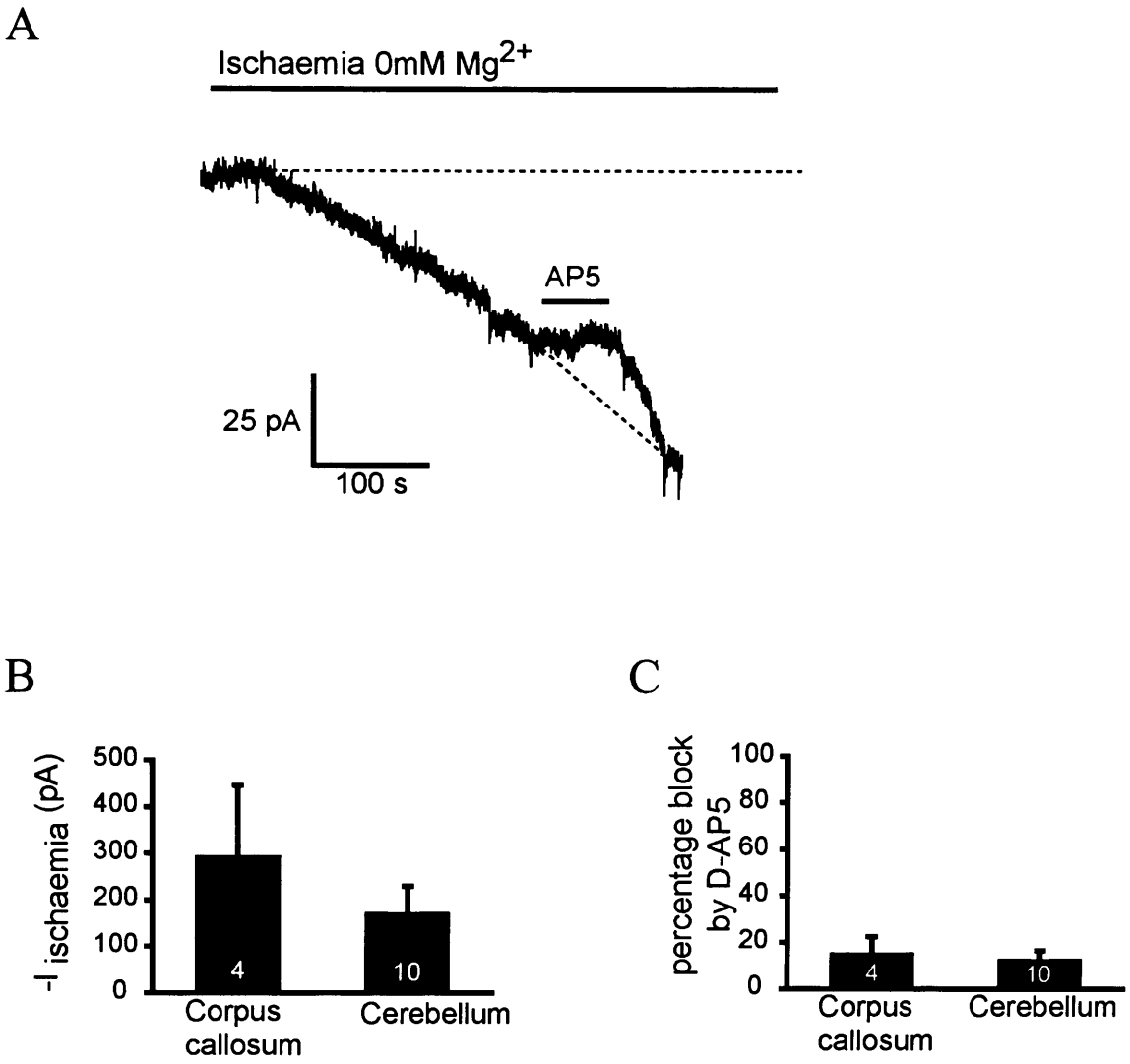

Figure 6.3 Ischaemia induces an inward current in mature oligodendoytes in the corpus callosum which is partially blocked by D-AP5. **A** Ischaemia-evoked current in a mature oligodendrocyte (0mM Mg^{2+}) and its block by 50 μM D-AP5 **B** Mean ischaemia-induced current in 4 mature oligodendrocyte in the corpus callosum and 10 mature cells in the cerebellum (not significantly different, p=0.64). **C** Fractional block by D-AP5 of the ischaemia evoked inward currents in B; no significant difference is seen between the regions (p=0.75). All at -63mV, 33°C, number of cells are shown in the bars.

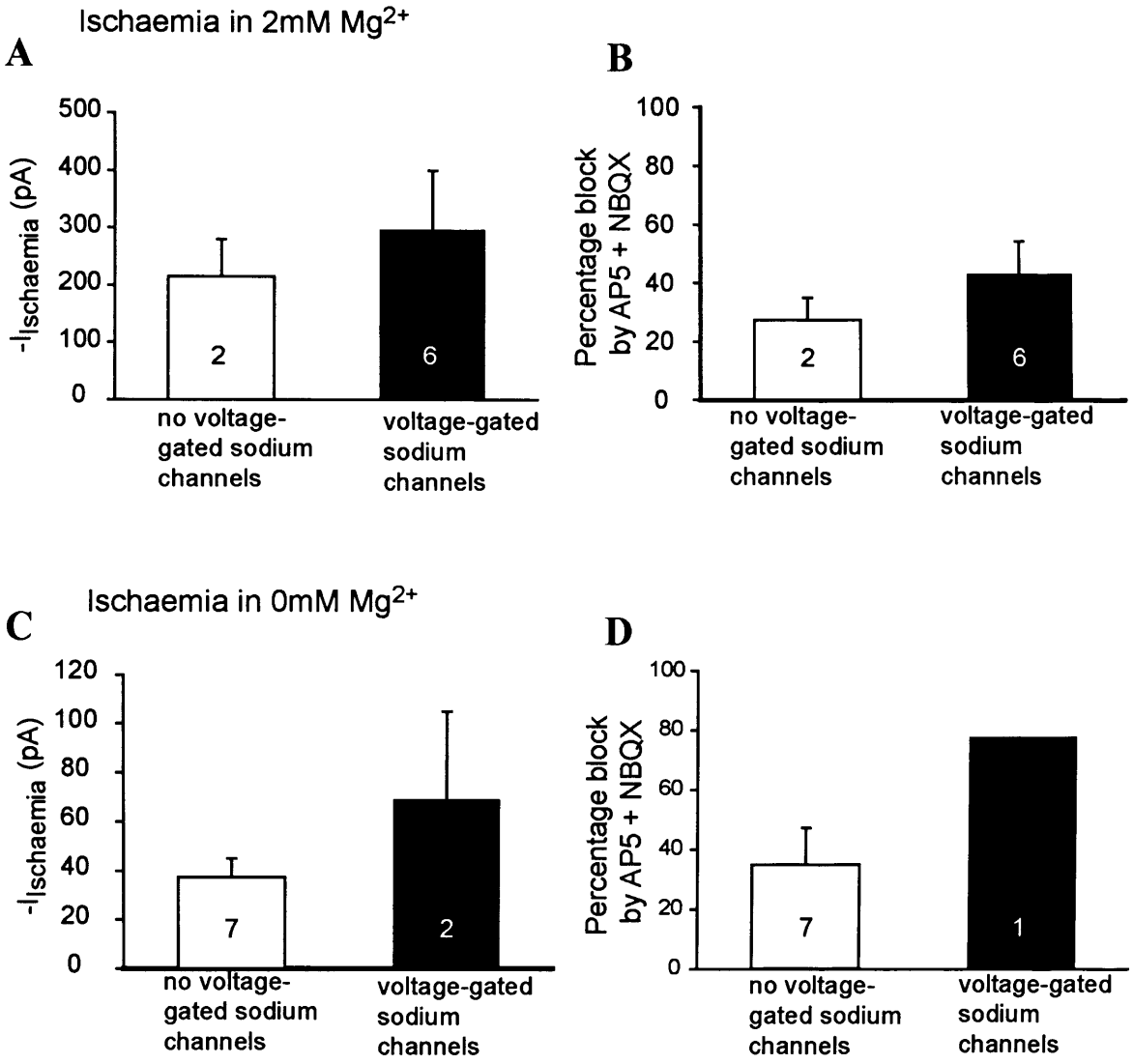

Figure 6.4 The two classes of $NG2^+$ cell do not differ significantly in their ischaemic responses. **A** Mean ischaemia-evoked current, with 2mM Mg^{2+} present, in $NG2^+$ cells that do not express voltage-gated sodium channels (n=2) or $NG2^+$ cells that do express sodium channels (n=6); not significantly different (p=0.7). **B** Mean percentage block by AP5 (50μM) plus NBQX (25μM) of the ischaemia evoked current in A, not significantly different (p=0.47). **C** Mean ischaemia-evoked current, in 0mM Mg^{2+}, in $NG2^+$ cells that do not express voltage-gated sodium channels (n=7) or $NG2^+$ cells that do express sodium channels (n=2); not significantly different (p=0.18). **D** Mean percentage block by AP5 (50μM) plus NBQX (25μM) of the ischaemia- evoked current in C. All cerebellum, -63mV, 33°C, number of cells are shown in the bars.

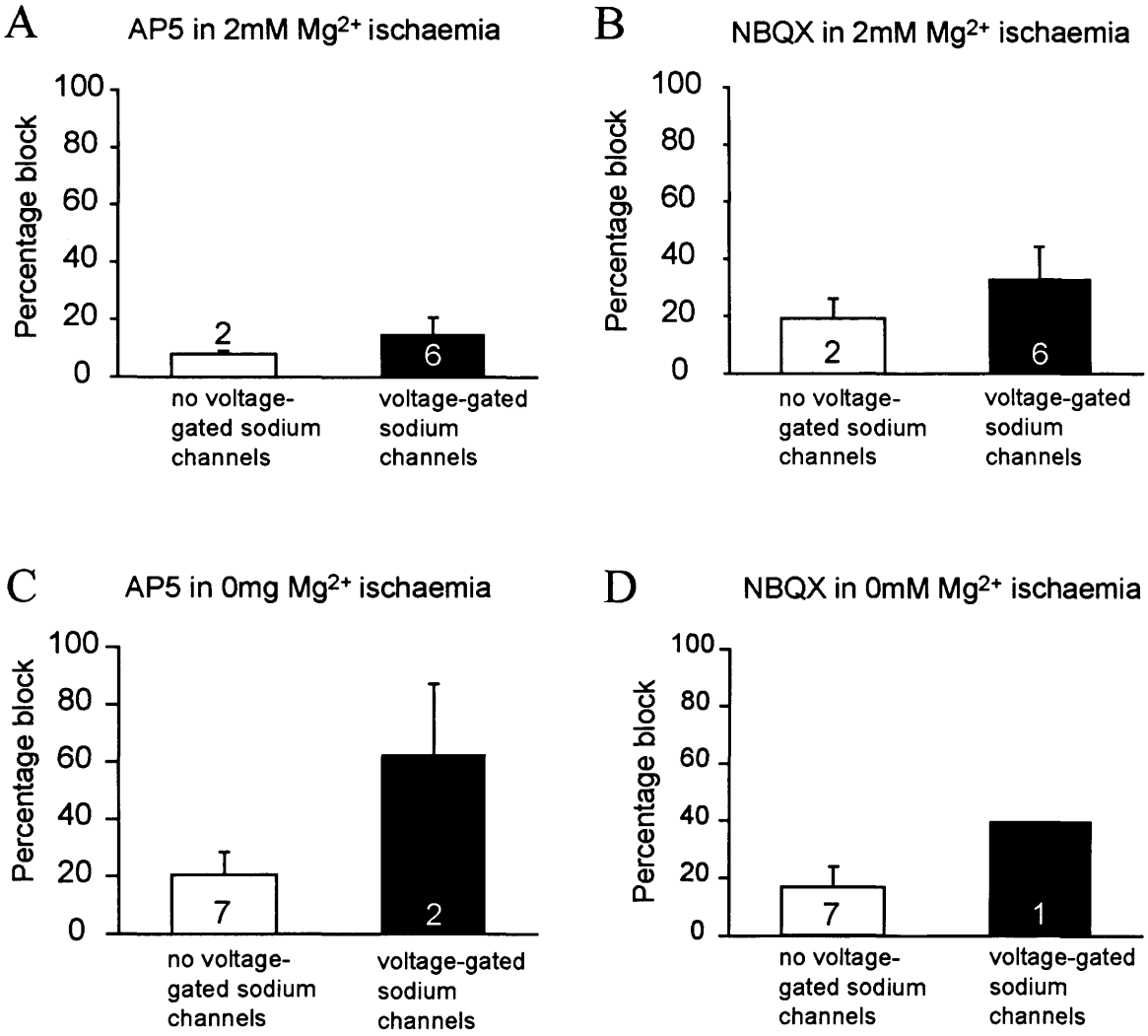

Figure 6.5 NMDA and AMPA receptors are activated in ischaemia in all NG2$^+$ cells. **A, B** Fractional block of the ischaemia-evoked inward current: in 2mM Mg^{2+} by 50μM D-AP5 (**A**) or by 25μM NBQX (**B**) in NG2$^+$ cells that either express voltage-gated sodium channels (n=6) or do not (n=2); not significantly different between the two classes of cell (p=0.47 for A and 0.51 for B). **C, D** Fractional block of the ischaemia-evoked inward current: in 0mM $Mg^{2+}$by 50μM D-AP5 (**C**) or by 25μM NBQX (**D**) in NG2$^+$ cells that either express voltage-gated sodium channels (n=2 for C and 1 for D) or do not (n=7); not significantly different between the two classes of cell (p=0.06 for C). All cerebellum, -63mV, 33°C, number of cells are shown in the bars.

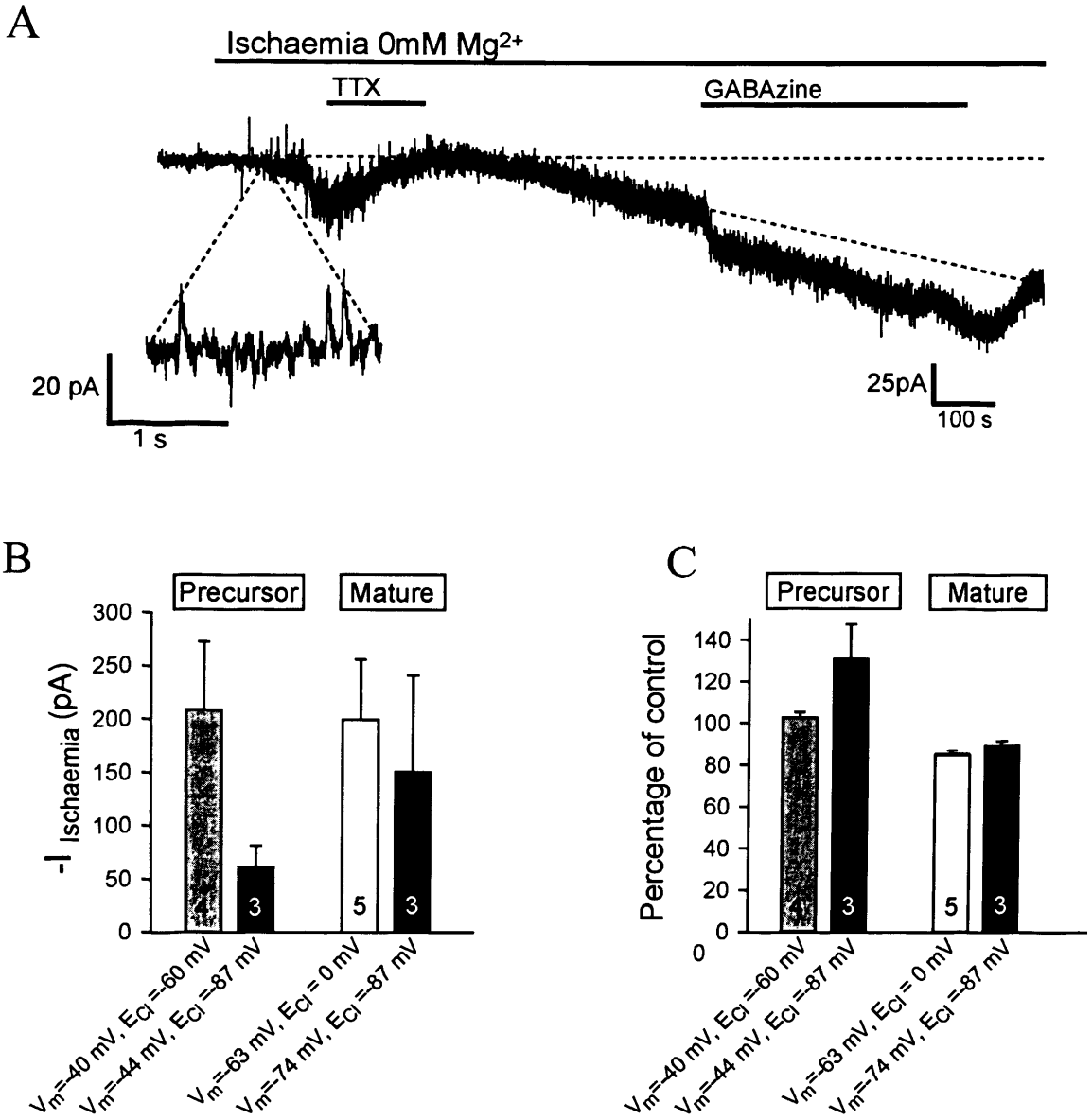

Figure 6.6 Oligodendrocyte $GABA_A$ receptors are activated in ischaemia **A** Ischaemia-evoked current at V_m= -44mV, in a precursor oligodendrocyte whole-cell clamped with E_{Cl}=-87mV, is made more inward by 10μM GABAzine. In this particular cell TTX (1μM) reduced the early development of the inward current. Inset: ischaemia-induced outward synaptic-like currents which are presumably evoked by exocytotic release of GABA. **B** Dependence of the peak inward current evoked by ischaemia on the pipette solution used and maturation stage (note different holding potentials used). **C** Mean effect of 10 μM GABAzine on the current in B. All in 0mM Mg^{2+}, cerebellum, 33°C, number of cells are shown in the bars.

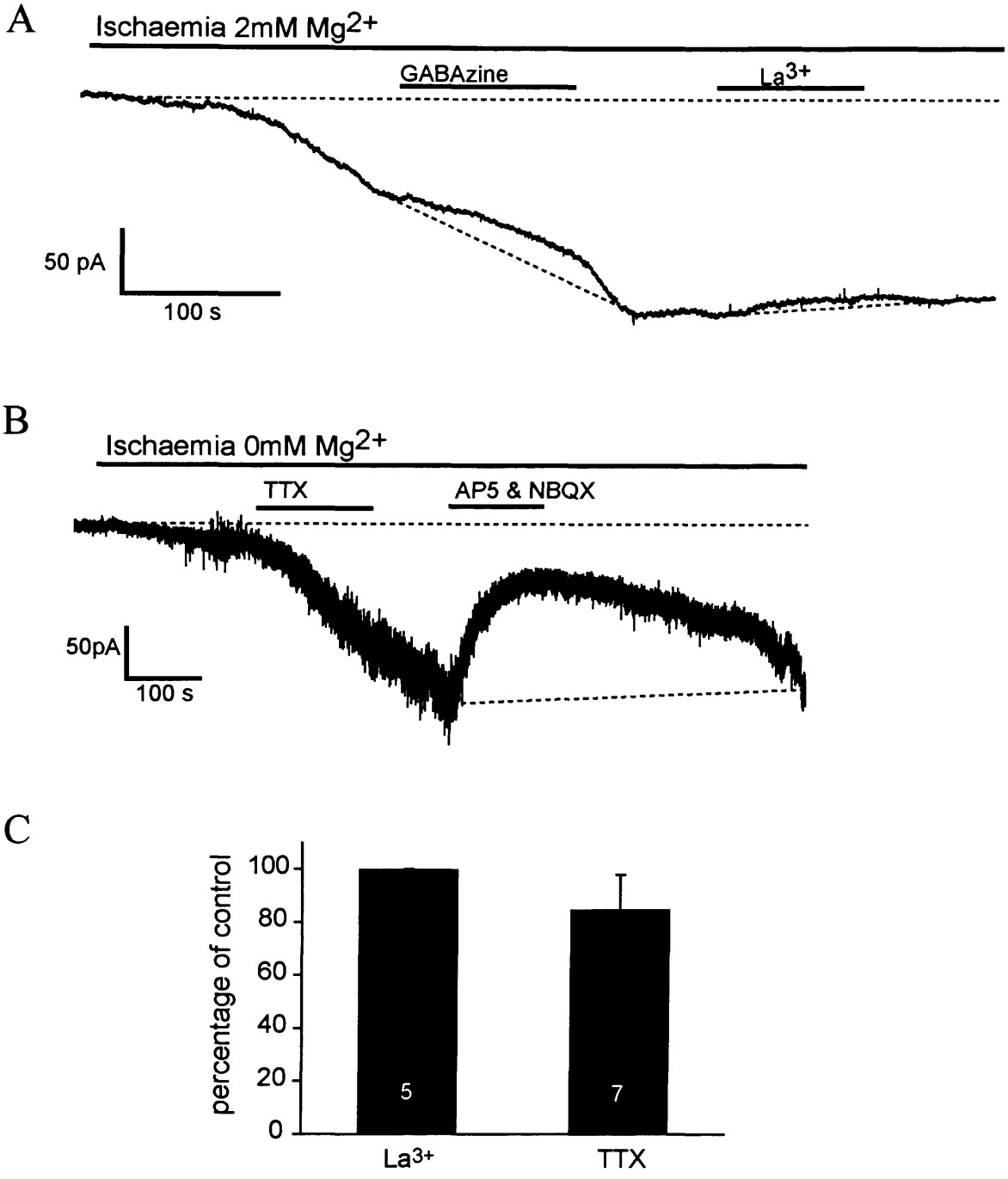

Figure 6.7 The ischaemia-evoked current in oligodendrocytes is not much affected by the TRP and voltage-gated calcium channel blocker La^{3+}, nor by TTX. **A** Ischaemia-evoked current in a mature oligodendrocyte (2mM Mg^{2+}), is not much reduced by 200 μM La^{3+} (p=0.4), at V_m=-63mV. However, 10μM GABAzine reduces the current (E_{Cl} = 0mV, so $GABA_A$ receptor current is inward). **B** Ischaemia-evoked current in a precursor oligodendrocyte (0mM Mg^{2+}), is not effected by 1 μM TTX (p=0.36), but the current is reduced in 200μM D-AP5 and 25μM NBQX, at V_m=-44mV,E_{Cl} = -87mV. **C** The effect on the ischaemia-evoked current of 200 μM La^{3+} in experiments like that shown in A on 5 mature cells (p=0.4), and of TTX on 7 precursor cells, like shown in B (p=0.36). All cerebellum, 33°C, numbers of cells are shown in the bars.

Chapter 7

Synaptic input to $NG2^+$ cells in cerebellar white matter

In this chapter I will explore the properties of events resembling synaptic currents that occur in the voltage-gated sodium channel expressing $NG2^+$ cells, and characterize how their frequency increases in ischaemia.

7.1 Introduction

In the grey matter, some $NG2^+$ cells not only express voltage-gated Na^+ channels (Chittajallu et al., 2004), as I also find for some white matter $NG2^+$ cells (see chapter 3, section 3.3.3), but they also have glutamatergic and GABAergic synaptic inputs, both in the hippocampus (Bergles et al., 2000; Jabs et al., 2005) and in the cerebellum (Lin et al., 2005). In chapter 6 I showed that, in ischaemia, some cerebellar white matter oligodendrocyte precursors ($NG2^+$ cells) exhibit similar synaptic currents (see e.g. Fig. 6.2A, B).

In neurons in the grey matter, ischaemia leads to an increase in synaptic activity, with both excitatory (Hershkowitz et al., 1993; Katchman & Hershkowitz, 1993b; Fleidervish et al., 2001) and inhibitory (Katchman et al., 1994; Fleidervish et al., 2001; Allen & Attwell, 2004; Allen et al., 2004b) synaptic currents increasing in frequency. This increase is independent of action potentials, as tetrodotoxin (TTX) does not affect these spontaneous synaptic events (Hershkowitz et al., 1993; Katchman & Hershkowitz, 1993b; Katchman et al., 1994; Fleidervish et al., 2001). The fact that some white matter oligodendrocyte precursors show synaptic currents in ischaemia suggests that exocytotic release of transmitter might contribute to the ischaemic activation of glutamate and GABA receptors, and raises the possibility that synaptic activity might have a function in these cells even in normal conditions.

I have therefore analyzed synaptic inputs to $NG2^+$ cells in the white matter, both for normal conditions and in simulated ischaemia.

7.2 Methods

Brain slices Cerebellar slices (225μm thick) were prepared from P7-P14 rats as described in Section 2.1. Slices were superfused at 33±1°C with bicarbonate Ringer's solution, composed of (in mM): NaCl 126, $NaHCO_3$ 24, NaH_2PO_4 1, KCl 2.5, $CaCl_2$ 2.5, $MgCl_2$ 2, D-glucose 10 (gassed with 95% O_2/5% CO_2), pH 7.4.

Recording & cell identification White matter cells were whole-cell clamped, as in chapter 3, with pipettes containing a CsCl-based solution, comprising (mM): 130 CsCl, 4 NaCl, 0.5 $CaCl_2$, 10 HEPES, 10 BAPTA, 2 MgATP, 0.5 Na_2GTP, K-Lucifer yellow 2, pH set to 7.3 with CsOH (E_{Cl} = 0mV) or a Cs-gluconate-based solution, comprising (mM): 130 Cs-gluconate, 4 NaCl, 0.5 $CaCl_2$, 10 HEPES, 10 BAPTA, 4 MgATP, 0.5 Na_2GTP, 2 K-Lucifer yellow, pH set to 7.3 (E_{Cl} = -87mV).

Analysis of synaptic currents Spontaneous synaptic currents (both inward and outward) were analysed using Strathclyde Electrophysiology Software. A synaptic current was defined to occur if its amplitude was larger than 3 times the standard deviation of the current noise (in regions of the record with no such currents), and its decay time was longer than its rise time, and its rise time was less than 10msec (most were faster than this, with a median value of 2ms). The decay of the current was fitted by one exponential.

Antibody labelling is described in detail in chapter 2, section 2.11.

Statistics These are described in chapter 2, section 2.13.

7.3 Results

7.3.1 $NG2^+$ cells receive synaptic input

In the cerebellar white matter there are two populations of $NG2^+$ cells, those that are $Olig2^+$ and hence in the oligodendrocyte lineage, and those which are not $Olig2^+$ (see chapter 3 for details). In addition, the $NG2^+$ cells fall into two electrophysiological groups: those that express voltage-gated Na^+ channels and those that do not, these two

classes having been shown in this thesis to respond differently to glutamate and NMDA, but similarly to GABA and to ischaemia.

In non-ischaemic conditions, all $NG2^+$ cells that expressed voltage-gated Na^+ channels (n=24) showed spontaneous synaptic events, with quite a range of frequencies. These events were sensitive to 1 μM tetrodotoxin (TTX), indicating that they require action potential dependent release of neurotransmitter (Fig. 7.1). In three cells, these events were analysed in more detail using an internal solution for which the reversal potential for chloride was set to 0mV (E_{Cl}=0mV) so that all spontaneous events were inward. They occurred with a mean frequency of 0.813±0.003 events per second, and were decreased in frequency by 95% in 1μM TTX (p=0.03). After the tetrodotoxin application it took a considerable time for these events to recover to their previous frequency (Figs. 7.1A, 7.2A) and size (Fig. 7.2B). In control conditions the amplitude of the events was 70.5±0.8 pA. The amplitude decreased in TTX (p=0.009), suggesting that smaller spontaneous events remain in TTX (Fig. 7.2B), or possibly (since these experiments were done with E_{Cl}=0mV, so that both glutamatergic and GABAergic currents are inward) that TTX abolishes action potential driven input mediated by one transmitter, leaving smaller spontaneous currents mediated by the other transmitter. The decay time of the currents was quite varied (23±10 ms in control conditions), so that although its mean value seemed to decrease in TTX (Fig. 7.2C) this decrease was not significant. This variable decay time of these events indicates that they are heterogeneous, perhaps because more than one neurotransmitter is released (see below). I therefore changed to an internal solution with a more negative reversal potential for chloride (E_{Cl}=-87mV) so that inhibitory inputs would generate outward, and excitatory inputs inward currents.

With E_{Cl} set to -87mV,these $NG2^+$ voltage-gated Na^+ channel expressing cells showed both inhibitory and excitatory inputs, exhibited as outward and inward currents, respectively, at -44mV (Fig. 7.3). In most cases the same cell had both types of input (Fig. 7.3A). However, in some cases they either only had inhibitory input (Fig. 7.3B) or only excitatory input (Fig. 7.3C). The presence of these two input types could explain the variable decay time reported above within and between cells studied with E_{Cl}=0mV.

7.3.2 Spontaneous synaptic-like events in $NG2^+$ cells increase in frequency in simulated ischaemia

The effect of simulated ischaemia on synaptic currents in neurons has been well studied in the grey matter. Tetrodotoxin-insensitive spontaneous synaptic currents, both glutamatergic and GABAergic, increase in frequency in the first minutes of ischaemia in hippocampal pyramidal cells (Hershkowitz et al., 1993; Katchman & Hershkowitz, 1993b; Katchman et al., 1994; Fleidervish et al., 2001). I therefore explored what effect simulated ischaemia had on the spontaneous events in $NG2^+$ cells expressing voltage-gated Na^+ channels.

In general, spontaneous events increased in frequency in the first minutes of simulated ischaemia, as can be seen in chapter 6, Figures 6.2A, B, and 6.6A. To quantify the frequency increase and to further understand the properties of these currents, I analysed these events in four cells with the chloride reversal potential set to -87mV, which all had both inhibitory and excitatory inputs.

In control (non-ischaemic) conditions the frequency of inhibitory inputs (0.12±0.04 Hz) tended to be lower than that of the excitatory inputs (0.47±0.24 Hz), however this difference was not significant (p=0.2; Fig. 7.4B top two traces). The average amplitude and decay time were 10.0±2.6pA and 20.1±3.7 ms for the inhibitory events, and 8.2±0.8pA and 13.3±4.7ms for the excitatory events.

After 1 minute of simulated ischaemia the spontaneous synaptic-like events increased in frequency 2.4-fold for the inhibitory events (Figs. 7.4B and 7.5A; p=0.04) and 5.0-fold for the excitatory events (Figs. 7.4B and 7.6A; p=0.035). With increased time in ischaemia, the frequency of both types of event continued to increase and this, along with a possibly increased rate of opening of ion channels, made the current noisier (Fig. 7.4A). This increase in noise, and the fact that the events go in two opposite directions, made it difficult to rely on the detection (by the software used) of synaptic-like events later in ischaemia. However, tetrodotoxin (1μM) did not seem to significantly decrease the frequency of either the outward events (Figs. 7.4A and 7.5A;

p=0.29) or the inward events (Figs. 7.4A and 7.6A; p=0.24), suggesting that (unlike the currents seen in control conditions in Fig. 7.1) these events that increase in frequency in ischaemia are independent of the propagation of action potentials. The decay time and amplitude of the outward and inward events did not change with increased time in ischaemia nor was it affected by TTX (Fig. 7.5B, C, Fig. 7.6B, C).

7.3.3 Strange unexplained transient currents in $NG2^+$ cells

Occasionally, additional transient current events were also sometimes encountered in $NG2^+$ cells, which had a spike-like phasic waveform (Fig. 7.7), resembling perhaps the inward current generating an action potential (these spikes were brief, ~1msec, with a similar rise and fall time, so they can not be synaptic currents as described above). These events were rare, but were seen in both the $NG2^+$ cells expressing voltage-gated Na^+ channels or those that do not express these channels, however in the cells expressing voltage-gated Na^+ channels these spiky events seemed to be more frequent. Most of these occurrences of these events were quite rare. More experiments are needed to understand further what these spikes are, and what role they have in these cells and in the white matter in general. One hypothesis is that they reflect the generation of action potentials in poorly voltage-clamped areas of the cell's processes, but this idea is undermined by the fact that they were also seen in $NG2^+$ cells that did not show a voltage-gated Na^+ current.

7.4 Discussion

I have shown that, as in the grey matter, white matter $NG2^+$ cells receive synaptic input, presumably from passing axons. I assume that the outward and inward transient currents that I see (with E_{Cl}=-87mV) are mediated by exocytotic release of GABA and glutamate respectively, although pharmacological experiments blocking $GABA_A$ and glutamate receptors are needed to test this. In grey matter $NG2^+$ cells the EPSCs and IPSCs are both evoked by action potentials, as they are abolished in TTX

(Bergles et al., 2000; Lin & Bergles, 2004; Jabs et al., 2005), which is identical to my findings in the white matter $NG2^+$ cells in non-ischaemic conditions. The decay time of the outward IPSC's in grey matter (hippocampus) $NG2^+$ cells has been found to be 20±12ms (Jabs et al., 2005) and 23.6±0.9 ms (Lin & Bergles, 2004) which is quite similar to the 20.1±3.7ms that I recorded in the cerebellar white matter $NG2^+$ cells (comparison of the amplitude of the currents in my work and in the preceding work is not possible because of the different holding potentials and values of E_{Cl} used). There is more disagreement over the properties of the glutamatergic EPSCs as in the hippocampus grey matter the decay time and amplitude have been reported to be either 1.2ms and 10pA (Bergles et al., 2000; Lin & Bergles, 2004) or 6.0ms and 5.6pA (Jabs et al., 2005). These figures are lower than the mean values for the decay time and the amplitude that I found in the white matter $NG2^+$ cells, i.e. 8.2 ms and 13.3pA respectively.

In hippocampal grey matter it has been shown that both EPSCs and IPSCs increase in frequency in ischaemia, and that this increased frequency is not generated by action potentials as it is unaffected by TTX (Katchman & Hershkowitz, 1993b; Katchman et al., 1994; Fleidervish et al., 2001; Allen & Attwell, 2004; Allen et al., 2004b). Similarly, I found that the spontaneous synaptic-like events in the white matter also increased in frequency during ischaemia, and that TTX did not prevent this. Presumably ischaemia leads to a rise of $[Ca^{2+}]_i$ in the cells releasing transmitter onto the $NG2^+$ cells, which increases spontaneous transmitter release.

The role of the synaptic-like currents in $NG2^+$ cells has yet to be understood. Perhaps they provide a mechanism for the cells to sense their environment and find axons to myelinate. On the other hand, as it is mainly the $NG2^+$ cells expressing voltage-gated sodium current that show the currents, it could be that these cells have a completely different role in the brain than to be reserve (precursor) cells for mature oligodendrocytes, as has been suggested previously (Butt et al., 2002), and they may become GABAergic interneurons (Belachew et al., 2003; Aguirre et al., 2004). Since the frequency of the synaptic-like currents increases in ischaemia, exocytosis could be a significant source of ischaemic neurotransmitter release, adding to the neurotransmitter

release by reversed uptake reported previously (Li & Stys, 2001a; Li & Stys, 2001b). If, during ischaemia, exocytotically released glutamate (and GABA) can diffuse out of the "synapses" onto $NG2^+$ cells, they may act on both precursor/immature and mature oligodendrocytes and will add to the deleterious effect of glutamate (and possibly GABA) in the white matter.

Finally, it seems that these cells also express some other kind of transient currents that are symmetrical in onset and offset, and fast: more experiments are needed to find out what these current events are and what role they serve.

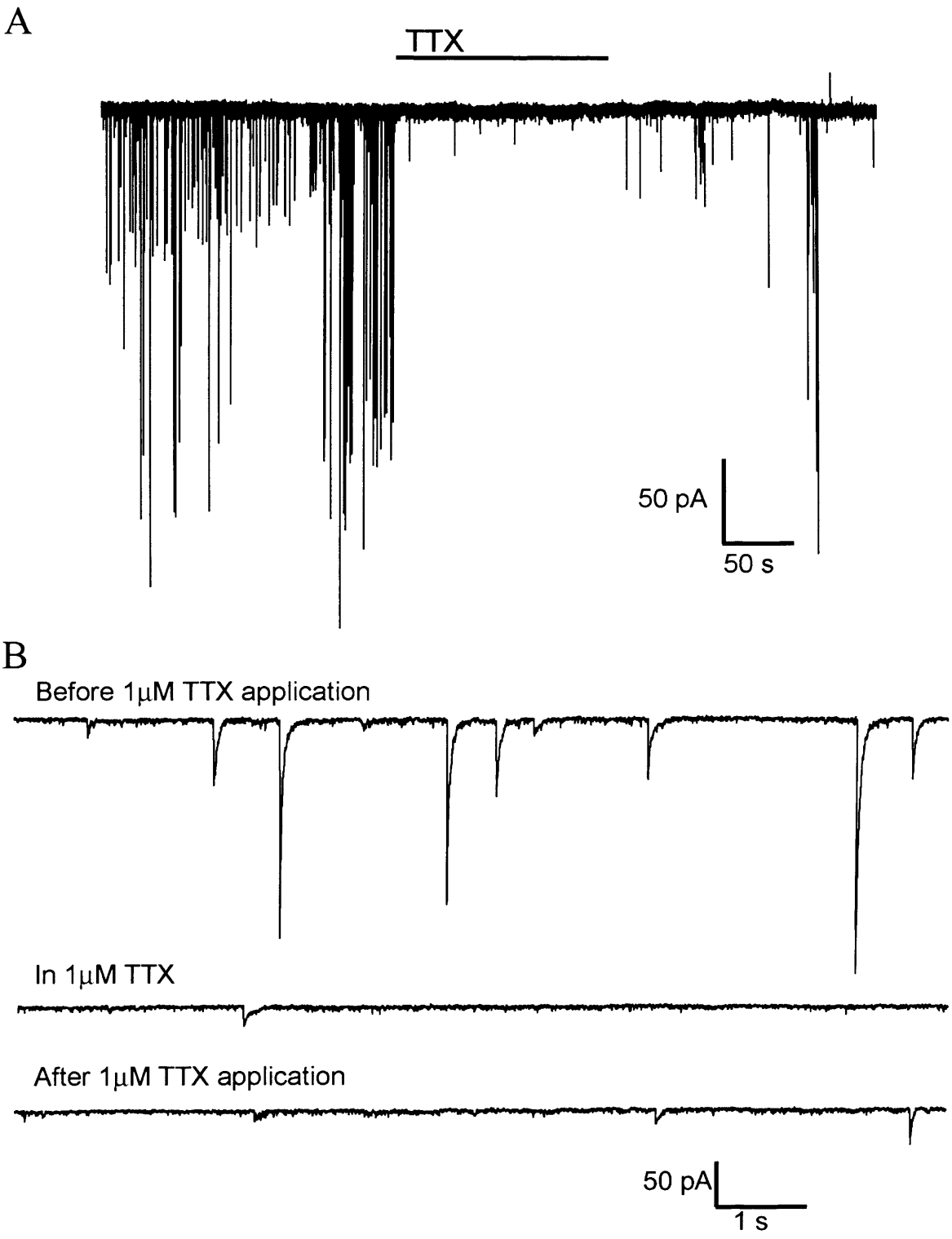

Figure 7.1 TTX-sensitive synaptic-like activity in $NG2^+$ cells. **A** An $NG2^+$ cell showing synaptic input (downward deflections), that was almost abolished in 1μM TTX. **B** Expanded traces from A, showing in more detail the synaptic-like currents in this cell. In 1μM TTX the currents almost disappear, then after washout of TTX they slowly reappear. Cerebellum, -63mV, 33°C, E_{Cl}=0mV.

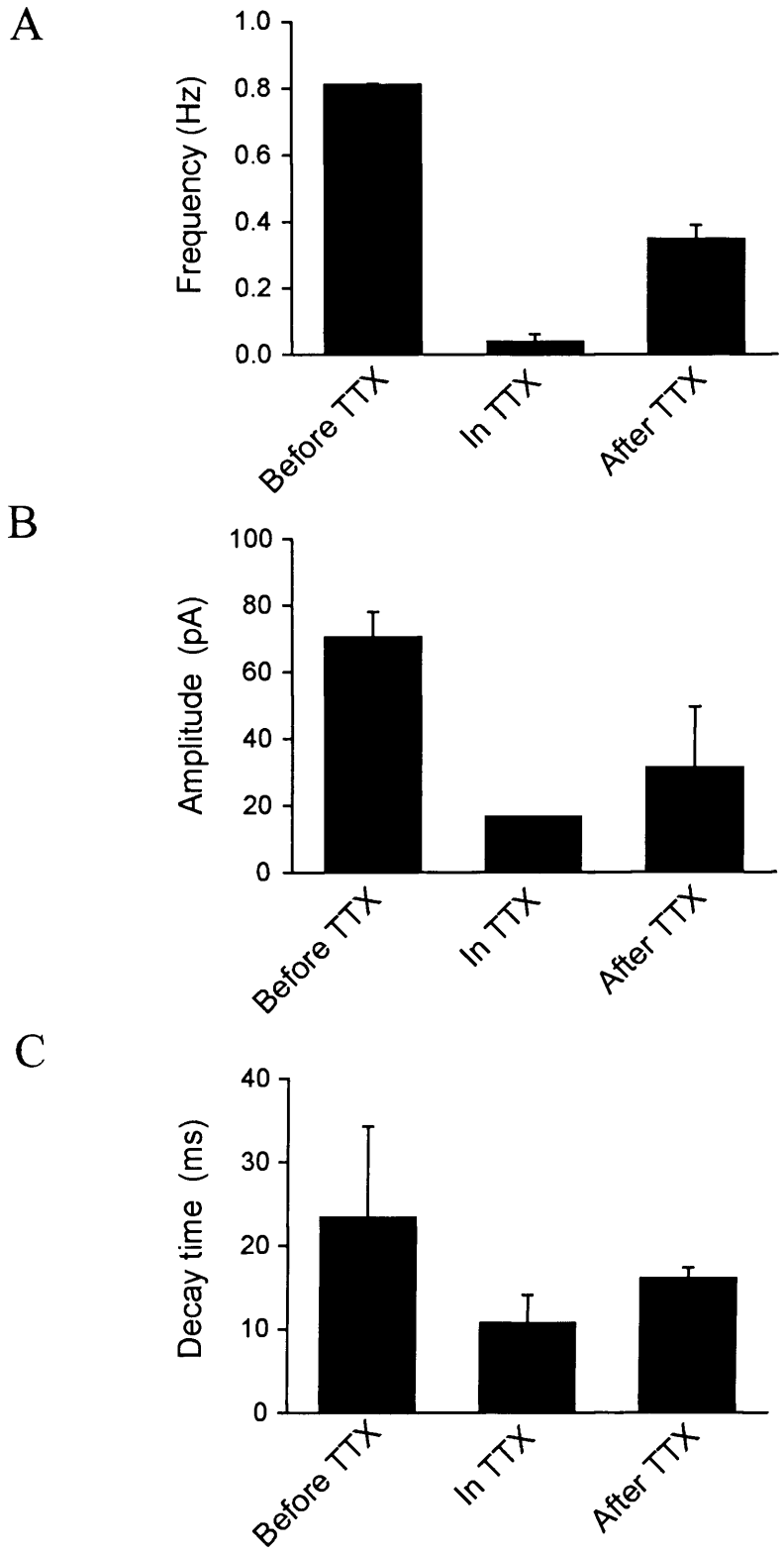

Figure 7.2 Effects of TTX on the spontaneous synaptic-like events in $NG2^+$ cells expressing voltage-gated sodium channels. Changes in frequency (**A**), amplitude (**B**) and decay time (**C**) of events before, during and after application of 1 μM TTX. All cerebellum, -63mV, 33°C, E_{Cl}=0mV.

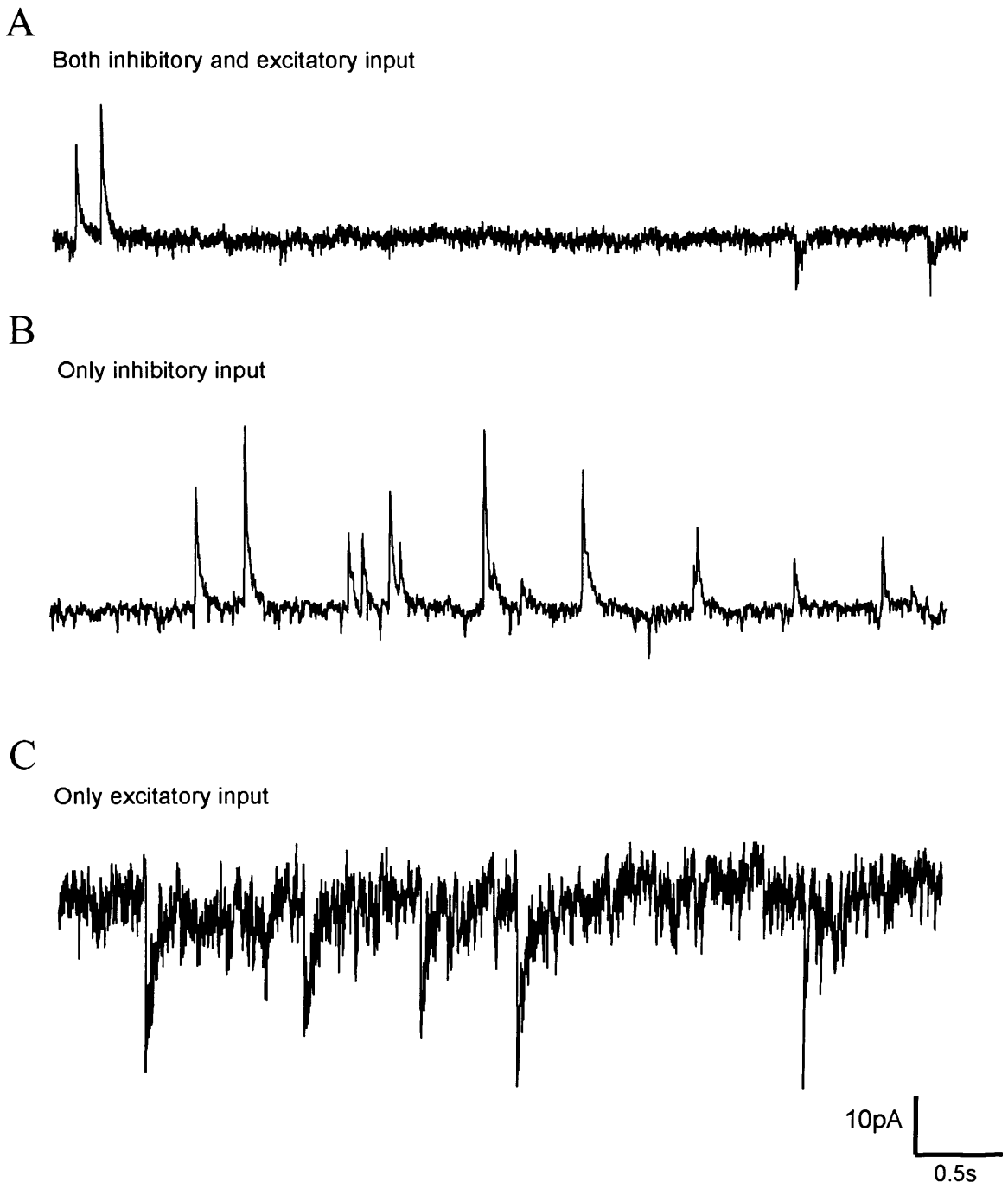

Figure 7.3 The spontaneous synaptic like currents in voltage-gated sodium channel expressing $NG2^+$ cells in the white matter fall into two classes. **A** Most cells had both inhibitory input (outward currents) and excitatory input (inward currents). However, some had either only inhibitory input (**B**) or only excitatory input (**C**). All cerebellum, -44mV, 33°C, with E_{Cl}=-87mV.

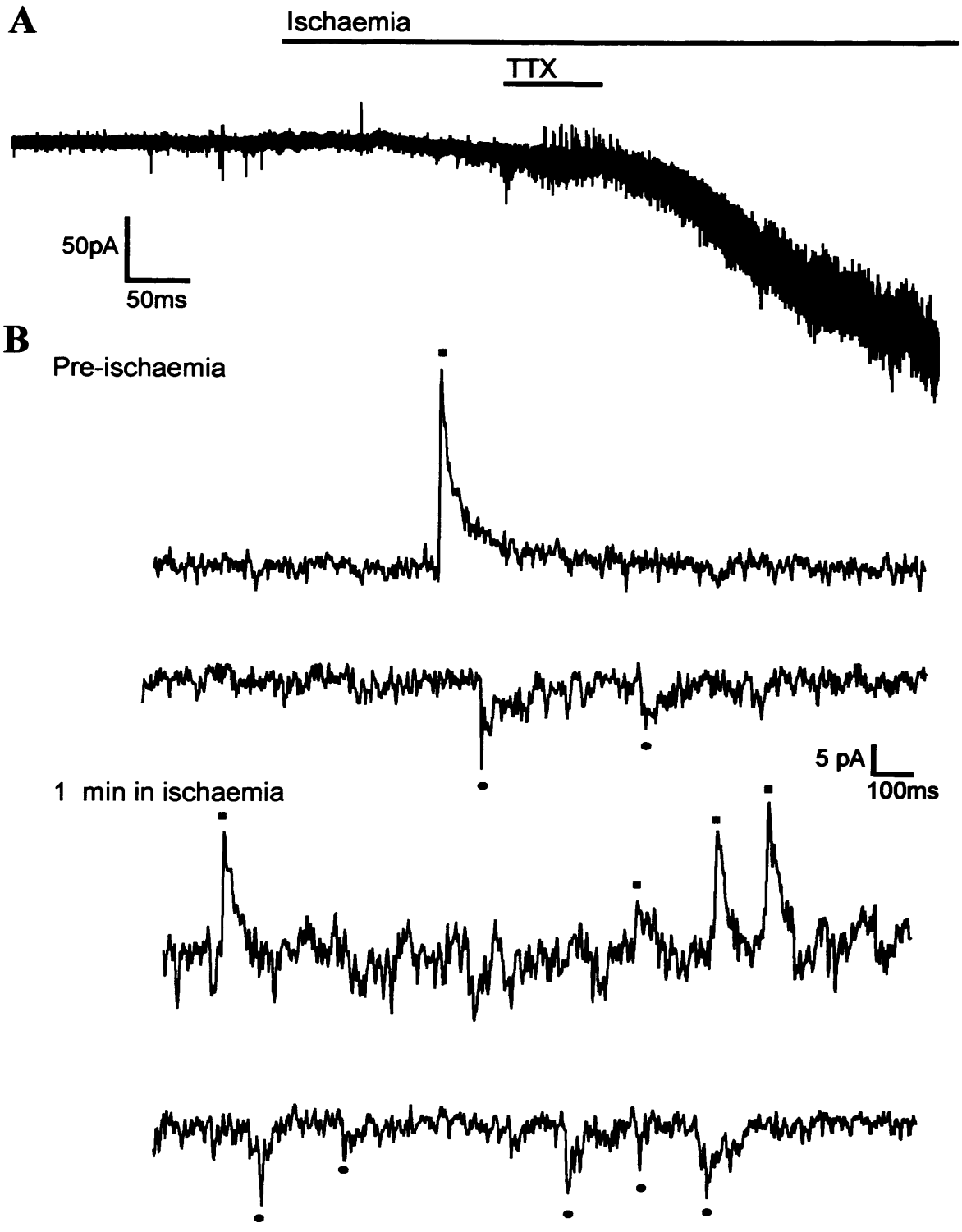

Figure 7.4 The spontaneous synaptic-like currents in the voltage-gated sodium channel expressing $NG2^+$ cells, in the white matter, increase in frequency during ischaemia. **A** Membrane current at -44mV before, and during ischaemia, including a period during which 1μM TTX was applied (which did not affect the occurrence of spontaneous synaptic currents: see text). **B** The cell exhibited both inhibitory inputs (shown as red circles) and excitatory inputs (shown as blue squares). Specimen sections of record illustrate both types of event. In ischaemia the summation of spontaneous events, and possibly increased opening of ion channels, makes the trace more noisy. All from cerebellum, -44mV, 33°C, with E_{Cl}=-87mV.

A

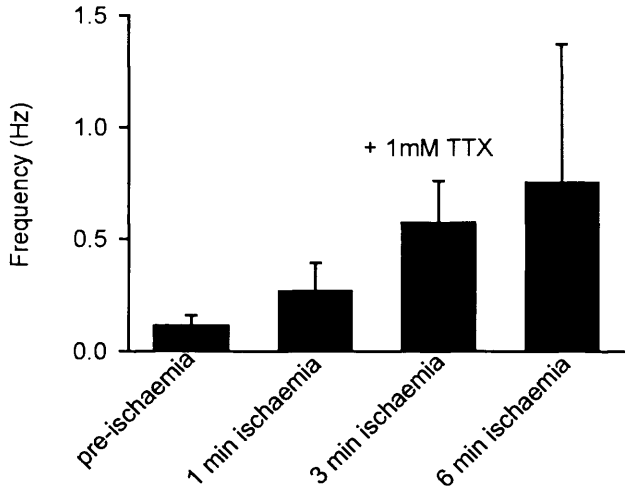

B

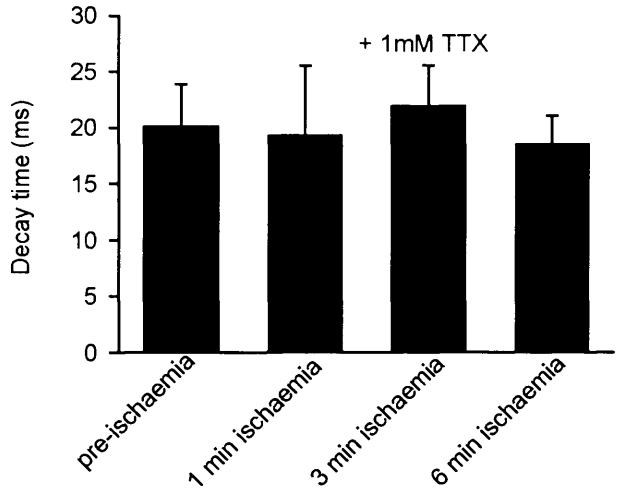

C

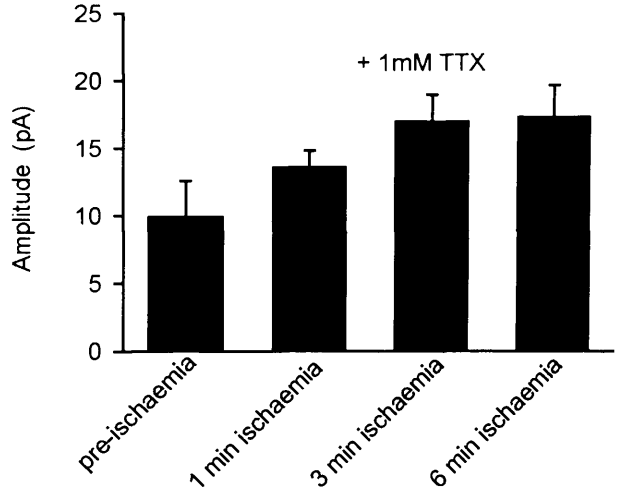

Figure 7.5 Analysis of the increase of frequency during ischaemia of the inhibitory synaptic-like currents in the voltage-gated sodium channel expressing $NG2^+$ cells, in the white matter. **A** The mean frequency of events increases (p=0.04) and TTX does not block this. **B, C** The decay time (p=0.96, **B**) and amplitude (p=0.099, **C**) do not change significantly with ischaemia (p values were derived in ANOVA analysis over all time points). Mean data from 4 cells that exhibited both inhibitory and excitatory currents. All cerebellum, -44mV, 33°C, with E_{Cl}=-87mV.

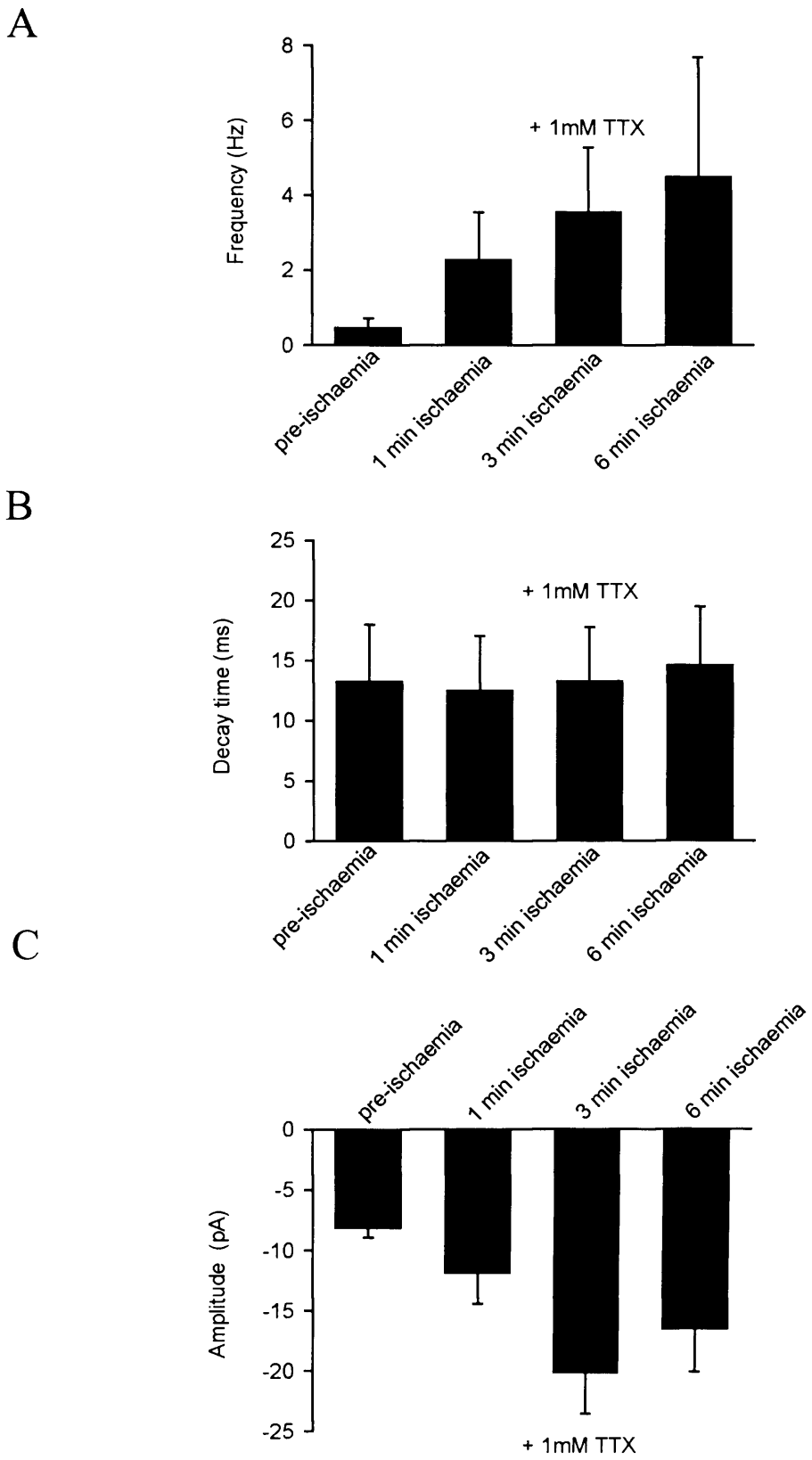

Figure 7.6 Analysis of the increase in frequency in ischaemia of the excitatory spontaneous synaptic like currents in the voltage-gated sodium channel expressing $NG2^+$ cells in the white matter. **A** The mean frequency of events increases (p=0.04) and TTX does not block this. **B, C** The decay time (p=0.96), **B** does not change and the amplitude increases slightly (p=0.04), **C** (p values were derived in ANOVA analysis over all time points.) Mean data from 4 cells that exhibited both inhibitory and excitatory currents. All cerebellum, -44mV, 33°C, with E_{Cl}=-87mV.

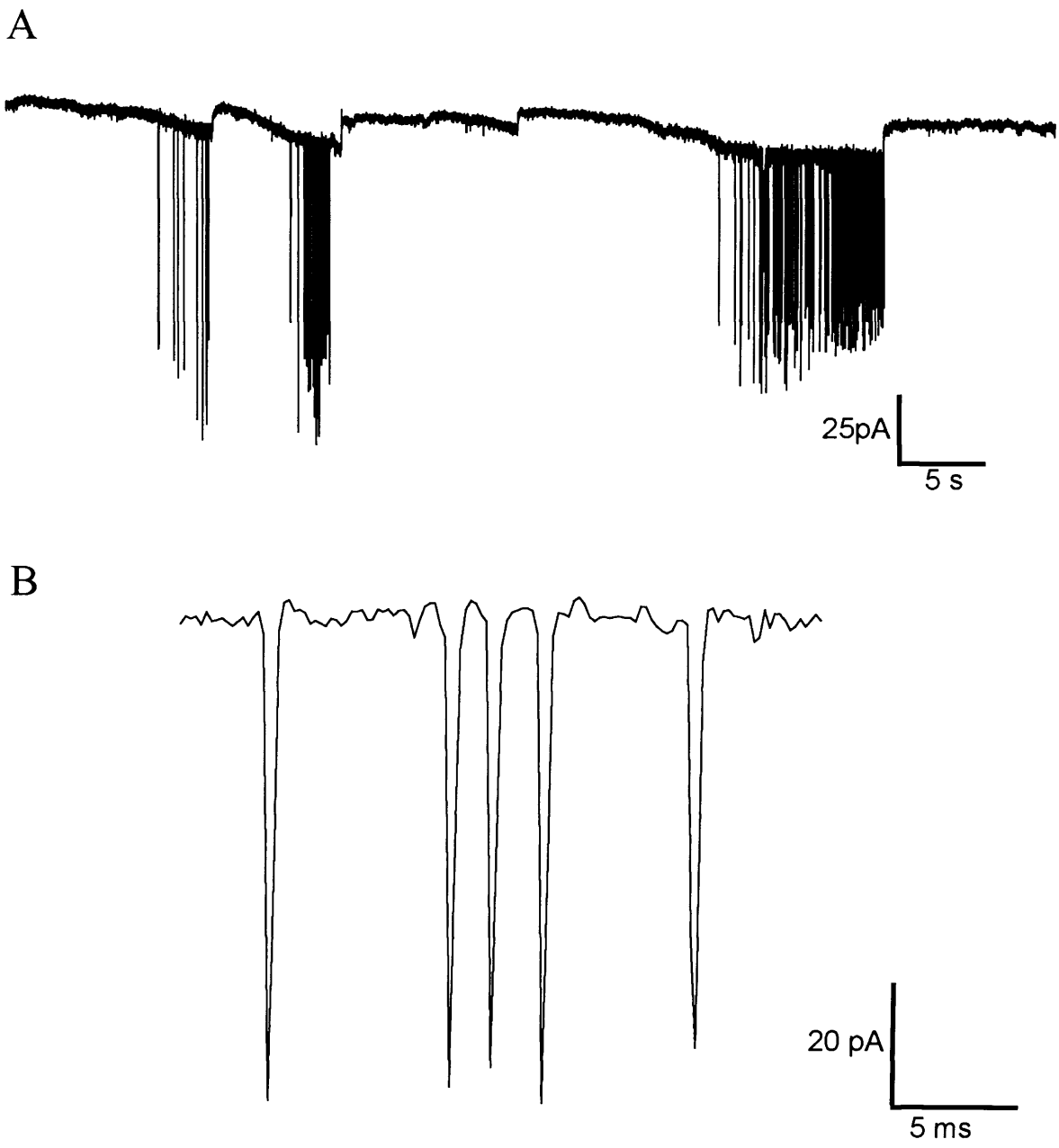

Figure 7.7 Spontaneous bursting events in the voltage-gated sodium channel expressing $NG2^+$ cells, in the white matter. **A** A cell showing repeated bursts of activity. **B** Expanded part of the trace shown in A, showing that these events do not look like synaptic inputs. All cerebellum, -63mV, 33°C, E_{Cl}=0mV.

Chapter 8

The roles of glycolysis and oxidative phosphorylation in the generation of the anoxic depolarization in grey matter

8.1 Introduction

As explained in Section 1.7, when the blood supply to part of the grey matter of the brain is cut off (for example in stroke) the plasma membrane sodium/potassium pump loses its ATP supply, and trans-membrane ion gradients start to run down. This run-down is initially slow, but after a few minutes the extracellular potassium concentration rises rapidly to about 60mM (Fig. 1.6), which depolarizes neurons to about -20mV: an event called the anoxic depolarization (or AD). Whether an AD occurs during transient ischaemia, and its time of occurrence, will be determined by how much stored energy the brain has to maintain ion gradients in the face of a temporary interruption of its energy supply. Brain ATP is largely derived from glucose: glycolysis is followed by oxidative phosphorylation in mitochondria (Fig. 8.1). It has been suggested (but disputed: Chih et al., 2001b) that neuronal activity-evoked glycolysis (Pellerin et al., 1998; Magistretti & Pellerin, 1999) or almost all glycolysis (Sibson et al., 1998) is in glia, which export lactate to neurons as a substrate for their mitochondria. Since neurons consume most brain energy (Attwell & Laughlin, 2001), this lactate export might explain how the brain's main energy store (assumed to be glial glycogen: Gruetter, 2003a; Brown, 2004) could sustain the activity of the neurons during energy deprivation, but no information is available on which CNS energy stores delay the occurrence of the AD.

In this chapter I will examine the effect of different types of metabolic inhibition on hippocampal area CA1, using the glutamate receptors in pyramidal cells to monitor the large rise of $[glutamate]_o$ produced by the AD. There were five aims, as follows. First, to ascertain the extent to which glycolysis can delay the regenerative decrease of

ion gradients that generates the AD, since plasma membrane ion pumps may be preferentially fuelled by glycolysis (Rosenthal & Sick, 1992). Second, to determine the period for which glycogen can sustain glycolysis in the absence of extracellular glucose. Third, to test whether superfused lactate can prevent the AD occurring when glycolysis is blocked, as expected if most ATP is generated from lactate supplied to neurons from glia. Fourth, to compare the effect of a commonly used mitochondrial blocker, cyanide, with that of other blockers (rotenone, antimycin), since cyanide can potentiate or inhibit NMDA receptors according to their subunit composition (Patel et al., 1994; Arden et al., 1998). Finally, to examine whether, in addition to preventing oxidative phosphorylation, removal of oxygen had direct effects on membrane currents contributing to the AD, since some K^+ and Na^+ currents can sense oxygen directly and are activated or inhibited when O_2 is removed (Jiang & Haddad, 1994; Hammarstrom & Gage, 2000). My results demonstrate a preferential role for glycolysis in preventing the AD.

Forty percent of the work in this chapter was done by my colleague Nicola Allen.

8.2 Methods

8.2.1 Electrophysiology

Pyramidal cells in hippocampal area CA1 were whole-cell clamped in order to use their NMDA and AMPA receptors to monitor the sudden inward current associated with the rise of glutamate concentration which is triggered by the decrease of ion gradients occurring at the time of the AD (Rossi et al., 2000). The time of the AD recorded in this way is indistinguishable from that recorded with extracellular field recording (Allen et al., 2004b), showing that neither the presence of ATP in the internal solution for the whole-cell clamped cell (see below), nor the clamping of the voltage of that cell, affects the generation of the AD: thus the clamped cell acts simply as a sensor of the ion gradient decrease and glutamate release which is produced by the large number of surrounding cells. Using whole-cell clamping to record the time of the AD offers two advantages over using extracellular field potential recording. First, the change of extracellular potential associated with the AD becomes very small if the AD

onset is slow, so whole-cell clamping gives more definite information on whether an AD has occurred, indeed it is only by the use of whole-cell clamping that I could be sure that there had not been a slow AD occurring in experiments described below when glucose was present. Second, whereas measuring the AD onset by field recording only gives data on the time of the AD, using whole-cell clamping enables me to examine in addition the time course of the pre-AD and post-AD current changes generated by ischaemia, and to monitor exocytotic transmitter release as miniature synaptic currents. Hippocampal slices, 225μm thick, were prepared from P12 rats (or in some experiments P28 rats, as noted in the text) as described in Chapter 2, with Na-kynurenate (1mM) in the slicing solution to block glutamate receptors, and were recorded from 2-5 hours after slicing, at which time glycogen levels should have largely recovered from the slicing process (Fiala et al., 2003). Recordings were at 33±1°C, with slices submerged in flowing solution (10ml/min) which normally contained (mM) NaCl 126, $NaHCO_3$ 24, NaH_2PO_4 1, KCl 2.5, $MgCl_2$ 2, $CaCl_2$ 2.5, glucose 10, bubbled with 95% O_2/5% CO_2, pH 7.4. Cells were whole-cell voltage-clamped with a pipette solution containing (mM): KCl 130, NaCl 5, HEPES 10, BAPTA 10, MgATP 2, $MgCl_2$ 2, pH set to 7.2 with KOH. Pipette series resistance was ~5MΩ before compensation by ~60% to reduce it to ~2MΩ. The large size of the current changes evoked by ischaemia (up to 6nA at the peak of the AD) means that, even after compensation, significant series resistance voltage errors will inevitably occur (a detailed analysis is presented in Hamann et al., 2002). Data are presented in this chapter without correction for this, because the series resistance was similar in different experimental conditions, and correcting for series resistance voltage errors would not alter the conclusions reached. Junction potentials were compensated for. Cells were clamped at -33mV to enhance the current generated by NMDA receptors. In a small number of experiments, non-invasive recording of the time of the anoxic depolarization was carried out by recording the field potential with an extracellular recording electrode (a patch pipette filled with external solution) placed in the pyramidal cell proximal apical dendrite layer (Rader & Lanthorn, 1989). Evoked synaptic transmitter release was studied by recording the field EPSP in the stratum

radiatum in response to 0.1 Hz stimulation of the Schaffer collaterals using a glass pipette, and quantified as the initial slope of the field EPSP.

8.2.2 Choice of agents to mimic energy deprivation

Experiments mimicking brain ischaemia in vitro inhibit glycolytic and mitochondrial ATP production by removing glucose and O_2, but often use metabolic blockers as well (Reiner et al., 1990). This is because, in open recording chambers, oxygen from the room air can rapidly diffuse through the solution to the tissue, preventing true inhibition of oxidative phosphorylation as would occur in vivo. In this chapter, energy deprivation was simulated by replacing 10mM glucose with 7mM sucrose and/or bubbling with 95% N_2/5% CO_2 and, in some experiments as described in the text, glycolysis was blocked with iodoacetate (2mM) and oxidative phosphorylation was blocked with rotenone (100μM) and antimycin (100μM) or NaCN (1mM). Using 100μM antimycin alone to block mitochondrial ATP production (along with iodoacetate to block glycolysis, and removal of oxygen and glucose) produced an AD with the same latency as that seen with rotenone present as well (429±16 sec in 5 cells and 440±17 sec in 29 cells, respectively, p=0.6). Reducing the antimycin concentration to 50μM, 25μM or 10μM also produced an AD with the same latency (423±11, 430±22, 499±61 sec respectively, 5 cells for each, p values compared with 100 μM antimycin plus rotenone were 0.43, 0.75 and 0.39 respectively), although the time of occurrence was more variable when 10μM antimycin was used. This suggests that block of complex 3 alone is sufficient to block mitochondrial ATP production and that 25μM antimycin is a sufficient concentration. Employing rotenone alone to block mitochondrial ATP production (along with iodoacetate to block glycolysis, and removal of oxygen and glucose) delayed the AD by about 2 minutes (to 569±42 sec, p=0.033, 5 cells), suggesting that rotenone alone may not completely prevent mitochondrial ATP production. This may be because it blocks the electron transport chain at complex 1 (see Fig. 8.1), so any metabolites that can enter the chain at complex 2 (such as $FADH_2$) will still be able to generate ATP (in the presence of residual oxygen), or because the rotenone dose used was not saturating. When Na-lactate was added, it replaced NaCl.

8.2.3 Experimental design

Every cell studied was from a different slice. Experiments comparing different metabolic blockers were done in an alternating interleaved manner (one cell with one condition, followed by another cell with the other condition, etc.).

8.2.4 Simulation of diffusion into and out of the hippocampal slice

The glucose distribution through the extracellular space of the slice was calculated by solving the modified diffusion equation

$$\frac{\delta c}{\delta t} = \frac{D}{\lambda^2}\frac{\delta^2 c}{\delta x^2} - \frac{Uc/\alpha}{c+K} \qquad (8.1)$$

where c is the concentration, x is the distance through the slice, D is the diffusion coefficient (assumed to be 7.6×10^{-10} $m^2 s^{-1}$, the value for glutamine (Longsworth, 1953), λ and α are the tortuosity factor and extracellular volume fraction (1.7 and 0.13 respectively: McBain et al., 1990), and U and K are the maximum uptake rate and EC_{50} for glucose uptake. I set K=1.6 mM (Erecinska & Silver, 1994), and set U to 0.055 moles/m^3/sec in order to reproduce a glucose uptake rate of 0.013 moles/m^3/sec (equivalent to the mean uptake rate of 79 moles/100g/min measured for rat hippocampus: Sokoloff et al., 1977) at the measured normal extracellular brain glucose level of 0.5mM (Fellows et al., 1992), assuming for simplicity that hippocampal slices at 33°C have the same glucose uptake rate as *in vivo* hippocampus (since brain slices, particularly at P12, may be less energetically demanding than the adult *in vivo* brain, the effect of assuming a lower glucose uptake rate is also considered below). The steady state distribution of glucose across the slice was determined by allowing the simulation to run until a steady state was reached. To simulate glucose diffusion out of the slice, after this steady state was reached, the glucose concentration at the surface of the slice was stepped to zero and equation (8.1) was solved to determine the time course of glucose removal from the slice. The resulting amount of glucose uptake remaining at different times was obtained by transforming the concentration at each point through the equation *Uc/(c+K)*. To estimate the time needed for drugs to diffuse into the slice the

simulation was run with U set to zero (i.e. ignoring uptake of drugs into the cells) and the concentration at the centre of the slice was found to reach half the value at the surface in less than 20 sec.

8.3 Results

8.3.1 The anoxic depolarization response to block of glycolysis and oxidative phosphorylation

Figure 8.1 is a schematic diagram of energy production in the brain, with glycolysis consuming external glucose and internal glycogen, and with most (94%: Rolfe & Brown, 1997) of the ATP being produced by mitochondria (possible compartmentation of metabolic function between neurons and glia will be considered later). There are several potential energy reservoirs in this scheme which can delay the decrease of the ion gradients maintained by the plasma membrane Na^+/K^+-ATPase when supplies of external glucose and O_2 are cut off. ATP can be made from phosphocreatine, glycolysis can use glucose-6-phosphate derived from glycogen as a substrate, and (if glucose levels fall while O_2 is still present, as in hypoglycaemia) metabolites downstream of glycolysis such as pyruvate can be used by mitochondria until they are used up.

To test the response of pyramidal cells to severe energy deprivation, I first removed external oxygen and glucose and simultaneously blocked glycolysis with iodoacetate (2mM) and blocked mitochondrial ATP production with a combination of rotenone (100μM) and antimycin (100μM). The resulting current response of a cell in a P12 slice, clamped at -33 mV, is shown in Figure 8.2A. For the first ~ 7 minutes the current became slightly more inward, but then (440±17 sec after the start of ischaemia in 29 slices) a large inward current occurred (the anoxic depolarization or AD current) which sagged back over about 30 sec to a more slowly decaying plateau of inward current. Applying glutamate receptor blockers during this plateau suppressed much of the inward current showing that it was mediated by glutamate release, as shown

previously by Rossi et al. (Rossi et al., 2000) using cyanide as a mitochondrial blocker, and in Figure 8.8 below.

8.3.2 Glycolysis fuelled by glycogen delays the AD when mitochondrial ATP production is blocked

Repeating the experiment of Figure 8.2A with iodoacetate omitted, in order to allow glycolysis to occur in the absence of external glucose using glucose-6-phosphate derived from glycogen (Fig. 8.1), the latency of the anoxic depolarization was increased by 5.5 mins (from ~7.5 to ~13 mins, $p=10^{-5}$: Fig. 8.2B; mean data are in Fig. 8.4A). The amplitude of the anoxic depolarization was also reduced (Fig. 8.4B), suggesting that allowing glycolysis to continue reduces the severity or the speed of the ion gradient decrease occurring at the time of the anoxic depolarization (AD), resulting in less glutamate release or more time for desensitization of glutamate receptors to occur.

Glucose remaining in the extracellular space of the slice after it has been removed from the superfusate could still be taken up and used to generate ATP in the absence of iodoacetate, but the extra 5.5 minute delay is unlikely to reflect the time needed for glucose to diffuse out of the slice. Simulation of glucose diffusion out of the slice, and of the resulting decline in glucose uptake (see section 8.2.4), showed that glucose uptake should be reduced to <10% of its initial value (averaged across the slice) 17 sec after removing glucose from the superfusate (see section 8.2.4; assuming a 10-fold lower glucose uptake rate than is seen *in vivo,* e.g. if there is less energy consumption as a result of removing excitatory input from outside the slice, would only prolong this to 60 sec). These data suggest, therefore, that (with mitochondria inhibited) glycogenolysis provides a reserve of ATP production which lasts ~5.5 mins in ischaemic conditions.

To check this interpretation of the data, I repeated this experiment after depleting glycogen stores by superfusing with solution containing 2mM glucose (instead of the normal 10mM, replaced by sucrose) for at least one hour before applying the ischaemic solution. Simulations of the diffusion of glucose into the slice (see section

8.2.4) suggested that with 10mM superfused glucose the extracellular glucose concentration at the centre of the slice will be 3mM, and the mean $[glucose]_o$ through the slice will be 5.2mM, while with 2mM superfused glucose the extracellular glucose concentration at the centre of the slice will be 0.17mM, and the mean $[glucose]_o$ through the slice will be 0.66mM, which is more similar to the extracellular glucose concentration of 0.5mM measured *in vivo* by a zero net flux microdialysis method (Fellows et al., 1992). (The predicted mean glucose concentration values are higher but still different, 9.4mM instead of 5.2mM, and 1.66mM instead of 0.66mM, if I assume that hippocampal slices have (e.g.) only 10% of the glucose uptake rate of *in vivo* hippocampus: see section 8.2.4). Thus, after incubation in the lower glucose solution, a decrease of glycogen stores and a lower intracellular glucose concentration are expected, and indeed have been found by Lipton (1989, lower glycogen: cf. their Table 1 data for 0 min with their Fig. 2) and Folbergrova et al. (1997, lower glucose).

Using ischaemic solution containing rotenone, antimycin and iodoacetate (and no glucose or O_2), the latency to the anoxic depolarization (AD) was not significantly different ($p=0.3$) after superfusion of 2mM glucose solution and after 10mM glucose solution (Fig. 8.2C, mean data in Fig. 8.4A). However, when the effect of omitting iodoacetate was tested after superfusion of 2mM glucose (Fig. 8.2D), the increase of latency described above after superfusion of 10mM glucose was reduced from 5.5 to 3 minutes (Fig. 8.4A), and this prolongation was not significant ($p=0.23$), consistent with glycogen stores having been depleted.

8.3.3 Glycolysis fuelled by glucose prevents the anoxic depolarization when mitochondria are blocked

If mitochondria are inhibited but glucose is present (e.g. in anoxia), extra production of ATP will be provided by glycolysis fuelled by glucose, on top of that fuelled by glycogen breakdown. To investigate this, I applied rotenone and antimycin in solution bubbled with N_2 but containing 10mM glucose (and no iodoacetate). Since glycolysis normally produces only 6% of the total ATP generated by the sequential

operation of glycolysis and oxidative phosphorylation (Rolfe & Brown, 1997), i.e. 2 of the total of 31 ATP molecules produced per glucose as shown in Figure 8.1, the latency to the anoxic depolarization in this condition might be expected to be only slightly prolonged compared to the situation with no glucose present as in Figure 8.2B. Contrary to this expectation, the presence of 10mM glucose prevented an anoxic depolarization occurring in 5 cells that I recorded from for over 40 mins (Fig. 8.3A), one of which was recorded from for 3.75 hours with no anoxic depolarization (AD) occurring (mean recording time was 5627±1817 sec: Fig. 8.4A). Including iodoacetate in the solution, to prevent the 10mM glucose present being metabolised, resulted in a normal early anoxic depolarization in all 5 cells studied (Fig. 8.3B, Fig. 8.4). Similarly, after 1 hour of superfusion with 2mM glucose, the maintained presence of 2mM glucose (in the rotenone and antimycin containing solution) greatly delayed the anoxic depolarization (AD). The anoxic depolarization latency (AD) was increased ($p=0.003$) from 676±126 sec in 6 slices with glucose removed during metabolic inhibition (Fig. 8.2D) to 3395±444 sec in 5 slices with 2mM glucose present (4 cells showed a very late anoxic depolarization, and one cell showed no anoxic depolarization by 4962 sec of recording; data not shown). Thus, glycolysis is able to prevent or greatly delay the occurrence of the anoxic depolarization.

Interestingly, external glucose not only prevented the anoxic depolarization occurring, but also prevented the massive increase in spontaneous release of GABA-containing vesicles that normally occurs in the first few minutes of ischaemia (Allen & Attwell, 2004; Allen et al., 2004b). Normally the fall of ATP levels in ischaemia leads to an increase of sIPSC rate, from 1-2Hz in control conditions to ~33Hz after 4 mins ischaemia (Allen & Attwell, 2004), whereas with mitochondria inhibited in the presence of 10mM glucose the sIPSC rate after 4 or even 40 mins metabolic inhibition (1.15±0.34 Hz and 1.98±0.47 Hz respectively) was not significantly increased ($p=0.86$ and 0.18, respectively) from its pre-ischaemic value (1.23±0.28 Hz in 4 cells). Thus, the presence of glucose maintains presynaptic transmembrane ion gradients sufficiently to prevent the rise of $[Ca^{2+}]_i$ which triggers the normal increase of sIPSC rate (Allen & Attwell, 2004).

In case the protective effect of external glucose was due to ATP production in the young (P12) animals used here being more dependent on glycolysis than is the case in older animals (Clark et al., 1993; Nabetani et al., 1995), I repeated this experiment in slices from P28 rats (in which enzymes of aerobic metabolism are at adult levels: Clark et al., 1993). The same abolition of the AD by 10mM glucose was obtained: in the absence of glucose the latency to the AD in N_2-bubbled solution containing rotenone, antimycin and iodoacetate was ~4 mins (230±8 sec, n=7, i.e. roughly one half of the latency seen in P12 slices), but in the presence of 10mM glucose and absence of iodoacetate no AD was seen for over 1 hour in 6 cells (recording time with no AD was 3 hours for one cell, and had a mean value of 4890±1230 sec: Fig. 8.4A).

Since it has been suggested that much of the brain's glycolysis occurs in astrocytes (Pellerin et al., 1998; Sibson et al., 1998; Magistretti & Pellerin, 1999), which also express a large fraction of the brain's glutamate transport capacity in the form of the GLT-1 transporter (Lehre et al., 1995), I considered whether the apparent importance of glycolysis for preventing the AD was related to a need to keep astrocytes polarised in order to power uptake by GLT-1 (Levy et al., 1998). To test this, in 3 cells exposed for about 20 minutes to rotenone and antimycin in N_2-bubbled solution containing 10mM glucose, I applied the GLT-1 blocker dihydrokainate (DHK, 200μM) to determine whether the resulting cessation of glutamate uptake would allow $[glu]_o$ to rise and suddenly trigger an AD. Experimentally no AD occurred (Fig. 8.3C), suggesting that glucose does not prevent an AD by maintaining glial glutamate uptake (although I cannot rule out the possibility that the residual uptake by the minority glial transporter GLAST, which is not blocked by DHK, is sufficient to prevent the glutamate concentration rising).

8.3.4 Oxygen-sensing channels do not determine the latency of the AD

Oxygen deprivation may directly inhibit K^+ channels (Jiang & Haddad, 1994) and increase Na^+ channel opening (Hammarstrom & Gage, 2000), both of which would tend to promote an earlier and larger AD. To test this, I applied solution lacking glucose

and containing iodoacetate to block glycolysis, and containing rotenone and antimycin to block mitochondrial ATP production, bubbled with 95% O_2/5% CO_2, and compared the response (Fig. 8.5A) with that produced by application of the same solution bubbled with 95% N_2/5% CO_2 (Fig. 8.2A). The latency to the AD was not significantly different (p=0.47) in the presence and absence of oxygen (Fig. 8.5B), indicating no significant contribution of these O_2-sensing channels to determining the time of the AD. However, the amplitude of the AD current was reduced in oxygen containing solution (Fig. 8.5C), and this may be due to an absence of low [O_2]-induced opening of oxygen-sensitive Na^+ channels or block of K^+ channels.

8.3.5 Metabolites downstream of glycolysis form an energy store to feed mitochondria

Applying iodoacetate alone in solution lacking oxygen and glucose (Fig. 8.6A) produced an AD with a latency that was 1 minute longer than (not significantly different from, p=0.11) that seen when rotenone and antimycin were included in the solution (Fig. 8.2A). However, when iodoacetate alone was applied in solution that lacked glucose but was bubbled with oxygen (Fig. 8.6B), the AD took an extra 5 minutes to occur (p=0.003; n=13, Fig. 8.6D). This suggests that there are sufficient substrates downstream of the GAPDH enzyme which is inhibited by iodoacetate (Fig. 8.1) for mitochondria to generate 5 minutes worth of ATP when oxygen is present. Again, the amplitude of the AD current was smaller in the presence of oxygen (Fig. 8.6E).

In case free-radical production by mitochondria in the presence of O_2 (Turrens, 2003) affected the time to the AD, I tested the effect of the cell-permeant free radical scavenger MnTBAP (Mn(III)tetrakis(4-benzoic acid) porphyrin, 200μM), in which the slices were soaked for 30 mins before recording and which was also present in the superfusion solution (Vergun et al., 2001). MnTBAP had no effect on the latency to the AD (754±149 sec in 6 slices, p=0.39 compared with no MnTBAP present) when iodoacetate was applied in the presence of oxygen, suggesting that free radical generation plays an insignificant role in determining the AD latency.

I independently estimated the ATP generating power of metabolites downstream of glycolysis by comparing the latency to the AD in the oxygen-bubbled iodoacetate containing solution (Fig. 8.6B) with that in the same solution to which rotenone and antimycin had been added to block mitochondria (Fig. 8.5A). The presence of the mitochondrial blockers reduced the time to the AD by nearly 6.5 minutes ($p=0.0005$, comparing the second column in Fig. 8.5B with the second column in Fig. 8.6D). This is slightly longer than the 5 minute change seen on omitting oxygen (Fig. 8.6A,B), which may reflect the presence of a small amount of residual oxygen in the N_2-bubbed iodoacetate containing solution of Figure 8.6A which would slightly increase the latency to the AD.

8.3.6 Lactate oxidation does not delay the AD when glycolysis is inhibited

According to the suggestion that activity-evoked glycolysis, or almost all glycolysis, is in glia, which export lactate to neurons as a substrate for their mitochondria (Pellerin et al., 1998; Sibson et al., 1998; Magistretti & Pellerin, 1999), one might expect that, with oxygen present during inhibition of glycolysis, neuronal ATP levels could be maintained if mitochondria are fuelled by the superfusion of lactate. Thus, if the AD is primarily produced by a decrease of neuronal transmembrane ion gradients (see section 8.4.2), then the AD evoked by iodoacetate in the presence of oxygen ought to be greatly delayed, or even prevented, by superfusion of lactate.

Experimentally, however, including 5mM lactate in the solution (a concentration reported to maintain synaptic transmission in the absence of glucose: Schurr et al., 1988; Saitoh et al., 1994) did not prevent the AD evoked by iodoacetate (Fig. 8.6C), which occurred (in 7 cells) at a time not significantly altered ($p=0.37$) from when lactate was absent. Lactate also did not prevent the increase in spontaneous release of GABA-containing vesicles that normally occurs during metabolic inhibition (Allen & Attwell, 2004; Allen et al., 2004b): after 4 mins in iodoacetate the sIPSC rate in 4 cells had increased from a pre-iodoacetate value of 2.8 ± 1.3Hz in 4 cells to 13.9 ± 2.8Hz (less than the 33Hz seen with combined inhibition of glycolysis and mitochondria (Allen &

Attwell, 2004) presumably because some ATP is initially still being made by mitochondria). The presence of 5mM lactate had no significant effect on this increase (the IPSC rate increased from 2.3±0.6Hz to 11.2±3.3Hz in 4 cells; p=0.55 compared with no lactate). Thus, the presence of lactate does not prevent [ATP] falling sufficiently in presynaptic terminals to evoke a large increase in spontaneous transmitter release.

Similarly 5mM pyruvate did not affect the AD latency (p=0.96) in 6 cells, and neither did 20mM lactate in 7 cells (p=0.34; Fig. 8.6D). In case this lack of effect of lactate was due to ATP production in the young (P12) animals used here being more dependent on glycolysis than is the case in older animals (Clark et al., 1993; Nabetani et al., 1995), I repeated this experiment in slices from P28 rats (in which the enzymes of aerobic metabolism are at adult levels: Clark et al., 1993). Again, neither 5mM nor 20mM lactate significantly delayed the AD (Fig. 8.6D): its latency changed from 1457±78 sec in 6 slices without lactate (twice as long as in P12 slices) to 1860±301 sec in 10 slices with 5mM lactate (p=0.16), while for 20mM lactate the latency was 1603±80 sec in 5 slices (p=0.22 compared with no lactate present).

To assess whether lactate might initially support synaptic transmission, even though it cannot prevent the anoxic depolarization occurring eventually, I carried out an experiment similar to that of Izumi et al. (1994, Fig. 4) measuring the field EPSP evoked by stimulating the Schaffer collaterals in P28 slices. Iodoacetate evoked an inhibition of the fEPSP slope (Fig. 8.6F), which fell to 50% of its initial value in approximately 3 mins (significantly faster than the 12 mins seen by Izumi et al. (1994) when they applied iodoacetate in the presence of glucose), and this was followed by a small recovery of the fEPSP. The initial depression of the fEPSP is due to adenosine release suppressing synaptic glutamate release (Fowler, 1990), and the subsequent recovery (Fowler, 1992) may reflect inhibition of the function of G protein-coupled adenosine receptors when the GTP concentration falls in presynaptic terminals. Again contrary to Izumi et al. (1994), I found that when 20mM lactate was present there was no change in the decline of the fEPSP (Fig. 8.6F).

I attribute the faster fEPSP decay that I see in iodoacetate, and the lack of effect of lactate, to the fact that Izumi et al. (1994) used a low concentration of iodoacetate (0.2mM) which blocks glycolysis incompletely (Zeevalk et al., 1995). Fitting a Michaelis-Menten relation to the data of Zeevalk et al. (1995) on the [iodoacetate]-dependence of glycolysis inhibition in retina, I estimate that 0.2mM iodoacetate only blocks glycolysis by 53%, while the 2mM that I use blocks it by 92%. Furthermore, Izumi et al. (1994) also left glucose present in the solution (presumably because if glycolysis were blocked it would not be metabolised). Repeating my experiment using only 0.2mM iodoacetate with 10mM glucose present, I found that the decay of the fEPSP slope to 50% of its initial size was delayed by 11 mins (Fig. 8.6F), consistent with some ATP being produced from external glucose and intracellular glycogen by unblocked glycolysis. Furthermore, if I employed 0.2mM iodoacetate with 20mM lactate (but no glucose) present, then the fEPSP decay was delayed by a further 4.5 mins (Fig. 8.6F), mimicking in part the protective effect of lactate observed by Izumi et al. (1994).

Taken together, these data suggest that when glycolysis is completely blocked (with 2mM iodoacetate), the amount of ATP made from lactate by mitochondria is too small to significantly delay the inhibition of the fEPSP, but that if some ATP is being made from glycogen by glycolysis (in only 0.2mM iodoacetate) then the addition of lactate-derived ATP can delay the fEPSP inhibition. In my experiments the presence of lactate did not prevent the fEPSP eventually being greatly reduced. This is not a discrepancy with the data of Izumi et al. (1994), who found that the fEPSP was only suppressed by 35% after 30 mins in lactate, for two reasons. First, it appears that they had glucose present in their lactate containing solution (see their Table 2 legend) which would have continued to make ATP via partially blocked glycolysis. Secondly, their recordings were at 30°C and mine were at 33°C. Assuming a Q_{10} of 3, I would expect that the time needed for the fEPSP to start its rapid decline in 0.2mM iodoacetate would be prolonged from the 18 mins in Fig. 8.6F to 25 mins, which is similar to the recording time of Izumi et al.: thus if they had recorded for longer, without glucose in the lactate-

containing solution, they would presumably have seen the large decrease of fEPSP in lactate-containing solution which I observe.

8.3.7 Blocking mitochondria with cyanide gives an earlier anoxic depolarisation than with rotenone/antimycin

I compared the effect of blocking mitochondrial function with cyanide ((Reiner et al., 1990; Ferreira et al., 1997) with the effect of using rotenone and antimycin (Fig. 8.7), since cyanide also modulates NMDA receptor activation (Patel et al., 1994; Arden et al., 1998). Solution containing iodoacetate and cyanide (1mM), and lacking O_2 and glucose, produced an AD (Fig. 8.7A) which was similar to that seen with rotenone and antimycin (Fig. 8.2A), except that it occurred approximately 1.5 minute earlier, after 6 mins instead of 7.5 mins (significantly different, $p= 2.6x10^{-5}$). Applying glutamate receptor blockers during the post-AD plateau suppressed much of the inward current (Fig. 8.8A) showing that it was mediated by glutamate release (Rossi et al., 2000), however much of the rest of the inward current is generated by GABA release (Allen et al., 2004b), E_{Cl} was 0mV in these experiments so $GABA_A$ receptors generate an inward current. The amplitude of the glutamate-mediated current was not significantly different between ischaemia induced by glucose- and oxygen-free solution containing either rotenone, antimycin and iodoacetate or cyanide and iodoacetate (Fig. 8.8B, C).

Omitting iodoacetate from the cyanide-containing solution, to allow glycolysis driven by glycogen breakdown, prolonged the latency to the AD by 6 mins (Fig. 8.7B, D; p=0.006), as described above when mitochondria were inhibited with rotenone and antimycin.

Surprisingly, if oxygen was present in the solution containing iodoacetate and cyanide and lacking glucose, the AD was delayed by nearly 11 minutes (p=0.007, n=7, Fig. 8.7C, D). In contrast, oxygen had no prolonging effect when mitochondria were blocked with rotenone and antimycin (Fig. 8.5). This suggests that cyanide does not completely block mitochondria (oxygen itself may reduce the cyanide block: Delhumeau et al., 1994).

8.3.8 The response to simple removal of oxygen and glucose

Figure 8.9A shows the response to removal of oxygen and glucose from the superfusion solution, without any metabolic blockers being added. The latency to the AD (Fig. 8.9D, 1st column) was longer by 4 mins ($p=0.04$) than when rotenone and antimycin were added as well (Fig. 8.4A, 2nd column; both in the absence of iodoacetate) presumably because in an open recording chamber it is hard to remove all the oxygen from the superfusing solution, and thus hard to completely inhibit mitochondrial ATP production from the substrate produced by glycogen breakdown. Consistent with the presence of a significant amount of residual O_2, simple removal of glucose (leaving oxygen present) produced an AD with a latency similar ($p=0.4$) to that seen when oxygen and glucose were both removed (Fig. 8.9B, D). However, the amplitude of the AD current was reduced in the presence of oxygen (Fig. 8.9E).

To check the role of glycogen breakdown, the experiment removing oxygen and glucose was repeated after soaking slices for at least an hour in solution containing 2mM glucose, to try to lower the cells' glycogen stores and intracellular glucose levels (as done above for Fig. 8.2C, D). After this treatment, the latency to the AD seen when glucose and O_2 were removed was reduced by 6.5 mins ($p=0.005$), as shown in Fig. 8.9C, D, again implying a significant role for glycogenolysis in delaying the AD.

8.3.9 Estimation of the relative size of hippocampal energy stores

In this section I use the data above to estimate the relative sizes of ATP reserves provided by various biochemical stores in slices from P12 rats. Most brain ATP is used to power ion pumping (Ames, 1992; Rolfe & Brown, 1997; Attwell & Laughlin, 2001), so here I focus on the supply of ATP to the Na^+ pump which prevents the decrease of ion gradients causing the AD.

8.3.9.1 How long can ATP stores sustain Na^+ pumping during severe metabolic inhibition?

When glucose and oxygen are removed, at the same time as blockers of ATP production by mitochondria and glycolysis are applied, it takes ~7.5 minutes (at 33°C) before the AD occurs in P12 hippocampal slices (Fig. 8.2). Part of this time will reflect the time needed for the ATP concentration to fall below the level needed to sustain operation of the plasma membrane Na^+/K^+-ATPase (the catalytic site for ATP hydrolysis has an EC_{50} of only 0.4μM, but the pump may stop working when [ATP] falls below the level needed to activate lower affinity ((EC50~0.4mM) ATP binding sites: Dagani & Erecinska, 1987). The remainder of the time will reflect the period needed for ion gradients to decrease once the Na^+/K^+-ATPase has stopped. The free ATP is initially 2.7mM (Folbergrova et al., 1997) and the hippocampus (*in vivo)* consumes ATP at a rate of 0.4mM/sec (calculated from the measured glucose utilization at 37°C of 79 μmol/100g/min (Sokoloff et al., 1977) assuming that 31 ATP are produced per glucose (Rolfe & Brown, 1997), so when ATP synthesis stops the existing ATP should be consumed in 2.7/0.4 = 6.8 sec at 37°C, or 10.5 sec at the temperature of 33°C which I use (assuming a Q_{10} of 3). In addition, ATP can be generated from phosphocreatine and from other nucleoside triphosphates (Fig. 8.1). The phosphocreatine concentration is twice as high as that of ATP (Raley & Lipton, 1990; Folbergrova et al., 1997), while the concentrations of UTP, GTP and CTP (which can be converted to ATP) when added together give about 1/3 the level of ATP (Pissarek et al., 1999). Thus, phosphocreatine is expected to contribute sufficient ATP to power about 21 sec of ion pumping, while other nucleoside triphosphates will power 3.5 sec of pumping. These durations will be increased in my experiments if the metabolic activity of hippocampal slices is lower than that of *in vivo* hippocampus, for example due to the removal of excitatory input from outside the hippocampus, or if energy use is down-regulated in the first few minutes of energy deprivation (as has been measured in cultured neurons after an hour's energy deprivation: Munns et al., 2003).

8.3.9.2 Glycogenolysis delays the AD by 5.5 minutes

When hippocampal slices were exposed to severe metabolic inhibition (removal of glucose and oxygen, and addition of rotenone and antimycin) but glycolysis was allowed to occur (i.e. no iodoacetate was applied) the AD occurred 5.5 minutes later (Fig. 8.2B), and this prolongation was reduced (indeed was not significant) for slices pre-soaked in low glucose, consistent with glycogen stores (and intracellular glucose) being the source of the extra latency (Fig. 8.2C, D). If I ignore metabolic compartmentation within the slice, by assuming that energy stored as glycogen predominantly in glia (Rosenberg & Dichter, 1985; Kato et al., 1989; Ignacio et al., 1990) can be freely passed to neurons (e.g. as lactate: Cambray-Deakin et al., 1988; Dringen et al., 1993; Pellerin et al., 1998; Sibson et al., 1998; Magistretti & Pellerin, 1999), and further assume that with mitochondria blocked there is no change in the rate of ATP consumption nor in the time needed for ion gradients to decrease after the sodium pump has stopped, then it appears that glycogenolysis can provide ~5.5 minutes worth of ATP to maintain sodium pumping and other energy consuming processes within the cell. Glycogen therefore provides a greater energy store than either free ATP or phosphocreatine.

8.3.9.3 Energy stored in metabolites downstream of GAPDH

Comparison of the latency to the AD produced by iodoacetate in solution including or lacking oxygen, or in oxygen-containing solution containing or lacking mitochondrial blockers, suggested that already generated products of glycolysis, downstream of the GAPDH enzyme that iodoacetate inhibits, can feed into mitochondria and generate ~6.5 minutes worth of ATP. Pyruvate, lactate, citric acid cycle intermediates, NADH, $FADH_2$ and amino acid oxidation may all contribute to this tail of substrate provision to mitochondria. Fatty acid metabolism, which generates $FADH_2$ for mitochondria, could also theoretically contribute to this increase of ATP production, but fatty acid oxidation is reported to be of little significance in the brain because of the absence of the enzyme 3-ketoacyl-CoA thiolase (Yang et al., 1987).

8.4 Discussion

I have investigated the role of different metabolic pathways in preventing the anoxic depolarization produced by energy deprivation in hippocampal slices. Formation of ATP from glycogen (via glycolysis) or from pyruvate, citric acid cycle intermediates and amino acids (via oxidative phosphorylation) can delay the AD. During transient ischaemia, hypoglycaemia or anoxia, these energy reserves might prevent an AD occurring, and be neuroprotective (Swanson & Choi, 1993; Gruetter, 2003a). My data indicate a particularly important role for glycolysis in this regard: when mitochondria are blocked external glucose prevents an AD occurring for hours, whereas when glycolysis is blocked lactate-driven oxidative phosphorylation does not significantly delay the AD.

8.4.1 External glucose prevents the AD occurring

Even with mitochondrial ATP production blocked, external glucose was sufficient to prevent the AD occurring. This is surprising, since normally glycolysis provides only 6% of the brain's ATP (assuming glycolysis does not become more important in brain slices). This might be taken to imply that only a small fraction of the brain's ATP production is needed to prevent the AD. However, when mitochondria are inhibited ATP production by glycolysis is increased, by the Pasteur effect, by a factor of 4-5, due to increased activity of phosphofructokinase, hexokinase and glucose transport (Lowry et al., 1964; Drewes & Gilboe, 1973; Dépre et al., 1998), so there should be much more ATP production than is normally generated by glycolysis. Although P12 animals may rely less on oxidative phosphorylation than older animals, and thus be able to maintain membrane potentials and neuronal excitability through glycolysis alone (Clark et al., 1993; Nabetani et al., 1995), I found identical results in older (P28) rat slices when the oxidative phosphorylation system is mature, i.e. external glucose was sufficient to prevent the AD.

8.4.2 Lactate oxidation does not delay the AD

While some papers report that lactate supports neuronal activity in the absence of glucose (in CA1: Schurr et al., 1988; Izumi et al., 1994; Izumi et al., 1997; optic nerve: Brown et al., 2003), others find that although lactate helps to maintain ATP levels it does not allow normal neuronal activity (CA3: Takata & Okada, 1995; Wada et al., 1998; in CA1: Chih et al., 2001a). Lactate is converted into pyruvate which produces ATP via oxidative phosphorylation (Fig. 8.1), so with glycolysis, but not mitochondria, inhibited one might expect lactate to maintain the majority of the ATP production and to prevent the AD. When glycolysis was inhibited with iodoacetate, however, adding 5-20mM lactate did not delay the AD either in P12 or P28 rats (Fig. 8.6C, D), and did not prevent a rise in sIPSC frequency or inhibition of excitatory synaptic transmission (Fig. 8.6F). Thus, in my experiments mitochondria do not produce significant ATP from superfused lactate (and hence not from lactate released by glia) when glycolysis is inhibited.

My data are consistent with the findings of Takata & Okada (1995) and Wada et al. (Wada et al., 1998) that replacing glucose with lactate abolished synaptic transmission in <20 mins (in guinea pig CA3 and dentate gyrus). By contrast in rat CA1, Schurr et al. (Schurr et al., 1988) found that replacing glucose by lactate preserved synaptic function, and Izumi et al. (1994, Fig. 4) found that after 30 mins in iodoacetate the field EPSP was reduced by 80% with glucose present, but reduced by only 35% in 10mM lactate. The results of Schurr et al. may reflect the use of an interface chamber rather than submerged slices, but the apparent discrepancy with Izumi et al. (1994) resulted from their using a low concentration of iodoacetate which does not completely block glycolysis (see section 8.3.6), and leaving glucose in their solutions. When I used their low concentration of iodoacetate and left glucose in the solution, it took longer for the fEPSP to be inhibited, as expected if ATP could still be made from glycogen and glucose by a glycolysis pathway that was only partially blocked (Fig. 8.6F). In addition, having lactate present (without glucose) further delayed the inhibition of the fEPSP. Thus, when glycolysis is completely blocked, the amount of ATP made from lactate by mitochondria is too small to delay the inhibition of the fEPSP, but if some ATP is being

made from glycogen when glycolysis is only partly blocked then the addition of lactate-derived ATP can delay (but not prevent) the fEPSP inhibition.

8.4.3 Metabolic compartmentation

Metabolic compartmentation in the brain, within cells or between cell types, may explain some of my results.

It has been suggested (Raffin et al., 1992; Rosenthal & Sick, 1992) that the plasma membrane Na^+/K^+-ATPase is preferentially fuelled by ATP produced from glycolysis (although it is unclear why mitochondrially-produced ATP cannot diffuse to plasma membrane Na^+ pumps, and an increase of glycolytic rate via the Pasteur effect might explain why mitochondrial block has relatively little effect). Consistent with a metabolic compartmentation within cells in which glycolysis powers ion pumping, glycolytic enzymes have been detected in synaptic locations where energy use on ion pumping is high (Wu et al., 1997; Ikemoto et al., 2003). This could explain why fuelling glycolysis with glucose while blocking mitochondria prevents an AD: glycolytic ATP might allow the Na^+/K^+-ATPase to function sufficiently to maintain transmembrane ion gradients. Indeed, external glucose maintained presynaptic ion gradients sufficiently to prevent the massive spontaneous exocytosis of GABA-containing vesicles that is normally triggered by energy deprivation.

Alternatively, if glycolysis is largely in glia, which export lactate to neurons to be metabolised by their mitochondria (Pellerin et al., 1998; Sibson et al., 1998; Magistretti & Pellerin, 1999; but see Chih et al., 2001b), then my data might suggest that the key step in triggering the AD is a fall in glial [ATP], leading to glial depolarization which releases K^+ and reduces glutamate uptake. This would explain why inhibition of (mainly glial) glycolysis with iodoacetate is sufficient to produce an AD after ~8 minutes (Fig. 8.6 A, D), whereas inhibition of (mainly neuronal) mitochondria with rotenone and antimycin (but no iodoacetate) produces an AD only after ~13 minutes (Figs. 8.2B, 8.4A). It would also explain why an AD can be prevented for over an hour when glucose is present during mitochondrial inhibition (Fig. 8.3A).

Finally, if maintaining ATP levels in glia were important for preventing an AD, it would explain why evolution has placed most glycogen in glia rather than neurons: during metabolic inhibition the ATP level in glia could be maintained by glycogenolysis.

However, it is not clear why a fall of ATP concentration in glia should trigger an AD. The ATP consumption and the expected K^+ leak when the sodium pump is inhibited are both larger in neurons than in glia (Attwell & Laughlin, 2001), suggesting that stopping ATP production will cause neuronal [ATP] to fall faster than glial [ATP] and that neurons will contribute more to the rise of $[K^+]_o$ which slows and then reverses glutamate transporters, releasing the glutamate which generates the AD (Rossi et al., 2000). The possibility that the AD is triggered by a decrease of glial ion gradients slowing or reversing the main GLT-1 glutamate transporter in glia is contradicted by the fact that blocking or knocking out GLT-1 does not alter the time of the AD (Rossi et al., 2000; Hamann et al., 2002), even when mitochondria are blocked (Fig. 8.3C). By contrast, knocking out the neuronal transporter EAAC1 delays the AD three-fold (Gebhardt et al., 2002), suggesting that the transporters which release glutamate are mainly in neurons. For all these reasons, one might expect a fall of ATP level in neurons, rather than glia, to be the factor precipitating the AD.

8.4.4 O_2-sensing ion channels do not influence AD latency

The latency of the AD seen during metabolic inhibition with rotenone, antimycin, iodoacetate and glucose removal was not affected by the presence or absence of oxygen (Fig. 8.5), suggesting that O_2-sensing channels play little role in determining the AD latency.

8.4.5 Comparison of cyanide and rotenone/antimycin as mitochondrial blockers

The AD produced using cyanide as a mitochondrial blocker (with iodoacetate to block glycolysis) was similar to that seen when blocking mitochondria with rotenone plus antimycin, but the AD latency was reduced by 20% when using cyanide. The

potentiating action of cyanide on NMDA receptors containing NR2A subunits (Patel et al., 1994; Arden et al., 1998), together with the fact that the AD is largely produced by activation of NMDA receptors (Rossi et al., 2000) seems a likely explanation for this slight acceleration.

8.4.6 A hierarchy of energy stores

The estimates of energy stores in P12 slices described in the Results can be summarised as the following hierarchy of times (at 33°C) for which ATP can be produced by the different stores: pyruvate/citric acid cycle intermediates/amino acid oxidation when mitochondria are functioning (390 sec) > glycogen when mitochondria are inhibited (330 sec) > phosphocreatine (21 sec) > ATP (10.5 sec) > other nucleoside triphosphates (3.5 sec). If a metabolic insult is of limited duration (e.g. a clot is rapidly cleared from a blood vessel), these stores may be able to prevent an AD occurring, and thus prevent the massive release of glutamate by transporter reversal which triggers neuronal death.

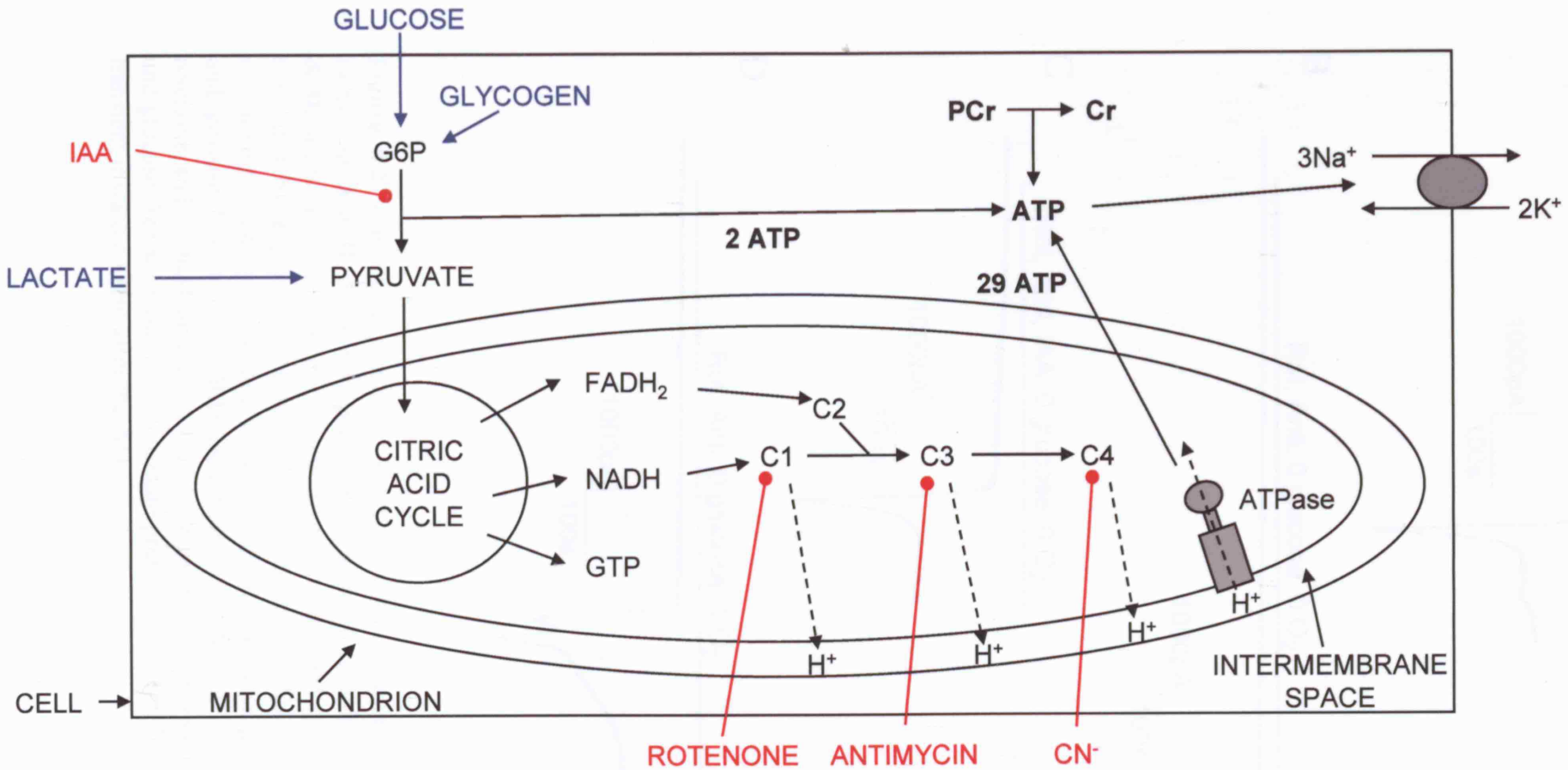

Figure 8.1 Schematic diagram of energy production pathways inhibited in this chapter. Conversion of glucose (or glycogen) to pyruvate by glycolysis generates 2 ATP molecules and can be inhibited with iodoacetate. G6P = glucose-6-phosphate. Pyruvate is converted to acetyl CoA to feed the citric acid cycle, which generates 2 GTP molecules (which are convertible to ATP) and exports NADH and $FADH_2$ to the electron transport chain, complexes 1, 3 and 4 (C1, C3 and C4) of which extrude H^+ across the mitochondrial membrane to power ATP synthesis (29 ATP/glucose; Rolfe and Brown, 1997). C1, C3 and C4 can be inhibited with rotenone, antimycin and cyanide respectively. ATP is used largely to fuel ion pumping (Attwell & Laughlin, 2001), indicated here as the plasma membrane sodium pump. Short term ATP reserves occur as phosphocreatine (PCr) and as nucleotide triphosphates (NTP) other than ATP (UTP, GTP, CTP).

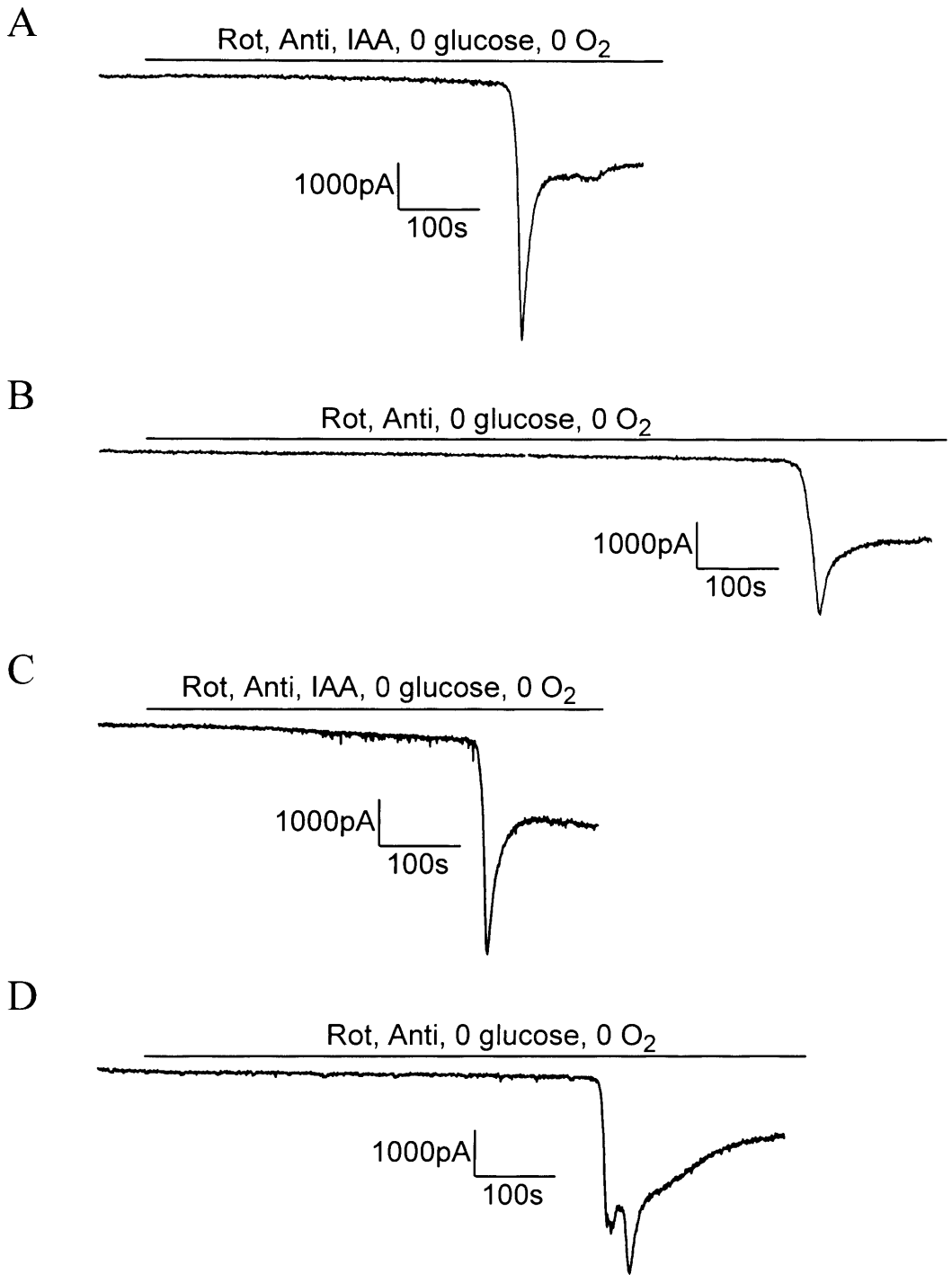

Figure 8.2. Current response at -33mV of CA1 pyramidal cells to simulated ischaemia. **A & B,** slices were presoaked in solution containing 10mM glucose. **C & D,** slices were presoaked in solution containing 2mM glucose. **A,C** Ischaemia simulated by application of 100μM rotenone and 100μM antimycin (to block oxidative phosphorylation), and 2mM iodoacetate (to block glycolysis), in oxygen and glucose free solution. **B,D** Ischaemia simulated by application of 100μM rotenone and 100μM antimycin (to block oxidative phosphorylation) in oxygen and glucose free solution (no iodoacetate present). The cell in D showed a second transient inward current after the AD.

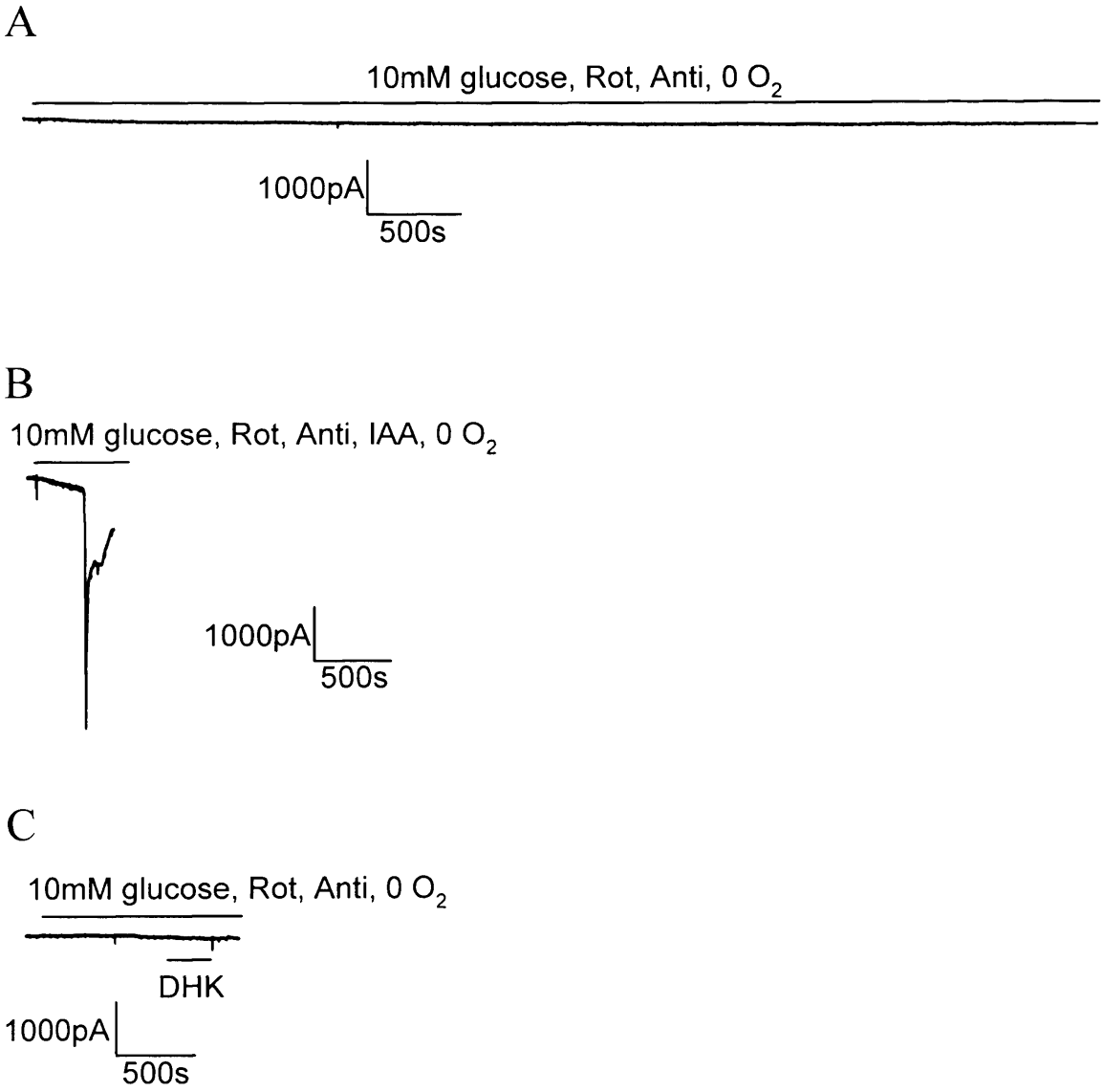

Figure 8.3. Glycolysis sustained by the presence of 10mM glucose prevented an AD from occurring in the presence of blockers of oxidative phosphorylation. Note the slow time scale compared with the other figures. **A** Blocking oxidative phosphorylation (with 100μM rotenone and 100μM antimycin) in oxygen free solution containing 10mM glucose did not induce an AD after 1 hour. **B** Repeating the experiment in A, but adding 2mM iodoacetate to block glycolysis, produced an AD as expected after 6 minutes. **C** Blocking the glutamate transporter GLT-1, by application of 200μM DHK, to a slice made ischaemic in the same way as in A, did not induce an AD.

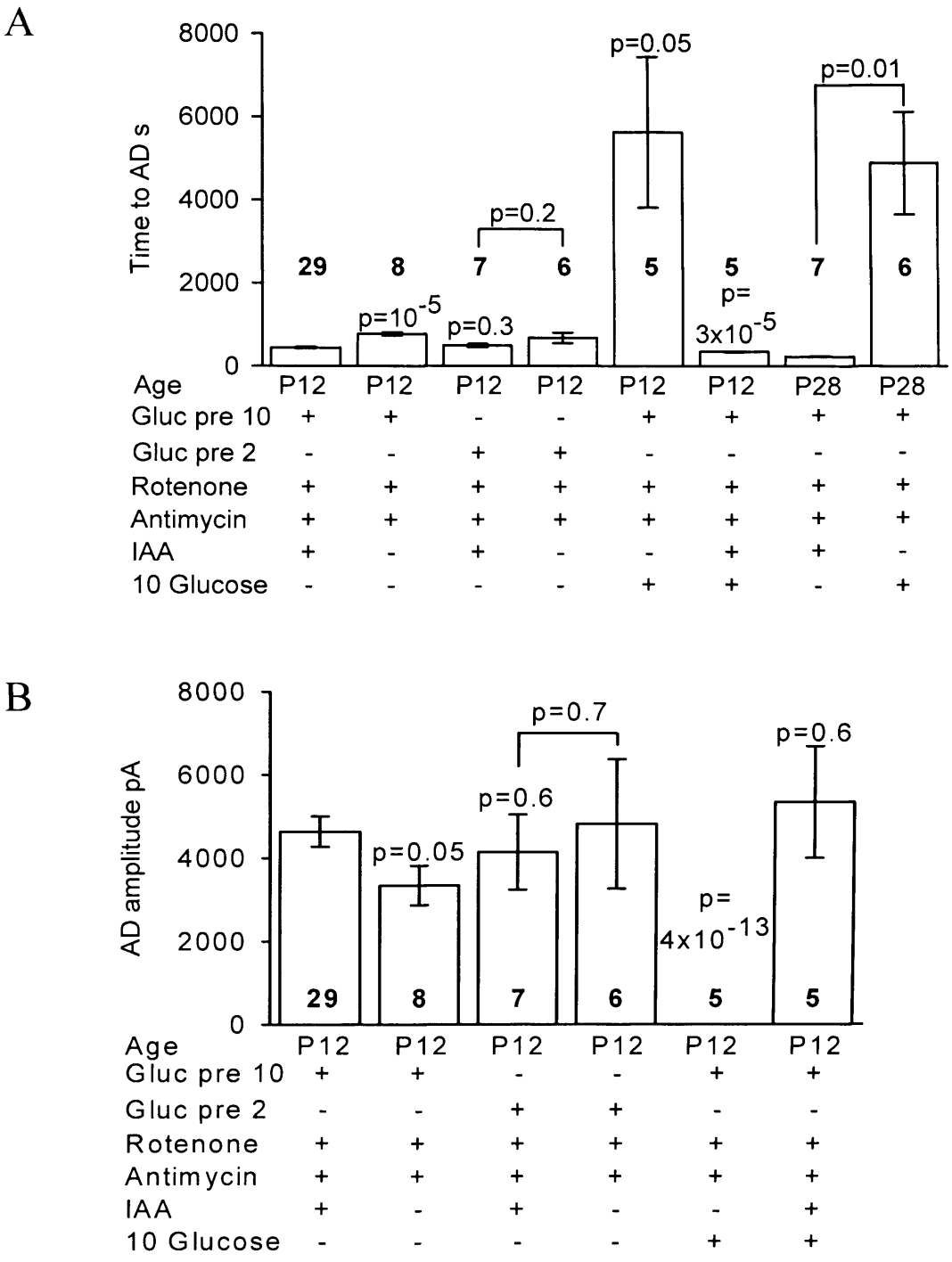

Figure 8.4. Summary of time taken for the AD to occur and the amplitude of the AD current in the ischaemic conditions presented in Figures 8.2 & 8.3. **A** Time taken for the AD to occur. For the 5th and 8th bars, no AD occurred and the bar shows the recording duration with no AD. **B** Amplitude of the AD current. In both graphs the numbers in bold represent the number of cells; p-values above bars compare values to the first condition (slice presoaked in 10mM glucose, application of solution containing rotenone, antimycin and iodoacetate, oxygen and glucose free), while p values between bars compare the indicated conditions. Gluc pre 10 or 2 means glucose was present at 10 or 2mM before ischaemia. No P28 data are shown for AD amplitude because in most of these experiments the AD latency was determined solely by extracellular recording.

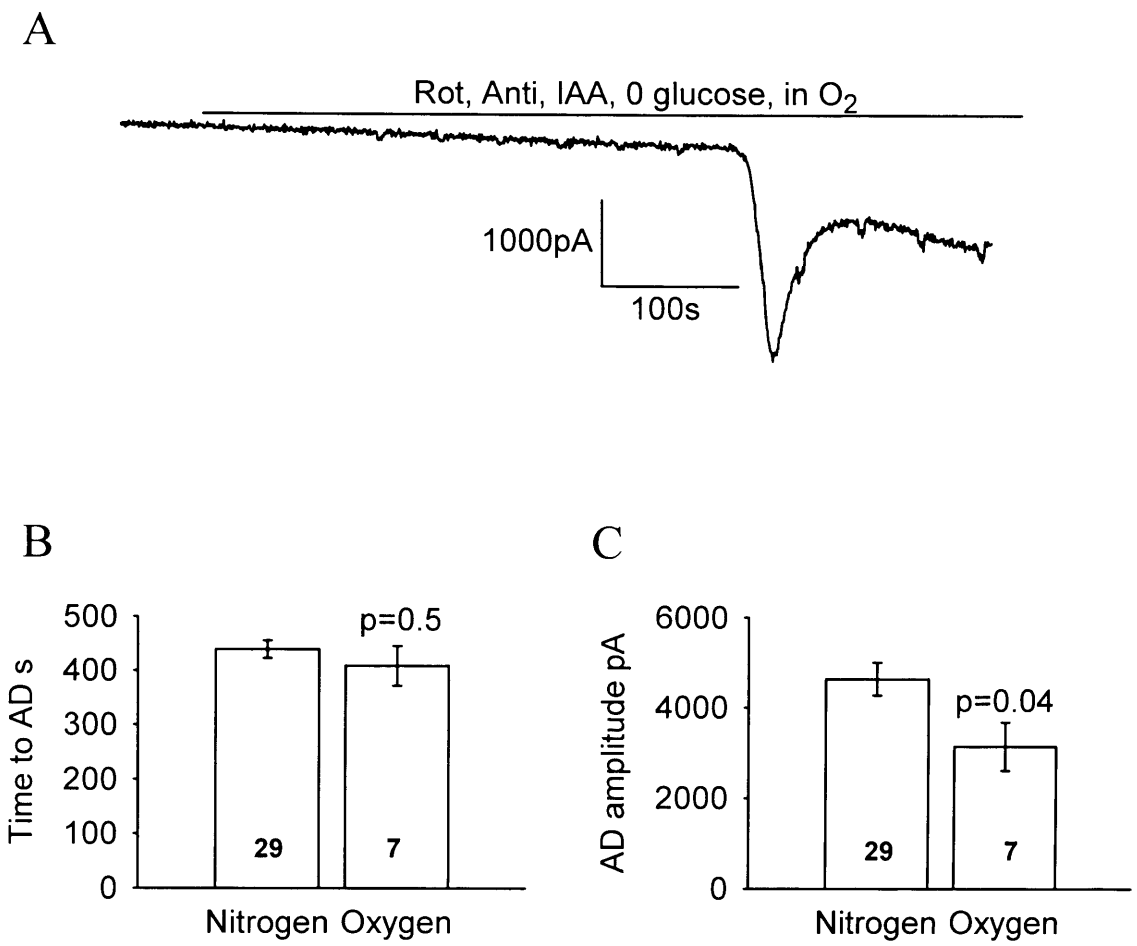

Figure 8.5. O_2 sensing ion channels do not affect the time at which the AD occurs. **A** An AD occurs in solution containing 100μM rotenone, 100μM antimycin and 2mM iodoacetate (glucose free, slice presoaked in 10mM glucose) bubbled with O_2, just as when the solution was bubbled with N_2 (Fig. 8.2A). Small steps on trace are in response to voltage jumps to check series resistance. **B** The time of the AD was not affected by the presence of oxygen in the ischaemia solution. **C** The amplitude of the AD current was reduced when oxygen was present in the ischaemia solution. Bold numbers show numbers of cells.

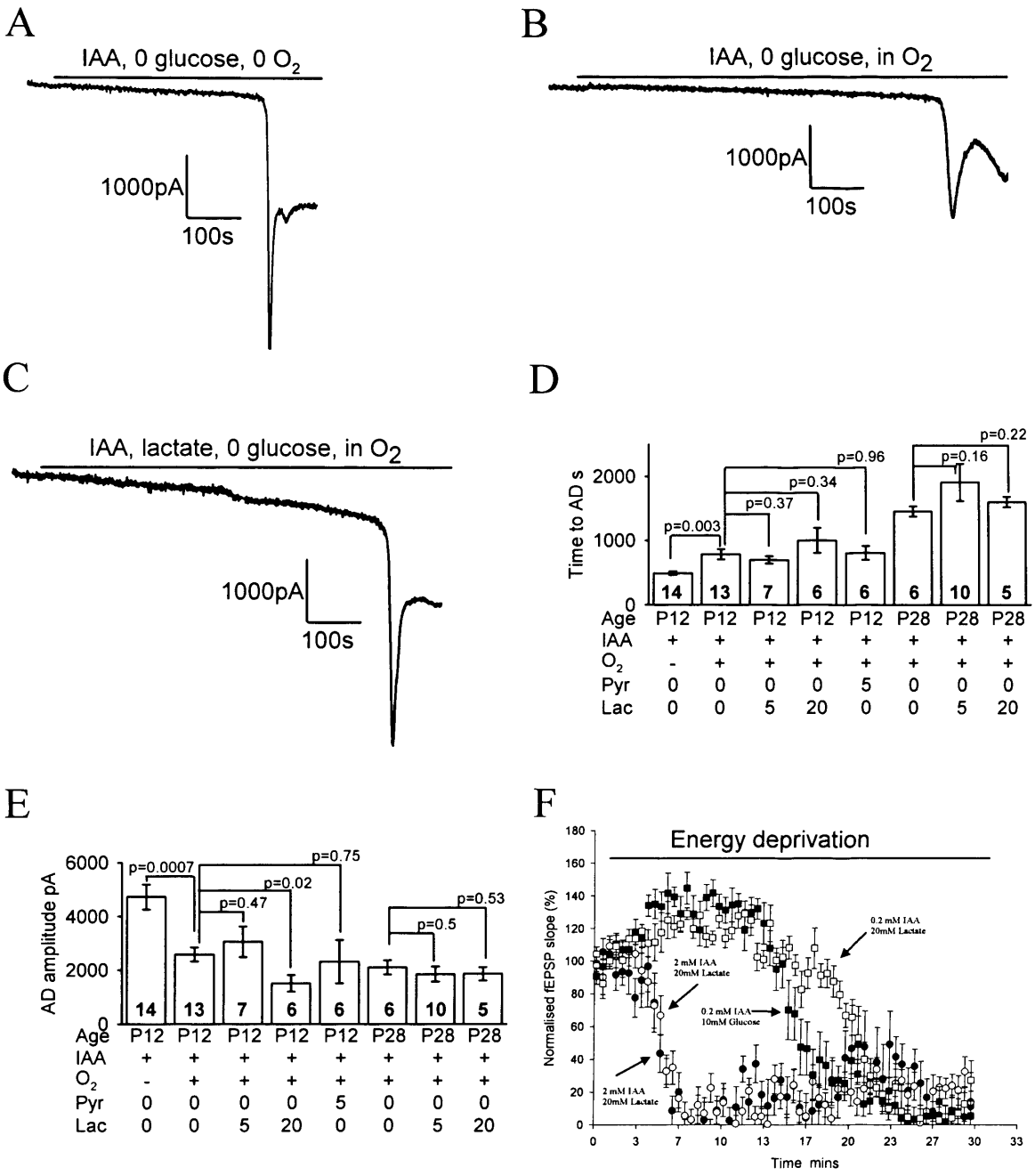

Figure 8.6. Blocking glycolysis alone is sufficient to induce an AD. **A-C** Data from P12 slices. **A** Blocking glycolysis with 2mM iodoacetate in oxygen and glucose free solution led to an AD after 8 minutes. **B** Adding oxygen to the solution used in A delayed the AD. **C** Adding 5mM lactate to the solution as in B had no effect on the time at which the AD occurred. **D** Mean time to the AD in the conditions of A-C and with 5mM pyruvate or 20mM lactate present for P12 slices, and with 0, 5 or 20mM lactate present for P28 slices. **E** Mean amplitude of the AD. Bold numbers denote the number of cells studied. **F** Decline of the field EPSP initial slope (normalised to value before metabolic inhibition) evoked by 0.1 Hz stimulation of the Schaffer collaterals in the presence (from t = 2mins) of 2mM iodoacetate (and no glucose), 2mM iodoacetate and 20mM lactate, 0.2mM iodoacetate and 10mM glucose, and 0.2mM iodoacetate and 20mM lactate.

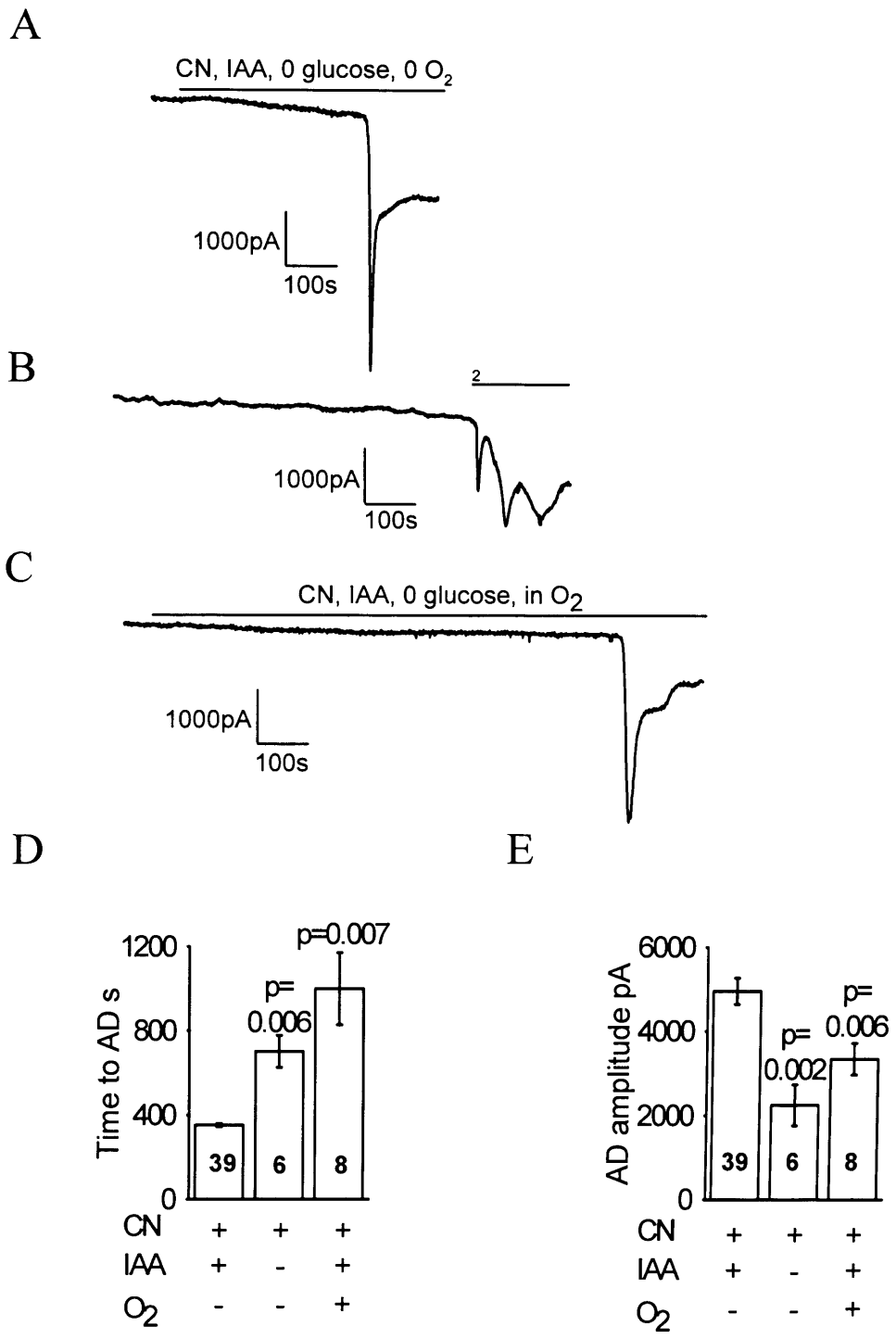

Figure 8.7. Use of cyanide to block oxidative phosphorylation. **A** Ischaemia induced by applying oxygen and glucose free solution containing 1mM cyanide (to block oxidative phosphorylation) and 2mM iodoacetate (to block glycolysis). **B** Omitting iodoacetate, when blocking oxidative phosphorylation using cyanide (in oxygen and glucose free solution) delayed the time to the AD (this cell showed repeated depolarizing currents after the AD). **C** Adding oxygen to glucose free solution containing 1mM cyanide and 2mM iodoacetate delayed the time to the AD. **D** Mean time to the AD in A-C. **E** Mean amplitude of the AD in A-C. Bold numbers show number of cells studied. P values compare the 2nd and 3rd bars with the 1st bar in D and E.

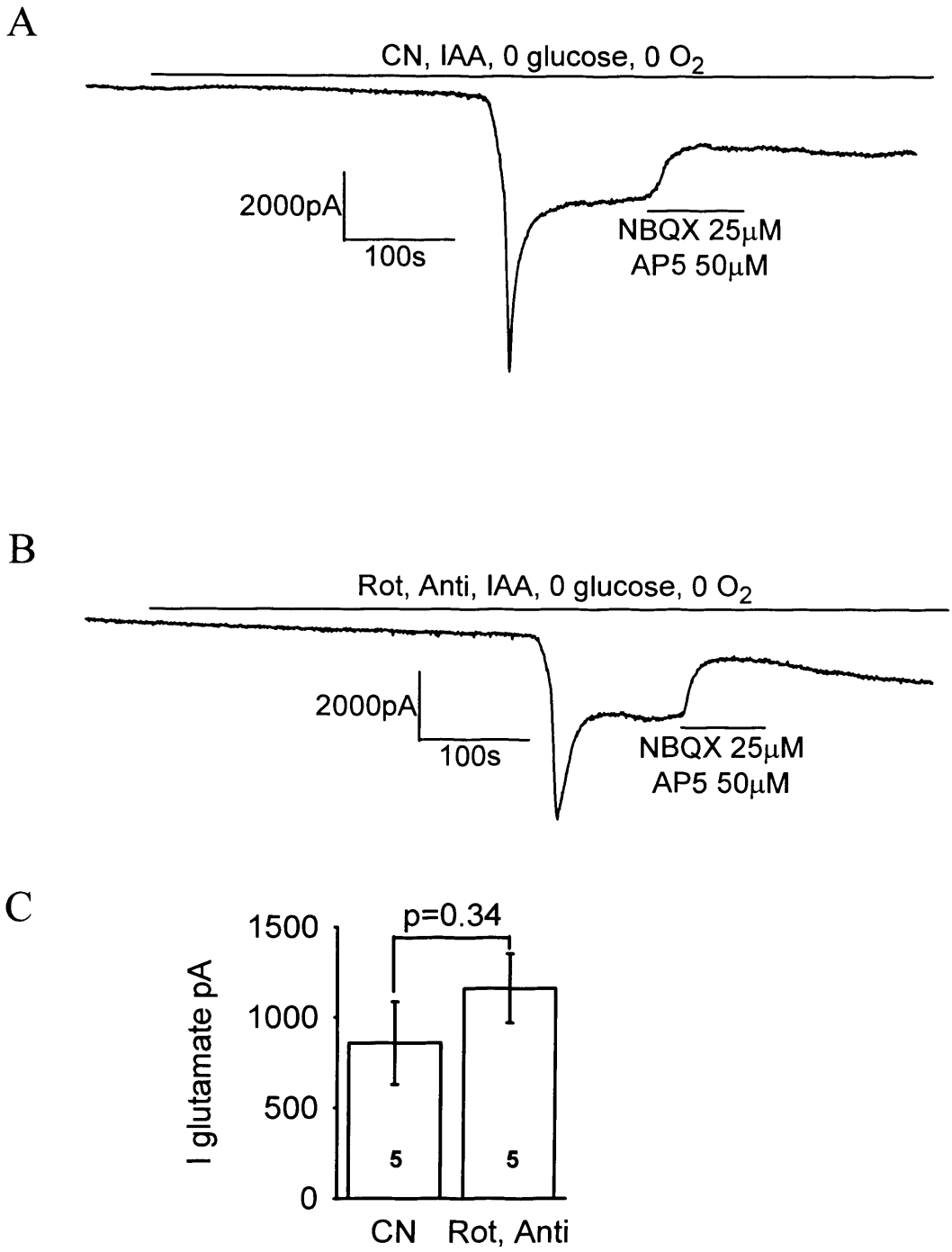

Figure 8.8. Glutamate receptor blockers reveal a similar amplitude of glutamate-mediated post-AD plateau current independent of how oxidative phosphorylation is inhibited. **A** Application of 25μM NBQX (to block AMPA receptors) and 50μM AP5 (to block NMDA receptors) to the post-AD plateau induced by cyanide (to block oxidative phosphorylation) and iodoacetate (to block glycolysis) in oxygen and glucose free solution. **B** Application of NBQX and AP5 to the post-AD plateau current induced by rotenone and antimycin (to block oxidative phosphorylation) and iodoacetate in oxygen and glucose free solution. **C** The amplitude of the glutamate-blockable current was not significantly different between the two methods of blocking oxidative phosphorylation. Bold numbers indicate number of cells studied.

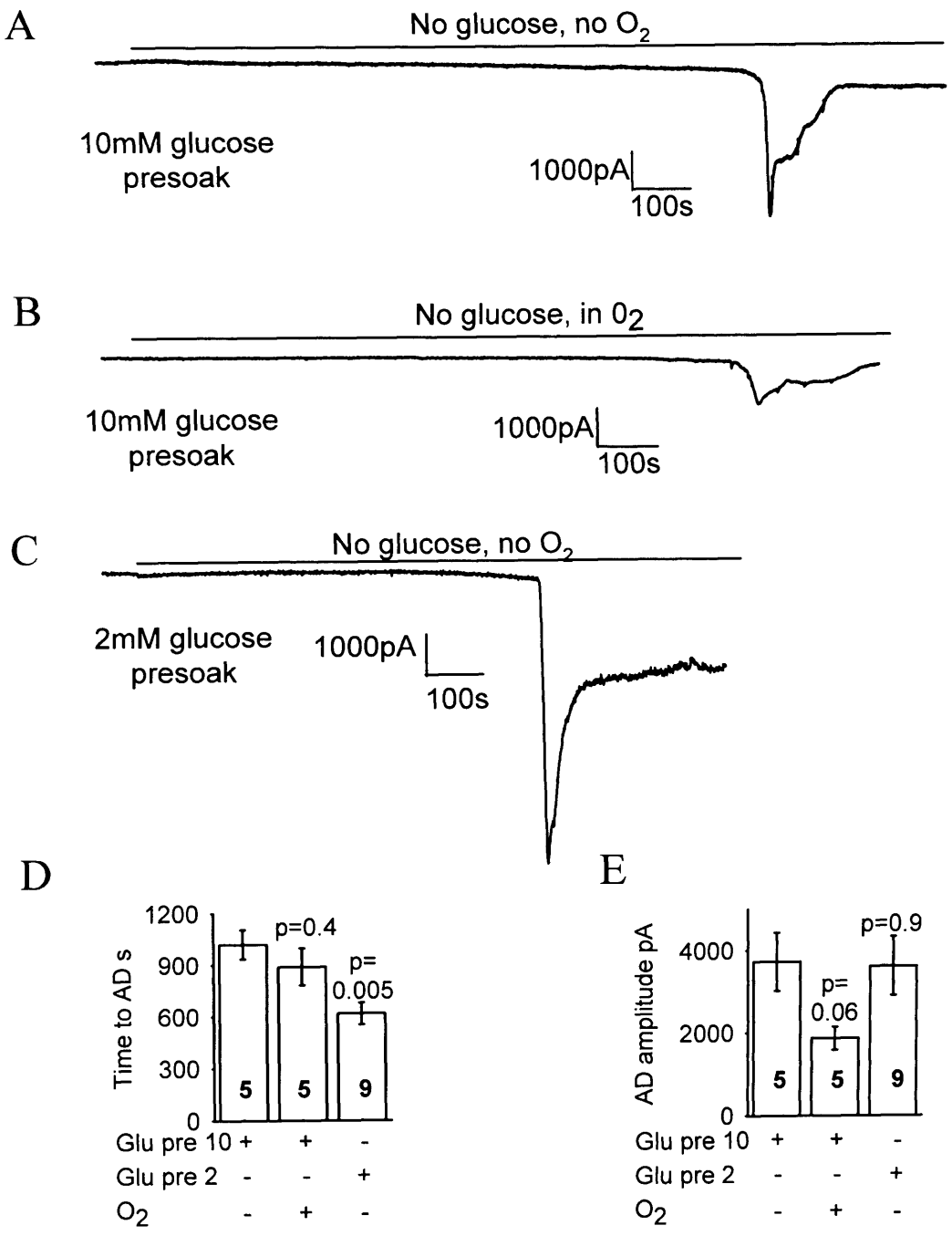

Figure 8.9. Response of CA1 pyramidal cells to oxygen and glucose deprivation without metabolic blockers. **A** Application of oxygen and glucose free solution to a pyramidal cell in a slice that had been presoaked in 10mM glucose induced an AD after ~18 minutes. **B** Applying glucose free solution in the presence of oxygen induced an AD at a time not significantly different from when oxygen was absent. **C** Oxygen and glucose deprivation in a slice that had been presoaked in 2mM glucose solution led to an earlier AD. **D** Mean time to AD. **E** Mean amplitude of the AD current. Bold numbers indicate number of cells studied. P values compare the 2nd and 3rd bars with the 1st bar in **D** and **E**.

Chapter 9

General discussion

In this chapter I will evaluate the findings presented within this thesis. At the end of the preceding results chapters, a detailed discussion has been given of the results obtained, so here I will only briefly review the results, and describe some possible experiments that could take the work further in the future.

9.1 Oligodendrocyte membrane properties and neurotransmitter receptor expression

In this thesis I have presented, for three developmental stages of oligodendrocytes, how their morphology, electrophysiological properties and protein expression change with development (chapter 3). In chapter 4, I showed that oligodendrocytes at all developmental stages express NMDA receptors, contradicting the current dogma, and I showed in chapter 6 that these receptors get activated during ischaemia. Interestingly, the NMDA receptors seem to be mainly expressed in the myelinating processes of the cells, indeed they were found at high density throughout the compact myelin. Notably, I identified that the NMDA receptors expressed by oligodendrocytes have properties that are somewhat different from those expressed in neurons, as they have a low magnesium sensitivity and hence can pass current at the cells' resting potential. The glutamate- and NMDA-evoked current was found to increase with development, possibly because the cell surface area is increasing as well. In addition, white matter astrocytes also responded to NMDA, as they do in the grey matter (Žiak et al., 1998; Schipke et al., 2001).

Oligodendrocytes were also found to express $GABA_A$ receptors and the GABA-evoked current also increased with maturation, possibly due to the increase in surface area with maturation. On the other hand, mature oligodendrocytes were found respond to glycine in only two out of nine cells tested. In addition, mature cells did not show any

current change in response to the neurotransmitters acetylcholine, adenosine, ATP, noradrenaline, dopamine, histamine, serotonin and melatonin. However, even though oligodendrocytes did not show any current change produced by these transmitters, they may express G-coupled receptors for the neurotransmitters, that will raise the calcium concentration in the oligodendrocytes without an effect on the membrane current.

9.1.1 Future experiments

In chapter 4, I showed via immunohistochemistry that the main NMDA receptor subunits expressed in oligodendrocytes are NR1, NR2C and NR3. Even though the co-labelling of NR2 and NR3 showed that these subunits are expressed in close vicinity to each other, it does not mean that the NMDA receptor in oligodendrocytes is a heteromer of NR1/NR2C/ NR3, because the antibody labelling I have performed does not give such resolution. It is would therefore be of great interest to try to immunoprecipitate NR1 and see what subunits are co-immunoprecipitated with it. It would be of great importance to know whether oligodendrocyte NMDA receptors have a different subunit combination to neuronal NMDA receptors. If they do, as is suggested by their low magnesium sensitivity, it might be possible to selectively inhibit the NMDA receptors expressed in oligodendrocytes without having an effect on the neuronal NMDA receptors. This would be beneficial for minimizing the damage caused by glutamate release in many white matter diseases.

The intriguing finding that the oligodendrocyte NMDA receptor is mainly found in the cells' processes and in the myelin, calls for further investigation. First of all, it would be interesting to look at whether these receptors play a role in myelination: they might then be "left-over" in the myelin sheet after myelination. The straightforward way to do this would be to use a co-culture of oligodendrocytes and neurons, which show myelination, and try either to inhibit or to activate the NMDA receptors and quantify the amount of myelin formed.

To identify possible G protein coupled receptor mediated responses to the neurotransmitters acetylcholine, adenosine, ATP, noradrenalin, dopamine, histamine,

serotonin and melatonin, it is desirable to use calcium imaging. This could be achieved by using a ratiometric calcium sensitive dye, like fura 2, in the internal solution.

9.2 Ischaemia of the grey and white matter

In chapter 8, I showed that glycolysis alone can provide neurons with enough ATP to maintain the ion gradient across the membrane and therefore prevent the sudden depolarization and subsequent increase in external glutamate concentration which occurs in ischaemia. Interestingly, during block of glycolysis, exogenous lactate (which should be converted to ATP by oxidative phosphorylation) did not generate enough energy to maintain the cells' ion gradients and prevent the sudden depolarization and consequent increase in extracellular glutamate concentration. In addition, in chapter 8 I demonstrated that using a new combination of metabolic blockers to mimic ischaemia, i.e. using in combination or alone antimycin or rotenone to block oxidative phosphorylation (rather than cyanide which is more commonly used) and iodoacetate to block glycolysis, gave results broadly similar to those seen using cyanide and iodoacetate. I then used this combination of blockers to mimic ischaemia in the white matter.

In chapter 6 I showed that simulated ischaemia generates an inward current in oligodendrocytes at all developmental stages. This inward current was reduced by blocking glutamate receptors, and importantly more current was blocked by blocking NMDA receptors than by blocking AMPA/kainate receptors. In line with my findings, the calcium concentration rises in oligodendrocytes in the adult optic nerve during ischaemia, and this can be prevented by blocking NMDA receptors (Žiak et al., 1998; Micu et al., 2005, online advanced publication). In addition, both in adult (Micu et al., 2005, online advanced publication) and neonatal optic nerve (Salter & Fern, 2005), the processes of the oligodendrocytes and the myelin get damaged in ischaemia, and this is prevented by inhibiting the NMDA receptors expressed in oligodendrocytes. These two other papers therefore provide results which are in complete agreement with my data.

Although in oligodendrocyte precursors the ischaemia-evoked current was almost completely inhibited by blocking glutamate receptors, and a small portion was generated via activation of $GABA_A$ receptors, the same was not true for mature cells. Although, glutamate blockers inhibited about 20% of the ischaemia-evoked current, the mechanism that generates the other 80% of the current remains unclear, as inhibiting GABA receptors had little effect and the current was not generated through activation of either TRP or voltage-gated calcium channels, and it is not generated as a result of action potentials evoked by axonal depolarization as TTX did not have any significant effect on the current.

9.2.1 Future experiments

It would be interesting to investigate the role of different metabolic pathways in delaying glutamate release during ischaemia in the white matter. To test whether glycolysis alone could prevent the generation of the inward current from occurring in oligodendrocytes, just as it did in pyramidal neurons, or if the white matter relies more on oxidative phosphorylation, one could repeat the experiments described for neurons in chapter 8, in which different metabolic blockers were used to detect the role of each pathway in providing the cells with enough energy to maintain their membrane potential during ischaemia and hence preventing the increase in external glutamate concentration.

An important question to be answered is from where, and how, is the glutamate released in white matter ischaemia? There are some reports showing that glutamate can be released via reversed uptake from both axons (Li et al., 1999) and oligodendrocytes (Li et al., 1999; Fern & Möller, 2000). In addition, Wilke et al. (2004) suggest that during white matter ischaemia astrocytes release glutamate through a mechanism dependent on the chloride co-transporter NKCC1, probably due to swelling. It would be possible to further test the mechanism of glutamate release during white matter ischaemia, by voltage-clamping oligodendrocytes or their precursors and using their glutamate receptors to sense the glutamate release, as Rossi et al (2000) did for grey matter ischaemia. One could test whether the glutamate release is via Ca^{2+}-dependent

exocytosis by removing extracellular calcium, assess whether glutamate is released via reversed uptake (Li et al., 1999; Fern & Möller, 2000), by preloading the slice with PDC, an inhibitor for reversed uptake, and investigate the contribution of exocytotic glutamate release from astrocytes by blocking it with furosemide (Parpura et al., 1994) and indomethacin (Bezzi et al., 1998).

To further advance our understanding of white matter ischaemia, it is also necessary to identify what mechanisms other than glutamate release may lay behind the generation of the inward current in mature oligodendrocyte during ischaemia. During ischaemia of the white matter, as in the grey matter, the potassium ion concentration increases in the extracellular space (Shimada et al., 1993; Vorisek & Sykova, 1997), and this could contribute to the inward current in oligodendrocytes as they express inward rectifying potassium channels (Chvatal et al., 1995; Gipson & Bordey, 2002). This could be tested by using a combination of potassium channel blockers applied during the steady state phase of the inward current. Furthermore, as oligodendrocytes express the Na/K/2Cl co-transporter (Plotkin et al., 1997; Chen & Sun, 2005) and the K/Cl exchangers KCC2 and KCC3 (Malek et al., 2003), and these transporters have all been suggested to participate in white matter damage (Malek et al., 2003; Wilke et al., 2004; Chen et al., 2005), it would be straightforward to use specific blockers that are available (like bumetanide and furosemide) to inhibit them and see whether this affects the ischaemia evoked current in mature oligodendrocytes (while using bumetanide it would be necessary have glutamate receptor blockers present, as it might also affect glutamate release from astrocytes during white matter ischaemia: (Wilke et al., 2004)).

9.3 The heterogeneity of the $NG2^+$ cells

In chapter 3 I showed that there exist two subtypes of $NG2^+$ cells, defined by their membrane properties, in the cerebral white matter. In addition, I showed in chapter 3, that 18% of $NG2^+$ cells in the cerebellar white matter do not express the oligodendrocyte lineage marker Olig2, presumably meaning that these 18% of $NG2^+$ cells are not going to become oligodendrocytes. In addition, I showed that white matter

$NG2^+$ cells, that express voltage-gated sodium channels, have TTX sensitive synaptic inputs, both GABAergic and glutamatergic, similar to those found for grey matter $NG2^+$ cells (Bergles et al., 2000; Lin & Bergles, 2004; Lin et al., 2005; Jabs et al., 2005), which must reflect transmitter release driven by axonal action potentials. Furthermore, in chapter 4 I showed that the glutamate response of the different types of $NG2^+$ cell differed significantly, in that $NG2^+$ cells expressing voltage-gated sodium channels have significantly larger glutamate- and NMDA- evoked responses. In contrast, there was no difference in their GABA evoked response (chapter 5). During ischaemia, there was also no difference between the responses of the two subsets of $NG2^+$ cells, either in the size of the ischaemia-evoked current or in the percentage block of that current produced by the glutamate receptor blockers AP5 and NBQX (see chapter 6). This result indicates that both subtypes of $NG2^+$ cells may be equally vulnerable to white matter ischaemia. However, although the synaptic activity in $NG2^+$ cells expressing voltage-gated sodium channels increased in ischaemia, it was independent of action potentials as TTX did not have any effect on the frequency of the currents (chapter 7).

The existence of two classes of $NG2^+$ cell with differing Olig2 expression, and and the difference in voltage-gated channel expression between $NG2^+$ cells, further contribute to the notion that there are two classes of $NG2^+$ cells in the CNS. It has previously been suggested that there is an $NG2^+$ adult oligodendrocyte precursor cell, functioning as a reserve cell to replace damaged mature oligodendrocytes, and that there is also a new type of glial cell that is also $NG2^+$ (Butt et al., 2002). Some oligodendrocyte precursors have been shown to express voltage-gated sodium channels similar to the $NG2^+$ cells that I have recorded from (Sontheimer et al., 1989; Barres et al., 1990c; Berger et al., 1991; Steinhauser et al., 1992; Berger et al., 1992a; Chvatal et al., 1995; Knutson et al., 1997; Žiak et al., 1998; Schools et al., 2003; Chittajallu et al., 2005), and in addition these cells have been shown to increase their migration rate in the presence of NMDA. This might explain why the glutamate-evoked current is larger in cells expressing voltage-gated sodium channels than in the ones that do not express sodium channels. It has been suggested that the "new" type of glial cell (Butt et al., 2002), the $NG2^+$ cell, is non-migratory, does not divide and is present at the Ranvier

nodes perhaps to sense the local environment (Butt et al., 2002; Butt et al., 2005), so this cell might not need to have as high a sensitivity to glutamate as the cells that use glutamate for migratory guidance.

These results might suggest that the voltage-gated sodium channel expressing $NG2^+$ cell that I find is the oligodendrocyte precursor cell, and the more ohmic cell is the "new" type of glia or the synantocyte. Contradicting that, however, is the fact that the ohmic cell is $Olig2^+$ and $NG2^+$, which one would not expect if the synantocyte is not of the oligodendrocyte lineage. In addition, the fact that the $NG2^+$ cell expressing voltage-gated sodium channels receives synaptic input, is not what one might naively expect for oligodendrocytes. To further identify these cells' properties, and to try to understand if there is a clear difference between the $Ng2^+/Olig2^+$ cells and the $NG2^+/Olig2^-$cells, further experiments are needed.

9.3.1 Future experiments

It would be interesting to attempt to identify the differences in the properties of $NG2^+$ cells in the cerebellar white matter. This could be achieved by voltage-clamping $NG2^+$ cells expressing voltage-gated sodium channels, fill them with a dye and do double antibody labelling against Olig2 and NG2, with the aim of determining whether all of these cells express Olig2, none express Olig2, or there are two classes of such cells. Furthermore, it would be desirable to expand the experiments to adult animals, as my results were only obtained in P7-P12 animals. The approach would be, first, to redo the immunohistochemistry labelling of Olig2 and NG2 to identify whether there is the same distribution of $Olig2^+$ $NG2^-$ cells in the white matter in adult brain, and second, to voltage-clamp the $NG2^+$ cells in the adult, record their membrane properties, and simultaneously dye-fill the cells and label them with antibodies against Olig2 and NG2.

It would also be interesting to explore whether the synaptic activity in $NG2^+$ cells is dependent on Purkinje cell activity. A possibility here would be to use a transgenic mouse that has EGFP expressed under the NG2 promoter to label oligodendrocyte lineage cells and then current-clamp a Purkinje cell with a dye in the

pipette, follow its axon and voltage-clamp an $EGFP^+/NG2^+$ cell that comes close to the axon. Inducing a depolarization in the Purkinje cell one would hope to record activity in the $NG2^+$ cell.

I hope to do experiments as suggested in the sections above during my post-doctoral research.

References

Aarts, M., Iihara, K., Wei, W.L., Xiong, Z.G., Arundine, M., Cerwinski, W., MacDonald, J.F., & Tymianski, M. (2003) A key role for TRPM7 channels in anoxic neuronal death. *Cell*, 115(7): 863-877.

Agrawal, S.K. & Fehlings, M.G. (1997) Role of NMDA and non-NMDA ionotropic glutamate receptors in traumatic spinal cord axonal injury. *J. Neurosci.*, 17(3): 1055-1063.

Aguirre, A.A., Chittajallu, R., Belachew, S., & Gallo, V. (2004) NG2-expressing cells in the subventricular zone are type C-like cells and contribute to interneuron generation in the postnatal hippocampus. *J. Cell Biol.*, 165(4): 575-589.

Allen, N.J. & Attwell, D. (2004) The effect of simulated ischaemia on spontaneous GABA release in area CA1 of the juvenile rat hippocampus. *J. Physiol*, 561(Pt 2): 485-498.

Allen, N.J., Karadottir, R., & Attwell, D. (2004a) Reversal or reduction of glutamate and GABA transport in CNS pathology and therapy. *Pflugers Arch.*, 449(2): 132-142.

Allen, N.J., Rossi, D.J., & Attwell, D. (2004b) Sequential release of GABA by exocytosis and reversed uptake leads to neuronal swelling in simulated ischemia of hippocampal slices. *J. Neurosci.*, 24(15): 3837-3849.

Ames, A. (1992) Energy requirements of CNS cells as related to their function and to their vulnerability to ischemia: a commentary based on studies on retina. *Can. J. Physiol Pharmacol.*, 70 Suppl: S158-S164.

Arden, S.R., Sinor, J.D., Potthoff, W.K., & Aizenman, E. (1998) Subunit-specific interactions of cyanide with the N-methyl-D-aspartate receptor. *J. Biol. Chem.*, 273(34): 21505-21511.

Armstrong, R.C., Harvath, L., & Dubois-Dalcq, M.E. (1990) Type 1 astrocytes and oligodendrocyte-type 2 astrocyte glial progenitors migrate toward distinct molecules. *J. Neurosci. Res.*, 27(3): 400-407.

Attwell, D. & Laughlin, S.B. (2001) An energy budget for signaling in the grey matter of the brain. *J. Cereb. Blood Flow Metab*, 21(10): 1133-1145.

Back, S.A., Han, B.H., Luo, N.L., Chricton, C.A., Xanthoudakis, S., Tam, J., Arvin, K.L., & Holtzman, D.M. (2002) Selective vulnerability of late oligodendrocyte progenitors to hypoxia-ischemia. *J. Neurosci.*, 22(2): 455-463.

Baron, W., Colognato, H., & ffrench-Constant, C. (2005) Integrin-growth factor interactions as regulators of oligodendroglial development and function. *Glia*, 49(4): 467-479.

Baron, W., de Jonge, J.C., de, V.H., & Hoekstra, D. (1998) Regulation of oligodendrocyte differentiation: protein kinase C activation prevents differentiation of O2A progenitor cells toward oligodendrocytes. *Glia*, 22(2): 121-129.

Barres, B.A., Burne, J.F., Holtmann, B., Thoenen, H., Sendtner, M., & Raff, M.C. (1996) Ciliary Neurotrophic Factor Enhances the Rate of Oligodendrocyte Generation. *Mol. Cell Neurosci.*, 8(2/3): 146-156.

Barres, B.A., Jacobson, M.D., Schmid, R., Sendtner, M., & Raff, M.C. (1993) Does oligodendrocyte survival depend on axons? *Curr. Biol.*, 3(8): 489-497.

Barres, B.A., Koroshetz, W.J., Chun, L.L., & Corey, D.P. (1990a) Ion channel expression by white matter glia: the type-1 astrocyte. *Neuron*, 5(4): 527-544.

Barres, B.A., Koroshetz, W.J., Swartz, K.J., Chun, L.L., & Corey, D.P. (1990c) Ion channel expression by white matter glia: the O-2A glial progenitor cell. *Neuron*, 4(4): 507-524.

Barres, B.A., Koroshetz, W.J., Swartz, K.J., Chun, L.L., & Corey, D.P. (1990b) Ion channel expression by white matter glia: the O-2A glial progenitor cell. *Neuron*, 4(4): 507-524.

Barres, B.A. & Raff, M.C. (1993) Proliferation of oligodendrocyte precursor cells depends on electrical activity in axons. *Nature*, 361(6409): 258-260.

Barres, B.A. & Raff, M.C. (1999) Axonal control of oligodendrocyte development. *J. Cell Biol.*, 147(6): 1123-1128.

Barres, B.A. & Raff, M.C. (1994) Control of oligodendrocyte number in the developing rat optic nerve. *Neuron*, 12(5): 935-942.

Baulac, M., Lachapelle, F., Gout, O., Berger, B., Baumann, N., & Gumpel, M. (1987) Transplantation of oligodendrocytes in the newborn mouse brain: extension of myelination by transplanted cells. Anatomical study. *Brain Res.*, 420(1): 39-47.

Baumann, N. & Pham-Dinh, D. (2001) Biology of oligodendrocyte and myelin in the mammalian central nervous system. *Physiol Rev.*, 81(2): 871-927.

Beattie, M.S., Hermann, G.E., Rogers, R.C., & Bresnahan, J.C. (2002) Cell death in models of spinal cord injury. *Prog. Brain Res.*, 137: 37-47.

Belachew, S., Chittajallu, R., Aguirre, A.A., Yuan, X., Kirby, M., Anderson, S., & Gallo, V. (2003) Postnatal NG2 proteoglycan-expressing progenitor cells are intrinsically multipotent and generate functional neurons. *J. Cell Biol.*, 161(1): 169-186.

Belachew, S., Malgrange, B., Rigo, J.M., Rogister, B., Coucke, P., Mazy-Servais, C., & Moonen, G. (1998a) Developmental regulation of neuroligand-induced responses in cultured oligodendroglia. *Neuroreport*, 9(6): 973-980.

Belachew, S., Malgrange, B., Rigo, J.M., Rogister, B., Leprince, P., Hans, G., Nguyen, L., & Moonen, G. (2000) Glycine triggers an intracellular calcium influx in oligodendrocyte progenitor cells which is mediated by the activation of both the

ionotropic glycine receptor and Na+-dependent transporters. *Eur. J. Neurosci.*, 12(6): 1924-1930.

Belachew, S., Rogister, B., Rigo, J.M., Malgrange, B., Mazy-Servais, C., Xhauflaire, G., Coucke, P., & Moonen, G. (1998b) Cultured oligodendrocyte progenitors derived from cerebral cortex express a glycine receptor which is pharmacologically distinct from the neuronal isoform. *Eur. J. Neurosci.*, 10(11): 3556-3564.

Benveniste, M. & Mayer, M.L. (1991) Kinetic analysis of antagonist action at N-methyl-D-aspartic acid receptors. Two binding sites each for glutamate and glycine. *Biophys. J.*, 59(3): 560-573.

Berger, T., Schnitzer, J., & Kettenmann, H. (1991) Developmental changes in the membrane current pattern, K+ buffer capacity, and morphology of glial cells in the corpus callosum slice. *J. Neurosci.*, 11(10): 3008-3024.

Berger, T., Schnitzer, J., Orkand, P.M., & Kettenmann, H. (1992a) Sodium and Calcium Currents in Glial Cells of the Mouse Corpus Callosum Slice. *Eur. J. Neurosci.*, 4(12): 1271-1284.

Berger, T., Walz, W., Schnitzer, J., & Kettenmann, H. (1992b) *J. Neurosci. Res.*, 31(1): 21-27.

Berger, T., Walz, W., Schnitzer, J., & Kettenmann, H. (1992c) GABA- and glutamate-activated currents in glial cells of the mouse corpus callosum slice. *J. Neurosci. Res.*, 31(1): 21-27.

Berger, T., Walz, W., Schnitzer, J., & Kettenmann, H. (1992d) *J. Neurosci. Res.*, 31(1): 21-27.

Bergles, D.E., Roberts, J.D., Somogyi, P., & Jahr, C.E. (2000) Glutamatergic synapses on oligodendrocyte precursor cells in the hippocampus. *Nature*, 405(6783): 187-191.

Bernard, F., Bossu, J.L., & Gaillard, S. (2001) Identification of living oligodendrocyte developmental stages by fractal analysis of cell morphology. *J. Neurosci. Res.*, 65(5): 439-445.

Bernstein, M., Lyons, S.A., Moller, T., & Kettenmann, H. (1996) Receptor-mediated calcium signalling in glial cells from mouse corpus callosum slices. *J. Neurosci. Res.*, 46(2): 152-163.

Berry, M., Hubbard, P., & Butt, A.M. (2002) Cytology and lineage of NG2-positive glia. *J. Neurocytol.*, 31(6-7): 457-467.

Berry, M., Ibrahim, M., Carlile, J., Ruge, F., Duncan, A., & Butt, A.M. (1995) Axon-glial relationships in the anterior medullary velum of the adult rat. *J. Neurocytol.*, 24(12): 965-983.

Bezzi, P., Carmignoto, G., Pasti, L., Vesce, S., Rossi, D., Rizzini, B.L., Pozzan, T., & Volterra, A. (1998) Prostaglandins stimulate calcium-dependent glutamate release in astrocytes. *Nature*, 391(6664): 281-285.

Bezzi, P., Gundersen, V., Galbete, J.L., Seifert, G., Steinhauser, C., Pilati, E., & Volterra, A. (2004) Astrocytes contain a vesicular compartment that is competent for regulated exocytosis of glutamate. *Nat. Neurosci.*, 7(6): 613-620.

Blumenfeld, H. (2002) Cerebellum. *Neuroanatomy Through Clinical Cases*: 653-688. Sunderland, Mass: Sinauer Associates.

Bongarzone, E.R., Howard, S.G., Schonmann, V., & Campagnoni, A.T. (1998) Identification of the dopamine D3 receptor in oligodendrocyte precursors: potential role in regulating differentiation and myelin formation. *J. Neurosci.*, 18(14): 5344-5353.

Borden, L.A. (1996) GABA transporter heterogeneity: pharmacology and cellular localization. *Neurochem. Int.*, 29(4): 335-356.

Borges, K. & Kettenmann, H. (1995) Blockade of K+ channels induced by AMPA/kainate receptor activation in mouse oligodendrocyte precursor cells is mediated by Na+ entry. *J. Neurosci. Res.*, 42(4): 579-593.

Borges, K., Ohlemeyer, C., Trotter, J., & Kettenmann, H. (1994) AMPA/kainate receptor activation in murine oligodendrocyte precursor cells leads to activation of a cation conductance, calcium influx and blockade of delayed rectifying K+ channels. *Neuroscience*, 63(1): 135-149.

Borges, K., Wolswijk, G., Ohlemeyer, C., & Kettenmann, H. (1995) Adult rat optic nerve oligodendrocyte progenitor cells express a distinct repertoire of voltage- and ligand-gated ion channels. *J. Neurosci. Res.*, 40(5): 591-605.

Boue-Grabot, E., Roudbaraki, M., Bascles, L., Tramu, G., Bloch, B., & Garret, M. (1998) Expression of GABA receptor rho subunits in rat brain. *J. Neurochem.*, 70(3): 899-907.

Bozzali, M. & Wrabetz, L. (2004) Axonal Signals and Oligodendrocyte Differentiation. *Neurochemical Research*, 29(5): 979-988.

Brown, A.M. (2004) Brain glycogen re-awakened. *J. Neurochem.*, 89(3): 537-552.

Brown, A.M., Tekkok, S.B., & Ransom, B.R. (2003) Glycogen regulation and functional role in mouse white matter. *J. Physiol*, 549(Pt 2): 501-512.

Bunge, R.P. (1968) Glial cells and the central myelin sheath. *Physiol Rev.*, 48(1): 197-251.

Butt, A.M., Duncan, A., & Berry, M. (1994) Astrocyte associations with nodes of Ranvier: ultrastructural analysis of HRP-filled astrocytes in the mouse optic nerve. *J. Neurocytol.*, 23(8): 486-499.

Butt, A.M., Duncan, A., Hornby, M.F., Kirvell, S.L., Hunter, A., Levine, J.M., & Berry, M. (1999) Cells expressing the NG2 antigen contact nodes of Ranvier in adult CNS white matter. *Glia*, 26(1): 84-91.

Butt, A.M., Hamilton, N., Hubbard, P., Pugh, M., & Ibrahim, M. (2005) Synantocytes: the fifth element. *J. Anat.*, 207(6): 695-706.

Butt, A.M., Hornby, M.F., Ibrahim, M., Kirvell, S., Graham, A., & Berry, M. (1997a) PDGF-alpha receptor and myelin basic protein mRNAs are not coexpressed by oligodendrocytes in vivo: a double in situ hybridization study in the anterior medullary velum of the neonatal rat. *Mol. Cell Neurosci.*, 8(5): 311-322.

Butt, A.M., Hornby, M.F., Kirvell, S., & Berry, M. (1997b) Platelet-derived growth factor delays oligodendrocyte differentiation and axonal myelination in vivo in the anterior medullary velum of the developing rat. *J. Neurosci. Res.*, 48(6): 588-596.

Butt, A.M., Ibrahim, M., Ruge, F.M., & Berry, M. (1995) Biochemical subtypes of oligodendrocyte in the anterior medullary velum of the rat as revealed by the monoclonal antibody Rip. *Glia*, 14(3): 185-197.

Butt, A.M., Kiff, J., Hubbard, P., & Berry, M. (2002) Synantocytes: new functions for novel NG2 expressing glia. *J. Neurocytol.*, 31(6-7): 551-565.

Butt, A.M., Pugh, M., Hubbard, P., & James, G. (2004) Functions of optic nerve glia: axoglial signalling in physiology and pathology. *Eye*, 18(11): 1110-1121.

Butt, A.M. & Ransom, B.R. (1989) Visualization of oligodendrocytes and astrocytes in the intact rat optic nerve by intracellular injection of lucifer yellow and horseradish peroxidase. *Glia*, 2(6): 470-475.

Butt, A.M. & Tutton, M. (1992) Response of oligodendrocytes to glutamate and gamma-aminobutyric acid in the intact mouse optic nerve. *Neurosci. Lett.*, 146(1): 108-110.

Cai, J., Qi, Y., Hu, X., Tan, M., Liu, Z., Zhang, J., Li, Q., Sander, M., & Qiu, M. (2005) Generation of oligodendrocyte precursor cells from mouse dorsal spinal cord independent of Nkx6 regulation and Shh signaling. *Neuron*, 45(1): 41-53.

Cambray-Deakin, M., Pearce, B., Morrow, C., & Murphy, S. (1988) Effects of neurotransmitters on astrocyte glycogen stores in vitro. *J. Neurochem.*, 51(6): 1852-1857.

Cenci Di Bello, I., Dawson, M.R., Levine, J.M., & Reynolds, R. (1999) Generation of oligodendroglial progenitors in acute inflammatory demyelinating lesions of the rat brain stem is associated with demyelination rather than inflammation. *J. Neurocytol.*, 28(4-5): 365-381.

Centonze, D., Saulle, E., Pisani, A., Bernardi, G., & Calabresi, P. (2001) Adenosine-mediated inhibition of striatal GABAergic synaptic transmission during in vitro ischaemia. *Brain*, 124(Pt 9): 1855-1865.

Chatterton, J.E., Awobuluyi, M., Premkumar, L.S., Takahashi, H., Talantova, M., Shin, Y., Cui, J., Tu, S., Sevarino, K.A., Nakanishi, N., Tong, G., Lipton, S.A., & Zhang, D. (2002) Excitatory glycine receptors containing the NR3 family of NMDA receptor subunits. *Nature*, 415(6873): 793-798.

Chen, H., Luo, J., Kintner, D.B., Shull, G.E., & Sun, D. (2005) Na(+)-dependent chloride transporter (NKCC1)-null mice exhibit less gray and white matter damage after focal cerebral ischemia. *J. Cereb. Blood Flow Metab*, 25(1): 54-66.

Chen, H. & Sun, D. (2005) The role of Na-K-Cl co-transporter in cerebral ischemia. *Neurol. Res.*, 27(3): 280-286.

Chen, Z.J., Negra, M., Levine, A., Ughrin, Y., & Levine, J.M. (2002) Oligodendrocyte precursor cells: reactive cells that inhibit axon growth and regeneration. *J. Neurocytol.*, 31(6-7): 481-495.

Chew, L.J., Fleck, M.W., Wright, P., Scherer, S.E., Mayer, M.L., & Gallo, V. (1997) Growth factor-induced transcription of GluR1 increases functional AMPA receptor density in glial progenitor cells. *J. Neurosci.*, 17(1): 227-240.

Chih, C.P., He, J., Sly, T.S., & Roberts, E.L., Jr. (2001a) Comparison of glucose and lactate as substrates during NMDA-induced activation of hippocampal slices. *Brain Res.*, 893(1-2): 143-154.

Chih, C.P., Lipton, P., & Roberts, E.L., Jr. (2001b) Do active cerebral neurons really use lactate rather than glucose? *Trends Neurosci.*, 24(10): 573-578.

Chittajallu, R., Aguirre, A., & Gallo, V. (2004) NG2-positive cells in the mouse white and grey matter display distinct physiological properties. *J. Physiol*, 561(Pt 1): 109-122.

Chittajallu, R., Aguirre, A.A., & Gallo, V. (2005) Downregulation of platelet-derived growth factor-alpha receptor-mediated tyrosine kinase activity as a cellular mechanism for K+-channel regulation during oligodendrocyte development in situ. *J. Neurosci.*, 25(38): 8601-8610.

Chiu, S.Y. & Kriegler, S. (1994) Neurotransmitter-mediated signaling between axons and glial cells. *Glia*, 11(2): 191-200.

Choi, D.W. (1988) Glutamate neurotoxicity and diseases of the nervous system. *Neuron*, 1(8): 623-634.

Choi, D.W., Maulucci-Gedde, M., & Kriegstein, A.R. (1987) Glutamate neurotoxicity in cortical cell culture. *J. Neurosci.*, 7(2): 357-368.

Chvatal, A., Pastor, A., Mauch, M., Sykova, E., & Kettenmann, H. (1995) Distinct populations of identified glial cells in the developing rat spinal cord slice: ion channel properties and cell morphology. *Eur. J. Neurosci.*, 7(1): 129-142.

Clapham, D.E., Runnels, L.W., & Strubing, C. (2001) The TRP ion channel family. *Nat. Rev. Neurosci.*, 2(6): 387-396.

Clark, J.B., Bates, T.E., Cullingford, T., & Land, J.M. (1993) Development of enzymes of energy metabolism in the neonatal mammalian brain. *Dev. Neurosci.*, 15(3-5): 174-180.

Coetzee, W.A., Amarillo, Y., Chiu, J., Chow, A., Lau, D., McCormack, T., Moreno, H., Nadal, M.S., Ozaita, A., Pountney, D., Saganich, M., Vega-Saenz de, M.E., & Rudy, B. (1999) Molecular diversity of K+ channels. *Ann. N. Y. Acad. Sci.*, 868: 233-285.

Colello, R.J., Devey, L.R., Imperato, E., & Pott, U. (1995) The chronology of oligodendrocyte differentiation in the rat optic nerve: evidence for a signaling step initiating myelination in the CNS. *J. Neurosci.*, 15(11): 7665-7672.

Coley, B.D. & Hogan, M.J. (1997) Cystic periventricular leukomalacia of the corpus callosum. *Pediatr. Radiol.*, 27(7): 583-585.

Collingridge, G.L. & Bliss, T.V. (1995) Memories of NMDA receptors and LTP. *Trends Neurosci.*, 18(2): 54-56.

Connors, B.W., Ransom, B.R., Kunis, D.M., & Gutnick, M.J. (1982) Activity-dependent K+ accumulation in the developing rat optic nerve. *Science*, 216(4552): 1341-1343.

Cotrina, M.L., Kang, J., Lin, J.H.C., Bueno, E., Hansen, T.W., He, L., Liu, Y., & Nedergaard, M. (1998) Astrocytic Gap Junctions Remain Open during Ischemic Conditions. *J. Neurosci.*, 18(7): 2520-2537.

Cull-Candy, S.G. & Leszkiewicz, D.N. (2004) Role of distinct NMDA receptor subtypes at central synapses. *Sci. STKE.*, 2004(255): re16.

Dagani, F. & Erecinska, M. (1987) Relationships among ATP synthesis, K+ gradients, and neurotransmitter amino acid levels in isolated rat brain synaptosomes. *J. Neurochem.*, 49(4): 1229-1240.

Dai, X., Lercher, L.D., Clinton, P.M., Du, Y., Livingston, D.L., Vieira, C., Yang, L., Shen, M.M., & Dreyfus, C.F. (2003) The trophic role of oligodendrocytes in the basal forebrain. *J. Neurosci.*, 23(13): 5846-5853.

Dan, Y., Song, H.J., & Poo, M.M. (1994) Evoked neuronal secretion of false transmitters. *Neuron*, 13(4): 909-917.

Davis, K.L., Stewart, D.G., Friedman, J.I., Buchsbaum, M., Harvey, P.D., Hof, P.R., Buxbaum, J., & Haroutunian, V. (2003) White matter changes in schizophrenia: evidence for myelin-related dysfunction. *Arch. Gen. Psychiatry*, 60(5): 443-456.

Dawson, M.R., Levine, J.M., & Reynolds, R. (2000) NG2-expressing cells in the central nervous system: are they oligodendroglial progenitors? *J. Neurosci. Res.*, 61(5): 471-479.

Dawson, M.R., Polito, A., Levine, J.M., & Reynolds, R. (2003) NG2-expressing glial progenitor cells: an abundant and widespread population of cycling cells in the adult rat CNS. *Mol. Cell Neurosci.*, 24(2): 476-488.

Dayer, A.G., Cleaver, K.M., Abouantoun, T., & Cameron, H.A. (2005) New GABAergic interneurons in the adult neocortex and striatum are generated from different precursors. *J. Cell Biol.*, 168(3): 415-427.

Delhumeau, G., Cruz-Mendoza, A.M., & Gomez, L.C. (1994) Protection of cytochrome c oxidase against cyanide inhibition by pyruvate and alpha-ketoglutarate: effect of aeration in vitro. *Toxicol. Appl. Pharmacol.*, 126(2): 345-351.

Delpire, E. (2000) Cation-Chloride Cotransporters in Neuronal Communication. *News Physiol Sci.*, 15: 309-312.

Demerens, C., Stankoff, B., Logak, M., Anglade, P., Allinquant, B., Couraud, F., Zalc, B., & Lubetzki, C. (1996) Induction of myelination in the central nervous system by electrical activity. *Proc. Natl. Acad. Sci. U. S. A*, 93(18): 9887-9892.

Deng, W., Rosenberg, P.A., Volpe, J.J., & Jensen, F.E. (2003) Calcium-permeable AMPA/kainate receptors mediate toxicity and preconditioning by oxygen-glucose deprivation in oligodendrocyte precursors. *Proc. Natl. Acad. Sci. U. S. A*, 100(11): 6801-6806.

Dépre, C., Rider, M.H., & Hue, L. (1998) Mechanisms of control of heart glycolysis. *Eur. J. Biochem.*, 258(2): 277-290.

Dewar, D., Underhill, S.M., & Goldberg, M.P. (2003) Oligodendrocytes and ischemic brain injury. *J. Cereb. Blood Flow Metab*, 23(3): 263-274.

Diamond, J.S. & Jahr, C.E. (1997) Transporters buffer synaptically released glutamate on a submillisecond time scale. *J. Neurosci.*, 17(12): 4672-4687.

Diers-Fenger, M., Kirchhoff, F., Kettenmann, H., Levine, J.M., & Trotter, J. (2001) AN2/NG2 protein-expressing glial progenitor cells in the murine CNS: isolation, differentiation, and association with radial glia. *Glia*, 34(3): 213-228.

Dingledine, R., Borges, K., Bowie, D., & Traynelis, S.F. (1999) The glutamate receptor ion channels. *Pharmacol. Rev.*, 51(1): 7-61.

Dolmetsch, R.E., Xu, K., & Lewis, R.S. (1998) Calcium oscillations increase the efficiency and specificity of gene expression. *Nature*, 392(6679): 933-936.

Drewes, L.R. & Gilboe, D.D. (1973) Glycolysis and the permeation of glucose and lactate in the isolated, perfused dog brain during anoxia and postanoxic recovery. *J. Biol. Chem.*, 248(7): 2489-2496.

Dringen, R., Gebhardt, R., & Hamprecht, B. (1993) Glycogen in astrocytes: possible function as lactate supply for neighboring cells. *Brain Res.*, 623(2): 208-214.

Edwards, F.A., Konnerth, A., Sakmann, B., & Takahashi, T. (1989) A thin slice preparation for patch clamp recordings from neurones of the mammalian central nervous system. *Pflugers Arch.*, 414(5): 600-612.

Eisenbarth, G.S., Walsh, F.S., & Nirenberg, M. (1979) Monoclonal antibody to a plasma membrane antigen of neurons. *Proc. Natl. Acad. Sci. U. S. A*, 76(10): 4913-4917.

Erecinska, M. & Silver, I.A. (1994) Ions and energy in mammalian brain. *Prog. Neurobiol.*, 43(1): 37-71.

Fatima-Shad, K. & Barry, P.H. (1993) Anion permeation in. *Proc. Biol. Sci.*, 253(1336): 69-75.

Fedrizzi, E., Inverno, M., Bruzzone, M.G., Botteon, G., Saletti, V., & Farinotti, M. (1996) MRI features of cerebral lesions and cognitive functions in preterm spastic diplegic children. *Pediatr. Neurol.*, 15(3): 207-212.

Fellows, L.K., Boutelle, M.G., & Fillenz, M. (1992) Extracellular brain glucose levels reflect local neuronal activity: a microdialysis study in awake, freely moving rats. *J. Neurochem.*, 59(6): 2141-2147.

Fenwick, E.M., Marty, A., & Neher, E. (1982) A patch-clamp study of bovine chromaffin cells and of their sensitivity to acetylcholine. *J. Physiol*, 331: 577-597.

Fern, R. & Möller, T. (2000) Rapid ischemic cell death in immature oligodendrocytes: a fatal glutamate release feedback loop. *J. Neurosci.*, 20(1): 34-42.

Fern, R., Ransom, B.R., & Waxman, S.G. (1995a) Voltage-gated calcium channels in CNS white matter: role in anoxic injury. *J. Neurophysiol.*, 74(1): 369-377.

Fern, R., Waxman, S.G., & Ransom, B.R. (1995b) Endogenous GABA attenuates CNS white matter dysfunction following anoxia. *J. Neurosci.*, 15(1 Pt 2): 699-708.

Ferreira, I.L., Duarte, C.B., & Carvalho, A.P. (1997) 'Chemical ischemia' in cultured retina cells: the role of excitatory amino acid receptors and of energy levels on cell death. *Brain Res.*, 768(1-2): 157-166.

Fiala, J.C., Kirov, S.A., Feinberg, M.D., Petrak, L.J., George, P., Goddard, C.A., & Harris, K.M. (2003) Timing of neuronal and glial ultrastructure disruption during brain slice preparation and recovery in vitro. *J. Comp Neurol.*, 465(1): 90-103.

Fleidervish, I.A., Gebhardt, C., Astman, N., Gutnick, M.J., & Heinemann, U. (2001) Enhanced spontaneous transmitter release is the earliest consequence of neocortical hypoxia that can explain the disruption of normal circuit function. *J. Neurosci.*, 21(13): 4600-4608.

Fogarty, M., Richardson, W.D., & Kessaris, N. (2005) A subset of oligodendrocytes generated from radial glia in the dorsal spinal cord. *Development*, 132(8): 1951-1959.

Folbergrova, J., Li, P.A., Uchino, H., Smith, M.L., & Siesjo, B.K. (1997) Changes in the bioenergetic state of rat hippocampus during 2.5 min of ischemia, and prevention of cell damage by cyclosporin A in hyperglycemic subjects. *Exp. Brain Res.*, 114(1): 44-50.

Follett, P.L., Rosenberg, P.A., Volpe, J.J., & Jensen, F.E. (2000) NBQX attenuates excitotoxic injury in developing white matter. *J. Neurosci.*, 20(24): 9235-9241.

Foster, R.E., Connors, B.W., & Waxman, S.G. (1982) Rat optic nerve: electrophysiological, pharmacological and anatomical studies during development. *Brain Res.*, 255(3): 371-386.

Fowler, J.C. (1990) Adenosine antagonists alter the synaptic response to in vitro ischemia in the rat hippocampus. *Brain Res.*, 509(2): 331-334.

Fowler, J.C. (1992) Escape from inhibition of synaptic transmission during in vitro hypoxia and hypoglycemia in the hippocampus. *Brain Res.*, 573(1): 169-173.

Friedman, S. & Shatz, C.J. (1990) The Effects of Prenatal Intracranial Infusion of Tetrodotoxin on Naturally Occurring Retinal Ganglion Cell Death and Optic Nerve Ultrastructure. *Eur. J. Neurosci.*, 2(3): 243-253.

Fujimoto, M., Munakata, M., & Akaike, N. (1995) Dual mechanisms of GABAA response inhibition by beta-lactam antibiotics in the pyramidal neurones of the rat cerebral cortex. *Br. J. Pharmacol.*, 116(7): 3014-3020.

Fujiwara, N., Higashi, H., Shimoji, K., & Yoshimura, M. (1987) Effects of hypoxia on rat hippocampal neurones in vitro. *J. Physiol*, 384: 131-151.

Gallo, V., Patneau, D.K., Mayer, M.L., & Vaccarino, F.M. (1994) Excitatory amino acid receptors in glial progenitor cells: molecular and functional properties. *Glia*, 11(2): 94-101.

Gallo, V., Zhou, J.M., McBain, C.J., Wright, P., Knutson, P.L., & Armstrong, R.C. (1996) Oligodendrocyte progenitor cell proliferation and lineage progression are regulated by glutamate receptor-mediated K+ channel block. *J. Neurosci.*, 16(8): 2659-2670.

Garcia-Barcina, J.M. & Matute, C. (1998) AMPA-selective glutamate receptor subunits in glial cells of the adult bovine white matter. *Brain Res. Mol. Brain Res.*, 53(1-2): 270-276.

Garcia-Barcina, J.M. & Matute, C. (1996) Expression of kainate-selective glutamate receptor subunits in glial cells of the adult bovine white matter. *Eur. J. Neurosci.*, 8(11): 2379-2387.

Gebhardt, C., Korner, R., & Heinemann, U. (2002) Delayed anoxic depolarizations in hippocampal neurons of mice lacking the excitatory amino acid carrier 1. *J. Cereb. Blood Flow Metab*, 22(5): 569-575.

Gill, R., Foster, A.C., & Woodruff, G.N. (1988) MK-801 is neuroprotective in gerbils when administered during the post-ischaemic period. *Neuroscience*, 25(3): 847-855.

Gipson, K. & Bordey, A. (2002) Analysis of the K+ current profile of mature rat oligodendrocytes in situ. *J. Membr. Biol.*, 189(3): 201-212.

Goddard, D.R., Berry, M., Kirvell, S.L., & Butt, A.M. (2002) Fibroblast growth factor-2 induces astroglial and microglial reactivity in vivo. *J. Anat.*, 200(Pt 1): 57-67.

Goddard, D.R., Berry, M., Kirvell, S.L., & Butt, A.M. (2001) Fibroblast growth factor-2 inhibits myelin production by oligodendrocytes in vivo. *Mol. Cell Neurosci.*, 18(5): 557-569.

Goldberg, M.P. & Ransom, B.R. (2003) New light on white matter. *Stroke*, 34(2): 330-332.

Gonchar, Y.A., Johnson, P.B., & Weinberg, R.J. (1995) GABA-immunopositive neurons in rat neocortex with contralateral projections to S-I. *Brain Res.*, 697(1-2): 27-34.

Greenwood, K. & Butt, A.M. (2003) Evidence that perinatal and adult NG2-glia are not conventional oligodendrocyte progenitors and do not depend on axons for their survival. *Mol. Cell Neurosci.*, 23(4): 544-558.

Gregori, N., Proschel, C., Noble, M., & Mayer-Proschel, M. (2002) The tripotential glial-restricted precursor (GRP) cell and glial development in the spinal cord:

generation of bipotential oligodendrocyte-type-2 astrocyte progenitor cells and dorsal-ventral differences in GRP cell function. *J. Neurosci.*, 22(1): 248-256.

Groom, A.J., Smith, T., & Turski, L. (2003) Multiple sclerosis and glutamate. *Ann. N. Y. Acad. Sci.*, 993: 229-275.

Gruetter, R. (2003a) Glycogen: the forgotten cerebral energy store. *J. Neurosci. Res.*, 74(2): 179-183.

Gruetter, R. (2003b) Glycogen: the forgotten cerebral energy store. *J. Neurosci. Res.*, 74(2): 179-183.

Gu, X. & Spitzer, N.C. (1995) Distinct aspects of neuronal differentiation encoded by frequency of spontaneous Ca2+ transients. *Nature*, 375(6534): 784-787.

Hamann, M., Rossi, D.J., Marie, H., & Attwell, D. (2002) Knocking out the glial glutamate transporter GLT-1 reduces glutamate uptake but does not affect hippocampal glutamate dynamics in early simulated ischaemia. *Eur. J. Neurosci.*, 15(2): 308-314.

Hamano, K., Takeya, T., Iwasaki, N., Nakayama, J., Ohto, T., & Okada, Y. (1998) A quantitative study of the progress of myelination in the rat central nervous system, using the immunohistochemical method for proteolipid protein. *Brain Res. Dev. Brain Res.*, 108(1-2): 287-293.

Hamill, O.P., Marty, A., Neher, E., Sakmann, B., & Sigworth, F.J. (1981) Improved patch-clamp techniques for high-resolution current recording from cells and cell-free membrane patches. *Pflugers Arch.*, 391(2): 85-100.

Hammarstrom, A.K. & Gage, P.W. (2000) Oxygen-sensing persistent sodium channels in rat hippocampus. *J. Physiol*, 529 Pt 1: 107-118.

Hansen, A.J. (1985) Effect of anoxia on ion distribution in the brain. *Physiol Rev.*, 65(1): 101-148.

He, W., Ingraham, C., Rising, L., Goderie, S., & Temple, S. (2001) Multipotent stem cells from the mouse basal forebrain contribute GABAergic neurons and oligodendrocytes to the cerebral cortex during embryogenesis. *J. Neurosci.*, 21(22): 8854-8862.

Herlenius, E. & Lagercrantz, H. (2004) Development of neurotransmitter systems during critical periods. *Exp. Neurol.*, 190 Suppl 1: S8-21.

Herrera, J., Yang, H., Zhang, S.C., Proschel, C., Tresco, P., Duncan, I.D., Luskin, M., & Mayer-Proschel, M. (2001) Embryonic-derived glial-restricted precursor cells (GRP cells) can differentiate into astrocytes and oligodendrocytes in vivo. *Exp. Neurol.*, 171(1): 11-21.

Hershkowitz, N., Katchman, A.N., & Veregge, S. (1993) Site of synaptic depression during hypoxia: a patch-clamp analysis. *J. Neurophysiol.*, 69(2): 432-441.

Hille, B. (2001) *Ion channels of excitable membranes*. Sunderland, Mass: Sinauer.

Holtzclaw, L.A., Gallo, V., & Russell, J.T. (1995) AMPA receptors shape Ca2+ responses in cortical oligodendrocyte progenitors and CG-4 cells. *J. Neurosci. Res.*, 42(1): 124-130.

Howd, A.G., Rattray, M., & Butt, A.M. (1997) Expression of GABA transporter mRNAs in the developing and adult rat optic nerve. *Neurosci. Lett.*, 235(1-2): 98-100.

Huang, J.K., Phillips, G.R., Roth, A.D., Pedraza, L., Shan, W., Belkaid, W., Mi, S., Fex-Svenningsen, A., Florens, L., Yates, J.R., III, & Colman, D.R. (2005) Glial membranes at the node of Ranvier prevent neurite outgrowth. *Science*, 310(5755): 1813-1817.

Hughes, S. & Chan-Ling, T. (2004) Characterization of smooth muscle cell and pericyte differentiation in the rat retina in vivo. *Invest Ophthalmol. Vis. Sci.*, 45(8): 2795-2806.

Husson, I., Mesples, B., Bac, P., Vamecq, J., Evrard, P., & Gressens, P. (2002) Melatoninergic neuroprotection of the murine periventricular white matter against neonatal excitotoxic challenge. *Ann. Neurol.*, 51(1): 82-92.

Hynd, M.R., Scott, H.L., & Dodd, P.R. (2004) Glutamate-mediated excitotoxicity and neurodegeneration in Alzheimer's disease. *Neurochem. Int.*, 45(5): 583-595.

Ignacio, P.C., Baldwin, B.A., Vijayan, V.K., Tait, R.C., & Gorin, F.A. (1990) Brain isozyme of glycogen phosphorylase: immunohistological localization within the central nervous system. *Brain Res.*, 529(1-2): 42-49.

Ikemoto, A., Bole, D.G., & Ueda, T. (2003) Glycolysis and glutamate accumulation into synaptic vesicles. Role of glyceraldehyde phosphate dehydrogenase and 3-phosphoglycerate kinase. *J. Biol. Chem.*, 278(8): 5929-5940.

Inglefield, J.R. & Schwartz-Bloom, R.D. (1998) Activation of excitatory amino acid receptors in the rat hippocampal slice increases intracellular Cl- and cell volume. *J. Neurochem.*, 71(4): 1396-1404.

Ishihara, K. & Hiraoka, M. (1994) Gating mechanism of the cloned inward rectifier potassium channel from mouse heart. *J. Membr. Biol.*, 142(1): 55-64.

Itoh, T., Beesley, J., Itoh, A., Cohen, A.S., Kavanaugh, B., Coulter, D.A., Grinspan, J.B., & Pleasure, D. (2002) AMPA glutamate receptor-mediated calcium signaling is transiently enhanced during development of oligodendrocytes. *J. Neurochem.*, 81(2): 390-402.

Izumi, Y., Benz, A.M., Katsuki, H., & Zorumski, C.F. (1997) Endogenous monocarboxylates sustain hippocampal synaptic function and morphological integrity during energy deprivation. *J. Neurosci.*, 17(24): 9448-9457.

Izumi, Y., Benz, A.M., Zorumski, C.F., & Olney, J.W. (1994) Effects of lactate and pyruvate on glucose deprivation in rat hippocampal slices. *Neuroreport*, 5(5): 617-620.

Jabs, R., Pivneva, T., Huttmann, K., Wyczynski, A., Nolte, C., Kettenmann, H., & Steinhauser, C. (2005) Synaptic transmission onto hippocampal glial cells with hGFAP promoter activity. *J. Cell Sci.*, 118(Pt 16): 3791-3803.

Jarjour, A.A. & Kennedy, T.E. (2004) Oligodendrocyte precursors on the move: mechanisms directing migration. *Neuroscientist.*, 10(2): 99-105.

Jensen, A.M. & Chiu, S.Y. (1993) Expression of glutamate receptor genes in white matter: developing and adult rat optic nerve. *J. Neurosci.*, 13(4): 1664-1675.

Jiang, C. & Haddad, G.G. (1994) A direct mechanism for sensing low oxygen levels by central neurons. *Proc. Natl. Acad. Sci. U. S. A*, 91(15): 7198-7201.

Johnston, D. & Amaral, D.G. (2004) Hippocampus. In G. M. Shepherd (Ed.), *The synaptic organization of the brain*: 455-498. Oxford: Oxford University Press.

Jonas, P., Bischofberger, J., & Sandkuhler, J. (1998) Corelease of two fast neurotransmitters at a central synapse. *Science*, 281(5375): 419-424.

Kakita, A. & Goldman, J.E. (1999) Patterns and dynamics of SVZ cell migration in the postnatal forebrain: monitoring living progenitors in slice preparations. *Neuron*, 23(3): 461-472.

Kakita, A., Zerlin, M., Takahashi, H., & Goldman, J.E. (2003) Some glial progenitors in the neonatal subventricular zone migrate through the corpus callosum to the contralateral cerebral hemisphere. *J. Comp Neurol.*, 458(4): 381-388.

Karschin, A., Wischmeyer, E., Davidson, N., & Lester, H.A. (1994) Fast inhibition of inwardly rectifying K+ channels by multiple neurotransmitter receptors in oligodendroglia. *Eur. J. Neurosci.*, 6(11): 1756-1764.

Katchman, A.N. & Hershkowitz, N. (1993b) Early anoxia-induced vesicular glutamate release results from mobilization of calcium from intracellular stores. *J. Neurophysiol.*, 70(1): 1-7.

Katchman, A.N. & Hershkowitz, N. (1993a) Adenosine antagonists prevent hypoxia-induced depression of excitatory but not inhibitory synaptic currents. *Neurosci. Lett.*, 159(1-2): 123-126.

Katchman, A.N., Vicini, S., & Hershkowitz, N. (1994) Mechanism of early anoxia-induced suppression of the GABAA-mediated inhibitory postsynaptic current. *J. Neurophysiol.*, 71(3): 1128-1138.

Kato, K., Shimizu, A., Kurobe, N., Takashi, M., & Koshikawa, T. (1989) Human brain-type glycogen phosphorylase: quantitative localization in human tissues determined with an immunoassay system. *J. Neurochem.*, 52(5): 1425-1432.

Kessaris, N., Jamen, F., Rubin, L.L., & Richardson, W.D. (2004) Cooperation between sonic hedgehog and fibroblast growth factor/MAPK signalling pathways in neocortical precursors. *Development*, 131(6): 1289-1298.

Kettenmann, H., Blankenfeld, G.V., & Trotter, J. (1991) Physiological properties of oligodendrocytes during development. *Ann. N. Y. Acad. Sci.*, 633: 64-77.

Kiernan, B.W. & ffrench-Constant, C. (1993) Oligodendrocyte precursor (O-2A progenitor cell) migration; a model system for the study of cell migration in the developing central nervous system. *Dev. Suppl*, 219-225.

Kimelberg, H.K. (2004) The problem of astrocyte identity. *Neurochem. Int.*, 45(2-3): 191-202.

Kimelberg, H.K. (1995) Receptors on astrocytes--what possible functions? *Neurochem. Int.*, 26(1): 27-40.

Kimura, F. & Baughman, R.W. (1997) GABAergic transcallosal neurons in developing rat neocortex. *Eur. J. Neurosci.*, 9(6): 1137-1143.

Kinney, H.C. (2005) Human myelination and perinatal white matter disorders. *J. Neurol. Sci.*, 228(2): 190-192.

Kirchhoff, F. & Kettenmann, H. (1992) GABA Triggers a [Ca2+]i Increase in Murine Precursor Cells of the Oligodendrocyte Lineage. *Eur. J. Neurosci.*, 4(11): 1049-1058.

Kirson, E.D., Schirra, C., Konnerth, A., & Yaari, Y. (1999) Early postnatal switch in magnesium sensitivity of NMDA receptors in rat CA1 pyramidal cells. *J. Physiol*, 521 Pt 1: 99-111.

Knobler, R.L., Saneto, R.P., Altman, A., Johnson, H.M., & de, V.J. (1988) Interleukin-2 blocks oligodendrocyte progenitor proliferation. *Ann. N. Y. Acad. Sci.*, 540: 324-326.

Knutson, P., Ghiani, C.A., Zhou, J.M., Gallo, V., & McBain, C.J. (1997) K+ channel expression and cell proliferation are regulated by intracellular sodium and membrane depolarization in oligodendrocyte progenitor cells. *J. Neurosci.*, 17(8): 2669-2682.

Koh, J.Y., Goldberg, M.P., Hartley, D.M., & Choi, D.W. (1990) Non-NMDA receptor-mediated neurotoxicity in cortical culture. *J. Neurosci.*, 10(2): 693-705.

Komuro, H. & Rakic, P. (1993) Modulation of neuronal migration by NMDA receptors. *Science*, 260(5104): 95-97.

Kriegler, S. & Chiu, S.Y. (1993) Calcium signaling of glial cells along mammalian axons. *J. Neurosci.*, 13(10): 4229-4245.

Kumar, S.S. & Huguenard, J.R. (2001) Properties of excitatory synaptic connections mediated by the corpus callosum in the developing rat neocortex. *J. Neurophysiol.*, 86(6): 2973-2985.

Kuner, T. & Schoepfer, R. (1996) Multiple structural elements determine subunit specificity of Mg2+ block in NMDA receptor channels. *J. Neurosci.*, 16(11): 3549-3558.

Landsend, A.S., miry-Moghaddam, M., Matsubara, A., Bergersen, L., Usami, S., Wenthold, R.J., & Ottersen, O.P. (1997) Differential localization of delta glutamate receptors in the rat cerebellum: coexpression with AMPA receptors in parallel fiber-

spine synapses and absence from climbing fiber-spine synapses. *J. Neurosci.*, 17(2): 834-842.

Le, B.B., Chatzopoulou, E., Heydon, K., Martinez, S., Ikenaka, K., Prestoz, L., Spassky, N., Zalc, B., & Thomas, J.L. (2005) Oligodendrocyte development in the embryonic brain: the contribution of the plp lineage. *Int. J. Dev. Biol.*, 49(2-3): 209-220.

Leblond, J. & Krnjevic, K. (1989) Hypoxic changes in hippocampal neurons. *J. Neurophysiol.*, 62(1): 1-14.

Lee, E.J., Lee, M.Y., Chen, H.Y., Hsu, Y.S., Wu, T.S., Chen, S.T., & Chang, G.L. (2005) Melatonin attenuates gray and white matter damage in a mouse model of transient focal cerebral ischemia. *J. Pineal Res.*, 38(1): 42-52.

Lee, M., Sakatani, K., & Young, W. (1993) A role of GABAA receptors in hypoxia-induced conduction failure of neonatal rat spinal dorsal column axons. *Brain Res.*, 601(1-2): 14-19.

Lehre, K.P., Levy, L.M., Ottersen, O.P., Storm-Mathisen, J., & Danbolt, N.C. (1995) Differential expression of two glial glutamate transporters in the rat brain: quantitative and immunocytochemical observations. *J. Neurosci.*, 15(3 Pt 1): 1835-1853.

Levine, J.M. & Card, J.P. (1987) Light and electron microscopic localization of a cell surface antigen (NG2) in the rat cerebellum: association with smooth protoplasmic astrocytes. *J. Neurosci.*, 7(9): 2711-2720.

Levine, J.M. & Stallcup, W.B. (1987) Plasticity of developing cerebellar cells in vitro studied with antibodies against the NG2 antigen. *J. Neurosci.*, 7(9): 2721-2731.

Levine, J.M., Stincone, F., & Lee, Y.S. (1993) Development and differentiation of glial precursor cells in the rat cerebellum. *Glia*, 7(4): 307-321.

Levine, J.M., Reynolds, R., & Fawcett, J.W. (2001) The oligodendrocyte precursor cell in health and disease. *Trends in Neurosciences*, 24(1): 39-47.

Levy, L.M., Warr, O., & Attwell, D. (1998) Stoichiometry of the glial glutamate transporter GLT-1 expressed inducibly in a Chinese hamster ovary cell line selected for low endogenous Na+-dependent glutamate uptake. *J. Neurosci.*, 18(23): 9620-9628.

Li, S., Jiang, Q., & Stys, P.K. (2000) Important role of reverse Na(+)-Ca(2+) exchange in spinal cord white matter injury at physiological temperature. *J. Neurophysiol.*, 84(2): 1116-1119.

Li, S., Mealing, G.A., Morley, P., & Stys, P.K. (1999) Novel injury mechanism in anoxia and trauma of spinal cord white matter: glutamate release via reverse Na+-dependent glutamate transport. *J. Neurosci.*, 19(14): RC16.

Li, S. & Stys, P.K. (2001a) Na(+)-K(+)-ATPase inhibition and depolarization induce glutamate release via reverse Na(+)-dependent transport in spinal cord white matter. *Neuroscience*, 107(4): 675-683.

Li, S. & Stys, P.K. (2001b) Na(+)-K(+)-ATPase inhibition and depolarization induce glutamate release via reverse Na(+)-dependent transport in spinal cord white matter. *Neuroscience*, 107(4): 675-683.

Li, S. & Stys, P.K. (2000) Mechanisms of ionotropic glutamate receptor-mediated excitotoxicity in isolated spinal cord white matter. *J. Neurosci.*, 20(3): 1190-1198.

Li, W., Llopis, J., Whitney, M., Zlokarnik, G., & Tsien, R.Y. (1998) Cell-permeant caged InsP3 ester shows that Ca2+ spike frequency can optimize gene expression. *Nature*, 392(6679): 936-941.

Lin, S.C. & Bergles, D.E. (2004) Synaptic signaling between GABAergic interneurons and oligodendrocyte precursor cells in the hippocampus. *Nat. Neurosci.*, 7(1): 24-32.

Lin, S.C., Huck, J.H., Roberts, J.D., Macklin, W.B., Somogyi, P., & Bergles, D.E. (2005) Climbing fiber innervation of NG2-expressing glia in the mammalian cerebellum. *Neuron*, 46(5): 773-785.

Lipton, P. (1989) Regulation of glycogen in the dentate gyrus of the in vitro guinea pig hippocampus; effect of combined deprivation of glucose and oxygen. *J. Neurosci. Methods*, 28(1-2): 147-154.

Lipton, P. (1999) Ischemic cell death in brain neurons. *Physiol Rev.*, 79(4): 1431-1568.

Liu, Y. & Rao, M.S. (2004) Olig genes are expressed in a heterogeneous population of precursor cells in the developing spinal cord. *Glia*, 45(1): 67-74.

Longsworth, L.G. (1953) Diffusion measurements at 25° of aqueous solutions of amino acids, peptides and sugars. *Journal of the American Chemical Society*, 75: 5705-5709.

LoTurco, J.J., Owens, D.F., Heath, M.J., Davis, M.B., & Kriegstein, A.R. (1995) GABA and glutamate depolarize cortical progenitor cells and inhibit DNA synthesis. *Neuron*, 15(6): 1287-1298.

Lowry, O.H., Passonneau, J.V., Hasselberger, F.X., & Schulz, D.W. (1964) Effect of Ischemia on Known Substrates and Cofactors of the Glycolytic Pathway in Brain. *J. Biol. Chem.*, 239(1): 18-30.

Lu, Q.R., Sun, T., Zhu, Z., Ma, N., Garcia, M., Stiles, C.D., & Rowitch, D.H. (2002) Common developmental requirement for Olig function indicates a motor neuron/oligodendrocyte connection. *Cell*, 109(1): 75-86.

Lu, Q.R., Yuk, D., Alberta, J.A., Zhu, Z., Pawlitzky, I., Chan, J., McMahon, A.P., Stiles, C.D., & Rowitch, D.H. (2000) Sonic hedgehog--regulated oligodendrocyte lineage genes encoding bHLH proteins in the mammalian central nervous system. *Neuron*, 25(2): 317-329.

Magistretti, P.J. & Pellerin, L. (1999) Cellular mechanisms of brain energy metabolism and their relevance to functional brain imaging. *Philos. Trans. R. Soc. Lond B Biol. Sci.*, 354(1387): 1155-1163.

Malayev, A., Gibbs, T.T., & Farb, D.H. (2002) Inhibition of the NMDA response by pregnenolone sulphate reveals subtype selective modulation of NMDA receptors by sulphated steroids. *Br. J. Pharmacol.*, 135(4): 901-909.

Malek, S.A., Coderre, E., & Stys, P.K. (2003) Aberrant chloride transport contributes to anoxic/ischemic white matter injury. *J. Neurosci.*, 23(9): 3826-3836.

Mallon, B.S., Shick, H.E., Kidd, G.J., & Macklin, W.B. (2002) Proteolipid promoter activity distinguishes two populations of NG2-positive cells throughout neonatal cortical development. *J. Neurosci.*, 22(3): 876-885.

Marcaggi, P. & Attwell, D. (2004) Role of glial amino acid transporters in synaptic transmission and brain energetics. *Glia*, 47(3): 217-225.

Marta, C.B., Paez, P., Lopez, M., de Iraldi, A.P., Soto, E.F., & Pasquini, J.M. (2003) Morphological Changes of Myelin Sheaths in Rats Intracranially Injected with Apotransferrin. *Neurochemical Research*, 28(1): 101-110.

Matthias, K., Kirchhoff, F., Seifert, G., Huttmann, K., Matyash, M., Kettenmann, H., & Steinhauser, C. (2003) Segregated expression of AMPA-type glutamate receptors and glutamate transporters defines distinct astrocyte populations in the mouse hippocampus. *J. Neurosci.*, 23(5): 1750-1758.

Matute, C., Alberdi, E., Domercq, M., Perez-Cerda, F., Perez-Samartin, A., & Sanchez-Gomez, M.V. (2001) The link between excitotoxic oligodendroglial death and demyelinating diseases. *Trends Neurosci.*, 24(4): 224-230.

Matute, C., Alberdi, E., Ibarretxe, G., & Sanchez-Gomez, M.V. (2002) Excitotoxicity in glial cells. *Eur. J. Pharmacol.*, 447(2-3): 239-246.

Matute, C., Sanchez-Gomez, M.V., Martinez-Millan, L., & Miledi, R. (1997) Glutamate receptor-mediated toxicity in optic nerve oligodendrocytes. *Proc. Natl. Acad. Sci. U. S. A*, 94(16): 8830-8835.

McDonald, J.W., Althomsons, S.P., Hyrc, K.L., Choi, D.W., & Goldberg, M.P. (1998) Oligodendrocytes from forebrain are highly vulnerable to AMPA/kainate receptor-mediated excitotoxicity. *Nat. Med.*, 4(3): 291-297.

McKinnon, R.D., Matsui, T., Aranda, M., & Dubois-Dalcq, M. (1991) A role for fibroblast growth factor in oligodendrocyte development. *Ann. N. Y. Acad. Sci.*, 638: 378-386.

McKinnon, R.D., Matsui, T., Dubois-Dalcq, M., & Aaronson, S.A. (1990) FGF modulates the PDGF-driven pathway of oligodendrocyte development. *Neuron*, 5(5): 603-614.

McKinnon, R.D., Piras, G., Ida, J.A., Jr., & Dubois-Dalcq, M. (1993) A role for TGF-beta in oligodendrocyte differentiation. *J. Cell Biol.*, 121(6): 1397-1407.

McMorris, F.A. & Dubois-Dalcq, M. (1988) Insulin-like growth factor I promotes cell proliferation and oligodendroglial commitment in rat glial progenitor cells developing in vitro. *J. Neurosci. Res.*, 21(2-4): 199-209.

Mehta, A.K. & Ticku, M.K. (1999) An update on GABAA receptors. *Brain Res. Brain Res. Rev.*, 29(2-3): 196-217.

Micu, I., Jiang, Q., Coderre, E., Ridsdale, A., Zhang, L., Woulfe, J., Yin, X., Trapp, B.D., McRory, J.E., Rehak, R., Zamponi, G.W., Wang, W., & Stys, P.K. (2005) NMDA receptors mediate calcium accumulation in myelin during chemical ischaemia. *Nature*.

Miller, R.H. (2002) Regulation of oligodendrocyte development in the vertebrate CNS. *Prog. Neurobiol.*, 67(6): 451-467.

Moran, M.M., Xu, H., & Clapham, D.E. (2004) TRP ion channels in the nervous system. *Curr. Opin. Neurobiol.*, 14(3): 362-369.

Müller, T., Fritschy, J.M., Grosche, J., Pratt, G.D., Mohler, H., & Kettenmann, H. (1994) Developmental regulation of voltage-gated K+ channel and GABAA receptor expression in Bergmann glial cells. *J. Neurosci.*, 14(5 Pt 1): 2503-2514.

Müller, T., Grosche, J., Ohlemeyer, C., & Kettenmann, H. (1993) NMDA-activated currents in Bergmann glial cells. *Neuroreport*, 4(6): 671-674.

Munns, S.E., Meloni, B.P., Knuckey, N.W., & Arthur, P.G. (2003) Primary cortical neuronal cultures reduce cellular energy utilization during anoxic energy deprivation. *J. Neurochem.*, 87(3): 764-772.

Nabetani, M., Okada, Y., Kawai, S., & Nakamura, H. (1995) Neural activity and the levels of high energy phosphates during deprivation of oxygen and/or glucose in hippocampal slices of immature and adult rats. *Int. J. Dev. Neurosci.*, 13(1): 3-12.

Nedergaard, M., Ransom, B., & Goldman, S.A. (2003) New roles for astrocytes: redefining the functional architecture of the brain. *Trends Neurosci.*, 26(10): 523-530.

Neusch, C., Rozengurt, N., Jacobs, R.E., Lester, H.A., & Kofuji, P. (2001) Kir4.1 potassium channel subunit is crucial for oligodendrocyte development and in vivo myelination. *J. Neurosci.*, 21(15): 5429-5438.

Nishiyama, A., Lin, X.H., Giese, N., Heldin, C.H., & Stallcup, W.B. (1996a) Co-localization of NG2 proteoglycan and PDGF alpha-receptor on O2A progenitor cells in the developing rat brain. *J. Neurosci. Res.*, 43(3): 299-314.

Nishiyama, A., Lin, X.H., Giese, N., Heldin, C.H., & Stallcup, W.B. (1996b) Interaction between NG2 proteoglycan and PDGF alpha-receptor on O2A progenitor cells is required for optimal response to PDGF. *J. Neurosci. Res.*, 43(3): 315-330.

Noble, M., Murray, K., Stroobant, P., Waterfield, M.D., & Riddle, P. (1988) Platelet-derived growth factor promotes division and motility and inhibits premature differentiation of the oligodendrocyte/type-2 astrocyte progenitor cell. *Nature*, 333(6173): 560-562.

Nowicky, A.V. & Duchen, M.R. (1998) Changes in [Ca2+]i and membrane currents during impaired mitochondrial metabolism in dissociated rat hippocampal neurons. *J. Physiol*, 507 (Pt 1): 131-145.

O'Neill, M.J., Bogaert, L., Hicks, C.A., Bond, A., Ward, M.A., Ebinger, G., Ornstein, P.L., Michotte, Y., & Lodge, D. (2000) LY377770, a novel iGlu5 kainate receptor antagonist with neuroprotective effects in global and focal cerebral ischaemia. *Neuropharmacology*, 39(9): 1575-1588.

Oka, A., Belliveau, M.J., Rosenberg, P.A., & Volpe, J.J. (1993) Vulnerability of oligodendroglia to glutamate: pharmacology, mechanisms, and prevention. *J. Neurosci.*, 13(4): 1441-1453.

Olney, J.W. (1978) Neurotoxicity of excitatory amino acids. In E. G. McGeer, J. W. Olney, & P. L. McGeer (Eds.), *Kainic acid as a tool in neurobiology*: 37-70. New York: Raven Press.

Ong, W.Y. & Levine, J.M. (1999) A light and electron microscopic study of NG2 chondroitin sulfate proteoglycan-positive oligodendrocyte precursor cells in the normal and kainate-lesioned rat hippocampus. *Neuroscience*, 92(1): 83-95.

Osterhout, D.J., Ebner, S., Xu, J., Ornitz, D.M., Zazanis, G.A., & McKinnon, R.D. (1997) Transplanted oligodendrocyte progenitor cells expressing a dominant-negative FGF receptor transgene fail to migrate in vivo. *J. Neurosci.*, 17(23): 9122-9132.

Othman, T., Yan, H., & Rivkees, S.A. (2003) Oligodendrocytes express functional A1 adenosine receptors that stimulate cellular migration. *Glia*, 44(2): 166-172.

Parpura, V., Basarsky, T.A., Liu, F., Jeftinija, K., Jeftinija, S., & Haydon, P.G. (1994) Glutamate-mediated astrocyte-neuron signalling. *Nature*, 369(6483): 744-747.

Passingham, R.E. (1973) Anatomical differences between the neocortex of man and other primates. *Brain Behav. Evol.*, 7(5): 337-359.

Pastor, A., Chvatal, A., Sykova, E., & Kettenmann, H. (1995) Glycine- and GABA-activated currents in identified glial cells of the developing rat spinal cord slice. *Eur. J. Neurosci.*, 7(6): 1188-1198.

Pastor, A., Kremer, M., Moller, T., Kettenmann, H., & Dermietzel, R. (1998) Dye coupling between spinal cord oligodendrocytes: differences in coupling efficiency between gray and white matter. *Glia*, 24(1): 108-120.

Patel, M.N., Peoples, R.W., Yim, G.K., & Isom, G.E. (1994) Enhancement of NMDA-mediated responses by cyanide. *Neurochem. Res.*, 19(10): 1319-1323.

Patneau, D.K. & Mayer, M.L. (1990) Structure-activity relationships for amino acid transmitter candidates acting at N-methyl-D-aspartate and quisqualate receptors. *J. Neurosci.*, 10(7): 2385-2399.

Patneau, D.K., Wright, P.W., Winters, C., Mayer, M.L., & Gallo, V. (1994) Glial cells of the oligodendrocyte lineage express both kainate- and AMPA-preferring subtypes of glutamate receptor. *Neuron*, 12(2): 357-371.

Pearce, I.A., Cambray-Deakin, M.A., & Burgoyne, R.D. (1987) Glutamate acting on NMDA receptors stimulates neurite outgrowth from cerebellar granule cells. *FEBS Lett.*, 223(1): 143-147.

Pellerin, L., Pellegri, G., Bittar, P.G., Charnay, Y., Bouras, C., Martin, J.L., Stella, N., & Magistretti, P.J. (1998) Evidence supporting the existence of an activity-dependent astrocyte-neuron lactate shuttle. *Dev. Neurosci.*, 20(4-5): 291-299.

Pende, M., Holtzclaw, L.A., Curtis, J.L., Russell, J.T., & Gallo, V. (1994) Glutamate regulates intracellular calcium and gene expression in oligodendrocyte progenitors through the activation of DL-alpha-amino-3-hydroxy-5-methyl-4-isoxazolepropionic acid receptors. *Proc. Natl. Acad. Sci. U. S. A*, 91(8): 3215-3219.

Peppiatt, C. & Attwell, D. (2004) Neurobiology: feeding the brain. *Nature*, 431(7005): 137-138.

Peters, A., Palay, S.L., & Webster, H.d. (1991) *The fine structure of the nervous system neurons and their supporting cells*. New York: Oxford University Press.

Piani, D. & Fontana, A. (1994) Involvement of the cystine transport system xc- in the macrophage-induced glutamate-dependent cytotoxicity to neurons. *J. Immunol.*, 152(7): 3578-3585.

Pissarek, M., Reinhardt, R., Reichelt, C., Manaenko, A., Krauss, G., & Illes, P. (1999) Rapid assay for one-run determination of purine and pyrimidine nucleotide contents in neocortical slices and cell cultures. *Brain Res. Brain Res. Protoc.*, 4(3): 314-321.

Pitt, D., Werner, P., & Raine, C.S. (2000) Glutamate excitotoxicity in a model of multiple sclerosis. *Nat. Med.*, 6(1): 67-70.

Plotkin, M.D., Snyder, E.Y., Hebert, S.C., & Delpire, E. (1997) Expression of the Na-K-2Cl cotransporter is developmentally regulated in postnatal rat brains: a possible mechanism underlying GABA's excitatory role in immature brain. *J. Neurobiol.*, 33(6): 781-795.

Porter, J.T. & McCarthy, K.D. (1997) Astrocytic neurotransmitter receptors in situ and in vivo. *Prog. Neurobiol.*, 51(4): 439-455.

Pringle, N.P., Guthrie, S., Lumsden, A., & Richardson, W.D. (1998) Dorsal spinal cord neuroepithelium generates astrocytes but not oligodendrocytes. *Neuron*, 20(5): 883-893.

Pringle, N.P., Mudhar, H.S., Collarini, E.J., & Richardson, W.D. (1992) PDGF receptors in the rat CNS: during late neurogenesis, PDGF alpha-receptor expression appears to be restricted to glial cells of the oligodendrocyte lineage. *Development*, 115(2): 535-551.

Pringle, N.P. & Richardson, W.D. (1993) A singularity of PDGF alpha-receptor expression in the dorsoventral axis of the neural tube may define the origin of the oligodendrocyte lineage. *Development*, 117(2): 525-533.

Pringle, N.P., Yu, W.P., Guthrie, S., Roelink, H., Lumsden, A., Peterson, A.C., & Richardson, W.D. (1996) Determination of neuroepithelial cell fate: induction of the oligodendrocyte lineage by ventral midline cells and sonic hedgehog. *Dev. Biol.*, 177(1): 30-42.

Puchalski, R.B., Louis, J.C., Brose, N., Traynelis, S.F., Egebjerg, J., Kukekov, V., Wenthold, R.J., Rogers, S.W., Lin, F., Moran, T., & . (1994) Selective RNA editing and subunit assembly of native glutamate receptors. *Neuron*, 13(1): 131-147.

Pulsinelli, W.A. (1985) Selective neuronal vulnerability: morphological and molecular characteristics. *Prog. Brain Res.*, 63: 29-37.

Puro, D.G., Yuan, J.P., & Sucher, N.J. (1996) Activation of NMDA receptor-channels in human retinal Muller glial cells inhibits inward-rectifying potassium currents. *Vis. Neurosci.*, 13(2): 319-326.

Rabacchi, S., Bailly, Y., Delhaye-Bouchaud, N., & Mariani, J. (1992) Involvement of the N-methyl D-aspartate (NMDA) receptor in synapse elimination during cerebellar development. *Science*, 256(5065): 1823-1825.

Rader, R.K. & Lanthorn, T.H. (1989) Experimental ischemia induces a persistent depolarization blocked by decreased calcium and NMDA antagonists. *Neurosci. Lett.*, 99(1-2): 125-130.

Raff, M.C., Abney, E.R., Cohen, J., Lindsay, R., & Noble, M. (1983a) Two types of astrocytes in cultures of developing rat white matter: differences in morphology, surface gangliosides, and growth characteristics. *J. Neurosci.*, 3(6): 1289-1300.

Raff, M.C., Lillien, L.E., Richardson, W.D., Burne, J.F., & Noble, M.D. (1988) Platelet-derived growth factor from astrocytes drives the clock that times oligodendrocyte development in culture. *Nature*, 333(6173): 562-565.

Raff, M.C., Miller, R.H., & Noble, M. (1983b) A glial progenitor cell that develops in vitro into an astrocyte or an oligodendrocyte depending on culture medium. *Nature*, 303(5916): 390-396.

Raffin, C.N., Rosenthal, M., Busto, R., & Sick, T.J. (1992) Glycolysis, oxidative metabolism, and brain potassium ion clearance. *J. Cereb. Blood Flow Metab*, 12(1): 34-42.

Ragheb, F., Molina-Holgado, E., Cui, Q.L., Khorchid, A., Liu, H.N., Larocca, J.N., & Almazan, G. (2001) Pharmacological and functional characterization of muscarinic receptor subtypes in developing oligodendrocytes. *J. Neurochem.*, 77(5): 1396-1406.

Rajantie, H. & Williams, D.E. (2001) Potentiometric titrations using dual microband electrodes. *Analyst*, 126(11): 1882-1887.

Raley, K.M. & Lipton, P. (1990) NMDA receptor activation accelerates ischemic energy depletion in the hippocampal slice and the demonstration of a threshold for ischemic damage to protein synthesis. *Neurosci. Lett.*, 110(1-2): 118-123.

Ransom, B., Behar, T., & Nedergaard, M. (2003) New roles for astrocytes (stars at last). *Trends Neurosci.*, 26(10): 520-522.

Ransom, B.R., Butt, A.M., & Black, J.A. (1991) Ultrastructural identification of HRP-injected oligodendrocytes in the intact rat optic nerve. *Glia*, 4(1): 37-45.

Rao, M.S., Noble, M., & Mayer-Proschel, M. (1998) A tripotential glial precursor cell is present in the developing spinal cord. *Proc. Natl. Acad. Sci. U. S. A*, 95(7): 3996-4001.

Reiner, P.B., Laycock, A.G., & Doll, C.J. (1990) A pharmacological model of ischemia in the hippocampal slice. *Neurosci. Lett.*, 119(2): 175-178.

Reynolds, R., Dawson, M., Papadopoulos, D., Polito, A., Di, B., I, Pham-Dinh, D., & Levine, J. (2002) The response of NG2-expressing oligodendrocyte progenitors to demyelination in MOG-EAE and MS. *J. Neurocytol.*, 31(6-7): 523-536.

Reynolds, R. & Wilkin, G.P. (1988) Development of macroglial cells in rat cerebellum. II. An in situ immunohistochemical study of oligodendroglial lineage from precursor to mature myelinating cell. *Development*, 102(2): 409-425.

Richardson, W.D., Pringle, N., Mosley, M.J., Westermark, B., & Dubois-Dalcq, M. (1988) A role for platelet-derived growth factor in normal gliogenesis in the central nervous system. *Cell*, 53(2): 309-319.

Rilling, J.K. & Insel, T.R. (1999) The primate neocortex in comparative perspective using magnetic resonance imaging. *J. Hum. Evol.*, 37(2): 191-223.

Ringo, J.L. (1991) Neuronal interconnection as a function of brain size. *Brain Behav. Evol.*, 38(1): 1-6.

Rogers, S.W., Gregori, N.Z., Carlson, N., Gahring, L.C., & Noble, M. (2001) Neuronal nicotinic acetylcholine receptor expression by O2A/oligodendrocyte progenitor cells. *Glia*, 33(4): 306-313.

Rolfe, D.F. & Brown, G.C. (1997) Cellular energy utilization and molecular origin of standard metabolic rate in mammals. *Physiol Rev.*, 77(3): 731-758.

Rosenberg, P.A., Dai, W., Gan, X.D., Ali, S., Fu, J., Back, S.A., Sanchez, R.M., Segal, M.M., Follett, P.L., Jensen, F.E., & Volpe, J.J. (2003) Mature myelin basic protein-expressing oligodendrocytes are insensitive to kainate toxicity. *J. Neurosci. Res.*, 71(2): 237-245.

Rosenberg, P.A. & Dichter, M.A. (1985) Glycogen accumulation in rat cerebral cortex in dissociated cell culture. *J. Neurosci. Methods*, 15(2): 101-112.

Rosenthal, M. & Sick, T.J. (1992) Glycolytic and oxidative metabolic contributions to potassium ion transport in rat cerebral cortex. *Can. J. Physiol Pharmacol.*, 70 Suppl: S165-S169.

Rosin, C., Colombo, S., Calver, A.A., Bates, T.E., & Skaper, S.D. (2005) Dopamine D2 and D3 receptor agonists limit oligodendrocyte injury caused by glutamate oxidative stress and oxygen/glucose deprivation. *Glia*, 52(4): 336-343.

Rossi, D.J., Hamann, M., & Attwell, D. (2003) Multiple modes of GABAergic inhibition of rat cerebellar granule cells. *J. Physiol*, 548(Pt 1): 97-110.

Rossi, D.J., Oshima, T., & Attwell, D. (2000) Glutamate release in severe brain ischaemia is mainly by reversed uptake. *Nature*, 403(6767): 316-321.

Rowitch, D.H. (2004) Glial specification in the vertebrate neural tube. *Nat. Rev. Neurosci.*, 5(5): 409-419.

Rowitch, D.H., Lu, Q.R., Kessaris, N., & Richardson, W.D. (2002) An 'oligarchy' rules neural development. *Trends Neurosci.*, 25(8): 417-422.

Runnels, L.W., Yue, L., & Clapham, D.E. (2001) TRP-PLIK, a bifunctional protein with kinase and ion channel activities. *Science*, 291(5506): 1043-1047.

Saitoh, M., Okada, Y., & Nabetani, M. (1994) Effect of mannose, fructose and lactate on the preservation of synaptic potentials in hippocampal slices. *Neurosci. Lett.*, 171(1-2): 125-128.

Sakatani, K., Hassan, A.Z., & Chesler, M. (1991) GABA-sensitivity of dorsal column axons: an in vitro comparison between adult and neonatal rat spinal cords. *Brain Res. Dev. Brain Res.*, 61(1): 139-142.

Salter, M.G. & Fern, R. (2005) NMDA receptors are expressed in developing oligodendrocyte processes and mediate injury. *Nature*, 438(7071): 1167-1171.

Salzer, J.L. (2003) Polarized domains of myelinated axons. *Neuron*, 40(2): 297-318.

Saneto, R.P., Altman, A., Knobler, R.L., Johnson, H.M., & de, V.J. (1986) Interleukin 2 mediates the inhibition of oligodendrocyte progenitor cell proliferation in vitro. *Proc. Natl. Acad. Sci. U. S. A*, 83(23): 9221-9225.

Sasaki, Y.F., Rothe, T., Premkumar, L.S., Das, S., Cui, J., Talantova, M.V., Wong, H.K., Gong, X., Chan, S.F., Zhang, D., Nakanishi, N., Sucher, N.J., & Lipton, S.A. (2002) Characterization and comparison of the NR3A subunit of the NMDA receptor in recombinant systems and primary cortical neurons. *J. Neurophysiol.*, 87(4): 2052-2063.

Satoh, M., Asai, S., Katayama, Y., Kohno, T., & Ishikawa, K. (1999) Real-time monitoring of glutamate transmitter release with anoxic depolarization during anoxic insult in rat striatum. *Brain Res.*, 822(1-2): 142-148.

Schäbitz, W.R., Li, F., & Fisher, M. (2000) The N-methyl-D-aspartate antagonist CNS 1102 protects cerebral gray and white matter from ischemic injury following temporary focal ischemia in rats. *Stroke*, 31(7): 1709-1714.

Schipke, C.G., Ohlemeyer, C., Matyash, M., Nolte, C., Kettenmann, H., & Kirchhoff, F. (2001) Astrocytes of the mouse neocortex express functional N-methyl-D-aspartate receptors. *FASEB J.*, 15(7): 1270-1272.

Schmidt, C., Ohlemeyer, C., Kettenmann, H., Reutter, W., & Horstkorte, R. (2000) Incorporation of N-propanoylneuraminic acid leads to calcium oscillations in oligodendrocytes upon the application of GABA. *FEBS Lett.*, 478(3): 276-280.

Schoenemann, P.T., Sheehan, M.J., & Glotzer, L.D. (2005) Prefrontal white matter volume is disproportionately larger in humans than in other primates. *Nat. Neurosci.*, 8(2): 242-252.

Schools, G.P., Zhou, M., & Kimelberg, H.K. (2003) Electrophysiologically "complex" glial cells freshly isolated from the hippocampus are immunopositive for the chondroitin sulfate proteoglycan NG2. *J. Neurosci. Res.*, 73(6): 765-777.

Schurr, A., West, C.A., & Rigor, B.M. (1988) Lactate-supported synaptic function in the rat hippocampal slice preparation. *Science*, 240(4857): 1326-1328.

Sheinin, A., Shavit, S., & Benveniste, M. (2001) Subunit specificity and mechanism of action of NMDA partial agonist D-cycloserine. *Neuropharmacology*, 41(2): 151-158.

Sheng, H.Z., Turnley, A., Murphy, M., Bernard, C.C., & Bartlett, P.F. (1989) Epidermal growth factor inhibits the expression of myelin basic protein in oligodendrocytes. *J. Neurosci. Res.*, 23(4): 425-432.

Shimada, N., Graf, R., Rosner, G., & Heiss, W.D. (1993) Ischemia-induced accumulation of extracellular amino acids in cerebral cortex, white matter, and cerebrospinal fluid. *J. Neurochem.*, 60(1): 66-71.

Shrager, P. & Novakovic, S.D. (1995) Control of myelination, axonal growth, and synapse formation in spinal cord explants by ion channels and electrical activity. *Brain Res. Dev. Brain Res.*, 88(1): 68-78.

Sibson, N.R., Dhankhar, A., Mason, G.F., Rothman, D.L., Behar, K.L., & Shulman, R.G. (1998) Stoichiometric coupling of brain glucose metabolism and glutamatergic neuronal activity. *Proc. Natl. Acad. Sci. U. S. A*, 95(1): 316-321.

Sibson, N.R., Mason, G.F., Shen, J., Cline, G.W., Herskovits, A.Z., Wall, J.E.M., Behar, K.L., Rothman, D.L., & Shulman, R.G. (2001) In vivo 13C NMR measurement of neurotransmitter glutamate cycling, anaplerosis and TCA cycle flux in rat brain during [2-13C]glucose infusion. *Journal of Neurochemistry*, 76(4): 975-989.

Sieghart, W., Fuchs, K., Tretter, V., Ebert, V., Jechlinger, M., Hoger, H., & Adamiker, D. (1999) Structure and subunit composition of GABA(A) receptors. *Neurochem. Int.*, 34(5): 379-385.

Simard, M. & Nedergaard, M. (2004) The neurobiology of glia in the context of water and ion homeostasis. *Neuroscience*, 129(4): 877-896.

Skundric, D.S. (2005) Experimental models of relapsing-remitting multiple sclerosis: current concepts and perspective. *Curr. Neurovasc. Res.*, 2(4): 349-362.

Small, R.K., Riddle, P., & Noble, M. (1987) Evidence for migration of oligodendrocyte--type-2 astrocyte progenitor cells into the developing rat optic nerve. *Nature*, 328(6126): 155-157.

Smith, T., Groom, A., Zhu, B., & Turski, L. (2000) Autoimmune encephalomyelitis ameliorated by AMPA antagonists. *Nat. Med.*, 6(1): 62-66.

Sokoloff, L., Reivich, M., Kennedy, C., Des Rosiers, M.H., Patlak, C.S., Pettigrew, K.D., Sakurada, O., & Shinohara, M. (1977) The [14C]deoxyglucose method for the measurement of local cerebral glucose utilization: theory, procedure, and normal values in the conscious and anesthetized albino rat. *J. Neurochem.*, 28(5): 897-916.

Solis, J.M. & Nicoll, R.A. (1992) Postsynaptic action of endogenous GABA released by nipecotic acid in the hippocampus. *Neurosci. Lett.*, 147(1): 16-20.

Soliven, B., Szuchet, S., Arnason, B.G., & Nelson, D.J. (1988) Voltage-gated potassium currents in cultured ovine oligodendrocytes. *J. Neurosci.*, 8(6): 2131-2141.

Somjen, G.G. (1988) Nervenkitt: notes on the history of the concept of neuroglia. *Glia*, 1(1): 2-9.

Sommer, I. & Schachner, M. (1981) Monoclonal antibodies (O1 to O4) to oligodendrocyte cell surfaces: an immunocytological study in the central nervous system. *Dev. Biol.*, 83(2): 311-327.

Sontheimer, H., Trotter, J., Schachner, M., & Kettenmann, H. (1989) Channel expression correlates with differentiation stage during the development of oligodendrocytes from their precursor cells in culture. *Neuron*, 2(2): 1135-1145.

Stallcup, W.B. (2002) The NG2 proteoglycan: past insights and future prospects. *J. Neurocytol.*, 31(6-7): 423-435.

Stallcup, W.B. & Beasley, L. (1987) Bipotential glial precursor cells of the optic nerve express the NG2 proteoglycan. *J. Neurosci.*, 7(9): 2737-2744.

Steinhauser, C., Berger, T., Frotscher, M., & Kettenmann, H. (1992) Heterogeneity in the Membrane Current Pattern of Identified Glial Cells in the Hippocampal Slice. *Eur. J. Neurosci.*, 4(6): 472-484.

Steinhauser, C., Jabs, R., & Kettenmann, H. (1994) Properties of GABA and glutamate responses in identified glial cells of the mouse hippocampal slice. *Hippocampus*, 4(1): 19-35.

Stensaas, L.J. & Stensaas, S.S. (1968) Astrocytic neuroglial cells, oligodendrocytes and microgliacytes in the spinal cord of the toad. II. Electron microscopy. *Z. Zellforsch. Mikrosk. Anat.*, 86(2): 184-213.

Stevens, B., Porta, S., Haak, L.L., Gallo, V., & Fields, R.D. (2002) Adenosine: a neuron-glial transmitter promoting myelination in the CNS in response to action potentials. *Neuron*, 36(5): 855-868.

Stys, P.K. (2004) White matter injury mechanisms. *Curr. Mol. Med.*, 4(2): 113-130.

Stys, P.K. (1998) Anoxic and ischemic injury of myelinated axons in CNS white matter: from mechanistic concepts to therapeutics. *J. Cereb. Blood Flow Metab*, 18(1): 2-25.

Sugimoto, Y., Taniguchi, M., Yagi, T., Akagi, Y., Nojyo, Y., & Tamamaki, N. (2001) Guidance of glial precursor cell migration by secreted cues in the developing optic nerve. *Development*, 128(17): 3321-3330.

Swanson, R.A. & Choi, D.W. (1993) Glial glycogen stores affect neuronal survival during glucose deprivation in vitro. *J. Cereb. Blood Flow Metab*, 13(1): 162-169.

Szatkowski, M., Barbour, B., & Attwell, D. (1990) Non-vesicular release of glutamate from glial cells by reversed electrogenic glutamate uptake. *Nature*, 348(6300): 443-446.

Takahashi, Y., Shirasaki, T., Yamanaka, H., Ishibashi, H., & Akaike, N. (1994) Physiological roles of glycine and gamma-aminobutyric acid in dissociated neurons of rat visual cortex. *Brain Res.*, 640(1-2): 229-235.

Takata, T. & Okada, Y. (1995) Effects of deprivation of oxygen or glucose on the neural activity in the guinea pig hippocampal slice--intracellular recording study of pyramidal neurons. *Brain Res.*, 683(1): 109-116.

Takebayashi, H., Nabeshima, Y., Yoshida, S., Chisaka, O., Ikenaka, K., & Nabeshima, Y. (2002) The basic helix-loop-helix factor olig2 is essential for the development of motoneuron and oligodendrocyte lineages. *Curr. Biol.*, 12(13): 1157-1163.

Takebayashi, H., Yoshida, S., Sugimori, M., Kosako, H., Kominami, R., Nakafuku, M., & Nabeshima, Y. (2000) Dynamic expression of basic helix-loop-helix Olig family members: implication of Olig2 in neuron and oligodendrocyte differentiation and identification of a new member, Olig3. *Mech. Dev.*, 99(1-2): 143-148.

Takeda, M., Nelson, D.J., & Soliven, B. (1995) Calcium signaling in cultured rat oligodendrocytes. *Glia*, 14(3): 225-236.

Tanaka, E., Yamamoto, S., Kudo, Y., Mihara, S., & Higashi, H. (1997) Mechanisms underlying the rapid depolarization produced by deprivation of oxygen and glucose in rat hippocampal CA1 neurons in vitro. *J. Neurophysiol.*, 78(2): 891-902.

Tekki-Kessaris, N., Woodruff, R., Hall, A.C., Gaffield, W., Kimura, S., Stiles, C.D., Rowitch, D.H., & Richardson, W.D. (2001) Hedgehog-dependent oligodendrocyte lineage specification in the telencephalon. *Development*, 128(13): 2545-2554.

Tekkök, S.B. & Goldberg, M.P. (2001) Ampa/kainate receptor activation mediates hypoxic oligodendrocyte death and axonal injury in cerebral white matter. *J. Neurosci.*, 21(12): 4237-4248.

Terada, N., Baracskay, K., Kinter, M., Melrose, S., Brophy, P.J., Boucheix, C., Bjartmar, C., Kidd, G., & Trapp, B.D. (2002) The tetraspanin protein, CD9, is expressed by progenitor cells committed to oligodendrogenesis and is linked to beta1 integrin, CD81, and Tspan-2. *Glia*, 40(3): 350-359.

Tessier-Lavigne, M., Attwell, D., Mobbs, P., & Wilson, M. (1988) Membrane currents in retinal bipolar cells of the axolotl. *J. Gen. Physiol*, 91(1): 49-72.

Trapp, B.D., Nishiyama, A., Cheng, D., & Macklin, W. (1997) Differentiation and Death of Premyelinating Oligodendrocytes in Developing Rodent Brain. *J. Cell Biol.*, 137(2): 459-468.

Tsai, H.H. & Miller, R.H. (2002) Glial cell migration directed by axon guidance cues. *Trends Neurosci.*, 25(4): 173-175.

Tsai, H.H., Tessier-Lavigne, M., & Miller, R.H. (2003) Netrin 1 mediates spinal cord oligodendrocyte precursor dispersal. *Development*, 130(10): 2095-2105.

Turrens, J.F. (2003) Mitochondrial formation of reactive oxygen species. *J. Physiol*, 552(Pt 2): 335-344.

Ueda, H., Levine, J.M., Miller, R.H., & Trapp, B.D. (1999) Rat optic nerve oligodendrocytes develop in the absence of viable retinal ganglion cell axons. *J. Cell Biol.*, 146(6): 1365-1374.

Vallstedt, A., Klos, J.M., & Ericson, J. (2005) Multiple dorsoventral origins of oligodendrocyte generation in the spinal cord and hindbrain. *Neuron*, 45(1): 55-67.

Vartanian, T., Szuchet, S., Dawson, G., & Campagnoni, A.T. (1986) Oligodendrocyte adhesion activates protein kinase C-mediated phosphorylation of myelin basic protein. *Science*, 234(4782): 1395-1398.

Vautier, F., Belachew, S., Chittajallu, R., & Gallo, V. (2004) Shaker-type potassium channel subunits differentially control oligodendrocyte progenitor proliferation. *Glia*, 48(4): 337-345.

Vergun, O., Sobolevsky, A.I., Yelshansky, M.V., Keelan, J., Khodorov, B.I., & Duchen, M.R. (2001) Exploration of the role of reactive oxygen species in glutamate neurotoxicity in rat hippocampal neurones in culture. *J. Physiol*, 531(Pt 1): 147-163.

Verkhratsky, A. & Steinhauser, C. (2000) Ion channels in glial cells. *Brain Res. Brain Res. Rev.*, 32(2-3): 380-412.

Volpe, J.J. (2001) Neurobiology of periventricular leukomalacia in the premature infant. *Pediatr. Res.*, 50(5): 553-562.

Vorisek, I. & Sykova, E. (1997) Ischemia-induced changes in the extracellular space diffusion parameters, K+, and pH in the developing rat cortex and corpus callosum. *J. Cereb. Blood Flow Metab*, 17(2): 191-203.

Wada, H., Okada, Y., Uzuo, T., & Nakamura, H. (1998) The effects of glucose, mannose, fructose and lactate on the preservation of neural activity in the hippocampal slices from the guinea pig. *Brain Res.*, 788(1-2): 144-150.

Wafford, K.A. (2005) GABAA receptor subtypes: any clues to the mechanism of benzodiazepine dependence? *Curr. Opin. Pharmacol.*, 5(1): 47-52.

Wallström, E., Diener, P., Ljungdahl, A., Khademi, M., Nilsson, C.G., & Olsson, T. (1996) Memantine abrogates neurological deficits, but not CNS inflammation, in Lewis rat experimental autoimmune encephalomyelitis. *J. Neurol. Sci.*, 137(2): 89-96.

Walz, W. (2000) Controversy surrounding the existence of discrete functional classes of astrocytes in adult gray matter. *Glia*, 31(2): 95-103.

Wang, C., Pralong, W.F., Schulz, M.F., Rougon, G., Aubry, J.M., Pagliusi, S., Robert, A., & Kiss, J.Z. (1996) Functional N-methyl-D-aspartate receptors in O-2A glial precursor cells: a critical role in regulating polysialic acid-neural cell adhesion molecule expression and cell migration. *J. Cell Biol.*, 135(6 Pt 1): 1565-1581.

Weinreich, D. & Hammerschlag, R. (1975) Nerve impulse-enhanced release of amino acids from non-synaptic regions of peripheral and central nerve trunks of bullfrog. *Brain Res.*, 84(1): 137-142.

Werner, P., Pitt, D., & Raine, C.S. (2001) Multiple sclerosis: altered glutamate homeostasis in lesions correlates with oligodendrocyte and axonal damage. *Ann. Neurol.*, 50(2): 169-180.

Wheeler, D.D., Boyarsky, L.L., & Brooks, W.H. (1966) The release of amino acids from nerve during stimulation. *J. Cell Physiol*, 67(1): 141-147.

Wilke, S., Thomas, R., Allcock, N., & Fern, R. (2004) Mechanism of acute ischemic injury of oligodendroglia in early myelinating white matter: the importance of astrocyte injury and glutamate release. *J. Neuropathol. Exp. Neurol.*, 63(8): 872-881.

Wilkins, A., Majed, H., Layfield, R., Compston, A., & Chandran, S. (2003) Oligodendrocytes promote neuronal survival and axonal length by distinct intracellular mechanisms: a novel role for oligodendrocyte-derived glial cell line-derived neurotrophic factor. *J. Neurosci.*, 23(12): 4967-4974.

Williams, K. (2001) Ifenprodil, a novel NMDA receptor antagonist: site and mechanism of action. *Curr. Drug Targets.*, 2(3): 285-298.

Williamson, A.V., Mellor, J.R., Grant, A.L., & Randall, A.D. (1998) Properties of GABA(A) receptors in cultured rat oligodendrocyte progenitor cells. *Neuropharmacology*, 37(7): 859-873.

Wilson, H.C., Onischke, C., & Raine, C.S. (2003) Human oligodendrocyte precursor cells in vitro: phenotypic analysis and differential response to growth factors. *Glia*, 44(2): 153-165.

Wood, P. & Bunge, R.P. (1984) The biology of the oligodendrocyte. In W. T. Norton (Ed.), *Oligodendroglia*: 1-46. New York: Plenum Press.

Wrathall, J.R., Teng, Y.D., & Marriott, R. (1997) Delayed antagonism of AMPA/kainate receptors reduces long-term functional deficits resulting from spinal cord trauma. *Exp. Neurol.*, 145(2 Pt 1): 565-573.

Wu, K., Aoki, C., Elste, A., Rogalski-Wilk, A.A., & Siekevitz, P. (1997) The synthesis of ATP by glycolytic enzymes in the postsynaptic density and the effect of endogenously generated nitric oxide. *Proc. Natl. Acad. Sci. U. S. A*, 94(24): 13273-13278.

Xu, Z.C. & Pulsinelli, W.A. (1994) Responses of CA1 pyramidal neurons in rat hippocampus to transient forebrain ischemia: an in vivo intracellular recording study. *Neurosci. Lett.*, 171(1-2): 187-191.

Xu, Z.C. & Pulsinelli, W.A. (1996) Electrophysiological changes of CA1 pyramidal neurons following transient forebrain ischemia: an in vivo intracellular recording and staining study. *J. Neurophysiol.*, 76(3): 1689-1697.

Yang, S.Y., He, X.Y., & Schulz, H. (1987) Fatty acid oxidation in rat brain is limited by the low activity of 3-ketoacyl-coenzyme A thiolase. *J. Biol. Chem.*, 262(27): 13027-13032.

Yoshioka, A., Ikegaki, N., Williams, M., & Pleasure, D. (1996) Expression of N-methyl-D-aspartate (NMDA) and non-NMDA glutamate receptor genes in neuroblastoma, medulloblastoma, and other cells lines. *J. Neurosci. Res.*, 46(2): 164-178.

Yu, W.P., Collarini, E.J., Pringle, N.P., & Richardson, W.D. (1994) Embryonic expression of myelin genes: evidence for a focal source of oligodendrocyte precursors in the ventricular zone of the neural tube. *Neuron*, 12(6): 1353-1362.

Yuan, X., Eisen, A.M., McBain, C.J., & Gallo, V. (1998) A role for glutamate and its receptors in the regulation of oligodendrocyte development in cerebellar tissue slices. *Development*, 125(15): 2901-2914.

Zajicek, J. & Compston, A. (1995) Mechanisms of damage and repair in multiple sclerosis--a review. *Mult. Scler.*, 1(2): 61-72.

Zeevalk, G.D., Schoepp, D., & Nicklas, W.J. (1995) Excitotoxicity at both NMDA and non-NMDA glutamate receptors is antagonized by aurintricarboxylic acid: evidence for differing mechanisms of action. *J. Neurochem.*, 64(4): 1749-1758.

Zhou, M., Schools, G.P., & Kimelberg, H.K. (2000a) GFAP mRNA positive glia acutely isolated from rat hippocampus predominantly show complex current patterns. *Brain Res. Mol. Brain Res.*, 76(1): 121-131.

Zhou, M., Schools, G.P., & Kimelberg, H.K. (2006) Development of GLAST(+) astrocytes and NG2(+) glia in rat hippocampus CA1: mature astrocytes are electrophysiologically passive. *J. Neurophysiol.*, 95(1): 134-143.

Zhou, Q. & Anderson, D.J. (2002) The bHLH transcription factors OLIG2 and OLIG1 couple neuronal and glial subtype specification. *Cell*, 109(1): 61-73.

Zhou, Q., Choi, G., & Anderson, D.J. (2001) The bHLH transcription factor Olig2 promotes oligodendrocyte differentiation in collaboration with Nkx2.2. *Neuron*, 31(5): 791-807.

Zhou, Q., Wang, S., & Anderson, D.J. (2000b) Identification of a novel family of oligodendrocyte lineage-specific basic helix-loop-helix transcription factors. *Neuron*, 25(2): 331-343.

Zipfel, G.J., Babcock, D.J., Lee, J.M., & Choi, D.W. (2000) Neuronal apoptosis after CNS injury: the roles of glutamate and calcium. *J. Neurotrauma*, 17(10): 857-869.

Žiak, D., Chvatal, A., & Sykova, E. (1998) Glutamate-, kainate- and NMDA-evoked membrane currents in identified glial cells in rat spinal cord slice. *Physiol Res.*, 47(5): 365-375.